UNIVERSITÀ
DEGLI STUDI
FIRENZE

Dottorato di ricerca in
Fisica e Astronomia

ciclo XXVI

Energy landscape of classical spin models

S.S.D. FIS/02 (fisica teorica)

Candidate
Rachele Nerattini

Supervisor
Dr. Lapo Casetti

PhD Coordinator
Prof. Roberto Livi

Anni 2011/2013

Università degli Studi di Firenze, Dipartimento di Fisica e Astronomia.

Acknowledgments

I would like to express my gratitude to my supervisor, Lapo Casetti, who has been supporting (and believing in) me since my first level degree. Thanks for the hints and the support, both in Physics as in life.

I also would like to thank Michael K. -H. Kiessling with whom I started an interesting and stimulating collaboration that I hope will continue in the future with the same strength and satisfaction. Special thanks to Michael Kastner for the interesting and stimulating discussions, to Dagash Mehta, Johann Brauchart and Andrea Trombettoni with whom I had the chance to collaborate even if from afar.

Warm thanks to Cesare Nardini for the work we have done together, for the long discussions and for the support. Thank to other Ph.D students with whom I shared my research experience; in particular, thank to Aurelio Patelli with whom I did have the chance to carry on useful discussions in many fields.

To conclude I would like to thank my friends, for their enthusiasm, my Family for the strong support that always gave to me and Lele for being with me.

Contents

Journal publications

This work is the result of a research activity that led to the following journal publications. The order in which the papers are listed reflects the order in which they will be discussed in the thesis; the specific Chapters in which the paper will be presented are reported under the references.

- **Kinetic energy and microcanonical nonanalyticities in finite and infinite systems**
  L. Casetti, M. Kastner and R. Nerattini,
  J. Stat. Mech: Theory Exp., P07036, (2009).
  Presented in Chapter 1.

- **Exploring the energy landscape of XY models**
  R. Nerattini, M. Kastner, D. Mehta and L. Casetti,
  Phys. Rev. E, 87, 032140 (2013).
  Presented in Chapter 2.

- **Microcanonical Relation between Continuous and Discrete Spin Models**
  L. Casetti, C. Nardini and R. Nerattini,
  Phys. Rev. Lett., 106, 057208 (2011).
  Presented in Chapter 3.

- **Density of states of continuous and discrete spin models: a case study**
  C. Nardini, R. Nerattini and L. Casetti,
  J. Stat. Mech: Theory Exp., P02007 (2012).
  Presented in Chapter 5.

- **Density of states of the two-dimensional XY model: an energy landscape approach**
  C. Nardini, R. Nerattini and L. Casetti,
  preprint arXiv:1312.5223 (2013); submitted to J. Phys. A: Math. Theor.
  Presented in Chapter 5.

- **"Magic" numbers in Smale's 7th problem**
  R. Nerattini, J. S. Brauchart and M. K. -H. Kiessling,
  preprint arXiv:1307.2834 (2013); submitted to J. Stat. Phys.
  Presented in Chapter 6.

Paper in preparation:

- **Critical energy densities of classical three-dimensional $\mathbf{O}(n)$ models**
  R. Nerattini, L. Casetti and A. Trombettoni,
  work in preparation.
  Presented in Chapter 4.

Introduction

The stationary points of a function of many variables $f : M \mapsto \mathbb{R}$ are the points $p^{\mathrm{s}} \in M$ on a manifold M such that $\nabla f(p^{\mathrm{s}}) = 0$. Stationary points play an important role for quite a few methods in theoretical physics, as knowledge about these points can be used to infer physical properties of the system under investigation. When the function f is the energy of a many-body system and the manifold M is the phase space or the configuration space of the system, these methods are referred to as *energy landscape methods* [1]. Examples of applications include clusters [1], disordered systems and glasses [2, 3], biomolecules, and protein folding [4].

Based on knowledge about the stationary points of the energy function, landscape methods can be applied to estimate dynamic as well as static properties. In most applications, like for example Stillinger and Weber's thermodynamic formalism [5, 6] and other 'superposition approaches' [1] for the study of equilibrium properties, only minima of the energy landscape are taken into account. In some later work, also first-order saddles (see e.g. [7,8]) and stationary points of arbitrary index[1] have been considered, for instance to characterize glassy behavior [9, 10].

The potential relevance of energy landscape properties for equilibrium phase transitions was suggested after it was realized that stationary points of the Hamiltonian are related to topology changes of the phase space accessible to the system. It was conjectured that some of these topology changes, and therefore some of the stationary points, are at the origin of thermodynamic phase transitions [11–15]; quite some research activity followed, some focused on specific models, others trying to shed light on the general mechanisms (see [16, 17] for reviews).

Although equilibrium phase transitions in systems with non-fluctuating

[1]The index of a stationary point $p^{\mathrm{s}} \in M$ of a function $f : M \mapsto \mathbb{R}$ is the number of unstable directions, i.e., the number of negative eigenvalues of the Hessian of f at p^{s}.

particle numbers have been mainly studied within the canonical ensemble, the connection between stationary points of the Hamiltonian and equilibrium statistical properties is more transparent in a microcanonical setting [18]. This can be understood by observing that, for a system with N degrees of freedom, the entropy density is defined as[2]

$$s(\varepsilon) = \frac{1}{N} \log \omega(\varepsilon), \tag{1}$$

where $\varepsilon = E/N$ is the energy density and ω is the density of states. For a system described by continuous variables, ω can be written as

$$\omega(\varepsilon) = \int_\Gamma \delta(\mathcal{H} - N\varepsilon)\, d\Gamma = \int_{\Gamma \cap \Sigma_\varepsilon} \frac{d\Sigma}{|\nabla \mathcal{H}|}, \tag{2}$$

where Γ denotes the phase space and $d\Gamma$ its volume measure, Σ_ε is the hypersurface of constant energy $E = N\varepsilon$, and $d\Sigma$ stands for the $N-1$-dimensional Hausdorff measure. The rightmost integral stems from a co-area formula [19]. At a stationary point p^{s}, the gradient $\nabla \mathcal{H}(p^{\mathrm{s}})$ vanishes by definition and the integrand diverges, while at the same time the measure $d\Sigma$ shrinks such that ω in general remains finite for finite systems. Indeed, a more refined analysis [20] shows that, although the integral on the right-hand side of (2) remains finite in the vicinity of a stationary point, the density of states will be nonanalytic at stationary values $\varepsilon^{\mathrm{s}} := \mathcal{H}(p^{\mathrm{s}})/N$ of the energy density for any finite[3] N.

The microcanonical nonanalyticities appearing at finite N are found to be in correspondence with stationary configurations; however, the 'strength' of such nonanalyticities generically decreases linearly with N, i.e., the first k derivatives of the entropy are continuous, where k is $\mathcal{O}(N)$, see Chapter 1 and [20, 22]. The usual thermodynamic quantities, like equations of state, are given by low-order derivatives of the entropy, and the observation of nonanalyticities of order $\mathcal{O}(N)$ from noisy data is therefore restricted to very small system sizes N. Taking this to its logical conclusion, we expect the order of the nonanalyticities to diverge in the thermodynamic limit, leading to a vanishing effect of stationary points and smooth results for the thermodynamic functions.

[2] Throughout the thesis we set Boltzmann's constant k_B to unity.

[3] Such a behavior differs from the canonical ensemble where the canonical free energy or other thermodynamic functions may develop nonanalyticities only in the thermodynamic limit $N \to \infty$ [21].

Superficially, this seems to challenge the conjecture that phase transitions stem from stationary points of the energy, as it suggests that finite-N nonanalyticities due to stationary points are unrelated to thermodynamic phase transitions. And indeed, for several model systems, phase transitions have been found to occur at energies at which no stationary points of the Hamiltonian are present [23–30]. On the other hand, a substantial amount of evidence (in the form of model calculations) has accumulated in favor of the conjecture that stationary points often do play a relevant role for the emergence of phase transitions, and the presence of a transition reflects prominently in properties of the stationary points. This evidence comes mostly from exactly solvable systems (often with mean-field interactions) where the connection between stationary points and thermodynamic phase transitions has been shown explicitly [11, 13, 14, 31–33].

Subsequently a possible scenario of how certain finite-N singularities may survive in the thermodynamic limit has been proposed in [34, 35] (KSS criterion) and will be discussed in Chapter 1. The KSS criterion asserts that only singularities related to asymptotically flat stationary points may survive in the thermodynamic limit and induce a thermodynamic phase transition. *Asymptotically flat* here refers to stationary points whose determinant of the Hessian matrix of the potential energy V vanishes in the thermodynamic limit.

This indeed was verified to happen in the exactly solvable mean-field models where the connection between stationary points of the Hamiltonian and phase transitions had been previously demonstrated, see [34] and Chapter 2, and also in a non-solvable toy model of a self-gravitating particles with a phase transition between a homogeneous and a collapsed phase [36]. The KSS criterion, applicable also in case of partial knowledge of the stationary configurations of a system, could then allow to extend the above presented energy landscape analysis to non-trivial models, like e.g. short-range models in $d > 1$, for whom an analytic knowledge of *all* the stationary configurations is essentially impossible.

The present work mainly concerns classical $\mathrm{O}(n)$ spin models. In particular, it originates from the following observation: A particular class of stationary configurations of classical $\mathrm{O}(n)$ models defined on regular $d-$dimensional hypercubic lattices and with ferromagnetic interactions[4] is in one-to-one cor-

[4]The observation is valid independently of the range of the interactions, that could be either short-range, e.g. nearest-neighbor, or long-range, e.g. mean-field, interactions.

respondence with the configurations of an Ising model defined on the same lattices and with the same interactions. This configurations will be denoted as Ising stationary configurations. Such an observation suggests the possibility that the thermodynamic behavior of classical O(n) spin models can be intimately related to the thermodynamic behavior of Ising models. As it will be shown in the following, this fact will allow us to make predictions on the thermodynamics of the O(n) models—in particular on the form of the density of states of the O(n) models with $n > 1$—making use of the known results about the thermodynamics of the $n = 1$ (Ising) models.

The thesis is organized as follows.

In Chapter 1 some theoretical results useful for the following will be recalled, with special attention to the energy landscape results for equilibrium phase transitions in classical spin models. In particular, the KSS theorem will be introduced and its formulation as a criterion for the search of phase transitions will be discussed in detail, being one of the technical tools involved in our analysis. At the end of the Chapter a recent debate about the validity of a previous result, the Franzosi and Pettini theorem, will be briefly discussed in connection with our analysis.

In Chapter 2 classical O(n) spin models will be introduced, the Ising stationary points will be defined and their properties discussed. Then, the thermodynamics of O(n) systems will be recalled with special attention to the O(2) models (the XY models) that are among the simplest lattice spin models with short-range interactions amenable of an energy landscape approach based on stationary points of the Hamiltonian. In Secs. 2.2.1 and 2.2.2 the results on the application of the KSS criterion to the one-dimensional and to the mean-field XY models, respectively, will be recalled given their relevance for our analysis. From Sec. 2.3 on, we are going to present the content of [37] concerning our original application of the KSS criterion to two- and three-dimensional nearest-neighbor XY models. As we are going to show, at variance with the already studied cases, the KSS criterion is not able to detect any signature of the phase transitions present in these systems. This fact will allow us to make some remarks on the applicability of the KSS criterion and will suggest to ask ourselves which alternative mechanism, based on an energy landscape approach, could be at the basis of the thermodynamic behavior of the continuous models.

In Chapter 3 the content of [38] will be presented, regarding a possible

mechanism for the emergence of phase transitions in continuous O(n) models. More precisely, an approximate form of the density of states $\omega^{(n)}$ will be proposed, based on the assumption that the Ising stationary configurations are the 'most important' class of stationary configurations for what concerns the thermodynamics of the continuous models. The approximations performed to derive $\omega^{(n)}$ will appear rather crude and uncontrolled but will lead to the following consequence: if an O(n) model with ferromagnetic interactions on a hypercubic lattice has a phase transition, its critical energy density has to be equal to that of the $n = 1$ case, i.e., a system of Ising spins with the same interactions. The reliability of this consequence will be discussed in the light of the results known in the literature. It will turn out that in case of one-dimensional and mean-field O(n) models the consequence holds exactly; for what concerns short-range systems, instead, it gives extremely good estimates of the critical energy density values at which the transitions are located.

In Chapter 4 the content of [39] will be discussed. The accuracy of the prediction on critical energies proposed in Chapter 3 will be numerically studied for the three-dimensional nearest-neighbor O(n) models. More precisely, we will derive an interpolation formula to compute the critical energy density of a generic O(n) model with $n \in [2, \infty]$ in $d = 3$. This formula shows that the critical energy densities $\varepsilon_c^{(n)}$ differ from the numerically determined critical value of the energy density $\varepsilon_c^{(1)}$ of the corresponding Ising model by a quantity that is less then 3% for any value of $n > 1$. For $n < 8$, that is for the O(n) models involved in usual physical problems, the difference is even smaller and is less than 1%. This study, besides giving useful informations on the critical behavior of O(n) models in $d = 3$, supports the idea at the basis of the approximations made in Chapter 3 for $\omega^{(n)}$ and defines its level of accuracy.

In Chapter 5 the content of [40, 41] will be presented, concerning some developments of the concepts presented in Chapter 3. As we are going to show, our derivation of $\omega^{(n)}$ can be followed rigorously in the simple cases of mean-field and one-dimensional XY models. The difficulties in generalizing such results to the case of short-range O(n) models will be discussed at the end of the Chapter. Some approximation techniques valid for O(n) models with $n \geq 2$ in $d \geq 2$ will be proposed and tested on the two-dimensional nearest-neighbor XY model.

A collaboration with M. K. -H. Kiessling and J. Brauchart, that is still

in force, regards the study of the Smale's 7th problem concerning stationary configurations of N interacting points constrained on the $\mathbb{S}^2$ sphere. This topic, although embedded in the general framework of the thesis, moves a bit apart from the rest of the work and we decided not to go into its full details. We will simply summarize the main features of the analysis in Chapter 6 and refer the reader to the paper [42] for a deeper discussion of the subject.

The results presented in this thesis and the future perspectives originated from our analysis will be discussed in the final section of this work.

Chapter 1

Energy landscapes and equilibrium statistical properties

The study of the *energy landscape* of a system is the study of the graph of the potential energy function and of its possible connection to some dynamical or equilibrium properties. This quite recent point of view finds applications in several fields of research varying from biology, to physics, to chemistry [1]. Our purpose is to explain some of the equilibrium properties of a system in terms of some topological and geometrical properties of its energy landscape. In particular, we are interested in the occurrence of equilibrium phase transitions.

The present chapter is devoted to recall some general results; we address the reader to [16, 17] for quite recent reviews on the subject both for what concerns the technical details and the applications to some specific model systems. The chapter is organized as follows. In the first paragraph we will briefly recall some general basic concepts of statistical ensembles and equilibrium phase transitions. In §1.1.2 we will nail the notion of energy landscape and we will mention the different approaches involved in its analysis. From §1.2 on we will analyze in more detail the connection between phase transitions and geometrical and topological properties of energy landscapes. In Sec. §1.2 we will summarize the basic concepts of Morse theory, the main tool to connect the topology of the energy landscape with the non-analytic points of the entropy function. In §1.3 we will discuss the so-called "topological conjecture" [15] which suggests a relation between phase transitions and

sufficiently strong topology changes in the accessible phase space. We will then present the Franzosi and Pettini theorem that proves a weak version of the conjecture. In §1.4 we will analyze a specific property of the microcanonical ensemble: the presence of non-analytic points of the entropy function in systems with a finite number N of degrees of freedom. In §1.5 we will present the so-called KSS theorem that suggests a possible mechanism for the finite-N singularities to survive in the thermodynamic limit, $N \to \infty$. We will then re-formulate this result as a criterion for the search of a phase transition, naming it as the KSS criterion. In §1.6 we will discuss a recent debate regarding the validity of the Franzosi and Pettini theorem.

1.1 The microcanonical ensemble, phase transitions and energy landscapes

If not stated otherwise, we are going to consider classical systems with N degrees of freedom described by the Hamiltonian

$$H(p,q) = \sum_{i=1}^{N} \frac{p_i^2}{2} + V(q). \tag{1.1}$$

$(p,q) = (p_1, \ldots, p_N, q_1, \ldots, q_N) \in \Lambda_N$ are the coordinates of the phase space Λ_N of the system; $V : (q_1, \ldots, q_N) \in \Gamma_N \to \mathbb{R}$ is the interaction potential and Γ_N the configuration space of the system. We will assume Γ_N to be a differentiable manifold at variance with what happens in some classical spin models, like the Ising or the Potts model, which have a discrete configuration space.

Starting from Eq. (1.1), equilibrium statistical mechanics allows to infer macroscopic properties of a system from suitable averages over the microscopic variables. Averages are performed according to statistical weights that depend on the particular statistical ensemble chosen for the analysis. The choice of the statistical ensemble is dictated by the physical conditions under which the system is studied. For instance the *canonical* ensemble is the correct framework for a statistical description of a system in contact with an external thermostat at temperature T, the *grand canonical* ensemble is the framework for a statistical description of a system in which neither the energy nor the temperature nor the number of particles are constant but can

fluctuate around a fixed mean value, and so on. In this work all the analysis will be performed in the *microcanonical* ensemble that represents the operational background of a statistical description in which the total energy $H(p,q) = E$ is conserved and the system can be considered as isolated. To fix the notations we will briefly recall the main results for the microcanonical ensemble; we address the reader to [43, 44] or to any primer book on statistical physics for a general introduction on this topic.

1.1.1 The microcanonical ensemble

In the microcanonical ensemble the fundamental quantity is the entropy density s_N as a function of the energy density $\varepsilon = E/N$,

$$s_N(\varepsilon) = \frac{1}{N} \log \omega_N(\varepsilon), \tag{1.2}$$

where $\omega_N(\varepsilon)$ is the density of states, given by

$$\omega_N(\varepsilon) = \int_{\Lambda_N} dp\, dq\, \delta\left[H(p,q) - N\varepsilon\right]; \tag{1.3}$$

δ is the Dirac distribution[1]. A related quantity is the configurational microcanonical entropy, given by

$$s_N^c(v) = \frac{1}{N} \log \omega_N^c(v) = \frac{1}{N} \log \int_{\Gamma_N} dq\, \delta\left[V(q) - Nv\right] \tag{1.4}$$

where $v = V/N$ and

$$\omega_N^c(v) = \int_{\Gamma_N} dq\, \delta\left[V(q) - Nv\right] \tag{1.5}$$

is the corresponding configurational density of states. The configurational entropy equals the entropy when the Hamiltonian simply consists of a configuration-dependent potential energy, $H \equiv V$. This is often the case when studying spin systems. This will also be the case in this work where classical O(n) models will be considered. In Chapter 2 we will come back to this point.

[1] Here and in the following we set the Boltzmann constant $k_B = 1$ and we consider the normalization factor $\frac{1}{h^N N!}$ already included in the integration measure.

The usual thermodynamic functions can be obtained from the entropy (1.2) by derivation. For instance the microcanonical caloric curve is given by

$$T^{\mu}(\varepsilon) = \left(\frac{ds}{d\varepsilon}\right)^{-1} \tag{1.6}$$

while the microcanonical expression of the specific heat per degree of freedom is given by

$$c^{\mu}(\varepsilon) = \frac{C^{\mu}(\varepsilon)}{N} = \left(\frac{dT^{\mu}}{d\varepsilon}\right)^{-1} = -\frac{(s')^2}{s''}, \tag{1.7}$$

where s' and s'' denote respectively the first and the second derivative of $s(\varepsilon)$ with respect to the energy density ε. It is worth noticing that the microcanonical specific heat is negative whenever $s''(\varepsilon) > 0$.

In the following we are going to analyze the analyticity properties of thermodynamic functions in the microcanonical setting. For what concerns such properties, thermodynamic functions obtained from different statistical ensembles can differ drastically. This is the case, for instance, for systems with a finite number of degrees of freedom, the average operations strongly relying on the statistical description chosen for the analysis, see e.g. [45–48]. This notwithstanding, in the case of short range interactions, different statistical descriptions, i.e. the microcanical and the canonical one, lead to equivalent results when $N \to \infty$ so that the canonical and the microcanonical results are related via a Legendre-Fenchel transformation, see e.g. [49, 50]. In the case of long-range interactions[2], instead, equivalence is not guaranteed anymore and usually different statistical descriptions lead to different results, see e.g. [51] and reference therein. However, even if the equivalence does not hold, the canonical results can always be derived from the microcanonical results while the vice versa is not true; loosely speaking this fact seems to suggest that the microcanonical descriptions happens to be the most fundamental.

In our work we are going to consider systems both with short and long range (mean-field) interactions for which different statistical descriptions are equivalent in the thermodynamic limit. This means that, when $N \to \infty$, we can switch from one statistical description to the other according to our

[2]Long-range interactions are such that $V(r) \sim r^{-\alpha}$ with $\alpha \leq d$ where d is the spatial dimension of the system.

convenience. The only fact to be worried about is the correct definition of the thermodynamic quantities in the different ensembles; i.e. if a system undergoes a phase transition and its critical behavior is expressed in terms of the energy instead of temperature, the correspondent critical exponent has to be modified by a factor $(1-\bar{\alpha})^{-1}$, with $\bar{\alpha}$ usual canonical specific heat critical exponent, stemming from the "translation" of temperatures into energies [48]. As an example, the microcanonical specific heat critical exponent α^{μ} is related to $\bar{\alpha}$ by the relation $\alpha^{\mu} = \frac{\bar{\alpha}}{1-\bar{\alpha}}$. Such a relation will be useful in Sec. 5.1.3.

1.1.2 Equilibrium phase transitions and energy landscapes

Phase transitions, like the melting of ice or the magnetization of a ferromagnet, are very common phenomena in our daily life as well as in several branches of physics. Loosely speaking, phase transitions can be seen as abrupt changes in the macroscopic properties of a system that happen for a particular value of an external control parameter (like the pressure or the temperature) but are not associated with any mutations in the microscopic interactions among its constituents [52]. In equilibrium statistical mechanics phase transitions are associated with nonanalyticities of thermodynamic functions: more precisely, one commonly defines a phase transition point as the value of an external parameter where some thermodynamic function is non-analytic[3]. Such an identification is satisfactory in the canonical ensemble: as originally suggested by Kramers [53], nonanalyticities of thermodynamic functions calculated in the canonical ensemble may show up only in the thermodynamic limit $N \to \infty$, where N is the number of degrees of freedom [21]. Moreover, such nonanalyticities separate different phases, i.e., regions of the parameters where the collective properties of the system are different. When studying physical models, one usually finds that thermodynamic functions have only a small number of nonanalyticities, if any. In the microcanonical ensemble, however, the situation is different; in fact, as will be discussed in Sec. 1.4, nonanalyticities of the microcanonical entropy may be present even at finite N and can be hardly associated to phase transitions,

[3]Departing slightly from the standard definition, we use the notion of analyticity in the sense of a real function being infinitely-many times differentiable.

at least to phase transitions as defined above.

The mathematical description of phase transitions developed in the past years yielded several important results; see i.e. [43, 54] for a general introduction and [55] for a summary. This notwithstanding, some conceptual and practical questions are still without an answer.

From a conceptual point of view, the research of sufficient conditions for the occurrence of a phase transition is an open problem and general results are still missing. For what concerns the necessary conditions only few general results are known: Van Hove [56] showed that phase transitions cannot be present in classical one dimensional systems of identical hard-sphere particles with finite-range interactions; Griffiths [57] showed that a spontaneous magnetization can be present in the Ising model only in spatial dimension $d > 1$; the Mermin and Wagner theorem [58] asserts that a phase transitions with the spontaneous breaking of a continuous symmetry can be present in a system with short-range interactions only if the spatial dimension of the system is $d > 2$.

Even the necessity of the thermodynamic limit is somehow an arguable argument. "Transitional phenomena", indeed, have been observed in systems with a small number of degrees of freedom like atomic clusters or proteins [1]. Moreover, physical systems have a finite number of degrees of freedom, although possibly extremely large, and so the limit $N \to \infty$ could sound like a mathematical expedient. Furthermore, critical behavior of some systems like supercooled liquids, glasses or disordered systems shows both equilibrium and dynamical features and a proper equilibrium statistical description may not be fully appropriated in these cases. Lastly the classical description of phase transitions has been mainly developed in the canonical (or grand-canonical) ensembles, as in the Lee and Yang theory [59] and its extension made by Fisher [60], and its application to the microcanonical ensemble is not straightforward. All these facts make the usual approach somehow incomplete, especially when the canonical and microcanonical descriptions are not equivalent, and point out the necessity of a more flexible approach to the study of these phenomena.

A possible idea is then to study the *energy landscape* of a system to infer some informations on its thermodynamic properties in a microcaconical framework. The notion of energy landscape strictly depends on the specific field of research considered. Usually the study of the energy landscape of a system is the study of the properties of the graph of its energy function

$H : \Lambda_N \to \mathbb{R}$, with Λ_N phase space of the system. In this kind of analysis a special role is played by the stationary points of the energy function that are all those points $(\tilde{p}_c)$ of the phase space such that $\nabla H(\tilde{p}_c) = 0$. Examples of applications include clusters [1], disordered systems and glasses [2, 3], biomolecules, and protein folding [4]. Based on the knowledge about the stationary points of the energy function, landscape methods can be applied to estimate dynamic as well as static properties of a system; in our work we are going to focus our attention only on the equilibrium properties.

In most applications, like Stillinger and Weber's thermodynamic formalism [5, 6] and other "superposition approaches" [1, 61] for the study of equilibrium properties, only the minima of the energy landscape are taken into account. In some later works, first-order saddles (see, i.e., [7, 8]) and stationary points of an arbitrary index[4] have also been considered, for instance, to characterize glassy behavior [9, 10].

The natural setting to understand the connection between the stationary points of the Hamiltonian and equilibrium statistical properties is the microcanonical one [18]. This can be understood by observing that, for a system with N degrees of freedom and described by continuous variables, the density of states in Eq. (1.3) can been written with the co-area formula [19] as

$$\omega_N(\varepsilon) = \int_{\Lambda_N \cap \Sigma_\varepsilon} \frac{d\Sigma}{|\nabla H(p, q)|} \tag{1.8}$$

where Λ_N is the phase space, Σ_ε is the hypersurface of constant energy $E = N\varepsilon$, and $d\Sigma$ stands for the $(N-1)$-dimensional Hausdorff measure. At a stationary point $\tilde{p}_c$, the gradient $\nabla H(\tilde{p}_c)$ vanishes by definition and the integrand diverges, while at the same time the measure $d\Sigma$ shrinks such that ω_N in general remains finite for finite systems. Indeed, a more refined analysis [20] showed that, although the integral on the right-hand side of Eq. (1.8) is finite in the vicinity of a stationary point, the density of states will be nonanalytic at stationary values $\varepsilon_c := H(\tilde{p}_c)/N$ of the energy density for any finite N.

On the other side, for systems described by the Hamiltonian (1.1), the integration over the momentum variables can be performed separately and

[4] For the definition of the index of a stationary point see Sec. 1.2.

the integration domain of Eq.(1.8) becomes

$$M_\varepsilon = \{q \in \Gamma_N | V(q) \leq N\varepsilon\} \tag{1.9}$$

that is, the configuration space accessible to the system at a given energy density value ε. It is reasonable to conjecture that "sufficiently strong" changes in the topology of (1.9) can be connected with nonanalytic points of $\omega_N(\varepsilon)$. As will become clear in the next section, changes in the topology of (1.11) happen in correspondence of critical points of the potential energy. It was then conjectured that some of these topology changes, and therefore some of the stationary points, are at the origin of thermodynamic phase transitions [11–15]; quite a bit of research activity followed, see i.e. [23–25, 27, 28, 30, 31, 33, 36, 37, 55, 62–69, 71–76], some focused on specific models, others trying to shed light on the general mechanisms (see Refs. [16, 17] for reviews).

The mathematical tool to connect the stationary points of the Hamiltonian (1.1) with the topology of the set (1.9) is finite-dimensional Morse theory. In the following paragraph we are going to recall some basic concepts of this theory.

1.2 Morse theory

The aim of this paragraph is to recall the basic concepts of finite dimensional Morse theory with particular attention to its application to the study of the topology of energy landscapes. We address the reader to [77] for technical details and for the mathematical proofs that we will omit here.

Let us consider a smooth function V from a manifold M to the space of real numbers, $V : M \subseteq \mathbb{R}^N \to \mathbb{R}$. We call *stationary points* or *critical points* or *saddle points* of V all those points $q_c \in M$ such that $dV(q_c) = 0$ including minima and maxima. Let $\mathcal{H}_V(q_c)$ denote the Hessian matrix of V evaluated in q_c. If $\det[\mathcal{H}_V(q_c)] \neq 0$ then q_c is said to be a non-degenerate stationary point, otherwise q_c is said to be degenerate. All those points $v_c \in \mathbb{R}$ image of (at least) one stationary point are said stationary values or critical values of the function V. If q_c is a non degenerate point, the *index* of q_c is the number of negative eigenvalues of the Hessian matrix evaluated in q_c. V is said to be a *Morse function* if $\det \mathcal{H}_V(q_c) \neq 0$ for *every* $q_c \in M$.

An important result of Morse theory is that all the critical points of a Morse function are isolated. This result is stated in the following

Theorem 1.2.1 (Morse Lemma)**.** *Let q_c be a non-degenerate critical point of V with index k.*

Then, in a neighborhood U_{q_c} of q_c a local coordinate system $(x_1, \ldots, x_N)$ exists such that

$$V = V(q_c) - x_1^2 - ... - x_k^2 + x_{k+1}^2 + ... + x_N^2 \tag{1.10}$$

is exact in U_{q_c}.

To study the topology of the energy landscape of a system, that is the topology of the set

$$M_v = V^{-1}(v) = \left\{ q \in M \middle| \frac{V(q)}{N} \leq v \right\}, \tag{1.11}$$

we are going to consider only potential functions V that are Morse functions. This is not a limiting restriction. In fact it can be shown that Morse function are an open and dense subset of all C^∞ functions [78]. This means that, even if the interaction potential is not a Morse function, it can be made a Morse function simply by adding a generic, arbitrarily small, perturbation. As an example, every potential function with continuous symmetry is not a Morse function. In this case, a generic perturbation changes the structure of the stationary points and explicitly breaks the continuous symmetry. A rather useful trick is to consider the system after having fixed a finite number of coordinates. In our work we are going to apply this prescription to study our potential functions. For further details and a more extended discussion on the subject, see Chapter 2.

The connection between Morse functions and the topology of the set (1.11) is established by the following

Theorem 1.2.2. *: Let us consider a smooth Morse function V such that $V : M \subseteq \mathbb{R}^N \to \mathbb{R}$. Suppose that $[a, b] \in \mathbb{R}$ contains a single critical value v_c which corresponds to a single critical point q_c with index k.*

If M_a and M_b are compact, then M_b is homeomorphic to a manifold obtained attaching[5] *a $k-$handle to M_a, where a $k-$handle is the direct product of a $k-$disc with a $(N-k)-$disc.*

[5]For a rigorous definition of the operation of "attaching", we address the reader to [77].

Theorem 1.2.2 asserts that the topology of the set (1.11) changes any time v passes through a stationary value and it is characterized by the stationary points of V and by their indices. This notwithstanding, the topology of M_v could be very complicated when N becomes large. A topological invariant easy to evaluate once all the stationary points are known is the Euler characteristic $\chi(M_v)$ of the manifold M_v. This quantity is given by

$$\chi(M_v) = \sum_{i=0}^{N} (-1)^i \mu_i \tag{1.12}$$

where μ_i is the $i-$th Morse number, defined as the number of critical points of V with index i and critical values smaller than v. To evaluate the Euler characteristic it is necessary to know *all* the stationary points and their indices; this informations could be hard to determine for generic potential functions.

1.3 Topological conjecture

The study of some simple models (see [16, 17] for reviews) has shown that strong changes in the topology of M_v for a certain value of the potential energy density v_c are often associated to a singular behavior of thermodynamic quantities at the same value of the potential energy per degree of freedom. This led the authors of [12] to conjecture that phase transitions could be due to "sufficiently strong" changes in the topology if M_v. This idea has been named "topological conjecture" in [15]. The precise meaning of "sufficiently strong" changes is still under debate. However a weaker version of the topological conjecture is believed to be correct; the so-called "weak" topological conjecture asserts that:

Conjecture 1.3.1 ("weak" topologic conjecture)**.** *A change in the topology of* $\{M_v\}$ *at* $v = v_c$ *is a necessary condition for a phase transition to occur in the system at* $v = v_c$*.*

Franzosi and Pettini announced in [79–81] the proof of a theorem that sustains the validity of Conjecure (1.3.1) for a certain class of physically relevant potential functions.

Theorem 1.3.2 (Franzosi-Pettini theorem)**.** *Let V be a potential function of the form*

$$V_N(q) = \sum_{i=1}^{N} \phi(q_i) + \sum_{i,j=1}^{N} c_{i,j}\psi(|q_i - q_j).$$

Let V be smooth, confining, short ranged and limited from below.

If there exists a number N_0 and an interval $[v_1, v_2] \in \mathbb{R}$ such that $\forall N > N_0$ the hypersurfaces $(M_v)_{v\in[v_1,v_2]}$ do not change topology, then the free energy is at least $C^2\left[\beta(v_1), \beta(v_2)\right]$ when $N \to \infty$. $\beta(v) = \frac{1}{T}(v)$ is the value of the inverse temperature correspondent to the potential energy v.

Authors stated that the extension of the above results to higher order derivatives of the free energy is possible although laborious. We do not present here the proof of theorem 1.3.2 for which we address to [79, 80], we simply highlight here that every hypothesis of the theorem appears to be vital for the results. In fact, counterexamples of theorem 1.3.2 are known for non-confining, long-range or singular potential functions, see i.e. [16] or [55] for a basic comment on this point. See also Sec. 1.6 for a further discussion on the validity of this theorem.

Thanks to Morse theory the above mentioned theorem can be reformulated in terms of stationary configurations of the potential energy. Indeed, if V is a Morse function, topological changes of the set M_v correspond to the existence of stationary points of the potential function V whose stationary values belong to $[v_1, v_2]$.

The determination of the kind of topology change that can induce a phase transition in the thermodynamic limit is still an open question. This notwithstanding, the connection between stationary configurations of the potential energy V–or changes in the topology of M_v–and nonanalyticities of the microcanonical entropy for *finite* N has been completely understood, as we shall see in the next Section.

1.4 Microcanonical singularities

In the canonical and in the grand canonical ensemble the thermodynamic potentials are smooth functions for systems with a finite number of degrees of freedom [44]. On the other side, as pointed out at the end of Sec. 1.1.2, the microcanonical entropy shows singularities also for finite systems. In principle, this fact should have been known for a long time, because even

one-degree-of-freedom systems like a simple pendulum or a particle in a double-well potential do show nonanalyticities of the entropy. Still, it came as a surprise to many researchers in the field to see how frequently such nonanalyticities are encountered in many-particle systems [22, 32, 82–84].

In the following we are going to consider systems described by the Hamiltonian (1.1) with V Morse potential functions. More precisely, we are going to describe the effect of the stationary configurations on the analyticity properties of the microcanonical entropy. This paragraph is structured as follows. In §1.4.1 we are going to review the results due to Kastner, Schreiber and Schnetz reported in [20, 35] giving a complete characterization of the nonanalyticities of the configurational entropy and of their strength for finite systems. They found a one-to-one correspondence between the stationary values of the potential energy the singularities of the configurational entropy. The behavior of such nonanalyticities as a function of the number N of degrees of freedom is remarkable: their number may grow with N even exponentially, and their "strength" generically decreases linearly with N. In §1.4.2 we will take back the kinetic term to get Hamiltonian systems of the form given by Eq. (1.1) and we will discuss the effect of this term on the microcanonical nonanalyticities for finite systems and in the case $N \to \infty$. It will turn out that the kinetic term increases the regularity of the entropy although it remains a singular function [22].

1.4.1 Singularities in the configurational entropy

Let us consider a Hamiltonian system of the form (1.1) with a smooth and confining potential $V : \Gamma_N \subseteq \mathbb{R}^N \to \mathbb{R}$. In [20, 35] authors have analyzed the analyticity properties of the configurational density of states[6] defined in Eq. (1.5)–or equivalently of the configurational entropy (1.4)–as a function of v. The main observation is that the nonanalytic points of $\omega_N^c(v)$ are strictly related to the stationary points of V. In fact, if no stationary values of

[6]Similar results are valid for the integrated density of states $\Omega^c(v) = \int_{\Gamma_N} \Theta(V(q) - Nv)\, dq$, $\Theta(x)$ denotes the Heaveside step function of x, and for the corresponding entropy $\sigma_N^c(v) = \frac{1}{N} \log\, \Omega_N^c(v)$. Ω_N^c is related to the previous definition by

$$\omega_N^c(v) = \frac{d\Omega_N^c(v)}{dv}. \tag{1.13}$$

the potential energy are present in the interval $[v_1, v_2]$, then ω_N^c and s_N^c are analytic functions $\forall v \in [v_1, v_2]$ [80]. Let us consider a given value v of $\frac{V}{N}$ and the set (1.11) that we rewrite as

$$V^{-1}(v) = \left\{ q \in \Gamma_N \Big| \frac{V(q)}{N} = v \right\}; \tag{1.14}$$

if $V^{-1}(v)$ does not contain any stationary point of V, then $\omega_N^c(v)$ is a smooth function. On the other side, if at least one critical point of V belongs to $V^{-1}(v)$, then it must be isolated, V being a Morse function. This implies that neighborhoods $U_{q_c^i}$ of q_c^i can be built in such a way that $q_c^j \notin U_{q_c^i}$ if $j \neq i$. For this reason we can discuss the analyticity properties of $\omega_N^c(v)$ supposing that only one critical point q_c is present, the generalization to several stationary configurations is straightforward and consists in adding the different contributions. If only one stationary configuration q_c is present, then the configurational density of state in Eq. (1.5) can be written as

$$\omega_N^c(v) = \int_{U_{q_c}} \delta(V(q) - Nv)\, dq \; + \; \int_{\Gamma_N - U_{q_c}} \delta(V(q) - Nv)\, dq; \tag{1.15}$$

for the above mentioned reasons the second term of the sum in Eq. (1.15) gives a smooth contribution and nonanalytic points can derive exclusively from the first term.

Without loosing in generality we can set $V(q_c) = 0$. Thanks to the Morse Lemma (1.2.1), U_{q_c} and a coordinate system $x = (x_1, \ldots, x_N)$ can be chosen in such a way that

$$V(q(x)) = -\sum_{i=1}^{k} x_i^2 + \sum_{i=k+1}^{N} x_i^2 \tag{1.16}$$

in U_{q_c}; k is the index of the stationary point q_c. Denoting by $J(x)$ the determinant of the Jacobian of the coordinate transformation from the original coordinate system to the one defined in Eq.(1.16), let us consider its expansion around $x = 0$:

$$J(x) = \sum_{I=\{i_1,\ldots,i_N\}} a_I x^I, \tag{1.17}$$

where a multi-index notation $x^I = x^{i_1} \ldots x^{i_N}$, has been used. In Eq. (1.17), the $0-$th order is related to the second derivatives of the potential energy

function V evaluated in q_c, that is

$$J(0) = a_0 = \left| \det \left[\frac{\mathcal{H}_V(0)}{2} \right] \right|^{-\frac{1}{2}}. \tag{1.18}$$

$J(0)$ represents the leading order contribution to the non analytic term in Eq. (1.15). In [20] authors evaluated the non analytic contribution deriving from the first term in the sum of Eq. (1.15) at any order in the expansion (1.17). The $0-$th order term in Eq. (1.18) is enough to our purposes and we can finally present the following theorem[7]

Theorem 1.4.1 (Singularities of the configurational entropy for finite systems)**.** *Let $V : G \subseteq \mathbb{R}^N \to \mathbb{R}$ be a Morse function. Let q_c be the only stationary point of V in an open set G, having index k and stationary value $\frac{V(q_c)}{N} = v_c$. The configurational density of state ω_N^c can be written as*

$$\omega_N^c(v) = \omega_N^a(v) + \omega_N^{na}(v), \tag{1.19}$$

that is as the sum of an analytic function $\omega^a(v)$ and a non analytic function $\omega_N^{na}(v)$. The leading order of the non analytic term is given by

$$\omega_N^{na}(v) = \frac{(N\pi)^{N/2}}{N\Gamma\left(\frac{N}{2}\right)\sqrt{\left|\det\left[\frac{\mathcal{H}_V(q_c)}{2}\right]\right|}}\, h_{N,k(mod4)}^{na}(v) \tag{1.20}$$

where the singularity is given by the universal function

$$h_{N,k(mod4)}^{na}(v) = \begin{cases} (-1)^{k/2} v^{(N-2)/2}\Theta(v), & k \text{ even}, \\ (-1)^{(k+1)/2} v^{(N-2)/2}\pi^{-1}\log|v|, & N \text{ even, } k \text{ odd}, \\ (-1)^{(N-k)/2}(-v)^{(N-2)/2}\Theta(-v), & N, k \text{ odd}. \end{cases} \tag{1.21}$$

$h_{N,k(mod4)}^{na}(v)$ is universal in the sense that it does not depend on V. In case there are more then one critical points of V, their contributions sum up. Finally, the contribution of the singularities due to higher order terms in the expansion (1.17) simply changes the pre-factor in Eq. (1.20) but leaves the universal function $h_{N,k(mod4)}^{na}(v)$ unchanged.

[7] For the general statement of the theorem at any order in the expansion of the determinant of the Jacobian and for its proof, we address the reader to [20].

In all the three cases of Eq. (1.21), ω_N^c is $\lfloor (N-3)/2 \rfloor$ times differentiable[8], where $\lfloor x \rfloor$ denotes the largest natural number smaller than x. In short, the results of Theorem 1.4.1 can be rephrased as follows:

(i) Every stationary point q_c of V gives rise to a nonanalyticity of the configurational entropy $s^c(v)$ at the corresponding stationary value $v = v_c = V(q_c)/N$.

(ii) The order of this nonanalyticity is $\lfloor (N-3)/2 \rfloor$, i.e., $s^c(v)$ is precisely $\lfloor (N-3)/2 \rfloor$ times differentiable at $v = v_c$.

The second observation could lead to the conclusion that in the thermodynamic limit $N \to \infty$ these non analytic points disappear. Actually this is not the case, as we will discuss in §1.5, in agreement with the conclusions of Theorem 1.3.2.

It is worth noticing that in Theorem 1.4.1 the request of a Morse potential is a stronger requirement then what is actually needed. In fact the previous results remain valid simply asking for non degenerate stationary points of V in $\Gamma_N - U$, with U a suitable subset of the configuration space. In this case the previous analysis is valid for every value of v except those included in $V(U)$ upon which nothing could be concluded. This is the situation in the mean field XY model that we are going to discuss in §2.2.1. In the following we will assume the potential energy $V(q)$ to be a Morse function unless explicitly stated otherwise.

1.4.2 Role of the kinetic energy

A kinetic term of the form in Eq.(1.1) gives a trivial contribution to the canonical partition function both in the case of finite systems and in the $N \to \infty$ limit; its effect is simply to shift the thermodynamic functions by a constant. In the microcanonical ensemble, instead, its effect is more tricky and it has been analyzed in [22] both in the case of finite systems and in the thermodynamic limit. The analysis has been done considering Hamiltonian systems with Morse potential functions and the results can be summarized as follows:

[8]The integrated density of states $\Omega_N^c(v)$ defined in Eq.(1.13) is $\lfloor (N-1)/2 \rfloor$ differentiable.

1. *finite* systems. If the configurational density of states $\omega_N(v)$ is nonanalytic at $v = v_c$, then the density of states $\omega_N(\varepsilon)$ and the entropy $s_N(\varepsilon)$ are nonanalytic at $\varepsilon = v_c$; moreover the density of states $\omega_N(\varepsilon)$ and the entropy $s_N(\varepsilon)$ at $\varepsilon = v_c$ are differentiable $\lfloor N/2 \rfloor$-times more often than the configurational density of states $\omega_N(v)$[9].

2. *Infinite* systems. If $s^c_\infty(v)$ is nonanalytic at $v = v_c$, then $s^\infty(\varepsilon)$ will be nonanalytic at $\varepsilon = \varepsilon^*$, where ε^* is defined implicitly by $\langle v \rangle(\varepsilon^*) = v_c$ with $\langle v \rangle$ denoting the average potential energy density. Apparently ε^* differs from the value of v_c, unless the average kinetic energy per particle vanishes at ε^*.

Hence, despite their common origin from the nonanalyticity of s^c at v_c, nonanalyticities of $s_\infty(\varepsilon)$ jump from their finite-N value of ε to a different value ε^* in the thermodynamic limit. Here we are going to give the sketch of the idea behind the above mentioned results, for a more rigorous proof we address the reader to [22].

We begin by noting that if the Hamiltonian $H(p, q)$ is of standard form (1.1), its stationary points[10] are of the form $\tilde{p}_c = (p_c, q_c) = (0, q_c)$. Hence the stationary value of the Hamiltonian coincides with the stationary value of the potential energy, i.e., $\varepsilon_c = v_c$, the kinetic energy is zero at stationary points and $H(p_c, q_c) = V(q_c)$ for all stationary points (p_c, q_c) of H. As a consequence, for all finite N the nonanalyticities of the configurational entropy–which we have traced back to stationary points in the previous section–show up at the very same stationary values as those of the entropy.

In case of systems described by Eq. (1.1) the density of states can be written as a convolution product [85] between a kinetic and configurational part. In fact we can define a kinetic density of states as

$$\omega^k_N(\gamma) = \int_{\mathbb{R}^N} \delta\left(\frac{1}{2}\sum_{i=1}^{N} p_i^2 - N\gamma\right)\, dp = \frac{2\pi^{N/2}}{\Gamma\left(\frac{N}{2}\right)}\left(2N^{\frac{N}{2}-1}\right)\gamma^{\frac{N}{2}-1}; \qquad (1.22)$$

[9] As far as the entropy is concerned, these statements hold if v_c is in the interior of its domain. Both statements hold also for the integrated densities of states $\Omega_N(\varepsilon)$ and $\Omega^c_N(\varepsilon)$.

[10] The present discussion holds also in case of magnetic systems for which a rather special precessional dynamics with constant kinetic energy is present. Indeed, their role is analogous to that of simple "rotor" systems where conjugate variables p and q can be separated and the relative Hamiltonian can be rewritten in the general form (1.1).

in this way the density of state $\omega_N(\varepsilon)$ is given by

$$\omega_N(\varepsilon) = \int_0^\infty \omega_N^k(\gamma)\omega_N^c(\varepsilon-\gamma)\, d\gamma = \int_{-\infty}^\varepsilon \omega_N^k(\varepsilon-\gamma)\omega_N^c(\gamma)\, d\gamma. \tag{1.23}$$

At any finite N, the effect of the kinetic energy term on the order of the nonanalyticities of the entropy can be computed explicitly from the convolution integral (1.23). Such a calculation is reported in the Appendix A of [22], and the only additional input used is that–in accordance with Theorem 1.4.1–the nonanalyticities of the configurational density of states ω_N^c are of algebraic type.

For what concerns the case of infinite systems, if $\lim_{N\to\infty} s_N^c$ exists, then also $\lim_{N\to\infty} s_N$ exists [85] and, apart from irrelevant constants, it is given by

$$\begin{aligned} s_\infty(\varepsilon) = &\lim_{N\to\infty} \frac{1}{N} \log \max_{\gamma\geq 0} \left[\omega_N^k(\gamma)\omega_N^c(\varepsilon-\gamma)\right] = \\ =&s_\infty^k\left[\tilde{\gamma}(\varepsilon)\right] + s_\infty^c\left[\varepsilon-\tilde{\gamma}(\varepsilon)\right], \end{aligned} \tag{1.24}$$

where $\tilde{\gamma}(\varepsilon)$ is the value of γ that maximize the above expression. In particular $\tilde{\gamma}(\varepsilon)$ represents the average kinetic energy per particle and the results for infinite systems follows from expression

$$s_\infty(\varepsilon) = s_\infty^k\left[\varepsilon - \langle v\rangle(\varepsilon)\right] + s_\infty^c\left[\langle v\rangle(\varepsilon)\right]. \tag{1.25}$$

Once again, in the proof the only requirement on the stationary points is that the nonanalyticities of the configurational density of state are of algebraic type. In case of Morse potentials this requirement is guaranteed by theorem 1.4.1 but the above mentioned results remain valid also for potentials that are not Morse functions (and so do not satisfy the hypotheses of theorem 1.4.1) but have nonanalyticities of the configurational density of state of algebraic type. An example of a system with this kind of potential function is given by the hypercubic model discussed in [22].

Let us conclude this section with some comments. The classical definition of phase transitions as nonanalytic points of the thermodynamic functions is perfectly meaningful in the canonical and grand-canonical ensembles but cannot be applied directly to the microcanonical ensemble. In this case the number of critical points of the potential energy typically increases exponentially with N. This would mean that one should encounter roughly $\mathcal{O}(e^N)$

phase transitions in finite systems. Moreover these nonanalyticities are irrelevant to the thermodynamics, as they affect derivatives of order N of the entropy. A possible mechanism for a microcanonical finite-N-singularity to survive in the thermodynamic limit has been proposed in [20,34] and will be discussed in the following Section.

1.5 The KSS criterion

It is natural to ask if some of the singularities of the microcanonical entropy of a finite system can survive in the $N \to \infty$ limit to give rise to a phase transition. In this Section we are going to discuss a theorem due to Kastner, Schreiber and Schnetz [20,34] that gives a necessary condition for a finite-N microcanonical singularity to survive in the thermodynamic limit. At the end of this Section this result will be re-formulated as a criterion for the search of phase transitions.

1.5.1 The KSS theorem

If not stated otherwise, in the following we are going to neglect the apex c to denote the configurational part of the thermodynamic functions to lighten the notations. Let us consider the configurational density of states in a small interval $(v_0 - \varepsilon, v_0 + \varepsilon)$ centered around a given value, v_0, of the potential energy density. We can write

$$\omega_N^{v_0,\varepsilon}(v) = A_N^{v_0,\varepsilon}(v) + B_N^{v_0,\varepsilon}(v), \tag{1.26}$$

where $B_N^{v_0,\varepsilon}(v)$ includes the singular contributions due to all the critical points whose energies belong to the interval $(v_0 - \varepsilon, v_0 + \varepsilon)$. From Theorem 1.4.1 we have:

$$B_N^{v_0,\varepsilon}(v) = \sum_{\{v_c | |v_c - v_0| < \varepsilon\}} \sum_{\{q_c | \frac{V(q_c)}{N} = v_c\}} \omega_{N,q_c}^{na}(v); \tag{1.27}$$

v_c denotes the stationary value of the potential energy and q_c denotes the stationary configurations. From Theorem 1.4.1 follows that we can add to $B_N^{v_0,\varepsilon}(v)$ a smooth function $A_N^{v_0,\varepsilon}(v)$ such that Eq. (1.26) coincides with the configurational density of states when $v \in (v_0 - \varepsilon, v_0 + \varepsilon)$.

We are interested in the regularity properties of the entropy density; in the set $(v_0 - \varepsilon, v_0 + \varepsilon)$ the latter can be written as

$$s_N^{v_0,\varepsilon}(v) = \lim_{N\to\infty} \frac{1}{N} \log\left[\omega_N^{v_0,\varepsilon}(v)\right] = \lim_{N\to\infty} \frac{1}{N} \log\left[A_N^{v_0,\varepsilon}(v) + B_N^{v_0,\varepsilon}(v)\right]. \quad (1.28)$$

The above relation can be written as

$$s_N^{v_0,\varepsilon}(v) = \max\{a^{v_0,\varepsilon}(v), b^{v_0,\varepsilon}(v)\}, \quad (1.29)$$

where

$$a^{v_0,\varepsilon}(v) = \lim_{N\to\infty} \frac{1}{N} \log\left[A_N^{v_0,\varepsilon}(v)\right] \quad (1.30)$$

and

$$b^{v_0,\varepsilon}(v) = \lim_{N\to\infty} \frac{1}{N} \log\left[B_N^{v_0,\varepsilon}(v)\right], \quad (1.31)$$

unless

$$\lim_{N\to\infty} \frac{B_N^{v_0,\varepsilon}(v)}{A_N^{v_0,\varepsilon}(v)} = -1, \quad (1.32)$$

which is a very peculiar case that we neglect in this discussion. From Eq. (1.29) follows that nothing can be concluded on the regularity properties of $s^{v_0,\varepsilon}(v)$ unless both $a^{v_0,\varepsilon}(v)$ and $b^{v_0,\varepsilon}(v)$ are known. For example, a mechanism to induce a singularity in $s^{v_0,\varepsilon}(v)$ could be a crossover between the two terms in the maximization procedure; moreover, nothing is known about the uniform convergence of $A_N^{v_0,\varepsilon}(v)$ to $a^{v_0,\varepsilon}(v)$ in the $N \to \infty$ limit; this implies that in principle $a^{v_0,\varepsilon}(v)$ could be a singular function.

In [20, 34], necessary conditions have been found such that the singular term $B_N^{v_0,\varepsilon}(v)$ could give a non vanishing contribution for every neighborhood of v_0 whatever small, in the $N \to \infty$ limit. We report the reasoning followed in [20, 34] without entering the details for which we refer the reader to the cited papers.

Given the above mentioned results, the following observation can be done. In Eq. (1.20), the analytic pre-factor

$$\frac{(N\pi)^{N/2}}{N\Gamma\left(\frac{N}{2}\right)} \quad (1.33)$$

is exponential in N. Then, $B_N^{v_0,\varepsilon}(v)$ contributes to $\omega^{v_0,\varepsilon}(v)$ with a term that goes to zero when ε goes to zero. On the other hand, we need that $b^{v_0,\varepsilon}(v)$

dominates over $a^{v_0,\varepsilon}(v)$ independently of the value of ε. Apparently the only possibility for this to happen is that

$$\lim_{N\to\infty} |\det[\mathcal{H}_V(q_c)]|^{\frac{1}{N}} = 0. \tag{1.34}$$

The quantity $|\det[\mathcal{H}_V(q_c)]|^{\frac{1}{N}}$ in Eq. (1.34) will be called normalized or reduced determinant of the Hessian matrix evaluated in q_c.

This observation is far from being rigorous since it does not give any clue as to the order in which the limit $N \to \infty$ and the limit $\varepsilon \to 0$ have to be performed. In any case it gives the feeling of the reason for which the reduced determinant in Eq.(1.34) is one of the most important ingredients of the following theorem

Theorem 1.5.1 (KSS theorem)**.** *Let $V : \Gamma_N \subseteq \mathbb{R}^N \to \mathbb{R}$ be a smooth and confining Morse potential. Denoting by q_c the critical points of V and by $k(q_c)$ their index, we call "Jacobian densities" the following quantities:*

$$j_l(v_0) = \limsup_{N\to\infty} \frac{1}{N} \log \left[\frac{\sum_{q_c \in Q_l([v_0, v_0+\varepsilon])} J(q_c)}{\sum_{q_c \in Q_l([v_0, v_0+\varepsilon])} 1} \right], \tag{1.35}$$

where

$$J(q_c) = \frac{1}{\sqrt{\left|\det\left[\frac{\mathcal{H}_V(q_c)}{2}\right]\right|}} \tag{1.36}$$

and

$$Q_l(v_0) = \left\{ q_c \middle| \left(\frac{V(q_c)}{N} = v_0 \right) \wedge [k(q_c) = l(mod 4)] \right\}. \tag{1.37}$$

Thus, the contribution $b^{v_0,\varepsilon}(v_0)$ defined in Eq. (1.31) cannot induce a phase transition in the limit $N \to \infty$ at $v = v_0$ if

1. *the total number of critical points is limited by $\exp(CN)$ for a given constant $C > 0$;*
2. *$\forall \varepsilon$ small enough the Jacobian densities satisfy $j_l(v_0) < \infty$, $\forall l \in \{0, 1, 2, 3\}$.*

The proof of the theorem consists in finding an estimate from above of $b^{v_0,\varepsilon}(v)$ which depends only on ε and not on V. The estimate is:

$$b^{v_0,\varepsilon}(v) \leq \frac{1}{2} \log \varepsilon + \sqrt{2\pi e} + \max_{\{l\in\{0,1,2,3\}, |v-v'|<\varepsilon\}} [n_l + j_l(v')], \tag{1.38}$$

where

$$n_l = \lim_{N\to\infty} \frac{1}{N} \log \sum_{q_c \in Q_l(\mathbb{R})} 1 \tag{1.39}$$

is the total density of critical points. If the hypotheses of the theorem are satisfied, the last term in Eq. (1.38) is finite and we can choose ε small enough and such that $a^{v_0,\varepsilon}(v)$ dominates over $b^{v_0,\varepsilon}(v)$; in this case the contribution of critical points of V is negligible in the limit $N \to \infty$.

1.5.2 The KSS criterion and its applicability

The KSS Theorem 1.5.1 allows to detect, among all the finite-N singularities of the microcanonical entropy, those that are possibly associated to a phase transition in the thermodynamic limit. In particular it asserts that, in the $N \to \infty$ limit, it is not possible to have a phase transition induced by a finite N microcanonical singularity if its two hypotheses are satisfied.

It is commonly believed that the total number of critical points in a generic Hamiltonian system grows exponentially with the number of degrees of freedom [1, 86]. A general proof of this property is not still available and some systems are known to show a different behavior, see i.e. the mean field spherical model [20] in which the number of stationary points does not increase with N. This notwithstanding the exponential behavior is certainly the most common one; for this reason the first hypothesis of the KSS Theorem has probably a technical nature and we are going to assume that it is satisfied for Morse potential functions.

Instead, the second hypothesis of the KSS theorem appears to be the key request to select, among the finite-N stationary points of the potential energy, the few that can "survive" in the thermodynamic limit. Its practical utility becomes clear when we re-formulate it in the following way:

In the thermodynamic limit, it is possible to have a nonanalytic point of the configurational microcanonical entropy at a given value of the potential energy density $v = v_0$ if at least one of the jacobian densities $j_l(v)$ in Eq. (1.35) diverges in $v = v_0$; that is if the second hypothesis of Theorem 1.5.1 is not satisfied.

Following a chronological order, in literature the above criterion has been applied to the study of the following models:

1. the mean-field XY model that we are going to discuss in §2.2.1, and the mean-field $k-$trigonometric model [20];

2. the spherical model with nearest-neighbors interactions. In this case a singularity of the Euler characteristic in a value of the potential energy v_t does not correspond to a phase transition; coherently the criterion is not satisfied [75].

3. The Self Gravitating Ring (SGR) model [36, 87]. This case is quite remarkable in that it is the first application of the above criterion to a non solvable model with long range interactions. The thermodynamics of the model is known thanks to numerical simulations [88, 89] and it shows a phase transition from a homogeneous high-energy phase to a clustered low-energy phase. The criterion is able to single out the phase transition and also suggests the presence in the system of another phase transition not previously known. All the analysis can be conducted in an analytical way and the SGR results had strongly encouraged researchers in the applications of such techniques to the analysis of the thermodynamics of a wider class of non-solvable models.

4. The one dimensional XY model [69] that will be analyzed in detail in §2.2.2.

In the first two cases it has been possible to find an invertible relation between the stationary configurations and their stationary values: $q_c = q_c(v_c)$. Thanks to this relation the Jacobian densities $j_l(v)$ have been evaluated analytically. Analogous relations have been found in the last two cases, but the quantities under analysis have been the reduced determinants present in Eq. (1.34) and related to the Jacobian densities by definition.

To find an invertible relation $q_c = q_c(v_c)$ could be an essentially impossible task for generic models. This fact is a strong limitation for the applicability of the criterion and in some cases it can seriously compromise the whole analysis. However the problem can be partially avoided in a way that will be discussed in details in the following Chapter; essentially it consists in a numerical sample of the stationary configurations of the potential energy stored with the respective stationary values. Of course numerical samplings, in general, cannot provide all the stationary configurations of the model but only a small subset of them. However, a remarkable property of the KSS criterion is that it can be applied even in the case of a partial knowledge of the stationary points of the potential energy function and of their stationary values. Indeed, let us assume that a particular class of stationary

configurations of a Morse potential energy function V is known and that this class does not include all the stationary configurations. Let us further suppose that we want to check the criterion for a certain value of the energy density, v_0. This scenario is the most common one when we want to apply the criterion to nontrivial systems. What we have to do is to prove that $l \in \{0, 1, 2, 3\}$ exists such that, in the thermodynamic limit $N \to \infty$ the quantity

$$\frac{1}{N} \log \left[\frac{\sum_{q_c \in Q_l([v_0, v_0+\varepsilon])} J(q_c)}{\sum_{q_c \in Q_l([v_0, v_0+\varepsilon])} 1} \right] \tag{1.40}$$

is not definitively bounded. The first interesting fact is that the index does not play any role: in fact if the above quantity is not definitively bounded, then at least one of its four subsequences must be unbounded as well. Given this fact and the fact that $J(q_c) > 0$, the quantity in Eq. (1.40) can be limited from below by restricting the sums present in Eq. (1.40) to a subset $\tilde{Q} \subseteq Q$ of the critical points,

$$\frac{1}{N} \log \left[\frac{\sum_{q_c \in Q_l([v_0, v_0+\varepsilon])} J(q_c)}{\sum_{q_c \in Q_l([v_0, v_0+\varepsilon])} 1} \right] \geq \frac{1}{N} \log \left[\sum_{q_c \in \tilde{Q}} J(q_c) \right] - \text{constant}. \tag{1.41}$$

As stated above, here we have assumed that the first hypothesis of the KSS theorem is satisfied so that the denominator of Eq. (1.40) can be neglected. From these observations and recalling the results of Section 1.4.2, we can formulate the following criterion for the search of phase transition [36, 55, 72, 87] (KSS criterion):

KSS Criterion 1.5.2. *Consider a classical Hamiltonian system of the form 1.1. Assume that the stationary points of V are isolated and that their number grows at most exponentially with N. Then, in the $N \to \infty$ limit, a singularity in the microcanonical entropy $s(\varepsilon)$ at energy density ε_c induced by saddles of V can be present only if the following conditions are satisfied. First, there must bu a sequence of stationary points $\{q_c^N\}_{N=1}^{\infty}$ whose corresponding stationary values converge to $v_0 = \langle v \rangle(\varepsilon_c)$, where the brackets denote the statistical average. This means:*

$$\lim_{N \to \infty} v(q_c^N) = v_0. \tag{1.42}$$

Second, the Hessian matrix $\mathcal{H}_V$ evaluated on the stationary configurations q_c^N is such that

$$\lim_{N \to \infty} \left| \mathcal{H}_V(q_c^N) \right|^{\frac{1}{N}} = 0. \tag{1.43}$$

Since the eigenvalues of $\mathcal{H}_V$ can be seen as curvatures of the potential energy landscape, Eq.(1.43) means that the saddles become asymptotically "flat".

It is not necessary to know all the stationary points of the potential energy V to show that the KSS criterion is satisfied: the only request is to find the "right" sequence of stationary configurations, the one that satisfies the two conditions (1.42) and (1.43). This observation will be useful in the following Chapter. This is the main difference between the KSS criterion and other energy landscapes techniques where the evaluation of topology invariants, such as the Euler characteristic, requires the knowledge of all the stationary configurations of the potential energy and their indices. However it is important to underline that without a complete knowledge of the critical points of V, it is impossible to prove the validity of the first hypothesis of the KSS Theorem.

1.6 On the Franzosi–Pettini theorem

In this last paragraph we are going to present a very recent debate around the validity of Theorem 1.3.2. The content of this paragraph concerns very recent results, in part already published and in part deriving from private communications with the authors, that have to be taken as very preliminary.

In [29] Kastner and Mehta claimed that a counterexample to the Franzosi and Pettini Theorem 1.3.2 was provided by the φ^4 model described by the following potential energy function

$$V_\varphi = \sum_{i\in\Lambda} \left[\frac{\lambda}{4!}\varphi_i^4 - \frac{\mu^2}{2}\varphi_i^2 + \frac{J}{4} \sum_{j\in\mathcal{N}(i)} (\varphi_i - \varphi_j)^2 \right] , \tag{1.44}$$

where J, λ, $\mu > 0$, $\Lambda \subset \mathbb{Z}^2$ is a finite square lattice and $\mathcal{N}(i)$ denotes the four nearest-neighboring sites of i.

After the claim, in a second paper [92], they proved that the potential function in Eq. (1.44) satisfies the hypotheses of the Franzosi-Pettini theorem although it is not a Morse function for every value of λ, μ, J and N, see particularly the appendix of [92].

Then two facts became relevant: (i) in [29] authors showed that, for every value of N, the φ^4 model has no critical points at energy density greater than

zero. (*ii*) Performing Monte Carlo simulations of the same system authors showed in [29,92] that the φ^4 model undergoes a phase transition at a value of the energy density well separated from zero; this fact happens for a wide range of parameters.

Assumed that the potential function (1.44) really satisfies all the hypothesis of the Franzosi–Pettini theorem 1.3.2, the two facts stated above are in contradiction with the latter and make the φ^4 model a counterexample of the Franzosi–Pettini theorem 1.3.2.
From private communications with R. Franzosi, M. Pettini, D. Mehta and M. Kastner, it turned out that the flaw in the Franzosi–Pettini theorem may be the absence of an extra-hypothesis in its statement. More precisely the theorem would need this:

additional hypotesis 1.6.1. *there must be no sequences of stationary configurations* $q_c^N \in \Gamma_N$ *such that*

$$\lim_{N\to\infty} \frac{V(q_c^N)}{N} = v_0, \ with\ v_0 \in [v_1, v_2]\ and\ \lim_{N\to\infty} ||\nabla V(q_c^N)|| = 0.$$

Actually, it looks like this extra hypothesis has been already used in the proof of the theorem but it is missing in its present statement. We recall that in the Franzosi–Pettini theorem the requests were that there should be a number N_0 and an interval $[v_1, v_2]$ such that $\forall N > N_0$ the hypersurfaces $(M_v)_{v\in[v_1,v_2]}$ do not change topology. If these requests are satisfied then the free energy is at least $C^2[\beta(v_1), \beta(v_2)]$. The extra-hypothesis 1.6.1 is much stronger than simply asking for the absence of critical points with critical values in $[v_1, v_2]$ for N large enough. From a qualitative point of view, the new request corresponds to ask that "changes in the topology of $(M_v)_{v\in[v_1,v_2]}$ cannot happen even asymptotically". In Sec.1.2 we have reviewed some results concerning the finite-dimensional Morse theory; it is important to stress that infinite-dimensional Morse theory is not a direct generalization of its finite-dimensional counterpart, so that our previous interpretation can be taken at most at a qualitative level.

The new request 1.6.1 appears anyhow reasonable. Indeed the structure of the stationary points can be changed easily by applying arbitrarily small perturbations to the system that do not affect its macroscopic thermodynamical behavior. For instance a stationary point of the potential energy can be transformed in a non-stationary point by changing the boundary conditions

or by applying a small external field to the system. On the contrary, a request like 1.6.1 is more "robust", in the sense that it should not be altered unless the changes in the boundary conditions or the applied external fields become so strong that also the thermodynamical behavior changes. Anyway, the fact that these results are very recent (and partially not yet published) makes mandatory to revisit them with care before drawing any conclusion.

For what concerns the results presented in this Chapter we can say that some of the results from [80] have been used to prove the Theorem 1.4.1 on the singularities in the microcanonical entropy of finite systems. However authors of Theorem 1.4.1 ensure that the theorem is not affected by the extra hypothesis (1.6.1); in absence of any explicit correction by the authors we can consider it as correct as all the other results reviewed in the previous sections with the special exception of the Franzosi–Pettini theorem.

For what concerns our results that will be presented in the rest of this work, they are not touched by the above discussion since they are not influenced by the possible addition of the extra-hypothesis 1.6.1. In fact they have been mostly derived before the debate on the Franzosi–Pettini theorem started.

We considered worthwhile to present here the above discussion even if it concerns still open questions. Anyway every statement has to be analyzed with special care in the future before drawing any conclusion on the subject.

Chapter 2

Energy landscapes and classical O(n) spin models

The energy landscape approach presented in the previous Chapter has been applied to study the equilibrium properties of several systems. As discussed in Sec.1.5.1 the KSS criterion has been tested on exactly solvable models, i.e., models with mean-field interactions or one-dimensional systems, the only exception being the non-solvable SGR model. In all cases the results were correct and encouraged us to go beyond "simple" models by performing an analysis of the stationary points and their Hessian determinants for classical O(n) spin models with nearest-neighbor ferromagnetic interactions. Our investigation starts with the analysis of the $n = 2$ case, the XY model, defined on a two-dimensional square lattice and on a three-dimensional cubic lattice [37,55]. The results of this study are collected in the present Chapter.

The Chapter is organized as follows. In Sec. 2.1 we will introduce the class of classical O(n) spin models and we will briefly review their thermodynamic behavior. In Sec. 2.1.1 we will construct a special class of stationary configurations: the Ising stationary configurations. As we will show, this class is given by all the configurations of an Ising model defined on the same lattice and with the same interactions as the corresponding O(n) model, see [38, 55]. Sec 2.2 will be mostly devoted to the application of the KSS criterion to nearest-neighbor XY models in two and three spatial dimensions. For the mean-field (fully connected) XY model as well as for the one-dimensional XY model, indeed, the stationary points and their relation to phase transitions have already been studied in earlier works, see [14, 34] and [69]; given their relevance for our work, the result of these analyses will

be reviewed in Secs. 2.2.1 and 2.2.2, respectively. From Sec. 2.3 on, we will finally present the application of the KSS criterion to the two- and three-dimensional XY models [37, 55] on the Ising configurations. Unlike in the mean-field case, however, no signature of the phase transitions will be visible from the data obtained both in two and in three spatial dimensions. In Sec. 2.3.3 we will then construct another class of stationary points which have the character of spin waves. Since their number is small (subexponential), they are not expected to significantly influence the thermodynamic behavior of the model. In Sec. 2.3.4, we will construct another exponentially large class of particularly interesting stationary points whose Hessian determinant is zero. Moreover, we will be able to prove that, even after explicitly breaking the global $O(2)$ symmetry of the XY model, these stationary points are not isolated but occur in continuous families. This finding has interesting consequences which will be discussed at the end of Sec. 2.3.4. In Sec. 2.3.5 we will investigate how the presence of inhomogeneous external magnetic fields may destroy the continuous families and lead to isolated, nonsingular stationary points. A summary of the results and concluding remarks will be presented in Sec. 2.3.6.

2.1 O(n) spin models

Classical O(n) spin models constitute a paradigmatic class of models for the study of magnetic phase transitions (the prototype of all continuous phase transitions). In our analysys we are going to consider O(n) models defined on d-dimensional hypercubic lattices with periodic boundary conditions. To each lattice site i an n-component classical spin vector $\boldsymbol{S}_i = (S_i^1, \ldots, S_i^n)$ of unit length is assigned. The energy of the model is given by the Hamiltonian

$$H^{(n)} = -J \sum_{\langle i,j \rangle} \boldsymbol{S}_i \cdot \boldsymbol{S}_j = -J \sum_{\langle i,j \rangle} \sum_{a=1}^{n} S_i^a S_j^a, \tag{2.1}$$

where the angular brackets denote a sum over all pairs of nearest-neighboring lattice sites[1]. The exchange coupling J will be assumed to be positive,

[1]Our class of models is such that $H^{(n)} \equiv V^{(n)}$. In principle a standard kinetic term could be added to Eq. (2.1) and a similar analysis could be performed on the systems, see Sec. 1.4.2. However we are only interested in the configurational quantities and so

resulting in ferromagnetic interactions, and without loss of generality we set $J = 1$ in the following. The Hamiltonian (2.1) is globally invariant under the O(n) group; when $n = 1$ the symmetry group becomes the discrete group $\mathrm{O}(1) \equiv \mathbb{Z}_2$ and the Hamiltonian (2.1) becomes the Ising Hamiltonian

$$H^{(1)} = -\sum_{\langle i,j \rangle} \sigma_i \sigma_j, \tag{2.2}$$

where $\sigma_i \in \{-1, +1\}\ \forall i$. In all the other cases $n \geqslant 2$, the O(n) group is a continuous one. Two special representatives of the O(n) models are the XY model ($n = 2$) and the Heisenberg model ($n = 3$). For the XY model, spins live on the unit circle $\mathbb{S}^1$ and the components of the ith spin can be parametrized by a single angular variable $\vartheta_i \in [0, 2\pi)$ such that

$$\begin{cases} S_i^1 &= \cos\vartheta_i, \\ S_i^2 &= \sin\vartheta_i. \end{cases} \tag{2.3}$$

The Hamiltonian of the XY model can thus be conveniently written as

$$H^{(2)} = -\frac{1}{2}\sum_{i=1}^{N} \sum_{j \in \mathcal{N}(i)} \cos\left(\vartheta_i - \vartheta_j\right), \tag{2.4}$$

where $\mathcal{N}(i)$ denotes the set of nearest neighbors of lattice site i. The energy density $\varepsilon = H^{(2)}/N$ lies in the energy range $[-d, d]$ where d is the lattice dimension.

The thermodynamics of the O(n) models is a well known topic in statistical physics. We simply recall here the main results useful in the following and we address the reader to the cited papers for further details.

When mean-field interactions are considered, the Hamiltonian (2.1) becomes

$$H_{MF}^{(n)} = -\frac{1}{2N}\sum_{i,j=1}^{N} \boldsymbol{S}_i \cdot \boldsymbol{S}_j, \tag{2.5}$$

where, according to the Kac prescription [51], the normalization $1/N$ is understood to obtain an extensive energy. In the mean-field case O(n) models

"energy density, ε" and "potential energy density, v" will be treated as synonyms in the following.

are exactly solvable for every n and show a phase transition with spontaneous symmetry breaking at the maximum value of ε ($\varepsilon_c = v_c = 0$ with our choice of units) [93].

As to systems with nearest-neighbor interactions, the energy density range is $\varepsilon \in [-d, d]$ with our choice of units. In $d = 1$ the models are exactly solvable for every n, see [44, 94] and references therein. For these models it can be shown that no spontaneous magnetization is present for any value of n except when $\varepsilon_c = v_c = -d$ (or, correspondingly, $T = 0$).

In $d = 2$, the case $n = 1$ (the Ising model) has been exactly solved by Lars Onsager in 1944 [95] and the model exhibits a ferromagnetic phase transition with spontaneous symmetry breaking at $\varepsilon_c = -\sqrt{2}$. In $d = 2$ the Mermin and Wagner theorem [58] rules out the possibility of a phase transition with spontaneous symmetry breaking for $n > 1$. However, the case $n = 2$ (the XY model) exhibits a Berežinskij-Kosterlitz-Thouless (BKT) transition [96, 97] with no long-range order. An analytical solution of the two-dimensional XY model is still missing; some theoretical results are known to estimate its thermodynamics in certain limits, see e.g. [98–101], and the thermodynamics has been reproduced through numerical investigations, see e.g. [102,103]. No phase transitions are believed to be present in $d = 2$ and $n > 2$.

In $d = 3$ a ferromagnetic phase transition with spontaneous symmetry breaking is present for every n. The models are not exactly solvable and their thermodynamics is known only through numerical simulations, see e.g. [104–106].

If we want to deal with an energy landscape approach to infer the equilibrium properties of the class of models in Eq. (2.1), the first thing we have to do is to determine the stationary configurations of $H^{(n)}$. This will be the subject of the next section.

2.1.1 Ising stationary configurations

The stationary points of $H^{(n)}$ for $n \geq 2$ are given by the solutions $\overline{S} = (\overline{S}_1, \ldots, \overline{S}_N)$ of the N vector equations $\nabla H^{(n)} = 0$. Inserting back for a moment the exchange coupling J in Eq. (2.1), the latter can be written as nN scalar equations,

$$-\sum_{j=1}^{N} J S_j^a + \lambda_k S_k^a = 0 \ , \quad a = 1, \ldots, n, \ k = 1, \ldots, N \ , \tag{2.6}$$

where the λ's are N Lagrange multipliers, plus the N nonlinear constraints $\sum_{a=1}^{n} \left(S_i^a\right)^2 = 1$, which prevent the above equations from being easily solved. However, a particular class of solutions can be found by assuming that all the spins are parallel or antiparallel: $S_i^1 = \cdots = S_i^{n-1} = 0 \ \forall i$. In this case, the $N(n-1)$ equations (2.6) with $a = 1, \ldots, n-1$, corresponding to the first $n-1$ components of the spins, are trivially satisfied. As to the n-th component, the constraints $(S_i^n)^2 = 1$ imply $S_i^n = \sigma_i \ \forall i$, so that the remaining N equations read as

$$-\sum_{j=1}^{N} J\,\sigma_j + \lambda_k \sigma_k = 0 \ , \qquad k = 1, \ldots, N \, . \tag{2.7}$$

The above equations are satisfied by any of the 2^N possible choices of the σ's provided one puts $\lambda_k = \left(\sum_{j=1}^{N} J\sigma_j\right)/\sigma_k$, $k = 1, \ldots, N$. The Hamiltonian (2.1) becomes the Ising Hamiltonian (2.2) when the spins belong to this class of stationary configurations. Therefore we have a one-to-one correspondence between a class of stationary configurations of the Hamiltonian (2.1) of a O(n) spin model and all the configurations of the Ising model (2.2), i.e., the Ising model defined on the same graph with the same exchange coupling[2] J; the corresponding stationary values are just the energy levels of this Ising Hamiltonian. We shall refer to the class of stationary configurations $\overline{S}_i = (0, \ldots, 0, \sigma_i) \ \forall i = 1, \ldots, N$ as "Ising stationary configurations".

The Ising stationary configurations do not complete all the stationary configurations of the O(n) models; on the contrary, we know that there are other classes of stationary configurations in these models, see e.g. [37], and we expect that many other classes are still not known in general (two exceptions are the mean-field XY model and the one-dimensional XY model that will be discussed respectively in Sec. 2.2.2 and 2.2.1). Nonetheless, the 2^N Ising ones are a non-negligible fraction of the whole, especially at large N because the number of stationary points of a generic function of N variables is expected to be exponentially growing with N [86].

The above results hold for O(n) and Ising models defined on any graph and with any interaction matrix J. From now on we shall restrict to regular d-dimensional hypercubic lattices and to ferromagnetic interactions: $J = 1$.

[2]The above considerations are valid also for a generic interaction matrix J_{ij} in Eq. (2.1).

In this case, in the thermodynamic limit $N \to \infty$, the energy density levels of the Ising Hamiltonian (2.2),

$$H^{(1)}(\sigma_1, \ldots, \sigma_N)/N \qquad \forall \sigma_i = \pm 1,$$

become dense and cover the whole energy density range of all the O(n) models.

There is another fact that has to be highlighted. The O(n) invariance of the Hamiltonian (2.1) implies that the solutions of (2.6) are not isolated points in configuration space, but occur in continuous curves, see e.g. [37] for the case $n = 2$. Several of the theoretical tools and results mentioned in Chapter 1, and in particular the Hessian determinant criterion (1.43), require energy functions with only isolated stationary points. It is therefore necessary to explicitly break the global O(n) symmetry of O(n) models and this can be done in different ways. One possibility is to add a generic perturbation to the system. For instance the Hamiltonian (2.1) can be perturbed by adding (small) external fields parallel to (and concord with) a fixed direction, let say the $n-$th direction $h_i = (0, \ldots, h_i^n)$, and whose strength may change from site to site,

$$H_p^{(n)} = -\sum_{a=1}^{n} S_i^a S_j^a + \sum_{i=1}^{N} h_i^n S_i^n. \tag{2.8}$$

At the end of the calculations the thermodynamic limit must be taken as $\lim_{|\boldsymbol{h}|\to 0} \lim_{N\to\infty}$ and the system is forced to break its symmetry in the direction dictated by the external field. Alternatively, as we are going to do, we can choose to fix one spin (that is a global phase), e.g. $\boldsymbol{S}_N = (S_N^1, S_N^2 \ldots, S_N^n) = (0, 0, \ldots, 1)$. In the large-$N$ limit, the only effect of this global phase fixing is to dictate the direction of the spontaneous symmetry breaking, but otherwise thermodynamic quantities remain unaffected. The interesting thing is that the class of the Ising stationary configurations remains unaffected either by the prescription in Eq. (2.8) and by the global phase fixing. This is not true, in gneral, for other stationary points that usually are destroyed when such modifications are applied.

All these facts may suggests that Ising stationary configurations are not merely a subclass of stationary points of the O(n) models but they could actually be the "most important" class. In particular we may hope to infer some of the thermodynamic properties of the O(n) models from what is

known about the corresponding Ising model. In the following of this Chapter we are going to take seriously this statement to understand if some prediction can be obtained from it. Our analysis starts with one representative of the O(n) models, the XY model, hoping that this choice yields the simplest possible O(n) models amenable to the energy landscape analysis we have in mind[3].

2.2 Exploring the energy landscape of XY models

The present Section is mainly devoted to the presentation of the results reported in [37] concerning the analysis of the energy landscape of the XY models in two and three spatial dimensions and with nearest-neighbors interactions. The mean-field (fully connected) XY model [14, 20] and the one-dimensional XY model [69] have already been studied in the spirit of the criterion presented in Chapter 1. The results showed a clear signature, in stationary-point properties, of the presence of a finite-temperature phase transition in the mean-field XY model and no signature of a transition in the one-dimensional XY model, in agreement with the known thermodynamic behavior of these models. Before going in the details of the application of the KSS criterion to the XY models in two and three dimensions, we will recall the above mentioned results for the mean-field and the one-dimensional case, given their relevance for the our analysis.

We recall here the main results of Sec. 1.5.2 that are necessary for the application of the KSS criterion 1.5.2. Let us consider a classical Hamiltonian of the form (1.1) without the kinetic term, and let us assume that the stationary points of the potential energy V are isolated and grows at most exponentially[4] with N. The microcanonical entropy density of the system $s(\varepsilon)$ can be non-analytic in $\varepsilon = v = v_c = \frac{V_c}{N}$ only if a sequence q_c^N of stationary configurations of V can be found such that the following conditions are

[3] In the even simpler Ising model such an analysis is impossible due to the discrete character of the spin variables.

[4] In the case of the XY models in $d = 2$ and $d = 3$ this condition will be assumed as satisfied even if the total number of stationary configurations is unknown.

satisfied:

$$(i)\ \lim_{N\to\infty} \frac{V(q_c^N)}{N} = v_c; \tag{2.9}$$

$$(ii)\ \lim_{N\to\infty} \left|\det \mathcal{H}_V(q_c^N)\right|^{\frac{1}{N}} = 0 \tag{2.10}$$

where $\mathcal{H}_V$ denotes the Hessian matrix of the potential energy function evaluated on the stationary configurations q_c^N. The second conditions can be equivalently replaced by the request that at least one of the Jacobian densities $j_l(v_c)$ given by Eq. (1.35), diverges when $N \to \infty$. Remember that a complete knowledge of all the stationary points is not necessary to apply the criterion; the only requirement is to find the "right" sequence for which Eq. (2.9) and Eq. (2.10) are satisfied. The results on the Ising stationary configurations reported in Sec. 2.1.1 indicate this class of stationary configurations as the "favourite" for the application of the KSS criterion. However, if the KSS criterion is not satisfied on this class (or on other classes of stationary configurations), it is possible that some of the unknown stationary points could satisfy requests (i) and (ii) and so nothing can be rigorously concluded on the thermodynamics of the model.

2.2.1 The mean-field XY model

The mean-field XY model is described by the Hamiltonian (2.5) and represents the first model for which the KSS criterion has been verified [20]. Following the results reported in [14] an external field h is introduced in the system such that $0 \lesssim h \ll 1$ and the continuous O(2) symmetry of the Hamiltonian (2.5) is explicitly broken in the low energy phase. In this way Eq. (2.5) becomes

$$H_{MF}^{(2)} = V_{XY_{MF}} - \frac{1}{2N}\sum_{i,j=1}^{N} \cos(\vartheta_i - \vartheta_j) - h\sum_{i=1}^{N} \cos\vartheta_i \tag{2.11}$$

where the angular variables $\vartheta_i \in [0, 2\pi)$ univocally determine the position of the ith spin on the unit circle $\mathbb{S}^1$, see Eq. (2.3). The thermodynamics of the model is well known [70] and shows a continuous phase transition in $\varepsilon_c = v_c = 0$ when $N \to \infty$ and $h \to 0$. When $h \neq 0$ no phase transitions are present for any finite value of the temperature.

For this model *all* the stationary configurations of the Hamiltonian (2.11) are known [14, 55] and can be grouped in two classes:

1. *Ising stationary points.* This is the class of stationary points presented in Sec.2.1.1. In terms of the angular variables ϑ_i the Ising stationary configurations are given by all those configurations $(\vartheta_i, \dots, \vartheta_N)$ such that[5] $\vartheta_i = \{0, \pi\}\ \forall i = 1, \dots, N$. For the mean-field XY model the energy density of an Ising stationary point can be parametrized in terms of the number of the angular variables equal to π: denoting by N_π the number of the angular variables equal to π and by $n_\pi = \frac{N_\pi}{N}$ their number density, we get:

$$v_{n_\pi} = -\frac{1}{2}\left(1 - 2n_\pi\right)^2 - h\left(1 - 2n_\pi\right). \tag{2.12}$$

   v_{n_π} is such that $v_{n_\pi} \in \left[-\frac{1}{2} - h, \frac{h^2}{2}\right]$.

2. *Stationary points characterized by the value of the magnetization.* This class consists in all the configurations $(\vartheta_1, \dots, \vartheta_N)$ such that

$$m_x(\vartheta_1, \dots, \vartheta_N) = \frac{1}{N}\sum_{i=1}^{N} \cos\vartheta_i = -h \tag{2.13}$$

$$m_y(\vartheta_1, \dots, \vartheta_N) = \frac{1}{N}\sum_{i=1}^{N} \sin\vartheta_i = 0, \tag{2.14}$$

   where m_x and m_y denotes respectively the x component and the y component of the magnetization vector $\boldsymbol{M} = \sum_{i=1}^{N}\langle \boldsymbol{S}_i \rangle$ of the model[6]. These stationary points are not isolated and have the same energy density v given by the maximum available for this model:

$$v = \frac{h^2}{2}. \tag{2.15}$$

Although the Hamiltonian (2.11) is not a Morse function on the stationary points characterized by the value of the magnetization, it becomes a Morse function once this degenerate-in-energy class of stationary points is excluded from the analysis. For this reason the KSS criterion has been applied only

[5] For this reason they are also called $0 - \pi$ stationary points in [36, 55].

[6] More precisely, $m_x(\vartheta_1, \dots, \vartheta_N)$ and $m_y(\vartheta_1, \dots, \vartheta_N)$ denotes the observables whose statistical average is respectively given by the x and y components of the magnetization.

to the Ising stationary configurations. Let us review here the results obtained from this analysis. Since the Ising stationary points are given by all the configurations of the correspondent Ising model, their number grows exponentially with N; for this reason the first condition of the KSS Theorem 1.5.1 is satisfied. Let us denote by $\vartheta_N^{n_\pi}$ a stationary point of the potential energy (2.11) having n_π angular variables equal to π and with $\mathcal{H}_{V_{XY_{MF}}}(\vartheta_N^{n_\pi})$ the Hessian matrix of the potential (2.11) evaluated on the stationary point $\vartheta_N^{n_\pi}$. We can now discuss the second condition of Theorem 1.5.1 regarding the Jacobian densities in Eq. (1.35). The results reported in [14] allow to show that

$$\lim_{N\to\infty} \left|\det\left[\mathcal{H}_{V_{XY_{MF}}}(\vartheta_N^{n_\pi})\right]\right|^{\frac{1}{N}} = \lim_{N\to\infty} |\det D|^{\frac{1}{N}} \tag{2.16}$$

where D is a diagonal matrix obtained by $\mathcal{H}_{V_{XY_{MF}}}(\vartheta_N^{n_\pi})$ erasing the out-of-diagonal elements. In this way the Jacobian densities (1.35) can be computed as functions of the energy density[7]

$$j_l(v_{n_\pi}) = \frac{1}{2}\log 2 - \frac{1}{4}\log\left(|h^2 - 2v_{n_\pi}|\right), \qquad \forall l \in \{0,1,2,3\}, \tag{2.17}$$

with v_{n_π} given by Eq. (2.12). From Eq. (2.17) follows that:

1. if $h = 0$, $j_l(v_{n_\pi})$ diverges when $v_{n_\pi} = 0$. In this case the second condition of the KSS criterion given by Eq. (2.10) is satisfied and a phase transition can be present at $v_{n_\pi} = 0$. Indeed this is exactly what happens in the mean-field XY model in the limit $N \to \infty$ and $h \to 0$ [70]; a phase transition is present at the maximum value of the energy density v given by $v_{n_\pi} = 0$ with our conventions.

2. If $h \neq 0$ we have that

$$j_l(v_{n_\pi}) < \infty \tag{2.18}$$

since $v_\pi < \frac{h^2}{2}$. In this case the condition (2.10) is not satisfied and the KSS criterion exclude the presence of a singularity in the microcanonical entropy induced by the class of the Ising stationary configurations when $N \to \infty$. Indeed, the mean-field XY model does not have any a phase transitions when $h \neq 0$.

[7] We refer the reader to [20] for the details on this calculation.

The above results are in agreement with the known results on the thermodynamics of this model. It is worth noticing that the class of Ising stationary configurations seems to be the one relevant for the thermodynamic behavior of the mean-field XY model. This may confirm our considerations made in Sec. 2.1.1.

2.2.2 The one-dimensional XY model

The one-dimensional XY model is described by the Hamiltonian (2.4) that in $d = 1$ can be written as

$$H_{1d}^{(2)}(\vartheta_1, \ldots, \vartheta_N) = -\sum_{i=1}^{N} \cos(\vartheta_i - \vartheta_{i+1}) . \tag{2.19}$$

Although the model does not have a phase transition for any finite value of the temperature (see §2.1), it has been studied several times in the past years with the techniques presented in Chapter 1 (see i.e. [14]). Recently, it has been studied by Kastner and Mehta in the light of the KSS criterion 1.5.2, see [69]. The main results of their study are recalled in this Section, with special emphasis on the results that will be useful for our work. Let us consider the case of periodic boundary conditions and set $\vartheta_N = 0$ to break explicitly the continuous O(2) symmetry of the Hamiltonian (2.19). Let us define a new set of angular variables φ_i such that

$$\begin{aligned} \varphi_i &= \vartheta_{i+1} - \vartheta_i \qquad \mod 2\pi \qquad \forall i = 1, \ldots, N-1, \\ \varphi_N &= \vartheta_1 \qquad\qquad\quad \mod 2\pi. \end{aligned} \tag{2.20}$$

The variables φ_i's measure the relative shift (mod 2π) of the nearest-neighbor angles ϑ_i and ϑ_{i+1} $\forall i = 1, \ldots, N-1$. Let us consider the case in which N is an odd number. In this case it can be shown that the stationary points of Eq. (2.19) are given by the configurations $(\varphi_1, \ldots, \varphi_N)$ such that

$$\varphi_i = (-1)^{q_i} \varphi_N + q_i \pi \qquad \forall i = 1, \ldots, N-1 \tag{2.21}$$

and

$$\varphi_N = \frac{2\pi l - \pi \sum_{i=1}^{N-1} q_i}{1 + \sum_{i=1}^{N-1} (-1)^{q_i}}; \tag{2.22}$$

$q_i \in \{0, 1\}$ while $l \in \{1, \ldots, 1 + \sum_{i=1}^{N-1}(-1)^{q_i}\}$ is a natural integer number. The request of N to be an odd number ensures that the denominator of

Eq. (2.22) is different from zero. The case of N being an even number is not analyzed in [69]. Anyway it is believed that, apart from changes in the technical details of the calculations, the asymptotic results do not depend on whether N is even or odd; for this reason the N-even case will not be considered here. Among all the stationary configurations of Eq. (2.19), two special class of stationary points can be recognized in Eq. (2.21) and Eq. (2.22):

1. *the Ising stationary points* (or $0 - \pi$ stationary points). In terms of the new variables φ_i they are given by the configurations $(\varphi_1, \ldots, \varphi_N)$ such that $\varphi_i \in \{0, \pi\}$ $\forall i = 1, \ldots, N-1$.

2. *Polygonal stationary configurations*[8]. These configurations are given by any sequence of variables $(\varphi_1, \ldots, \varphi_N)$ such that $\varphi_i \equiv \frac{2\pi m}{N}$ $\forall i = 1, \ldots, N-1$ with $m = 1, \ldots, N$. These configurations are such that all the nearest-neighbor spin variables are shifted of the same quantity. The periodic boundary conditions force the shift to be a multiple of 2π.

Denoting by $\#(\vartheta^s)$ the number of stationary points ϑ^s, for the above presented classes of stationary points we have

$$\#(\vartheta^s) = \begin{cases} \frac{N!}{\left[\left(\frac{N-1}{2}\right)!\right]^2} & \text{for the Ising class,} \\ N & \text{for the polygonal class.} \end{cases} \tag{2.23}$$

This means that the Ising stationary points are exponentially many in N at variance with what happens for instance for the polygonal class of stationary configurations.

To apply the KSS criterion we have to check the conditions (2.9) and (2.10). To this end we have to express the energy density $v_N(\vartheta^s)$ and the reduced determinant $\mathcal{D}_N(\vartheta^s)$ of the Hessian matrix of Eq. (2.19), in terms of θ^s. As in the mean-field case also in the one-dimensional model these expressions can be found analytically [69] and are given by

$$v_N\left(\vartheta^s\right) = -\frac{1}{N}\left(1 + \sum_{k=1}^{N}(-1)^{q_k}\right)\cos\varphi_N \tag{2.24}$$

[8]Their name derives from an analogous class detected in the SGR model [36, 87].

and

$$\mathcal{D}_N(\vartheta^s) = |\det \mathcal{H}(\vartheta^s)|^{\frac{1}{N-1}} = |\cos\varphi_N| \left| \sum_{k=1}^{N-1} (-1)^{q_k} \right|^{\frac{1}{N-1}}; \tag{2.25}$$

At this point, a suitable sequence of stationary points $\{\vartheta^s\}_{N=N_0}^{\infty}$ has to be chosen such that $v_N(\vartheta^s) < \infty$ in the thermodynamic limit. This can be done considering sequences of stationary points with fixed values of φ_N and of $l_q = \frac{1}{N}\left(1 + \sum_{k=1}^{N-1}(-1)^{q_k}\right) \in [-1, 1]$. In this way and for every finite value of N, Eqs. (2.24) and (2.25) become, respectively,

$$v_N(\vartheta^s) = -l_q \cos\varphi_N \tag{2.26}$$

and

$$\mathcal{D}_N(\vartheta^s) = |\cos\varphi_N||N l_q|^{\frac{1}{N-1}}. \tag{2.27}$$

In the thermodynamic limit, $N \to \infty$, Eq.(2.27) does not depend on l_q anymore and we get

$$\mathcal{D} = \lim_{N\to\infty} \mathcal{D}_N(\vartheta^s) = |\cos\vartheta_N|. \tag{2.28}$$

Moreover, when $N \to \infty$, the values of φ_N given by Eq. (2.22) become dense in $(-\pi, \pi]$. Combining Eq. (2.26) with Eq. (2.28) we finally get

$$\mathcal{D} = \left| \frac{-v_N(\vartheta^s)}{l_q} \right|. \tag{2.29}$$

It can be shown that, for all the possible sequences of stationary configurations ϑ^s, every couple $(v_N, \mathcal{D})$ falls inside the blue triangle in Fig. 2.1 (or on its edges), and the triangle is densely filled in the thermodynamic limit. The KSS criterion is satisfied only for $v = 0$; this means that only for this value of the energy density the necessary conditions for the occurrence of a phase transition are fulfilled. From the exact solution of the model it is known that no phase transitions are present in it for any finite value of the temperature. The results summarized in Fig. 2.1 confirms the known results; ideed, the value $v = 0$ is a rather special value of the energy corresponding to an infinite value of the temperature ($T = \pm\infty$). Although this analysis does not add too much to the well known thermodynamics of the one-dimensional XY model, some considerations can be made about the above results that will be useful for the following.

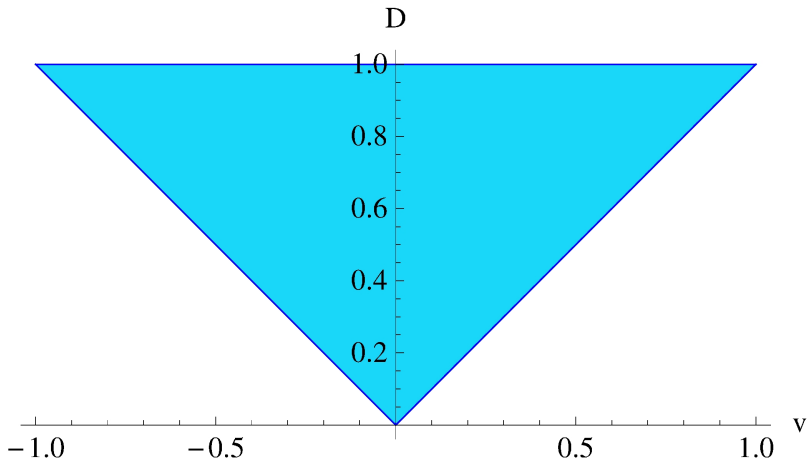

Figure 2.1: Behavior of $\mathcal{D} = \left|\frac{-v_N(\theta^s)}{l_q}\right|$ as a function of the energy density v. Figure adapted from [69].

At variance with what happens for the mean-field XY model, the reduced determinant in Eq.(2.29) is not a function of the energy density alone. In fact, given a certain value of v, the quantity $\mathcal{D}$ fills densely a certain interval of values in the thermodynamic limit.

Among all the stationary configurations given by Eq. (2.21) and Eq. (2.22), two special classes of stationary points have been pointed out: the Ising stationary configurations and the polygonal configurations. From Eq. (2.28) it turns out that the reduced determinant of the Hessian matrix is constant and equal to 1 if evaluated on an Ising stationary point. Moreover, on the Ising stationary points the reduced determinant covers in a dense way the basis of the reverse triangle in Fig. 2.1 when $N \to \infty$. On the other side, the polygonal configurations are selected once q_i are set equal to 0 $\forall i = 1, \ldots, N-1$ (and correspondingly $l_q = 1$). From Eq. (2.29) is possible to see that this kind of solutions produce the values of the reduced determinant $\mathcal{D}$ that cover the two oblique edges of equal length of the reverse triangle in Fig. 2.1. They provide the lower bound of $\mathcal{D}$ in the whole energy density range accessible to the system.

Even if in the one-dimensional XY model a huge number of stationary configurations is present (see Eqs. (2.21) and (2.22)), the class of the Ising stationary points seems to be again a remarkable class of stationary configurations. In fact these points fill densely the whole energy density range of the system, their number grows exponentially with the number of degrees

of freedom of the system –the number of the polygonal configurations grows only linearly with N– and they are present both in the case of periodic and anti-periodic boundary conditions [107] at variance with what happens e.g. for the polygonal configurations. This last fact is quite relevant since we expect that the thermodynamic behavior of the system should be independent on the choice of the boundary conditions when $N \to \infty$. Moreover the reduced determinant $\mathcal{D} \neq 0$ on the Ising points for every value of the energy density; this fact is coherent with the known thermodynamic behavior of the model.

The results reported for the mean-field XY model and for the one-dimensional XY model are in agreement with the theoretical directives of Chapter 1 and prepare the ground for the application of the KSS criterion to XY models in $d = 2$ and $d = 3$. This is one of the main topic of our work and we are going to present our results in the following sections.

2.3 The two- and three- dimensional XY models

In this Section we are going to apply the KSS criterion to the two-dimensional XY model defined on a square lattice and to the three-dimensional XY model defined on a cubic lattice with nearest-neighbors ferromagnetic interactions and periodic boundary conditions. The models are described by the Hamiltonian (2.4) that we recall here for our convenience

$$H^{(2)} = -\frac{1}{2}\sum_{i=1}^{N}\sum_{j\in\mathcal{N}(i)}\cos\left(\vartheta_i - \vartheta_j\right). \tag{2.30}$$

The difference between the $d = 2$ and $d = 3$ case is simply made by the definition of the set of nearest-neighbors $\mathcal{N}(i)$ of the $i-$th spin and it is given by 4 spins in $d = 2$ and 6 spins in $d = 3$.

The stationary points of the energy are given by all the configurations ϑ^{s} that satisfies the vector equation $\nabla\mathcal{H}^{(2)}(\vartheta^{\mathrm{s}}) = 0$. Using (2.30), the kth component of this equation can be written as

$$\sum_{j\in\mathcal{N}(k)}\sin\left(\vartheta_k - \vartheta_j\right) = 0. \tag{2.31}$$

To explicitly break the O(2) invariance of Eq. (2.30) we choose to fix one spin, e.g. $\vartheta_N \equiv 0$; as already discussed in Sec. 2.1.1, there are other possibilities

to break the symmetry, and we will come back to this point in Sec. 2.3.5. In order to apply the KSS criterion, we have to evaluate, at the stationary points, the determinant of the Hessian matrix of the Hamiltonian [which for the XY model (2.30) coincides with the potential energy]. The elements of the Hessian matrix are defined as

$$\mathcal{H}_{kl} = \frac{\partial^2 H}{\partial \vartheta_k \partial \vartheta_l}. \tag{2.32}$$

The constraint $\vartheta_N \equiv 0$ makes the Hessian an $(N-1)\times(N-1)$ matrix and, for the XY Hamiltonian (2.30), its diagonal elements are given by

$$\mathcal{H}_{kk} = \sum_{j\in\mathcal{N}(k)} \cos\left(\vartheta_k - \vartheta_j\right), \tag{2.33}$$

while the off-diagonal elements are

$$\mathcal{H}_{kl} = \begin{cases} -\cos\left(\vartheta_k - \vartheta_l\right) & \text{for } l \in \mathcal{N}(k), \\ 0 & \text{else,} \end{cases} \tag{2.34}$$

for $k, l = 1, \ldots, N-1$. Finding *all* stationary points of the Hamiltonian (2.30) is unlikely to be feasible for large lattices. This notwithstanding, we know that the Ising stationary points are stationary configurations of the Hamiltonian (2.30). In fact, inspection of the stationary point conditions (2.31) reveals that any configuration where $\vartheta_i^{\mathrm{s}} = \{0, \pi\}\ \forall i$ is a stationary point, as in this case each term of the sum on the left-hand side of (2.31) vanishes separately. In the notation of (2.3) such stationary points can be written as

$$\begin{cases} S_i^1 &= \sigma_i, \\ S_i^2 &= 0, \end{cases} \tag{2.35}$$

where $\sigma_i \in \{-1, +1\}$. Therefore, as already discussed in Sec.2.1.1, each Ising stationary point ϑ^{s} of the XY Hamiltonian (2.30) corresponds to a configuration of the Ising model (2.2) defined on the same lattice. Moreover, the corresponding stationary values $\mathcal{H}^{(2)}(\vartheta^{\mathrm{s}})$ of these 'Ising stationary configurations' are just the energy levels of the Ising Hamiltonian (2.2).

Evaluated at the Ising stationary configurations, the Hessian matrix elements (2.33) and (2.34) can be written as

$$\mathcal{H}_{kk} = \sigma_k \sum_{j\in\mathcal{N}(k)} \sigma_j \tag{2.36}$$

and

$$\mathcal{H}_{kl} = \begin{cases} -\sigma_k \sigma_l & \text{for } l \in \mathcal{N}(k), \\ 0 & \text{else,} \end{cases} \tag{2.37}$$

for $k, l = 1, \ldots, N-1$ and $k \neq l$. As recalled in Sec. 2.2.1 and in Sec. 2.2.2, in the mean-field XY model, and also in the one-dimensional XY model, the energy and the Hessian determinant of Ising stationary configurations depend on only a single collective variable, thus allowing an analytical search of stationary points satisfying Eq.s (2.9) and (2.10). Unfortunately, for the two- and three-dimensional nearest-neighbor models this is not the case and we have to resort to numerical methods. We computed the determinant of the Hessian of the Hamiltonian on a numerically obtained sample of the Ising stationary configurations. The sample was obtained by standard Metropolis Monte Carlo simulations of the two-dimensional and three-dimensional Ising models, exploiting the above mentioned one-to-one relation between configurations of the Ising model and Ising stationary configurations of the XY models.

2.3.1 Two-dimensional XY model

We considered $L \times L$ square lattices of side lengths $L = 16$, 24, 32 and 64, so that the number of degrees of freedom ranges from $N = L^2 = 256$ to 4096. Compared to those typically considered in simulations nowadays, these are not very big lattices, and indeed obtaining the sample was easy and fast. The practical limit on the number of degrees of freedom was set by the time-consuming calculation of the Hessian determinant for each configuration of the sample. Although in principle Ising configurations occur over the entire range $[-2, 2]$ of accessible energy densities, only configurations with negative energy were sampled in the Monte Carlo runs. This is a consequence of using canonical simulations at positive simulation temperature so that, for sufficiently large lattice sizes, the Boltzmann weight narrowly focuses the sampled distribution on a range of negative energies. However, by using also negative temperatures we would have obtained symmetric results with respect to zero energy, without adding any relevant information. For each lattice of side lengths $L = 16$, 24 and 32, we considered a total sample of 250000 configurations. For $L = 64$ we considered only 48000 configurations, the Hessian determinant being quite heavy to compute. Results for the

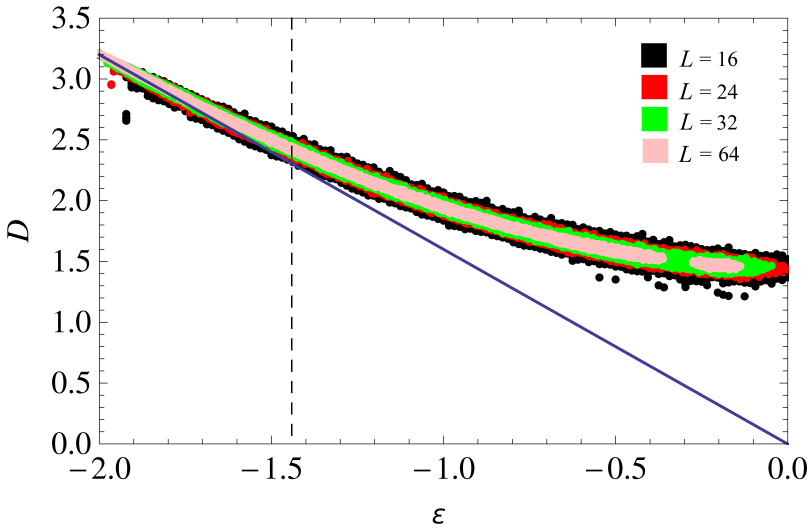

Figure 2.2: Rescaled Hessian determinant $\mathcal{D}$ of Ising stationary configurations for the two-dimensional XY model, plotted as a function of the energy density ε. Data symbols correspond to lattices of side lengths $L = 16$ (black), 24 (red), 32 (green) and 64 (lighter red). The critical energy density $\varepsilon_{\mathrm{c}}^{2d} \approx -1.446$ of the BKT transition is marked by a vertical dashed line. The solid lines are the values calculated for the polygonal configurations in the large-N limit according to (2.46).

rescaled Hessian determinant

$$\mathcal{D} = \left|\det \mathcal{H}_{H^{(2)}}\left(\vartheta^{\mathrm{s}}\right)\right|^{1/N} \tag{2.38}$$

as a function of the energy density are shown in Fig. 2.2.

In order to further characterize the sampled stationary points we computed, for the same lattices, the index density

$$\iota = \frac{\mathrm{index}(\vartheta^{\mathrm{s}})}{N-1}, \tag{2.39}$$

where the index of a stationary point ϑ^{s} is the number of negative eigenvalues of the Hesse matrix at ϑ^{s}. The results for the index density ι as a function of the energy density are shown in Fig. 2.3.

Two features of the results shown in Figs. 2.2 and 2.3 are of particular interest.

1. As N grows, the rescaled determinant $\mathcal{D}$ as well as the index density ι show a tendency to concentrate onto a single curve, so that, at least for Ising stationary configurations, these quantities appear to be good

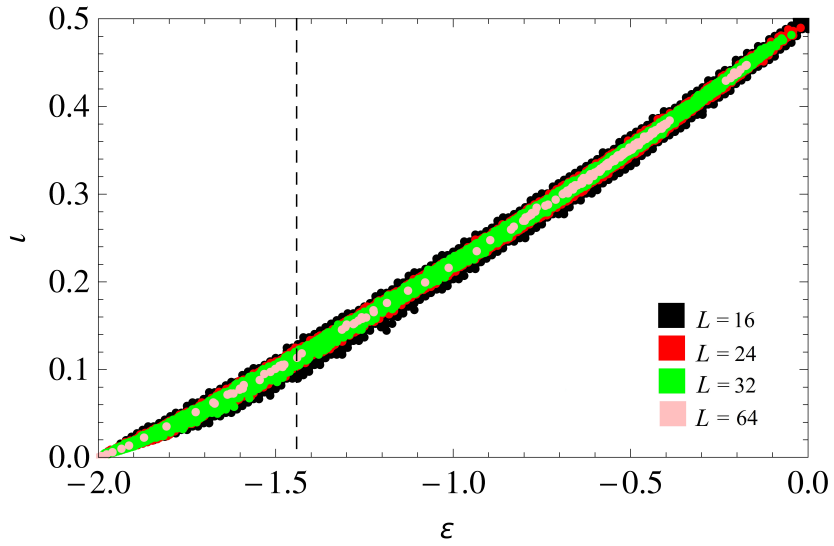

Figure 2.3: As in Fig. 2.2 for the index density ι. Data for the polygonal configurations are not shown.

thermodynamic observables. Moreover, both quantities appear to be monotonic functions of the energy density.

2. The Hessian determinant shows no tendency to vanish for any value of the energy density. Hence there are no indications of the presence of asymptotically flat stationary points, i.e., of the validity of Eq. (2.10) around the transition energy density $\varepsilon_{\rm c}^{2d} \approx -1.446$ of the BKT transition. Also the index density $\iota(\varepsilon)$ does not show any remarkable feature close to $\varepsilon_{\rm c}^{2d}$.

Our sample has variable magnetization and, in particular for low energies, configurations typically have nonzero magnetizations while in the two-dimensional XY model the typical magnetization is zero at any energy. In order to rule out the possibility that this may affect our results, we repeated the calculation of the Hessian determinant on a sample of configurations with vanishing magnetization, obtained by Monte Carlo with Kawasaki dynamics [55]. The results (not shown) display no appreciable differences with respect to Fig. 2.2.

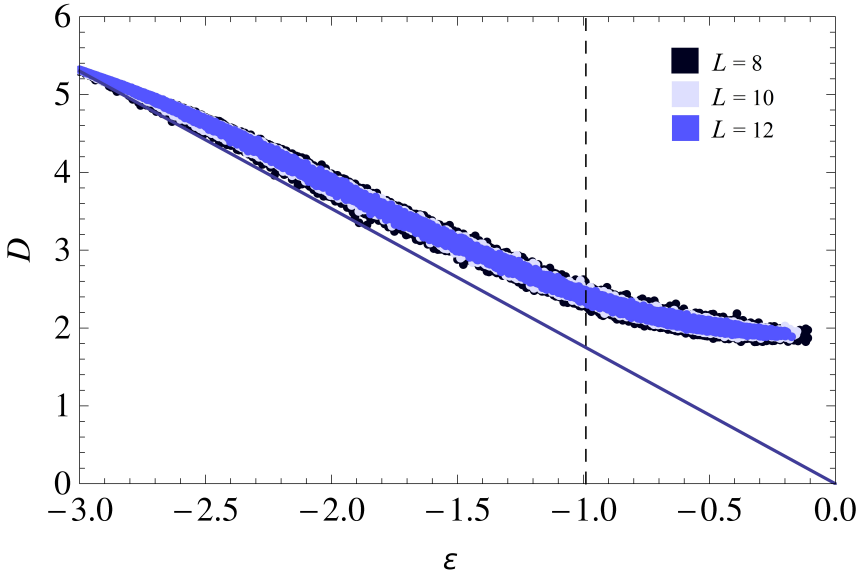

Figure 2.4: Rescaled Hessian determinant $\mathcal{D}$ as a function of the energy density ε for the three-dimensional XY model. Data symbols correspond to lattices of side lengths $L = 8$ (darker blue), 10 (lighter blue) and 12 (blue). The critical energy density $\varepsilon_{\mathrm{c}}^{3d} \approx -0.99$ of the ferromagnetic transition is marked by a vertical dashed line. The solid lines are the values calculated for the polygonal configurations in the large-N limit according to (2.47).

2.3.2 Three-dimensional XY model

In the three-dimensional case we proceeded analogously to the two-dimensional case, considering $L \times L \times L$ lattices of side lengths $L = 8$, 10 and 12, so that the number of degrees of freedom ranged from $N = L^3 = 512$ to 1728. For each lattice we considered a total sample of 57000 configurations. Results for the rescaled Hessian determinant $\mathcal{D}$ and for the index density ι as a function of the energy density are shown in Figs. 2.4 and 2.5, respectively. The similarities to Figs. 2.2 and 2.3 are striking, so that the considerations made for the two-dimensional case carry over to three dimensions.

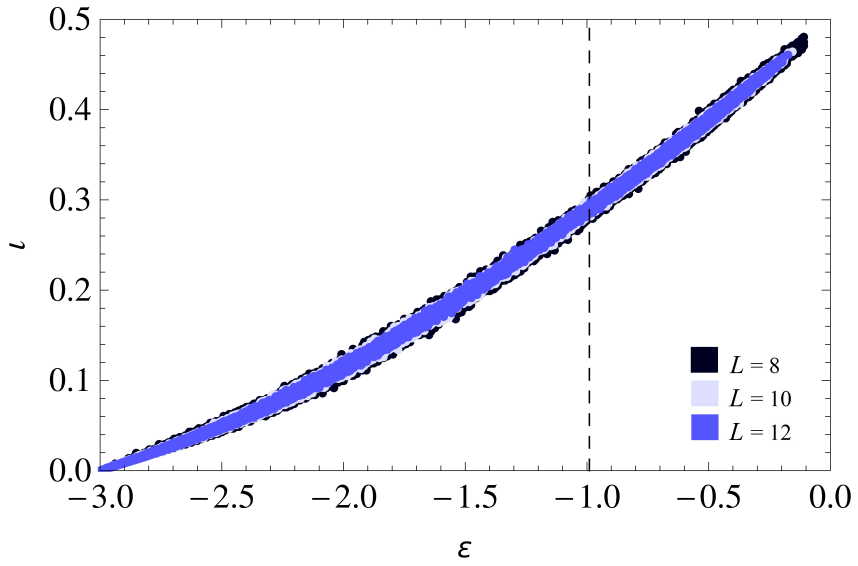

Figure 2.5: As in Fig. 2.4 for the density of index ι. Data for the polygonal configurations are not shown.

2.3.3 Polygonal stationary points

Another class of stationary configurations of the XY model that can be easily identified are those for which neighboring spins differ by the same angle[9] φ,

$$\vartheta_j = \vartheta_i \pm \varphi \qquad \forall i = 1, \ldots, N,\ j \in \mathcal{N}(i). \tag{2.40}$$

Periodic boundary conditions restrict these angles to values $\varphi = 2\pi m/L$ with $m \in \{0, \ldots, L-1\}$. The stationary configurations (2.40) are analogous to the polygonal stationary points for the 1-d XY model of Sec.2.2.2, for this reason we decided to denote them with the same name.

For the two-dimensional XY model, the energy density of a polygonal stationary configuration is

$$\varepsilon(\varphi) = -2\cos\varphi, \tag{2.41}$$

and the Hessian determinant of the Hamiltonian has the simple form

$$\mathcal{H}_{ij}(\varphi) = A_{i,j}\cos\varphi, \tag{2.42}$$

[9]These configurations can be generalized to the case in which there is a different constant angle for each of the d independent directions of the lattice; however, for simplicity we shall restrict to the case of just one angle, equal for all the directions.

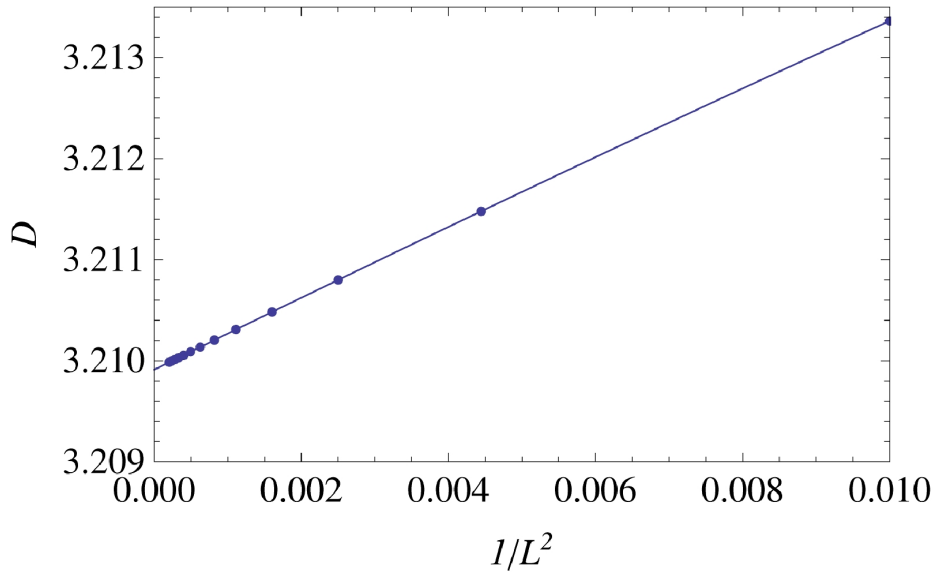

Figure 2.6: Rescaled determinant $\mathcal{D} = |\det A|^{1/(N-1)}$ of the matrix A as defined in (2.43), plotted as a function of the inverse system size. The line is obtained from a linear least-square fit, and an extrapolation to $1/L^2 = 0$ yields $a = \lim_{N\to\infty} \mathcal{D} \approx 3.21$.

where A is an $(N-1) \times (N-1)$ matrix with elements

$$A_{ij} = \begin{cases} 4 & \text{if } i = j, \\ -1 & \text{if } j \in \mathcal{N}(i), \\ 0 & \text{else.} \end{cases} \tag{2.43}$$

We have analyzed the determinant of A numerically, and the results shown in Fig. 2.6 provide strong evidence that, asymptotically for large N, the determinant behaves as

$$\det A \sim a^{N-1} \tag{2.44}$$

with $a \approx 3.21$. The rescaled Hessian determinant computed on these configurations in the thermodynamic limit is then given by

$$\lim_{N\to\infty} |\det \mathcal{H}(\varphi)|^{1/(N-1)} = a|\cos\varphi| \tag{2.45}$$

and, using (2.41), we can write

$$\lim_{N\to\infty} |\det H(\varphi)|^{1/(N-1)} = \frac{a}{2}|-\varepsilon|. \tag{2.46}$$

This result is plotted in Fig. 2.2 along with the data for the Ising stationary points.

For the polygonal stationary points of the three-dimensional XY model, the calculation proceeds along very similar lines, yielding as a final result

$$\lim_{N\to\infty} |\det \mathcal{H}(\varphi)|^{1/(N-1)} = \frac{b}{3}|-\varepsilon| \tag{2.47}$$

with $b \approx 5.3$. This result is plotted in Fig. 2.4, along with data for the Ising stationary configurations.

2.3.4 Singular stationary points

To apply the KSS criterion the starting assumption is that the Hamiltonian H of the system under consideration is a Morse function, meaning that at any stationary point of H the Hessian determinant is nonzero. To be sure that this is the case for the XY models under analysis, we set $\vartheta_N = 0$. Although this reasonable prescription, in the following we prove that, in lattice dimensions $d = 2$ and $d = 3$, the XY Hamiltonian (2.30) is not still a Morse function, but instead has an exponentially (in N) large number of singular stationary points. Moreover, the stationary energy densities $H(\vartheta^{\rm s})/N$ of all these singular stationary points become dense on the interval $[-d, d]$ of accessible energy densities in the thermodynamic limit. The proof is constructive, and for simplicity we restrict the presentation to two-dimensional square lattices of size $L \times L$ with periodic boundary conditions. The three-dimensional case is treated in the Appendix A.1. Generalizations to higher-dimensional lattices should be possible along similar lines, but we did not work this out in detail.

For a configuration $\vartheta = (\vartheta_1, \ldots, \vartheta_N)$ to have a vanishing Hessian determinant, it is sufficient that one row of the Hessian matrix given in (2.33) and (2.34) has only zero entries. This is a local property, as all the nonzero entries in the kth row are fully determined by the kth spin and its nearest neighbors. Consider for example a configuration which, somewhere on the lattice, locally looks like

$$\begin{array}{ccc} \cdot & \downarrow & \cdot \\ \uparrow & \leftarrow & \uparrow \\ \cdot & \downarrow & \cdot \end{array} \tag{2.48}$$

where arrows $\uparrow$, $\rightarrow$, $\downarrow$, $\leftarrow$ correspond to angle variables $\vartheta_i = 0$, $\pi/2$, π, $3\pi/2$. The dots in (2.48) are place holders for arbitrary spin orientations, as their

values do not matter for the moment. Assigning to the center (left-pointing) spin of this configuration the label k, we find

$$\mathcal{H}_{kk} = \sum_{j \in \mathcal{N}(k)} \cos(\pm\pi/2) = 0, \qquad \mathcal{H}_{kl} = 0 \; \forall l \tag{2.49}$$

for the elements of the Hessian matrix. The matrix therefore does not have full rank and its determinant is zero.

Next, in addition to this local condition guaranteeing that the Hessian determinant vanishes, we also have to ensure that the overall configuration is a stationary point of $H^{(2)}$. This is a global property as, in order for a configuration to be stationary, the constraint

$$\sum_{l \in \mathcal{N}(k)} \sin\left(\vartheta_k - \vartheta_l\right) = 0 \tag{2.50}$$

has to be satisfied for all lattice sites k. Starting from the pattern in (2.48), it is not too difficult to construct an embedding of such patterns into larger lattices while at the same time satisfying the stationarity constraints (2.50). For the example of an 8×8 square lattice, the following class of configurations does the job,

$$\begin{array}{cccccccc}
\uparrow & \updownarrow & \updownarrow & \updownarrow & \updownarrow & \updownarrow & \uparrow & \leftarrow \\
\updownarrow & \updownarrow & \updownarrow & \updownarrow & \updownarrow & \downarrow & \rightarrow & \downarrow \\
\updownarrow & \updownarrow & \updownarrow & \updownarrow & \uparrow & \leftarrow & \uparrow & \updownarrow \\
\updownarrow & \updownarrow & \updownarrow & \downarrow & \rightarrow & \downarrow & \updownarrow & \updownarrow \\
\updownarrow & \updownarrow & \uparrow & \leftarrow & \uparrow & \updownarrow & \updownarrow & \updownarrow \\
\updownarrow & \downarrow & \rightarrow & \downarrow & \updownarrow & \updownarrow & \updownarrow & \updownarrow \\
\uparrow & \leftarrow & \uparrow & \updownarrow & \updownarrow & \updownarrow & \updownarrow & \updownarrow \\
\rightarrow & \downarrow & \updownarrow & \updownarrow & \updownarrow & \updownarrow & \updownarrow & \downarrow
\end{array} \tag{2.51}$$

The lattice sites marked with gray $\updownarrow$-arrows can be filled with an arbitrary 'Ising-type'-pattern of $\uparrow$ and $\downarrow$ arrows. Independently of the precise pattern of these up- and down-pointing arrows, the resulting configuration will always be stationary. In this way, we have obtained a class of stationary points of the Hamiltonian $H^{(2)}$ with vanishing Hessian determinant, and the scheme works in just the same way for larger lattice sizes.

This class of singular stationary points ϑ^{s} is ample enough to allow us to adjust the energy density $H(\vartheta^{\mathrm{s}})/N$ almost freely: By choosing an appropriate Ising-type pattern of $\uparrow$ and $\downarrow$ for the gray $\updownarrow$-arrows in (2.51), the energy of the configuration is varied. Since the number of gray $\updownarrow$-arrows in such a configuration scales as L^2, their contribution to the overall energy will, in the large-L limit, dominate over the fixed (black) arrows in (2.51) whose number increases only linearly in L. As a result, the corresponding stationary energy densities $H(\vartheta^{\mathrm{s}})/N$ are dominated by the Ising-type pattern chosen for the gray $\updownarrow$-arrows and, like the Ising energy densities, become dense on the interval $[-2, 2]$ of accessible energy densities in the thermodynamic limit.

Singular stationary points come in two flavors: They can either be isolated stationary points, like at the minimum $x^{\mathrm{s}} = 0$ of the quartic $f_1(x) = x^4$. Or they can form continuous families of non-isolated stationary points, like for the Mexican hat potential $f_2(x, y) = (x^2 + y^2)^2 - (x^2 + y^2)$ where the points on the circle $x^2 + y^2 = 1/2$ form a continuous curve of minima of f_2. Our singular stationary points of the two-dimensional XY Hamiltonian fall into the latter category. This can be seen by starting from a configuration like the one depicted in (2.51) and then simultaneously rotating by some arbitrary angle α all the $\rightarrow$ and $\leftarrow$ spins situated on the diagonal. It is easily checked that the resulting configuration still satisfies the stationarity condition (2.50). This proves that the singular stationary points we have constructed are not isolated, but occur in continuous one-parameter families, parametrized by the angle α. Similarly, one can create two- and more-parameter families by generalizing (2.51) to contain more than one diagonal pattern,

$$
\begin{array}{cccccccc}
\uparrow & \updownarrow & \uparrow & \leftarrow & \uparrow & \updownarrow & \uparrow & \leftarrow \\
\updownarrow & \downarrow & \rightarrow & \downarrow & \updownarrow & \downarrow & \rightarrow & \downarrow \\
\uparrow & \leftarrow & \uparrow & \updownarrow & \uparrow & \leftarrow & \uparrow & \updownarrow \\
\rightarrow & \downarrow & \updownarrow & \downarrow & \rightarrow & \downarrow & \updownarrow & \downarrow \\
\uparrow & \updownarrow & \uparrow & \leftarrow & \uparrow & \updownarrow & \uparrow & \leftarrow \\
\updownarrow & \downarrow & \rightarrow & \downarrow & \updownarrow & \downarrow & \rightarrow & \downarrow \\
\uparrow & \leftarrow & \uparrow & \updownarrow & \uparrow & \leftarrow & \uparrow & \updownarrow \\
\rightarrow & \downarrow & \updownarrow & \downarrow & \rightarrow & \downarrow & \updownarrow & \downarrow
\end{array}
\tag{2.52}
$$

In this configuration the $\rightarrow$ and $\leftarrow$ spins situated on the main diagonal can be simultaneously rotated by some angle α, and those on the other diagonal (modulo periodic boundary conditions) by an independent angle β, resulting in a continuous two-parameter family of stationary points. The generalization to more parameters is straightforward, provided the lattice sizes are chosen large enough.

Note that this occurrence of continuous families of non-isolated stationary points is not due to the global O(2) invariance of the XY Hamiltonian: This global symmetry is a trivial effect that we have taken care of by fixing one angle variable, $\vartheta_N = 0$, as discussed in Sec. 2.1.1. From the examples (2.51) and (2.52), however, we have learned that this global phase fixing is not sufficient to ensure that the XY Hamiltonian is a Morse function with only isolated stationary points. The problem seems to be that certain spin environments, like the pattern

$$\begin{array}{cccccccc}
\uparrow & \cdot & \cdot & \cdot & \cdot & \cdot & \uparrow & \cdot \\
\cdot & \cdot & \cdot & \cdot & \cdot & \downarrow & \cdot & \downarrow \\
\cdot & \cdot & \cdot & \cdot & \uparrow & \cdot & \uparrow & \cdot \\
\cdot & \cdot & \cdot & \downarrow & \cdot & \downarrow & \cdot & \cdot \\
\cdot & \cdot & \uparrow & \cdot & \uparrow & \cdot & \cdot & \cdot \\
\cdot & \downarrow & \cdot & \downarrow & \cdot & \cdot & \cdot & \cdot \\
\uparrow & \cdot & \uparrow & \cdot & \cdot & \cdot & \cdot & \cdot \\
\cdot & \downarrow & \cdot & \cdot & \cdot & \cdot & \cdot & \downarrow
\end{array} \tag{2.53}$$

in (2.51), can build a 'cage' around a lattice region such that the overall phase of the enclosed region [the diagonal in the case of (2.51)] is shielded from the rest of the configuration. As a consequence, breaking of the *global* $O(2)$ invariance of the XY Hamiltonian by *locally* fixing $\vartheta_N = 0$ is not sufficient. Another way to eliminate the global $O(2)$ invariance is to use antiperiodic boundary conditions in all the d-directions, as proposed in Ref. [108]. However, we have verified numerically that even using antiperiodic boundary conditions, isolated singular solutions as well as continuous one- and more-parameter families of solutions exist.

2.3.5 Symmetry breaking fields

The observation of local versus global properties also suggests how the problem of non-isolated, singular stationary points might be solved: As mentioned at the end of Sec. 2.1.1, perturbations like

$$H^{(2)} = -\frac{1}{2}\sum_{i=1}^{N}\sum_{j\in\mathcal{N}(i)}\cos\left(\vartheta_i - \vartheta_j\right) - \sum_{i=1}^{N} h_i\vartheta_i^2 \tag{2.54}$$

and maybe also

$$H^{(2)} = -\frac{1}{2}\sum_{i=1}^{N}\sum_{j\in\mathcal{N}(i)}\cos\left(\vartheta_i - \vartheta_j\right) - \sum_{i=1}^{N} h_i\cos\vartheta_i, \tag{2.55}$$

for generic values of $(h_1,\ldots,h_N)\in\mathbb{R}^N$, should ensure that the Hamiltonian has only isolated and nondegenerate stationary points, but other forms of perturbations might do the job as well. For 3×3 lattices we have checked numerically that, up to numerical accuracy, the perturbations in (2.54) and (2.55) indeed destroy all singular stationary points of $H^{(2)}$: Firstly, we used the numerical polynomial homotopy continuation method (Bertini software package [109]) which finds all the solutions of a system of multivariate polynomial equations, including isolated singular solutions [110]. This method has been recently used to study the potential energy landscape in various areas of physics [71, 107, 111–116]. We studied at least 10 generic sets of $(h_1,\ldots,h_N)\in\mathbb{R}^N$ for both types of perturbations and verified that no isolated singular solution occur for these perturbed systems. We then used an extension of the numerical polynomial homotopy continuation method, called numerical algebraic geometry [117,118], which can find solution curves of a system of polynomial equations, combined with the method described in Ref. [119], and concluded that there is no continuous solution curve for any of the systems in the presence of a generic perturbation.

From a physical point of view, the cosine-perturbed Hamiltonian (2.55) appears particularly appealing as it has the form of a spatially inhomogeneous magnetic field in x-direction acting on the spins. Interestingly, this specific choice of the perturbation leaves the Ising stationary configurations: Every Ising configuration $(\vartheta_1^{\mathrm{s}},\ldots,\vartheta_N^{\mathrm{s}})$ with $\vartheta_i^{\mathrm{s}}\in\{0,\pi\}$ is also a stationary point of the perturbed Hamiltonian (2.55) for arbitrary perturbation fields h_i. Mathematically, this is due to the fact that the Taylor expansion of the

perturbation around an Ising stationary configuration

$$\sum_{i=1}^{N} h_i \cos\vartheta_i \Big|_{\vartheta_i=\vartheta_i^{\mathrm{s}}} = \sum_{i=1}^{N} \left[h_i \cos\vartheta_i^{\mathrm{s}} + \mathcal{O}\left(\vartheta_i - \vartheta_i^{\mathrm{s}}\right)^2 \right] \tag{2.56}$$

has vanishing linear contributions, thus leaving these stationary points unaffected. It is unclear to the authors whether there is any physical significance to this observation. This notwithstanding, this property can be used to check if all the singular solutions of $H^{(2)}$ are indeed destroyed by the perturbation (2.55) also in lattices larger than 3×3. For simplicity in the following we will restrict ourselves to two-dimensional square lattices, but we have checked that the conclusions remain valid in three dimensions.

In order to study the effect of the perturbation (2.55) on singular configurations, we want to construct a sample of such configurations, spread over a range of energies similar to the nonsingular ones in Figs. 2.2, 2.3, 2.4 and 2.5. One possible strategy to do so is to take the nonsingular sample as a starting point and transform each of the configurations into a singular one by imprinting the mask

$$\begin{array}{cccccccc}
\downarrow & \cdot & \cdot & \cdot & \cdot & \cdot & \downarrow & \uparrow \\
\cdot & \cdot & \cdot & \cdot & \cdot & \uparrow & \downarrow & \uparrow \\
\cdot & \cdot & \cdot & \cdot & \downarrow & \uparrow & \downarrow & \cdot \\
\cdot & \cdot & \cdot & \uparrow & \downarrow & \uparrow & \cdot & \cdot \\
\cdot & \cdot & \downarrow & \uparrow & \downarrow & \cdot & \cdot & \cdot \\
\cdot & \uparrow & \downarrow & \uparrow & \cdot & \cdot & \cdot & \cdot \\
\downarrow & \uparrow & \downarrow & \cdot & \cdot & \cdot & \cdot & \cdot \\
\downarrow & \uparrow & \cdot & \cdot & \cdot & \cdot & \cdot & \uparrow
\end{array} \tag{2.57}$$

(or a similar one for other lattice sizes), i.e., by rotating all spins of the configuration into the orientation indicated in (2.57), while leaving unchanged all sites indicated by dots. The configuration in (2.57) is similar to the one in (2.51), only that the spins on the diagonal are rotated by $\pi/2$. Such a configuration, as explained in Sec. 2.3.4, is also singular, and it preserves the Ising-type character of the configuration. Imprinting the mask (2.57) causes only a subextensive change of energy, and the distribution in energy

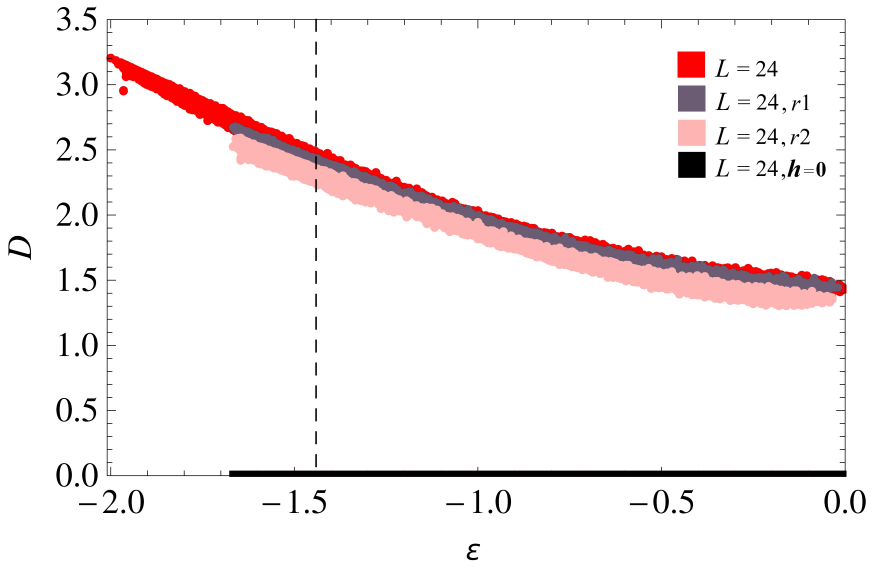

Figure 2.7: Rescaled Hessian determinant $\mathcal{D}$ as a function of the energy density for the two-dimensional XY model with $L = 24$ and cosine perturbation terms (2.55). See the legend in the plot for the color code: "original" stands for the original Ising configurations as in Fig. 2.2; "modified" stands for the singular Ising configurations (built from the original ones as described in the text), either with unperturbed Hamiltonian, so that $\mathcal{D} = 0$, or with a perturbed Hamiltonian with the fields h_i chosen randomly in the range $r_1 = [-0.5, 0.5]$ or $r_2 = [-10^{-7}, 10^{-7}]$.

density of the stationary points will therefore be similar to the distribution of the original (nonsingular) sample. Switching on the perturbation fields h_i in (2.55) should turn all singular solutions into regular ones, and it is this effect we want to study.

We performed the above analysis on 25000 configurations for a square lattice of side length $L = 24$. The fields h_i were chosen randomly in the ranges $r_1 = [-0.5, 0.5]$ and $r_2 = [-10^{-7}, 10^{-7}]$, to test the dependency of the reduced determinant on the strength of the fields h_i. Results are shown in Fig. 2.7. This analysis, like the one conducted for the 3×3 lattice by numerical homotopy continuation, confirms that generic perturbations as in (2.55) transform singular solutions of $H^{(2)}$ into nonsingular ones. Remarkably, the effect of the perturbations h_i on the rescaled determinant $\mathcal{D}$ is rather drastic: Already for tiny perturbations in the range $r_2 = [-10^{-7}, 10^{-7}]$, D is far away from zero and very close to the values of the original (nonsingular) Ising stationary configurations. This finding can be explained by the fact that, according to the scheme in Sec. 2.3.4, we constructed one-parameter

families of singular solutions. Accordingly, the Hessian determinant is expected to have a single vanishing eigenvalue. Switching on a perturbation affects the zero eigenvalue by making it nonzero and of order h, while all other eigenvalues remain constant (nonzero) to leading order. We therefore have

$$\mathcal{D}(h) = |ch|^{1/N} \left| \prod_{k=2}^{N} \lambda_k \right|^{1/N}, \tag{2.58}$$

where the eigenvalues λ_k are independent of h to leading order for all $k \geqslant 2$. No matter how small ch is, $|ch|^{1/N}$ will always be close to 1 for $N \gg 1$. The remaining $(N-1)$-fold product in (2.58) will generically yield a value close to the 'thermodynamic' one observed for generic Ising stationary configurations as shown in Fig. 2.2, even for tiny perturbations h. Intuitively, we would expect a stationary point with an extensive number of vanishing eigenvalues to be more relevant for the system's thermodynamic properties, while those with a few such eigendirections should not play a major role. But this is speculation going beyond what the KSS criterion claims and needs further examination.

In summary, we find that a generic perturbation as in (2.54) or (2.55) successfully destroys all singular stationary points. Moreover, the rescaled Hessian determinant $\mathcal{D}$ is rather insensitive to the actual strength of the perturbation. Similar behavior is observed for the three-dimensional XY model, but the results are not shown here.

2.3.6 The KSS criterion, concluding remarks

We have explored the energy landscape of the XY model with nearest-neighbor interactions on the two-dimensional square lattice and the three-dimensional cubic lattice. In particular, we have constructed certain classes of stationary points of the Hamiltonian (2.30). One of these classes consists of Ising stationary configurations (2.35), and their number is 2^N for a given lattice size N. While analytic expressions for all these exponentially many stationary points are readily obtained, an analysis of their properties is a much harder task. We resorted to Monte Carlo techniques for generating samples of Ising stationary configurations and then numerically calculated properties like the index ι and the rescaled Hessian determinant $\mathcal{D}$ of these points. The results, summarized in Figs. 2.2, 2.3, 2.4 and 2.5, indicate that $\mathcal{D}$ and ι are good thermodynamic observables in the sense that, with in-

creasing lattice size N (but already for small system sizes), the data points concentrate on a line in these plots and appear to be functions of the energy density ε alone. It is worth noticing that this effect was not obvious a priori especially for the two dimensional XY model where finite size effects are known to be relevant also in macroscopic systems [90, 91].

The original motivation for undertaking this energy landscape study was to test whether the KSS criterion, based on the Hessian determinant at stationary points of the Hamiltonian, reveals a signature of the phase transition of the XY model in two or three dimensions. In this respect, our results are not conclusive. The data for the rescaled Hessian determinant $\mathcal{D}$, shown in Figs. 2.2 and 2.4, are clearly bounded away from zero for all values of the energy density ε, and therefore do not signal the presence of a phase transition according to the criterion in Eq. (2.10). As far as the validity of the KSS criterion is concerned, however, this finding has little to say. It rather reveals the limitations of the numerical method we have been using: The Monte Carlo technique we have been using to generate a sample of Ising stationary configurations uses importance sampling with respect to the energy, resulting in a reasonably uniform distribution of data points on the energy axis in Figs. 2.2, 2.3, 2.4 and 2.5. But for a given energy density ε, stationary points are selected unbiased, resulting in the above mentioned behavior as 'good thermodynamic observables'. This implies, however, that stationary points with vanishing (or at least small) rescaled Hessian determinant $\mathcal{D}$ are found by this sampling technique only in case that $\mathcal{D} = 0$ is the most probable value at some energy density ε (see [92] for a numerical study of the nearest-neighbor ϕ^4 model on the square lattice reaching similar conclusions). According to our data, this is not the case.

Indeed, and rather surprisingly, we were able to show that singular stationary points, i.e., stationary points with $\mathcal{D} = 0$, do exist and are even in abundance: As proved in Sec. 2.3.4, even after breaking the global O(2) invariance of the XY model by fixing one spin, an exponentially (in N) large number of singular stationary points exists, densely covering the accessible range $[-d, d]$ of energy densities in the large-N limit. Moreover, these singular stationary points are non-isolated, i.e., they come in continuous families parametrized by one or several angular variables. But despite their ubiquitous presence and abundance, our Monte Carlo scheme failed to detect these points, as the value $\mathcal{D} = 0$ of their rescaled Hessian determinant is not the most probable one at any given ε. It must be noted that this is not a limita-

tion of the specific Monte Carlo technique we used here: it is expected to be a generic property of unbiased numerical sampling schemes. For instance, also a search of stationary points by means of a modified Newton-Raphson method analogous to that used in Ref. [92] did not reveal any tendency of $\mathcal{D}$ to vanish close to the phase transition energies but did not find any singular solutions either (data not shown). Hence our results suggest that from a practical point of view a purely numerical approach to the criterion in Eq.s (2.9) and (2.10) is not very useful unless a numerical sampling scheme able to efficiently detect stationary configurations with zero—or at least small—determinant is devised, which is currently lacking.

In addition to hinting at the inadequacy of commonly used numerical schemes to yield a sufficiently accurate exploration of the energy landscape of XY models from the point of view of the determinant criterion, the presence of singular, non-isolated stationary points (even after explicitly breaking the global O(2) symmetry by fixing one spin) has another relevant consequence. It implies that requirements for the validity of the determinant criterion (2.10) itself, as well as of the other theoretical tools developed for the study of phase transitions based on stationary points of the energy landscape, are not met by the XY Hamiltonian (2.30). Indeed, all these tools require that stationary points are nonsingular and isolated. This is typically assumed to be a 'safe' hypothesis once global invariances of the Hamiltonian have been removed, but our results show that this is not the case.

This observation may suggest that the application of theoretical tools based on the assumption of isolated, nonsingular stationary points is hopeless in the case of XY models. This is not necessarily true, because a way out consists in adding a generic perturbation to the Hamiltonian. We have shown in Sec. 2.3.5 that the singular stationary points can be removed by applying generic perturbations like (2.54) or (2.55). More precisely, the removal of all the singular stationary configurations has been shown for small lattices by the homotopy continuation method. For larger lattices we have considered a sample of Ising stationary configurations, that would be singular in absence of the perturbation and that remain stationary also in presence of a perturbation of the form (2.55), and we have shown that they become nonsingular when the Hamiltonian is perturbed. In previous works both the fixing of a single degree of freedom and the application of a perturbation, typically like (2.55) but with a homogeneous field h (see e.g. Ref. [14]), have been considered and were thought to be equally effective in removing singular,

non-isolated solutions. Our results show that the global $O(2)$ symmetry is not the only cause of singular solutions, and the 'local' strategy is therefore not sufficient for destroying them.

Remarkably, after switching on even a tiny perturbation, the rescaled determinant immediately takes on values in the vicinity of the thermodynamic average, far from the singular behavior with $\mathcal{D} = 0$. This result tells us that the study of the rescaled Hessian determinant $\mathcal{D}$ carried out in Sec. 2.3.1 directly gives us information on the behavior of $\mathcal{D}$ for the perturbed Hamiltonian (2.55) in the limit of very small external fields. Since we can now safely assume that the perturbed Hamiltonian has only isolated singular points, the results shown in Figs. 2.2 and 2.4 should be a faithful representation of what can be learned by standard unbiased numerical techniques as those employed in this work.

The presence of families of non-isolated stationary configurations with zero Hessian determinant (even after breaking the global $O(2)$ symmetry) has interesting implications reaching beyond the XY models investigated in the present paper. Previously, non-isolated stationary configurations had already been found in the mean-field XY model, but only at a specific value of the energy density (the maximum of the energy density achieved by the points with vanishing magnetization, see Sec. 2.2.1 and [14]), and also in the globally coupled Kuramoto model with homogeneous frequencies [120] (in this context a continuous family of singular solutions has been termed an 'incoherent manifold'). A numerical check by means of the homotopy continuation method gave similar results for a variety of other models, including the mean-field spherical p-spin model, particles interacting via a Lennard-Jones potential and the generalized Thomson problem, details of which will be reported elsewhere. Isolated and non-isolated singular solutions often play relevant roles also in field theories (see e.g. Ref. [69] and references therein).

The analysis presented in this Chapter regards the two- and three- dimensional ferromagnetic nearest-neighbors XY models. Despite the very different nature of the phase transition present in these two models, the results obtained are very similar and differ only at a qualitative level. This makes us suppose that similar results hold for general ferromagnetic short-range O(n) models and an analogous inspection in terms of application of the KSS criterion on other representatives of this class appeared to be worthless to our eyes. This fact naturally raised up the question of which mechanism

can produce a phase transition in this class of systems, hopefully based on energy landscape techniques. Although at this stage is not completely clear why the Ising configurations should be relevant for the thermodynamics of the O(n) models, we will keep on trusting in this idea and in the next Chapter we are going to present a possible scenario for this to happen.

Chapter 3

A microcanonical relation between O(n) and Ising models

In Chapter 2 a special class of stationary configurations of classical O(n) spin models has been constructed, present for every $n > 1$. This class is given by all the configurations of the corresponding Ising model, that is by the configurations of the Ising model defined on the same lattice and with the same interactions as the continuous model.

Results shown in Secs. 2.2.1 and 2.2.2 for the mean-field and the one-dimensional XY models suggested that Ising stationary points could play a major role in determining the thermodynamic behavior of the continuous systems, but the KSS criterion failed to single out the phase transitions for two- and three-dimensional XY models with short range interactions.

We then asked ourselves which kind of alternative mechanism based on an energy landscape approach—possibly focused on the Ising stationary points—could be at the basis of the emergence of a phase transition in these systems and in O(n) models in general.

In this Chapter we are going show how the microcanonical density of states $\omega^{(n)}$ of an O(n) model with $n > 1$ can be, indeed, approximated in terms of the density of states $\omega^{(1)}$ of the corresponding Ising model. The Chapter covers the results presented in [38] and has the following structure. In Sec. 3.1 we will derive an approximate expression for the density of state $\omega^{(n)}$ in terms of $\omega^{(1)}$. This expression implies an interesting relation between the critical values of the energy density of the continuous models and those of the Ising models: the critical energy densities should be exactly the same in the two cases. The relation will be discussed in Sec. 3.2.

3.1 Density of states and Ising stationary configurations

In Sec. 2.1.1 a special class of stationary configurations of the O(n) models (2.1) has been constructed, given by all the configurations of the corresponding Ising model. In case of O(n) models defined on regular $d-$dimensional hypercubic lattices with ferromagnetic interactions and periodic boundary conditions, the Ising stationary configurations show several interesting properties that make them outstanding with respect to other classes of stationary points (possibly) present in the systems. In particular, they are exponentially many in N, they become dense and cover all the energy density range $[-d, d]$ allowed for our systems in the $N \to \infty$ limit, and they are robust to external perturbations like i.e. the one in Eq.(2.55).

As discussed in the previous Chapter, the KSS criterion applied to two- and three- dimensional XY models on this particular class of stationary points is not able to select the right energy density values at which the transitions occur. This notwithstanding, the analysis conducted on the reduced determinant $\mathcal{D}$ and on the reduced index ι for this class of configurations led to a remarkable result. As shown in Figs. in Figs. 2.2, 2.3, 2.4 and 2.5, for $N \gg 1$ the above quantities behave as good thermodynamic observables: the data points concentrate on a line in these plots and appear to be functions of the energy density ε alone. This fact seems to suggest that the local properties of the energy landscape of the continuous models around every Ising configurations may depend only on the energy density value of the Ising point and not on the specific configuration considered[1]. This property was not obvious a priori and will be useful in the following.

Taking seriously the idea that Ising stationary configurations are the most important ones, we may approximate the density of states $\omega^{(n)}(\varepsilon)$ of an O(n) model in terms of these configurations. To this end, let us first rewrite Eq. (1.8) as

$$\omega^{(n)}(\varepsilon) = \sum_p \int_{U_p \cap \Sigma_\varepsilon} \frac{d\Sigma}{|\nabla H^{(n)}|} \tag{3.1}$$

[1]This observation holds for sure for the Ising stationary points that can be detected with a standard Monte Carlo algorithm as in Secs. 2.3.1 and 2.3.2. In the following we will assume that the observation is valid for every Ising stationary point.

where p runs over the 2^N Ising stationary configurations and U_p is a neighborhood of the p-th Ising configuration such that $\{U_p\}_{p=1}^{2^N}$ is a proper partition of the configuration space $\Gamma = (\mathbb{S}^{n-1})^N$, that coincides with phase space for spin models (2.1). Since Ising configurations are isolated points in the configuration space of a O(n) model, such a partition always exists.

Let us now introduce two assumptions allowing to write Eq. (3.1) in a more transparent, albeit approximate, way.

(i) We shall assume that the integrals in Eq. (3.1) depend only on ε, i.e., the neighborhoods U can be deformed such as

$$\int_{U_p \cap \Sigma_\varepsilon} \frac{d\Sigma}{|\nabla H^{(n)}|} = \int_{U_q \cap \Sigma_\varepsilon} \frac{d\Sigma}{|\nabla H^{(n)}|} = g^{(n)}(\varepsilon) \tag{3.2}$$

for any p, q such that $H^{(n)}(p) = H^{(n)}(q) = N\varepsilon$.

(ii) In the sum (3.1) we shall consider only Ising stationary configurations at energy density ε.

At a qualitative level, the first assumption is supported by the results on $\mathcal{D}$ and on ι shown in Secs. 2.3.1 and 2.3.2. Since the geometrical properties of the energy landscape of the continuous models around every Ising point seem to depend only on its energy density, we shall assume that Ising points with same energy density ε contribute with the same weight $g^{(n)}(\varepsilon)$ to the density of states $\omega^{(n)}(\varepsilon)$.

For what concerns the second assumption, for a given value of ε, the largest contribution to $\omega^{(n)}(\varepsilon)$ is likely to come from those U_p such that $H^{(n)}(p) = N\varepsilon$. In fact, if $H^{(n)}(q) \neq N\varepsilon$ then $\left|\nabla H^{(n)}(x)\right| \neq 0 \ \forall x \in U_q \cap \Sigma_\varepsilon$, unless a zero in $\left|\nabla H^{(n)}(x)\right|$ comes from a stationary configuration which does not belong to the Ising class. According to our previous considerations, we suppose that non-Ising stationary configurations can be neglected in our analysis and so assumption (ii) follows in a natural way. The validity of assumptions (i) and (ii) will be discussed again in Chapter 5.

Using (i) and (ii), Eq. (3.1) becomes

$$\omega^{(n)}(\varepsilon) \simeq g^{(n)}(\varepsilon) \sum_p \delta\left[H^{(n)}(p) - N\varepsilon\right] . \tag{3.3}$$

The sum on the r.h.s. of Eq. (3.3) is over Ising configurations, so that it equals the density of states $\omega^{(1)}(\varepsilon)$ of the corresponding Ising model. We can thus write

$$\omega^{(n)}(\varepsilon) \simeq \omega^{(1)}(\varepsilon)\, g^{(n)}(\varepsilon) . \tag{3.4}$$

3.2 Critical energy densities

Were Eq. (3.4) exact, it would imply that if $\omega^{(1)}(\varepsilon)$ is nonanalytic at $\varepsilon = \varepsilon_c$, then also $\omega^{(n)}(\varepsilon)$ is nonanalytic at $\varepsilon = \varepsilon_c$ for any n, unless the function $g^{(n)}(\varepsilon)$ precisely cancels this nonanalyticity, which seems a rather special case. We do not expect Eq. (3.4) to be exact, even in the thermodynamic limit $N \to \infty$, unless, again, $g^{(n)}(\varepsilon)$ has some very special features: with a generic $g^{(n)}(\varepsilon)$ a density of states of the form (3.4) would not reproduce the known critical exponents of the O(n) universality classes [121]. However, it can be shown that a generic $g^{(n)}(\varepsilon)$ in Eq. (3.4) correctly implies a negative value for the specific heat critical exponent of O(n) spin models (i.e., the specific heat of continuous models does not diverge at criticality, but rather has a cusp-like behavior), see Sec. 5.1.3 and Appendix C.1. This is a common feature of O(n) models [121] and reinforces the belief that the approximation (3.4), although rather crude, may properly capture the main features of the nonanalyticities of the density of states when $N \to \infty$, as their location. Therefore we end up with the following[2]

Consequence 3.2.1. *If a O(n) spin model defined on a d-dimensional hypercubic lattice with Hamiltonian (2.1) and ferromagnetic interaction matrix $J_{ij} > 0$ has a phase transition, its critical energy density $\varepsilon_c^{(n)} = E_c^{(n)}/N$ is equal to that of the $n = 1$ case, i.e., a system of Ising spins with the same interactions.*

We stress that the above implication concerns the critical value of the control parameter of the microcanonical ensemble, the energy density, and says nothing about critical temperatures, which may well be different–and typically are–at different n. Let us now review some results reported in literature for the critical energy densities, in order to assess the reliability of this Consequence for some representatives of the O(n) class of models. The results for some specific models are reported in Table 3.1.

Table 3.1 shows that Consequence 3.2.1 is true for systems with long-range interactions on d-dimensional lattices, $J_{ij} = N^{(\alpha/d)-1}|i-j|^{-\alpha}$ with $0 \leq \alpha < d$; $\alpha = 0$ is the mean-field case of models defined on complete graphs with the same interaction strength between any two sites, $J_{ij} = 1/N$. As recalled in Sec. 2.1, all these systems have a mean-field-like phase transition

[2]Consequence 3.2.1 is stated as a Conjecture in [38].

Table 3.1: Comparison of critical energy densities $\varepsilon_c^{(n)}$ and critical temperatures T_c for ferromagnetic models with long-range (LR) interactions (first row) and nearest-neighbor interactions on a $1d$ chain (second row) and a $2d$ square lattice (third row).

model		$\varepsilon_c^{(n)}$	$T_c^{(n)}$	derivation method
LR	Ising	0	1	exact solution
	$O(n)$	0	$1/n$	exact solution [93]
$d=1$	Ising	-1	0	exact solution
	$O(n)$	-1	0	exact solution
$d=2$	Ising	-1.414...	2.269...	exact solution
	$O(2)$	-1.4457(4)	0.8929(1)	numerical [102, 103]

at the maximum value of ε, with critical temperatures $T_c^{(n)} = 1/n$ [93]. We stress again that critical energy densities are equal but critical temperatures are not[3] and depend on n.

In case of nearest-neighbor interactions, the energy density range is $\varepsilon \in [-d, d]$ with our choice of units. Consequence 3.2.1 is true for $d = 1$ at any n, although this case is somehow trivial because there is no transition at finite temperature.

In $d = 2$, the Mermin-Wagner theorem excludes the possibility of a phase transition with spontaneous symmetry breaking for any $n > 1$ but a transition between a disordered and a quasi-ordered phase occurs for $n = 2$ (XY model), the (BKT) transition [96,97]. In Table 3.1 we report the best recent estimate of the critical temperature obtained by Hasenbusch and coworkers (see e.g. [103] and references quoted therein) and the corresponding critical energy density (estimated from a Monte Carlo simulation of a system with 256×256 spins [102]). The difference between this value and the exact value of the critical energy density of the Ising model on a square lattice is around 2%. This difference, though small, appears significant since it is orders of magnitude larger than the statistical error on the numerical estimate of the energy.

[3] In the case of quantum mean-field Ising and Heisenberg models one has instead a complete thermodynamic equivalence, i.e., their canonical free energies are equal, although in the microcanonical ensemble this is no longer true: see [122, 123]

Based on this result one should conclude that the approximations involved to derive Consequence 3.2.1 are less reasonable in the $d = 2$ case than in the long-range or in the one-dimensional case. However, the comparison in $d = 2$ is between an exact result in the thermodynamic limit[4] and a numerical estimate of the energy on a finite lattice, whose statistical accuracy does not consider the systematic error due to the finite size effects, which could be quite large in this particular case [124, 125]. Moreover, also the precise determination of the critical temperature of the BKT transition is a subtle and difficult task due to its elusive nature. This is witnessed by the remarkable spread of values of $T_c^{(2)}$ reported in different papers [55]: the summary given in Ref. [124] shows that estimated critical temperatures vary in the interval $[0.88, 0.99]$ while Ref. [126] gave $[0.85, 0.95]$ as confidence interval for $T_c^{(2)}$. The energy values given in Ref. [102] corresponding to both these temperature intervals do contain the Ising value $\varepsilon_c^{(1)} = -\sqrt{2}$; for instance, the temperature interval $[0.85, 0.95]$ corresponds to $\varepsilon_c^{(2)} \in [-1.48, -1.38]$. We thus believe that the available data are not conclusive as far as a deeper comprehension of the implications of Eq. (3.4) and of assumptions (i) and (ii) is concerned, in this particular case. It is also worth noticing that despite the difference in the nature of the 2-d Ising and of the BKT transitions, the two-dimensional Ising and XY models do share a "weak universality" [128]. Indeed, the critical exponent ratio β/ν and the exponent δ are equal in the two cases [129]. It is tempting to think that energy landscape arguments like those discussed above may explain such a relation between the features of phase transitions so different from each other. However, more work has to be done to clarify these aspects and to extabilish possible connections between "weak universality" and Eq. (3.4); we then reserve a deeper investigation of the two-dimensional case for future work.

For nearest-neighbor interacting O(n) models in $d = 3$, the comparison is entirely between simulation outcomes, since no exact solution exists even for the Ising case. For every value of n, the models show a phase transitions with spontaneous symmetry breaking from an high-energy paramagnetic phase to a low-energy ferromagnetic phase. Before Consequence 3.2.1 was proposed, results reported in literature showed that the critical energies measured for O(n) spin systems with $n = 1, 2$ and 3 looked almost consistent, if one

[4]Exact values are $\varepsilon_c^{(1)} = -\sqrt{2}$ and $T_c^{(1)} = \frac{2}{\log(1+\sqrt{2})}$.

considered quoted errors as statistical errors; see [38] for a discussion on the point and [104–106] for the critical values of the energy densities for $n = 1, 2$ and 3, respectively.

Motivated by Consequence 3.2.1, we went beyond these numerical estimations by determining highly accurate critical values of the energy densities for three-dimensional O(n) models with $n = 2, 3$ and 4; this has been done performing a finite-size scaling analysis of the numerical data produced with long Monte Carlo simulations of the systems. The results of this numerical analysis are reported in [39] and will be discussed in the next Chapter.

For what concerns models in the first two-rows of Table 3.1, they will be analyzed in more detail in Chapter 5. In the particular cases of the mean-field and of the one-dimensional XY models an expression for $\omega^{(2)}$ similar to (3.4) will be derived analytically, that reduces to Eq. (3.4) for $\varepsilon \to \varepsilon_c$. Moreover, in Sec. 5.2 an approximation scheme originating from Eq. (3.4) will be introduced, such that the short-range O(n) models in $d \geq 2$ can be studied in a natural way. The approximation procedure will be explicitly tested on the XY model in $d = 2$.

Chapter 4

Critical energy densities of O(n) models in $d = 3$: a numerical study

In Sec. 3.1 an approximate relation between the densities of states of continuous and discrete spin models was conjectured. As a main consequence, the relation, given by Eq. (3.4), would imply the equality of the critical values of the energy densities of the O(n) models for every value of $n = 1, 2, 3 \ldots$ and, in principle, also in the $n \to \infty$ limit.

For generic values of n and d, the assumptions made in Chapter 3 to derive Eq. (3.4) are difficult to control in a rigorous way. Hence, two different aspects have to be checked with special care: the energy range of validity of the approximation, and the error made by replacing the critical energy $\varepsilon_c^{(n)}$ of the O(n) model, with $\varepsilon_c^{(1)}$, as Consequence 3.2.1 implies. The first aspect has been fully understood in the case of the mean-field and of the one-dimensional XY models [40] and it is part of the analytical study that will be presented in Chapter 5. The second aspect, instead, has been checked so far only at a numerical level and for O(n) models defined on regular cubic lattices. The results of the analysis are presented in [39] and will be discussed in this Chapter.

The present Chapter is structured as follows: assuming the critical energy density of the Ising model in three-dimensions is known with enough accuracy [130], in Sec. 4.1.1 we are going to determine the critical values of the energy densities of the O(2), O(3) and O(4) models in $d = 3$. These values will be computed, in the thermodynamic limit, through a finite-size scaling (FSS)

analysis whose basic relations will be presented in Sec. 4.1.1. As discussed in Chapter 3, rather accurate values of the critical energy densities for the O(n) models with $n = 2, 3$ and 4 are present in the literature. However, our analysis will improve the accuracy in most of these results; this fact represents a crucial requirement when Consequence 3.2.1 has to be tested with numerical techniques. In Sec. 4.1.6 the spherical model in $d = 3$ will be introduced since its thermodynamics is supposed to be equivalent to the one of an O(n) model in the $n \to \infty$ limit. The spherical model can be solved analytically in any spatial dimensions d and, in particular, in $d = 3$; this results will be relevant for our analysis. In Sec. 4.2 a careful comparison between the critical values of the energy densities of the above mentioned models will be performed; the concluding remarks on the analysis will be presented in Sec. 4.3.

4.1 Determination of the critical energy densities

The validity of Consequence 3.2.1 can be discussed by answering the following question: For every given value of $n \in [2, \infty]$, what is the difference between the critical value $\varepsilon_c^{(n)}$ of the energy density of the O(n) model and the critical value $\varepsilon_c^{(1)}$ of the energy density of the related Ising model?

Before starting our analysis some preliminary observations can be made. In $d = 3$, O(n) models are not exactly solvable[1] and their thermodynamics is known only through numerical studies. The numerical simulations have been limited so far only to those representatives of the O(n) class of models that can be easily tackled with numerical techniques and that are relevant for most problems in statistical physics; see i.e. [104–106, 131] for $n = 1, 2, 3$ and 4, respectively.

The common feature of these kind of analyses is that the algorithms applied are canonical ones. Hence, especially before Consequence 3.2.1 was proposed in [38], an accurate evaluation of the critical energy densities $\varepsilon_c^{(n)}$ was out of the scope of the works, and the computation of $\varepsilon_c^{(n)}$ was usually a byproduct of a more general task possibly focused on the determination

[1] But in the case $n \to \infty$, that will be discussed in Sec. 4.1.6.

of other parameters, such as the critical temperatures $T_c^{(n)}$ or the critical exponents.

The aim of our study is to give an answer to the question raised by Consequence 3.2.1 in $d = 3$. To this end, we have to estimate accurate critical values of energy density $\varepsilon_c^{(n)}$ for as many O(n) models as possible and to compare them in the whole range $n \in [1, \infty]$. We then start performing a finite-size scaling (FSS) analysis of the critical energy density values of classical O(n) models with $n = 2, 3$ and 4. The case $n = 1$ has already been studied with high accuracy by Hasenbusch and Pinn in [130] and we will simply recall their results in Sec. 4.1.2.

The FSS analyses rely on numerical data computed with accurate canonical Monte Carlo simulations that make use of the optimized cluster algorithm `spinmc` for classical O(n) spin models, provided by the ALPS project [132]. The simulations were run in part on the PLX machine in the CINECA cluster in Casalecchio di Reno (Bologna) and in part on the cluster farm provided by the department of physics and astronomy of Università degli Studi di Firenze, in Sesto Fiorentino (Firenze), see Appendix B for details.

For each O(n) model, the simulations have been performed at the value of the critical temperature $T_c^{(n)}$, given in the literature with an uncertainty $\Delta T_c^{(n)}$. This quantity has to be taken into account in the computation of $\Delta\varepsilon_c^{(n)}$ and the propagation procedure needs the evaluation of the critical value of the specific heat. For this reason, in the Monte Carlo simulations, besides collecting the values of the energy densities we also computed the critical values of the specific heat. The FSS procedure and the uncertainties propagation-procedure will be discussed in the following section.

4.1.1 Finite-size scaling analysis

Let us denote by $\varepsilon_c^{(n)}(L)$ and $c^{(n)}(L)$ the critical values of the energy density and of the specific heat, respectively, of an O(n) model defined on a regular cubic lattice of edge $L = \sqrt[3]{N}$. The relation between $\varepsilon_c^{(n)}(L)$ and $\varepsilon_c^{(n)}(\infty) = \varepsilon_c^{(n)}$ is given by the FSS equation

$$\varepsilon_c^{(n)}(L) = \varepsilon_c^{(n)} + \varepsilon_n \, L^{\frac{\alpha_n - 1}{\nu_n}}. \tag{4.1}$$

An analogous expression holds for the specific heat, and it is given by

$$c^{(n)}(L) = c_c^{(n)} + c_n \, L^{\frac{\alpha_n}{\nu_n}} \tag{4.2}$$

where $c_c^{(n)} = c_c^{(n)}(\infty)$ denotes the critical value of the specific heat in the thermodynamic limit. In Eqs. (4.1) and (4.2), ε_n and c_n are model dependent fit parameters while α_n and ν_n are the specific heat and the correlation length canonical critical exponents, respectively. We are not discussing here the derivation of Eqs. (4.1) and (4.2), we instead refer the reader to the existing literature for an in-depth analysis on the subject; see i.e. [133–135] for reviews and [136] for an explicit derivation of Eqs. (4.1) and (4.2) for $n = 2$.

For every O(n) model, the critical energy density $\varepsilon_c^{(n)} \pm \Delta\varepsilon_c^{(n),stat}$ can be determined with a fit of the Monte Carlo data $\varepsilon_c^{(n)}(L)$ according to Eq. (4.1); here and in the following $\Delta\varepsilon_c^{(n),stat}$ will denote the statistical uncertainty on $\varepsilon_c^{(n)}$ due to the fitting procedure.

Since our purpose is to compare the values of $\varepsilon_c^{(n)}$ for different n, every source of error in the determination of $\Delta\varepsilon_c^{(n)}$ has to be checked separately. The fact that the energy data $\varepsilon_c^{(n)}(L)$ are computed with Monte Carlo simulations performed at $T_c^{(n)}$ becomes relevant. Indeed, the critical temperatures are provided in literature with an uncertainty $\Delta T_c^{(n)}$ whose effect in the determination of $\Delta\varepsilon_c^{(n)}$ has to be checked with special care. As a matter of fact, $\Delta T_c^{(n)}$ can be seen as the analogoue of a systematic source of error in an experimental setting; we will then denote by $\Delta\varepsilon_c^{(n),syst}$ its contribution to $\Delta\varepsilon_c^{(n)}$. The two contributions, $\Delta\varepsilon_c^{(n),stat}$ and $\Delta\varepsilon_c^{(n),syst}$, to the uncertainty $\Delta\varepsilon_c^{(n)}$ of $\varepsilon_c^{(n)}$ will be discussed separately in the following, and the final value of $\varepsilon_c^{(n)}$ will be given by

$$\varepsilon_c^{(n)} \pm \Delta\varepsilon_c^{(n)} = \varepsilon_c^{(n)} \pm \Delta\varepsilon_c^{(n),stat} \pm \Delta\varepsilon_c^{(n),syst}. \tag{4.3}$$

Once $\varepsilon_c^{(n)}$ is computed with the FSS analysis, $\Delta\varepsilon_c^{(n),syst}$ can be determined with two different methods. In both cases the critical value $c_c^{(n)}$ of the specific heat is necessary and will be computed with a fit[2] of the Monte Carlo data $c_c^{(n)}(L)$ according to Eq. (4.2). The two methods applied to compute $\Delta\varepsilon_c^{(n),syst}$ are the following.

- *Method 1.*

$$\Delta\bar{\varepsilon}_c^{(n),syst} = |\varepsilon_c^{(n)} - \bar{\varepsilon}_+^{(n)}| = |\varepsilon_c^{(n)} - \bar{\varepsilon}_-^{(n)}|. \tag{4.4}$$

[2]For $c_c^{(n)}$ only the statistical error $\Delta c_c^{(n),stat}$ will be computed since the interest in this quantity is only for the computation of $\Delta\varepsilon_c^{(n),syst}$.

$\bar{\varepsilon}_{\pm}^{(n)}$ denote the energy densities at $T_{\pm}^{(n)} = T_c^{(n)} \pm \Delta T_c^{(n)}$, computed with a first order Taylor expansion around $\varepsilon_c^{(n)}$; that is,

$$\begin{aligned}\bar{\varepsilon}_{\pm}^{(n)} =& \varepsilon_c^{(n)}\Big|_{T=T_c^{(n)}} + \frac{d\varepsilon}{dT}\Big|_{T=T_c^{(n)}} \left[\left(T_c^{(n)} \pm \Delta T_c^{(n)}\right) - T_c^{(n)}\right] = \\ =& \varepsilon_c^{(n)} \pm c_c^{(n)}\ \Delta T_c^{(n)}.\end{aligned} \tag{4.5}$$

- *Method 2.*

$$\Delta\tilde{\varepsilon}_c^{(n),syst} = \cdot^{|\varepsilon_c^{(n)} - \tilde{\varepsilon}_+^{(n)}|}_{|\varepsilon_c^{(n)} - \tilde{\varepsilon}_-^{(n)}|}, \tag{4.6}$$

with $\tilde{\varepsilon}_{\pm}^{(n)}$ denoting again the energy density values at $T_{\pm}^{(n)}$; at variance with $\bar{\varepsilon}_{\pm}^{(n)}$, $\tilde{\varepsilon}_{\pm}^{(n)}$ are computed with a fit of the energy density data $\tilde{\varepsilon}_{\pm}^{(n)}(L)$ at $T_{\pm}^{(n)}$. The values of $\tilde{\varepsilon}_{\pm}^{(n)}(L)$ for certain system sizes are computed with a first order Taylor expansion of the experimental data $\varepsilon_c^{(n)}(L)$ through the relation

$$\begin{aligned}\tilde{\varepsilon}_{\pm}^{(n)}(L) &= \varepsilon^{(n)}(L)\Big|_{T=T_c^{(n)}} + c_c^{(n)}(L)\Big|_{T=T_c^{(n)}} \left[\left(T_c^{(n)} \pm \Delta T_c^{(n)}\right) - T_c^{(n)}\right] = \\ &= \varepsilon^{(n)}(L) \pm c_c^{(n)}(L)\ \Delta T_c^{(n)},\end{aligned} \tag{4.7}$$

and for other system sizes, namely for $L = 32, 64$ and 128, numerically, by performing Monte Carlo simulations of the systems at $T_{\pm}^{(n)}$.

In the end, the fitting procedure is applied according to the relation[3]

$$\tilde{\varepsilon}_{\pm}^{(n)}(L) = \tilde{\varepsilon}_{\pm}^{(n)} + \varepsilon_{n,\pm} L^{D_n} \tag{4.8}$$

with $D_n = \frac{\alpha_n - 1}{\nu_n}$ as in Eq. (4.1).

At the end of the analysis, $\Delta\bar{\varepsilon}_c^{(n),syst}$ and $\Delta\tilde{\varepsilon}_c^{(n),syst}$ will be compared. According to the level of accuracy achieved, one of them will be chosen as final estimate of $\Delta\varepsilon_c^{(n),syst}$.

[3] Eqs. (4.1) and Eq. (4.8) hold for $T = T_c^{(n)}$. However, since $\frac{\Delta T_c^{(n)}}{T_c^{(n)}} \sim 10^{-5}$ for the models considered, we assume Eq. (4.8) is valid in the whole range $T \in \left[T_c^{(n)} - \Delta T_c^{(n)}, T_c^{(n)} + \Delta T_c^{(n)}\right]$.

4.1.2 $n = 1$, the Ising model

The derivation of the critical energy density $\varepsilon_c^{(1)}$ for the three-dimensional Ising model can be found in [130]. The authors performed a FSS analysis of data computed with canonical Monte Carlo simulations of the system, considering lattices up to 112^3 spins. The best final estimate of the critical energy density is given by

$$\varepsilon_c^{(1)} \pm \Delta\varepsilon_c^{(1)} = -0.99063 \pm 0.00004\,. \tag{4.9}$$

The above result has been computed by Hasenbusch et al. in [130] considering system sizes close to the maximum size achievable with our tools and represents one of the most accurate estimate of $\varepsilon_c^{(1)}$ available in the literature (see i.e. [105] for a comparison). Moreover, the uncertainty $\Delta\varepsilon_c^{(1)}$ in Eq. (4.9) has been computed combining the statistical and the systematic errors as we have discussed in the previous Section. These facts led us not to repeat the analysis on the Ising model and to consider Eq. (4.9) as the best final estimate of $\varepsilon_c^{(1)}$. We will come back on this point in Sec. 4.3.

4.1.3 $n = 2$, the XY model

We performed canonical Monte Carlo simulations of the XY model defined on regular cubic lattices with edges $L = 32, 40, 50, 64, 80, 100$ and 128. The simulations have been performed at the critical value of the temperature $T_c^{(2)} = 2.201673(97)$ reported in [104] and the technical details are summarized in Sec. B.1.1 of Appendix B. The values for $\varepsilon_c^{(2)}(L)$ and $c_c^{(2)}(L)$ obtained from the simulations are reported in Table 4.1: in parentheses are the statistical errors.

We fitted the energy density data in Table 4.1 according to the relation (4.1) and with different choices for the critical exponents: (*i*) the experimental values $\nu_2 = 0.6705(6)$ and $\alpha_2 = -0.0115(18)$ as reported in [137]; (*ii*) $\nu_2 = 0.662(7)$ obtained in [104] at the same critical value of the temperature as in our case and $\alpha_2 = -0.014(21)$ as derived from the scaling relation $\alpha_2 = 2 - d\nu_2$ with $d = 3$; (*iii*) $\nu_2 = 0.6723(3)[8]$ obtained in [138] with an high statistics simulation at a slightly different value of the critical temperature and $\alpha_2 = -0.017(3)$ as derived from the scaling relation $\alpha = 2 - d\nu$ with $d = 3$; (*iv*) $\alpha_2/\nu_2 = -0.0258(75)$ and $1/\nu_2 = 1.487(81)$ as obtained in [136] with an analogous analysis. The results of the fits for $\varepsilon_c^{(2)}$ and for the fitting parameter ε_2 are reported in Table 4.2.

Table 4.1: Monte Carlo results for the energy density $\varepsilon_c^{(2)}(L)$ and for the specific heat $c_c^{(2)}(L)$ at the critical temperature $T_c^{(2)} = 2.201673$.

L	$\varepsilon_c^{(2)}(L)$	$c_c^{(2)}(L)$
32	-0.9982(3)	2.611(31)
40	-0.99589(12)	2.709(18)
50	-0.99382(9)	2.825(24)
64	-0.99233(14)	2.923(59)
80	-0.99137(6)	3.074(34)
100	-0.99067(4)	3.199(38)
128	-0.99020(4)	3.282(54)

Table 4.2: Fitting values of the parameters $\varepsilon_c^{(2)}$ and ε_2 entering expression (4.1).

Fitting parameters	constants	results	$\chi^2/d.o.f$
$\varepsilon_c^{(2)}$, ε_2	$\nu_2 = 0.6705$ $\alpha_2 = -0.0115$	$\varepsilon_c^{(2)} = -0.98900(3)$ $\varepsilon_2 = -1.77(2)$	0.60
$\varepsilon_c^{(2)}$, ε_2	$\nu_2 = 0.662$ $\alpha_2 = -0.014$	$\varepsilon_c^{(2)} = -0.98904(3)$ $\varepsilon_2 = -1.92(2)$	0.57
$\varepsilon_c^{(2)}$, ε_2	$\nu_2 = 0.6723$ $\alpha_2 = -0.017$	$\varepsilon_c^{(2)} = -0.98901(3)$ $\varepsilon_2 = -1.79(2)$	0.59
$\varepsilon_c^{(2)}$, ε_2	$\alpha_2/\nu_2 = -0.0258$ $1/\nu_2 = 1.487$	$\varepsilon_c^{(2)} = -0.98901(3)$ $\varepsilon_2 = -1.79(2)$	0.59

We also performed a four-parameters fit considering α_2, ν_2, $\varepsilon_c^{(2)}$ and ε_2 as fitting parameters. However, no meaningful results could be extracted from the fit, the relative error on the parameters being larger than 100% on the critical exponents (data not shown).

All the fitting results reported in Table 4.2 have a $\chi^2/d.o.f \sim 0.6$ and the values of the critical energy densities $\varepsilon_c^{(2)}$ are all consistent with each other. This fact implies that $\varepsilon_c^{(2)}$ is rather insensitive to the choice of the critical exponents (and so to the values of the critical temperatures at which they have been computed). Anyway, as best estimate of the fitting parameters we chose:

$$\begin{aligned} \varepsilon_c^{(2)} \pm \Delta\varepsilon_c^{(2),stat} &= -0.98904 \ \pm \ 0.00003\,, \\ \varepsilon_2 &= -1.92 \ \pm \ 0.02 \end{aligned} \tag{4.10}$$

as reported in the second row of Table 4.2. These values correspond to a

choice of the critical exponents given by $\nu_2 = 0.662$ and $\alpha_2 = -0.014$ as derived in [104] at the same value of $T_c^{(2)}$ as in our case. The curve $\varepsilon_c^{(2)}(L)$ given by Eq. (4.1) for $n = 2$ and with the values of $\varepsilon_c^{(2)}$ and ε_2 as in Eq. (4.10), is shown in Fig. 4.1 together with the numerical data used in the analysis. The values of $\varepsilon_c^{(2)}$ and ε_2 reported in Eq. (4.10) are consistent with the same quantities reported in [136] where authors find $\varepsilon_c^{(2)} = -0.9890(4)$ and $\varepsilon_2 = -1.81(38)$ once adapted to our conventions[4]. It is worth noticing that our value of $\varepsilon_c^{(2)} = -0.98904(3)$ in Eq. (4.10) has a precision of one digit more with respect to the previous results present in literature and obtained with analogous techniques, see i.e. [136].

We fitted data of $c_c^{(2)}(L)$ reported in Table 4.1 according to the scaling relation given in Eq. (4.2) and keeping the value of the ratio α_2/ν_2 constant and equal to $\alpha_2/\nu_2 = -0.02$, as given in [104]. The result of the fit is reported in the first row of Table 4.3. To check the dependence of the specific heat on the value of the ratio α_2/ν_2, we also performed the same fit for different choices of the critical exponents: (*i*) $\alpha_2/\nu_2 = -0.0285$ as reported in [136]; (*ii*) $\alpha_2/\nu_2 = -0.025$ as obtained from data in [138]; (*iii*) $\alpha_2/\nu_2 = -0.0172$ as obtained from the numerical values of the critical exponents in [137]. The results of the fits for $c_c^{(2)}$ and c_2 with these choices of the critical exponents are reported in the second, third and forth row of Table 4.3, respectively.

Although the values of $c_c^{(2)}$ reported in Table 4.3 are not all consistent with each other, the results in the first three rows are comparable. Moreover, our results for $\alpha_2/\nu_2 = -0.0285$ are in agreement with the results computed in [136] for the same choice of the ratio of the critical exponents. Indeed, authors found $c_c^{(2)} = 20.45(66)$ and $c_2 = -19.61(72)$ with a fit based on data derived form Monte Carlo simulations at a different value of the critical temperature. Interestingly the values of the fitting parameters $c_c^{(2)}$ and c_2 are slightly larger than the others when experimentally determined critical exponents $\nu_2 = 0.6705$ and $\alpha_2 = -0.0115$ [137] are considered, see the last row of Table 4.3. This fact has been already pointed out in [136] where authors found $c_c^{(2)} = 30.3 \pm 1.0$ and $c_2 = -29.4 \pm 1.1$ for the same choice of the critical exponents. These results suggest that the value of $c_c^{(2)}$ strongly depends on the value of the ratio α_2/ν_2. In [136] authors considered lattice

[4] In [136] the definition of the energy density is such that $\varepsilon_c^{(2)} = E_0 - 3$ and $\varepsilon_2 = E_1$ with E_0 and E_1 as defined in [136].

sizes up to $L = 80$ and suggested that a wider range of lattice sizes should be necessary to determine the asymptotic value of $c_c^{(2)}$. In our analysis we considered lattices sizes up to $L = 128$, that is almost 4 times bigger than in [136], but the discrepancy is still visible. Lattice sizes bigger than 128^3 spins may be needed to improve the estimate of $c_c^{(2)}$. For our purposes, we can consider

$$\begin{aligned} c_c^{(2)} \pm \Delta c_c^{(2)} &= 28.4 \pm 0.6\,, \\ c_2 &= -27.7 \pm 0.7 \end{aligned} \tag{4.11}$$

as best final estimate values for the fitting parameters. These quantities, in fact, derive from the fit with $\alpha_2/\nu_2 = -0.02$ as obtained in [104] at the same value of $T_c^{(2)} = 2.201673$ as in our case. We refer the reader to [136] for a more detailed discussion on the problem. The curve $c_c^{(2)}(L)$ given by

Table 4.3: Fitting values of the parameters $c_c^{(2)}$ and c_2 entering expression (4.2).

Fitting parameters	constants	results	$\chi^2/d.o.f$
$c_c^{(2)}$, c_2	$\alpha_2/\nu_2 = -0.02$	$c_c^{(2)} = 28.4 \pm 0.6$ $c_2 = -27.7 \pm 0.7$	0.2
$c_c^{(2)}$, c_2	$\alpha_2/\nu_2 = -0.0258$	$c_c^{(2)} = 22.7 \pm 0.5$ $c_2 = -21.9 \pm 0.5$	0.2
$c_c^{(2)}$, c_2	$\alpha_2/\nu_2 = -0.025$	$c_c^{(2)} = 23.3 \pm 0.5$ $c_2 = -22.6 \pm 0.6$	0.2
$c_c^{(2)}$, c_2	$\alpha_2/\nu_2 = -0.0172$	$c_c^{(2)} = 32.5 \pm 0.7$ $c_2 = -31.8 \pm 0.8$	0.2

Eq. (4.2) for $n = 2$ with $c_c^{(2)}$ and c_2 as in Eq. (4.11), is plotted in Fig. 4.2 together with the numerical data.

In order to evaluate $\Delta\varepsilon_c^{(2),syst}$, we applied the two methods presented in Sec. 4.1.1.

- *Method 1.* From Eq. (4.5), we computed $\bar{\varepsilon}_+^{(2)}$ and $\bar{\varepsilon}_-^{(2)}$ at $T_+^{(2)} = 2.20177$ and $T_-^{(2)} = 2.201576$, respectively, assuming $\varepsilon_c^{(2)} = -0.98904$ as reported in Eq. (4.10). These quantities are given by $\bar{\varepsilon}_+^{(2)} = -0.98629$ and $\bar{\varepsilon}_-^{(2)} = -0.99180$ and are such that $|\varepsilon_c^{(2)} - \bar{\varepsilon}_+^{(2)}| = |\varepsilon_c^{(2)} - \bar{\varepsilon}_-^{(2)}| \simeq 0.003$. We then get

$$\Delta\bar{\varepsilon}_c^{(2),syst} = |\varepsilon_c^{(2)} - \bar{\varepsilon}_\pm^{(2)}| = 0.003. \tag{4.12}$$

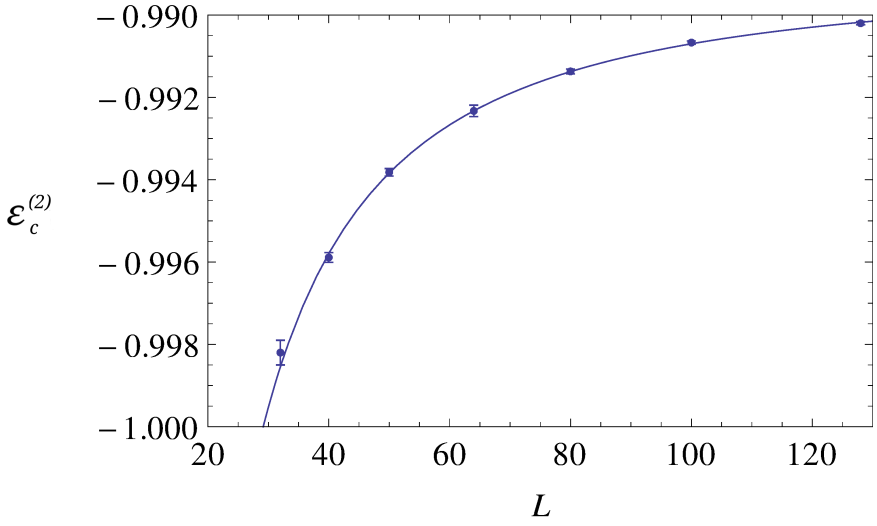

Figure 4.1: The energy density $\varepsilon_c^{(2)}(L)$ at the critical temperature $T_c^{(2)} = 2.201673$ as a function of L. The solid curve represents the fit to (4.10) with $\nu_2 = 0.662$ and $\alpha_2 = -0.014$.

- *Method 2.* We computed $\tilde{\varepsilon}_{\pm}^{(2)}$ with a fit of the energy density values $\tilde{\varepsilon}_{\pm}^{(2)}(L)$ for $L = 40, 50, 80$ and 100 at $T_+^{(2)} = 2.20177$ and $T_-^{(2)} = 2.201576$, respectively, according to relation in Eq. (4.8) with $n = 2$ and $D_2 = -1.5317$ as derived from data in [104]. $\tilde{\varepsilon}_{\pm}^{(2)}(L)$ for these $L-$values are computed with Eq. (4.7) from data given in Table 4.1.

  For some particular values of L, namely for $L = 32, 64$ and 128, we performed high-accurate canonical Monte Carlo simulations at $T_+^{(2)}$ and $T_-^{(2)}$, respectively, to compute the numerical values $\varepsilon_{\pm}^{(2)}(32)$, $\varepsilon_{\pm}^{(2)}(64)$ and $\varepsilon_{\pm}^{(2)}(128)$. The numerical results have been compared with the same quantities as derived with the Taylor expansion (4.7) and appeared to be consistent with them. This result reinforce the robustness of the analytical procedure implied to derive $\Delta\tilde{\varepsilon}_c^{(2),syst}$ and we considered the experimental values $\varepsilon_{\pm}^{(2)}(32)$, $\varepsilon_{\pm}^{(2)}(64)$ and $\varepsilon_{\pm}^{(2)}(128)$ in the fitting procedure for the derivation of $\tilde{\varepsilon}_{\pm}^{(2)}$. The data involved in the analysis are given in Table 4.4 in which we denote in **bold** data derived from Monte Carlo simulations and in plain text data derived with the Taylor expansion (4.7). The results of the fits are reported in Table 4.5; we get

$$\Delta\tilde{\varepsilon}_c^{(2),syst} = \cdot^{|\varepsilon_c^{(2)} - \tilde{\varepsilon}_+^{(2)}|}_{|\varepsilon_c^{(2)} - \varepsilon_-^{(2)}|} = \cdot^{0.0003}_{0.0003} = 0.0003. \tag{4.13}$$

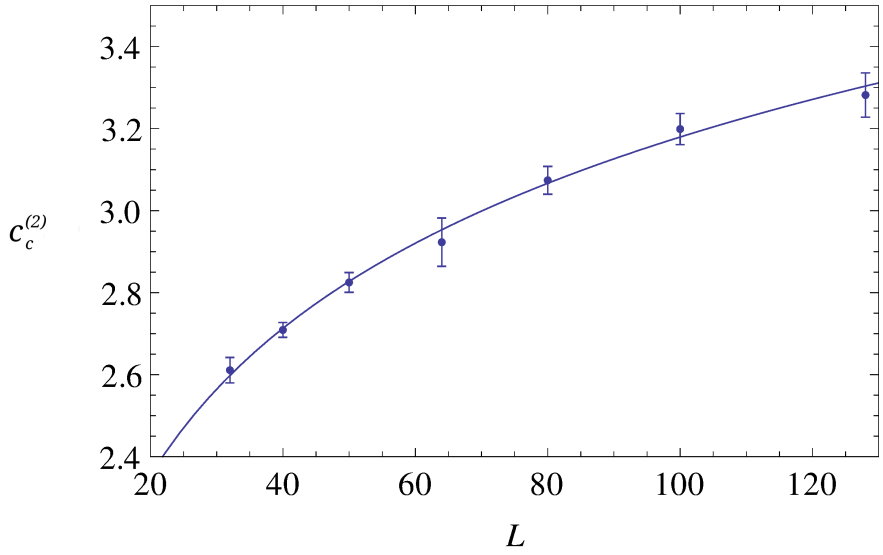

Figure 4.2: The specific heat $c_c^{(2)}(L)$ at the critical temperature $T_c^{(2)} = 2.201673$ as a function of L. The solid curve represents the fit to (4.11) with $\alpha_2/\nu_2 = -0.02$.

In Sec. 4.2 we are going to compare the critical values of the energy density of different O(n) models both in the limit of small n and in the limit $n \to \infty$; we should then consider $\Delta\varepsilon_c^{(2),syst} = \Delta\bar{\varepsilon}_c^{(2),syst}$ given in Eq. (4.12), being the largest among the two different estimates of the systematic uncertainties in Eqs. (4.12) and (4.13). However, this result depends on the value of $c_c^{(2)}$ given in Eq.(4.11) that, in turn, is strictly affected by the choice of the ratio α_2/ν_2. For this reason we prefer to consider $\Delta\tilde{\varepsilon}_c^{(2),syst}$ in Eq. (4.13) as best estimate of $\Delta\varepsilon_c^{(2),syst}$. We finally have

$$\varepsilon_c^{(2)} \pm \Delta\varepsilon_c^{(2),stat} \pm \Delta\varepsilon_c^{(2),syst} = -0.98904 \ \pm \ 0.00003 \ \pm \ 0.0003. \qquad (4.14)$$

as final best estimate for the critical energy density of the O(2) model in three-dimensions. The uncertainty $\Delta\varepsilon_c^{(2),syst}$ due to $\Delta T_c^{(2)}$ is one order of magnitude larger than the statistical error. This feature will be in common with all the other models considered.

4.1.4 $n = 3$, the Heisenberg model

We performed canonical Monte Carlo simulations of the Heisenberg model defined on a regular cubic lattices with edges $L = 32, 40, 50, 64, 80, 100$ and 128. As best estimate of the critical temperature of the system we considered

Table 4.4: Energy density data $\varepsilon_+^{(2)}$ and $\varepsilon_-^{(2)}$ obtained via Taylor expansion and numerical Monte Carlo simulations (**bold**), at $T_+^{(2)} = 2.20177$ and $T_-^{(2)} = 2.201576$, respectively.

L	$\varepsilon_+^{(2)}(L)$	$\varepsilon_-^{(2)}(L)$
32	**-0.99854(15)**	**-0.9984(3)**
40	-0.99563(12)	-0.99615(12)
50	-0.99355(9)	-0.99409(9)
64	**-0.99197(7)**	**-0.99270(7)**
80	-0.99107(6)	-0.99167(6)
100	-0.99036(4)	-0.99098(4)
128	**-0.98994(4)**	**-0.99049(4)**

Table 4.5: Fitting values of the parameters $\varepsilon_\pm^{(2)}$ and $\varepsilon_\pm^{(2)}$. In parentheses are the statistical errors due to the fitting procedure.

Fitting parameters	constants	results	$\chi^2/d.o.f$
$\varepsilon_+^{(2)}$, $\varepsilon_{2,+}$	$D_2 = -1.5317$	$\varepsilon_+^{(2)} = -0.98871(5)$ $\varepsilon_{2,+} = -1.95(3)$	1.46
$\varepsilon_-^{(2)}$, $\varepsilon_{2,-}$	$D_2 = -1.5317$	$\varepsilon_-^{(2)} = -0.98935(4)$ $\varepsilon_{2,-} = -1.91(3)$	0.8

the value $T_c^{(3)} = 1.44298(2)$ given in [106]; the details of the simulations are reported in Sec. B.1.2 of Appendix B. The values for $\varepsilon_c^{(3)}(L)$ and $c_c^{(3)}(L)$ obtained from the simulations are reported in Table 4.6: in parentheses are the statistical errors.

We fitted data reported in Table 4.6 according to relation (4.1) with $n = 3$ and considering $\varepsilon_c^{(3)}$ and ε_3 as fitting parameters. For the values of the critical exponents, we considered different choices: (*i*) the best theoretical estimates $\nu_3 = 0.705(3)$ and $\alpha_3 = -0.115(9)$ coming from a re-summed perturbation series analysis, [139]; (*ii*) we kept the value of $D_3 = (\alpha_3 - 1)/\nu_3$ in Eq. (4.1) constant to $D_3 = (\alpha_3 - 1)/\nu_3 = -1.586(19)$ as obtained in [140] from analogous analysis performed at $T_c = 1.4430$; (*iii*) we considered $D_3 = (\alpha_3 - 1)/\nu_3 = -1.5974$ as derived in [106] from analogous analysis performed at the same value of $T_c^{(3)}$ as in our case. The results of the fits for $\varepsilon_c^{(3)}$ and ε_3 are reported in Table 4.7.

We also performed a fit of all the parameters $\varepsilon_c^{(3)}$, ε_3 and D_3 with the scaling relation $\varepsilon_c^{(3)}(L) = \varepsilon_c^{(3)} + \varepsilon_3 L^{D_3}$. The results are given by $\varepsilon_c^{(3)} =$

Table 4.6: Monte Carlo results for the energy density $\varepsilon_c^{(3)}(L)$ and for the specific heat $c_c^{(3)}(L)$ at the critical temperature $T_c^{(3)} = 1.44298$.

L	$\varepsilon_c^{(3)}(L)$	$c_c^{(3)}(L)$
32	-0.99646(7)	2.863(15)
40	-0.99437(6)	2.938(19)
50	-0.99289(5)	3.030(19)
64	-0.99183(4)	3.126(23)
80	-0.99116(3)	3.197(28)
100	-0.99064(3)	3.259(32)
128	-0.990312(14)	3.367(28)

Table 4.7: Fitting values of the parameters $\varepsilon_c^{(3)}$ and ε_3 entering expression (4.1).

Fitting parameters	constants	results	$\chi^2/d.o.f$
$\varepsilon_c^{(3)}$, ε_3	$\nu_3 = 0.705$ $\alpha_3 = -0.115$	$\varepsilon_c^{(3)} = -0.989537(12)$ $\varepsilon_3 = -1.652(10)$	0.52
$\varepsilon_c^{(3)}$, ε_3	$D_3 = -1.586$	$\varepsilon_c^{(3)} = -0.989542(11)$ $\varepsilon_3 = -1.677(10)$	0.48
$\varepsilon_c^{(3)}$, ε_3	$D_3 = -1.5974$	$\varepsilon_c^{(3)} = -0.989556(10)$ $\varepsilon_3 = -1.744(9)$	0.40

$-0.98958(3)$, $\varepsilon_3 = -1.88(17)$ and $D_3 = -1.62(2)$ with a $\chi^2/d.o.f \sim 0.43$. These results are in agreement with those reported in Table 4.7 and with the results reported in literature, see i.e. [106, 140]. However, as they come from a three-parameters fit of a relative small set of experimental data, we chose to neglect them and to consider only results reported in Table 4.7 in our study.

The values of the parameters reported in the second row of Table 4.7 are consistent with the correspondent quantities reported in [140]. In there, authors give $\varepsilon_c^{(3)} = -0.9894(1)$, $\varepsilon_3 = -1.68(8)$ and $D_3 = -1.586(19)$ once adapted to our conventions[5]. These values come from a three parameter fit of the scaling relation $\varepsilon_c^{(3)}(L) = \varepsilon_c^{(3)} + \varepsilon_3 L^{D_3}$ with $D_3 = (\alpha_3 - 1)/\nu_3$, performed at $T_c = 1.4430 \neq T_c^{(3)}$. Beside supporting our results, this fact

[5]In [140] authors use a different notation with respect to ours. In particular: $\varepsilon_c^{(3)} = < e >^{reg} -3$ and $\varepsilon_3 = -d_0$.

seems to suggest that $\varepsilon_c^{(3)}$ does not depend too much on the value of the critical temperature.

For what concerns the third row of Table 4.7, the results of the fit have to be compared with the results computed in [106] at the same value of $T_c^{(3)}$ as in our case. In there, authors find

$$\varepsilon_c^{(3)}(L) = \varepsilon_c^{(3)} + \varepsilon_3 L^{D_3} \approx -0.9896 \pm 1.7225 L^{-1.5974} \tag{4.15}$$

once adapted to our conventions; the relative precision of the data fit being of 0.001% or better. Also in this case our results, obtained for $D_3 = -1.5974$, are perfectly consistent.

The values of the parameter $\varepsilon_c^{(3)}$ reported in Table 4.7 are consistent with each other. The results reported in the third row of Table 4.7 have been determined considering a combination of the critical exponents D_3 as derived in [106] at the same value of the critical temperature as in our case. Since the numerical value of α_3/ν_3 will be needed to determine $c_c^{(3)}$, we give

$$\begin{gathered} \varepsilon_c^{(3)} \ \pm \ \Delta\varepsilon_c^{(3),stat} = -0.989556 \ \pm \ 0.000010\,, \\ \varepsilon_3 = -1.744(9) \end{gathered} \tag{4.16}$$

as best estimate of the critical energy density value of $\varepsilon_c^{(3)}$. The curve $\varepsilon_c^{(3)}(L)$ given by Eq. (4.1) for $n = 3$ and with the values of $\varepsilon_c^{(3)}$ and ε_3 as in Eq. (4.16), is shown in Fig. 4.3 together with the numerical data used in the analysis. It is worth noticing that the value of $\varepsilon_c^{(3)}$ in Eq. (4.16) is given with a precision of one digit more with respect to the previous results in literature and obtained with analogous techniques, see i.e [106, 140].

We fitted data of $c_c^{(3)}(L)$ reported in Table 4.6 according to the scaling relation in Eq.(4.2) with $\alpha_3/\nu_3 = -0.1991$ as in reported [106]. The results of the fit are shown in the first row of Table 4.8. To check the dependence of our results from the ratio α_3/ν_3 we performed the same fit for two different choices of α_3/ν_3: (*i*) $\alpha_3/\nu_3 = -0.1631$ as derived in [139] and (*ii*) $\alpha_3/\nu_3 = -0.166$ as derived in [140]. The results of these fits are reported in the second and third rows of Table 4.8, respectively. At variance with what happens for the XY model, the values of the fitting parameters $c_c^{(3)}$ are consistent with each other and with the results in literature, see i.e. [106, 140]. The same holds for c_3. Interestingly, this fact is true for every choice of the ratio α_3/ν_3 suggesting that, for O(3) models, system sizes up to 128^3 spins are already large enough to infer the value of the specific heat in the thermodynamic

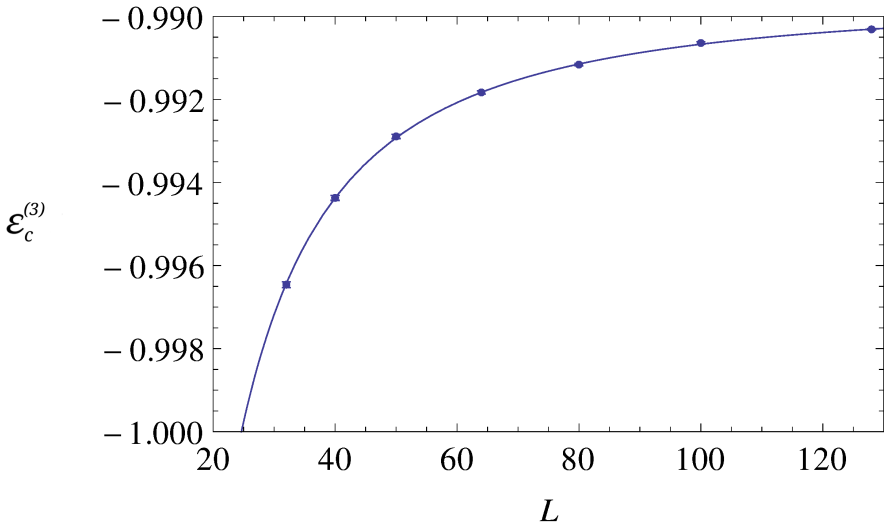

Figure 4.3: The energy density $\varepsilon_c^{(3)}(L)$ at the critical temperature $T_c^{(3)} = 1.4498$ as a function of L. The solid curve represents the fit to (4.16) with $(\alpha_3 - 1)/\nu_3 = -1.5974$.

limit. We choose

$$\begin{aligned} c_c^{(3)} &= 4.91(3)\,, \\ c_3 &= -4.09(9) \end{aligned} \tag{4.17}$$

as the best choice of the fitting parameters, being associated to a choice of the critical exponents derived in [106] at the same value of $T_3^{(3)}$ as in our case. The curve $c_c^{(3)}(L)$ given by Eq. (4.2) for $n = 3$ and the values of the fitting parameters $c_c^{(3)}$ and c_3 as in Eq. (4.17), is shown in Fig. 4.4 together with the numerical data used in the analysis.

Table 4.8: Fitting values of the parameters $c_c^{(3)}$ and c_3 entering expression (4.1) with $n = 3$.

Fitting parameters	constants	results	$\chi^2/d.o.f$
$c_c^{(3)}$, c_3	$\alpha_3/\nu_3 = -0.1991$	$c_c^{(3)} = 4.91(3)$ $c_2 = -4.09(9)$	0.18
$c_c^{(3)}$, c_3	$\alpha_3/\nu_3 = -0.1631$	$c_c^{(3)} = 5.31(5)$ $c_3 = -4.32(8)$	0.15
$c_c^{(3)}$, c_3	$\alpha_3/\nu_3 = -0.166$	$c_c^{(3)} = 5.27(4)$ $c_3 = -4.29(8)$	0.15

In order to evaluate $\Delta\varepsilon_c^{(3),syst}$, we applied the two methods presented in Sec. 4.1.1 and specialized to $n = 3$.

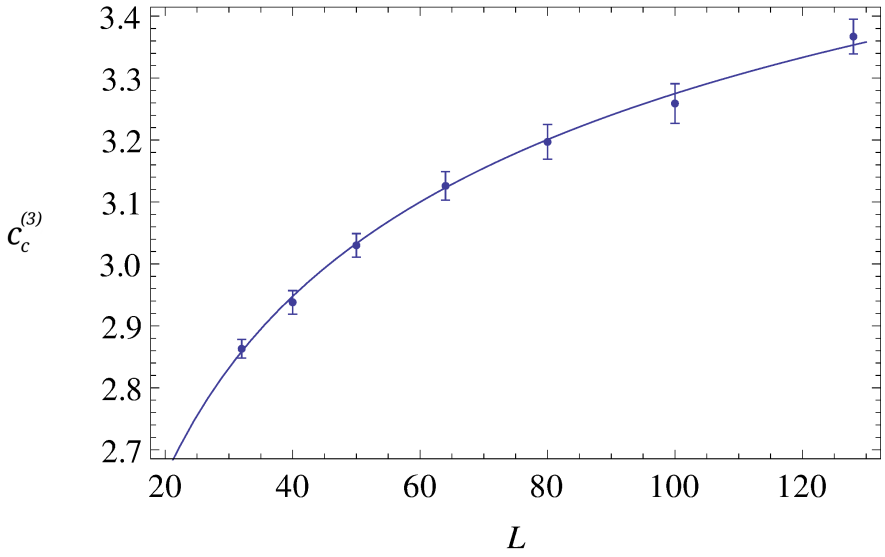

Figure 4.4: The specific heat $c_c^{(3)}(L)$ at the critical temperature $T_c^{(3)} = 1.4498$ as a function of L. The solid curve represents the fit to (4.17) with $\alpha_3/\nu_3 = -0.1991$

- *Method 1.* From Eq. (4.5), we computed the values of $\bar{\varepsilon}_+^{(3)}$ and $\bar{\varepsilon}_-^{(3)}$ at $T_+^{(3)} = 1.44300$ and $T_-^{(3)} = 1.44296$, respectively, assuming $\varepsilon_c^{(3)} = -0.989556$ as reported in Eq. (4.16). These quantities are given by $\bar{\varepsilon}_+^{(3)} = -0.989458$ and $\bar{\varepsilon}_-^{(3)} = -0.989654$ and are such that $|\varepsilon_c^{(3)} - \bar{\varepsilon}_+^{(3)}| = |\varepsilon_c^{(3)} - \bar{\varepsilon}_-^{(3)}| \simeq 0.00010$. In this way, we get

$$\Delta\bar{\varepsilon}_c^{(3),syst} = |\varepsilon_c^{(3)} - \bar{\varepsilon}_\pm^{(3)}| = 0.00010. \tag{4.18}$$

- *Method 2.* We computed $\tilde{\varepsilon}_\pm^{(3)}$ with a fit of the energy density data for $\tilde{\varepsilon}_\pm^{(3)}(L)$ for $L = 32, 40, 50, 64, 80, 100$ and 128 at $T_+^{(3)} = 1.44300$ and $T_-^{(3)} = 1.44296$, respectively, according to relation in Eq. (4.8) with $n = 3$ and $D_3 = -1.5974$ as in [106]. For $L = 40, 50, 80, 100$ we computed $\tilde{\varepsilon}_\pm^{(3)}(L)$ by applying Eq. (4.7) to data given in Table 4.6. As in the case of the XY model, the values of $\tilde{\varepsilon}_\pm^{(3)}(L)$ for $L = 32, 64$ and 128 are obtained with Monte Carlo simulations performed at $T_+^{(3)}$ and $T_-^{(3)}$, respectively; these numerical values are consistent with the same quantities computed with Eq. (4.7), not shown here. The data involved in the analysis are shown in Table 4.9; in **bold** are shown numerical values arising from the Monte Carlo simulations and in plain

Table 4.9: Energy density data $\varepsilon_+^{(3)}(L)$ and $\varepsilon_-^{(3)}(L)$ obtained via Taylor expansion (plain text) and numerical Monte Carlo simulations (**bold**), at $T_+^{(3)} = 1.44300$ and $T_-^{(3)} = 1.44296$, respectively. In parentheses are statistical errors from the simulations.

L	$\varepsilon_+^{(3)}(L)$	$\varepsilon_-^{(3)}(L)$
32	**-0.99636(7)**	**-0.99654(7)**
40	-0.99431	-0.99443
50	-0.99283	-0.99295
64	**-0.99164(6)**	**-0.99182(4)**
80	-0.99110	-0.99122
100	-0.99058	-0.99071
128	**-0.990232(19)**	**-0.99039(2)**

text values computed with Eq. (4.7). From the fits we get

$$\Delta\tilde{\varepsilon}_c^{(3),syst} = \cdot^{|\varepsilon_+^{(3)} - \varepsilon_c^{(3)}|}_{|\varepsilon_-^{(3)} - \varepsilon_c^{(3)}|} = \cdot^{0.00008}_{0.00006} \tag{4.19}$$

as reported in Table 4.10. Since our purpose is to compare the values of the critical energy density for different O(n) models, we choose to consider $\Delta\bar{\varepsilon}_c^{(3),syst}$ in Eq. (4.18) as best estimate of the systematic uncertainty on $\varepsilon_c^{(3)}$. From Eqs. (4.16) and (4.18) we finally get

$$\varepsilon_c^{(3)} \pm \Delta\varepsilon_c^{(3),stat} \pm \Delta\varepsilon_c^{(3),syst} = -0.989556 \pm 0.000010 \pm 0.00010, \tag{4.20}$$

as best estimate of the critical energy density of the three dimensional Heisenberg model, in the thermodynamic limit.

Table 4.10: Fitting values of the parameters $\varepsilon_\pm^3$ and $\varepsilon_{\pm,3}$.

Fitting parameters	constants	results	$\chi^2/d.o.f$
$\varepsilon_+^{(3)}$, $\varepsilon_{+,3}$	$D_3 = -1.5974$	$\varepsilon_+^{(3)} = -0.989479(19)$ $\varepsilon_{+,3} = -1.743(16)$	0.97
$\varepsilon_-^{(3)}$, $\varepsilon_{-,3}$	$D_3 = -1.5974$	$\varepsilon_-^{(3)} = -0.98962(2)$ $\varepsilon_{-,3} = -1.738(17)$	1.15

4.1.5 $n = 4$, the O(4) model

We performed canonical Monte Carlo simulations of the O(4) model defined on a regular cubic lattices with edges $L = 32, 40, 64, 80, 100$ and 128. For the

Table 4.11: Monte Carlo results for the energy density $\varepsilon_c^{(4)}(L)$ and for the specific heat $c_c^{(4)}(L)$ at the critical temperature $T_c^{(4)} = 1.06835$.

L	$\varepsilon_c^{(4)}(L)$	$c_c^{(4)}(L)$
32	-0.996930(67)	3.195(20)
40	-0.995431(53)	3.282(21)
64	-0.993374(35)	3.416(27)
80	-0.992875(20)	3.470(39)
100	-0.992482(23)	3.551(44)
128	-0.992260(20)	3.617(43)

critical temperature of the system we choose the value $T_c^{(4)} = 1.06835(13)$ given in [141]. Simulations have been performed at $T_c^{(4)} = 1.06835$ and the technical details are reported in Sec. B.1.3 of Appendix B. Table 4.11 shows the values for $\varepsilon_c^{(4)}(L)$ and $c_c^{(4)}(L)$ involved in the analysis, in parentheses are statistical errors.

We fitted data reported in Table 4.11 according to relation (4.1) with $n = 4$ and considering $\varepsilon_c^{(4)}$ and ε_4 as fitting parameters. For the values of the critical exponents, we considered different cases: (i) $\nu_4 = 0.7479(80)$ as reported in [141] at the same value of the critical temperature as in our case and $\alpha_4 = -0.244(24)$ as obtained from the scaling relation $\alpha = 2 - d\nu$ with $d = 3$; (ii) $\alpha_4 = -0.21312$ and $\nu_4 = 0.73771$ as obtained from the scaling relations $\alpha = 2-\beta(1+\delta)$ and $\nu = \frac{2-\alpha}{d}$ with $d = 3$, from data reported in [131] at $T_c = 1.06849$. In [131] the values of $\varepsilon_c^{(4)}$ and $c_c^{(4)}$ have been determined with a finite size scaling analysis considering an external field h and then extrapolating the results in the limit $h \to 0$. As will be shown in a moment and in support to our analysis, their results will be in excellent agreement with ours although derived with a slightly different approach. The results of the fits for $\varepsilon_c^{(4)}$ and ε_4 are reported in Table 4.12. We also performed a

Table 4.12: Fitting values of the parameters $\varepsilon_c^{(4)}$ and ε_4 entering expression (4.1).

Fitting parameters	constants	results	$\chi^2/d.o.f$
$\varepsilon_c^{(4)}$, ε_4	$\nu_4 = 0.7479$ $\alpha_4 = -0.244$	$\varepsilon_c^{(4)} = -0.99172(2)$ $\varepsilon_4 = -1.68(2)$	1.3
$\varepsilon_c^{(4)}$, ε_4	$\nu_4 = 0.73771$ $\alpha_4 = -0.21312$	$\varepsilon_c^{(4)} = -0.99170(2)$ $\varepsilon_4 = -1.57(2)$	1.3

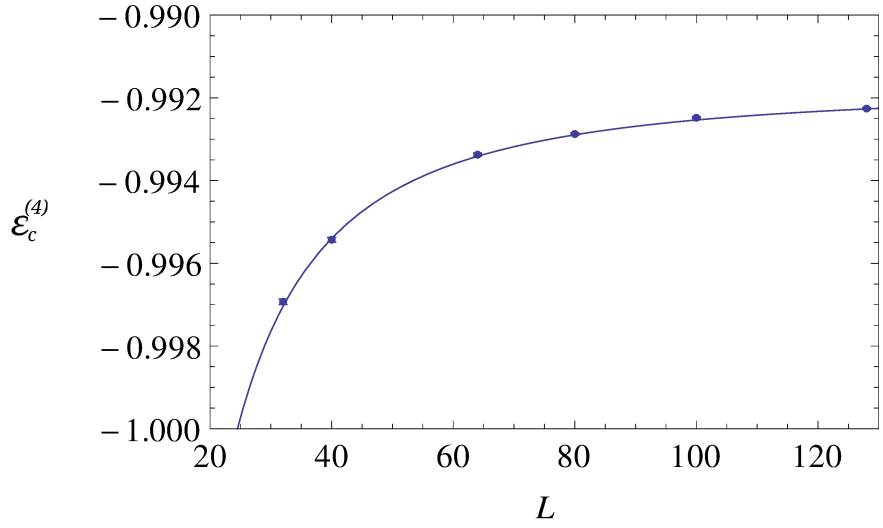

Figure 4.5: The energy density $\varepsilon_c^{(4)}(L)$ at the critical temperature $T_c^{(4)} = 1.06835$ as a function of L. The solid curve represents the fit to (4.21) with $\alpha_4 = -0.244$ and $\nu_4 = 0.7479$.

four-parameters fit to derive α_4, ν_4, $\varepsilon_c^{(4)}$ and ε_4. However, as in the $n = 2$ case, no meaningful results can be extracted from the fit, the relative error on the critical exponents being larger then 100%. The results of the fit are not shown here and will be neglected in the analysis.

The results for the critical energy density $\varepsilon_c^{(4)}$ shown in Table 4.12 are consistent with each other. As anticipated, they are also in agreement with the known results, see i.e. [131] where authors find $\varepsilon_c^{(4)} = -0.991792(28)$ from a FSS analysis involving an external magnetic field. However, we chose to consider

$$\begin{gathered} \varepsilon_c^{(4)} \pm \Delta\varepsilon_c^{(4),stat} = -0.99174 \pm 0.00002\,, \\ \varepsilon_4 = -1.69(2) \end{gathered} \tag{4.21}$$

as best estimate of the critical energy density $\varepsilon_c^{(4)}$ and of the fitting parameter ε_4, as reported in the first row of Table 4.12. These results, in fact, come from a choice of the critical exponents as in [141] and computed at the same value of the critical temperature as in our case. The curve $\varepsilon_c^{(4)}(L)$ given by Eq. (4.1) for $n = 4$ and for $\varepsilon_c^{(4)}$ and ε_4 as in Eq. (4.21), is shown in Fig. 4.5 together with the numerical data used in the analysis.

We fitted data of $c_c^{(4)}(L)$ reported in Table 4.11 according to the scaling relation in Eq.(4.2) with $n = 4$ and keeping the value of the ratio α_4/ν_4

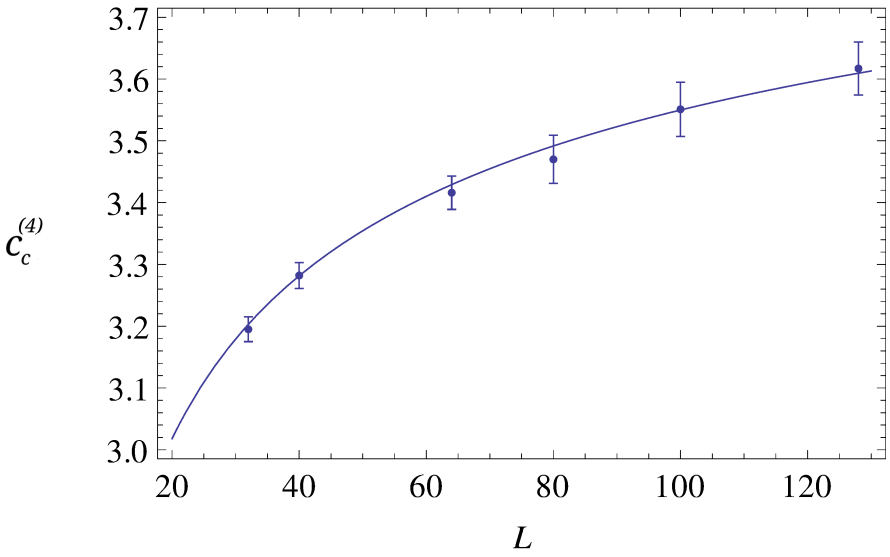

Figure 4.6: The specific heat $c_c^{(4)}(L)$ at the critical temperature $T_c^{(4)} = 1.06835$ as a function of L. The solid curve represents the fit to (4.22) with $\alpha_4/\nu_4 = -0.326$

constant to $\alpha_4/\nu_4 = -0.326$ as derived in [141] at the same $T_c^{(4)}$ as in our case. The results of the fit are given by

$$\begin{aligned} c_c^{(4)} &= 4.32(3)\,, \\ c_4 &= -3.46(10) \end{aligned} \tag{4.22}$$

and are reported in the first row of Table 4.13. To check the dependence of our results on the value of the ratio α_4/ν_4, we also performed the fit with a different choice for α_4/ν_4: $\alpha_4/\nu_4 = -0.289$ as derived from data reported in [131]. The results of this fit are reported in the second row of Table 4.13. The values of $c_c^{(4)}$ reported in Table 4.13 are in a good agreement with each other. Moreover the $c_c^{(4)}$ in the second row Table 4.13 is consistent with the correspondent quantity reported in [131] and derived with a rather different procedure. The curve $c_c^{(4)}(L)$ given by Eq. (4.2) for $n = 4$ and for $c_c^{(4)}$ and c_4 as in Eq. (4.22), is shown in Fig. 4.6 together with the numerical data used in the analysis.

In order to determine $\Delta\varepsilon_c^{(4),syst}$ we applied the two methods presented in Sec. 4.1.1 and specialized to $n = 4$.

- *Method 1.* From Eq. (4.5), we computed the values of $\bar{\varepsilon}_+^{(4)}$ and $\bar{\varepsilon}_-^{(4)}$ at $T_+^{(4)} = 1.06848$ and $T_-^{(4)} = 1.06822$, respectively, assuming $\varepsilon_c^{(4)} = -0.99174$ as reported in Eq. (4.21). These quantities are given by

Table 4.13: Fitting values of the parameters $c_c^{(4)}$ and c_4 entering expression (4.1) with $n = 4$.

Fitting parameters	constants	results	$\chi^2/d.o.f$
$c_c^{(4)}$, c_4	$\alpha_4/\nu_4 = -0.326$	$c_c^{(4)} = 4.32(3)$ $c_4 = -3.46(10)$	0.12
$c_c^{(4)}$, c_4	$\alpha_4/\nu_4 = -0.289$	$c_c^{(4)} = 4.43(3)$ $c_4 = -3.37(9)$	0.11

$\bar{\varepsilon}_+^{(4)} = -0.991178$ and $\bar{\varepsilon}_-^{(4)} = -0.992302$ and are such that $|\varepsilon_c^{(4)} - \bar{\varepsilon}_+^{(4)}| = |\varepsilon_c^{(4)} - \bar{\varepsilon}_-^{(4)}| \simeq 0.0006$. In this way, we get

$$\Delta\bar{\varepsilon}_c^{(4),syst} = |\varepsilon_c^{(4)} - \bar{\varepsilon}_\pm^{(4)}| = 0.0006. \tag{4.23}$$

- *Method 2.* We computed $\tilde{\varepsilon}_\pm^{(4)}$ with a fit of the energy density data $\tilde{\varepsilon}_\pm^{(4)}(L)$ with $L = 32, 64$ and 128 derived with Monte Carlo simulations performed at $T_+^{(4)} = 1.06848$ and $T_-^{(4)} = 1.06822$, respectively; the fits have been computed according to relation in Eq. (4.8) with $n = 4$ and $D_4 = -0.326$ as in [141]. At variance with what we have done for $n = 2$ and 3, in this case we did not consider the values of the critical energy density for other L-values, obtained with Eq.(4.7). Indeed, in this case, the fits produced extremely bad results when Taylor-expanded data are considered. The Monte Carlo data involved in the analysis are given in Table 4.14; in parentheses are the statistical errors coming from the simulations. The results of the fit, shown in Table 4.15, are such that

$$\Delta\tilde{\varepsilon}_c^{(4),syst} = \cdot^{|\varepsilon_+^{(4)} - \varepsilon_c^{(4)}|}_{|\varepsilon_-^{(4)} - \varepsilon_c^{(4)}|} = \cdot^{0.00006}_{0.00002} \tag{4.24}$$

As for the O(2) and for the O(3) model, we are going to consider $\Delta\varepsilon_c^{(4),syst} = \Delta\bar{\varepsilon}_c^{(4),syst} = 0.0006$ given by Eq. (4.23), being larger than $\Delta\tilde{\varepsilon}_c^{(4),syst}$ reported in Eq. (4.24).

We finally get

$$\varepsilon_c^{(4)} \pm \Delta\varepsilon_c^{(4),stat} \pm \Delta\varepsilon_c^{(4),syst} = -0.99174 \pm 0.00002 \pm 0.0006 \tag{4.25}$$

as the final value of the critical energy density of the three dimensional O(4) model in the thermodynamic limit. As for the O(2) and the O(3) models, the uncertainty on $\varepsilon_c^{(4)}$ due to $\Delta T_c^{(4)}$ is larger than the statistical uncertainty and has to be considered in our analysis.

Table 4.14: Energy density data $\varepsilon_+^{(4)}(L)$ and $\varepsilon_-^{(4)}(L)$ obtained with numerical Monte Carlo simulations performed at $T_+^{(4)} = 1.06848$ and $T_-^{(4)} = 1.06822$, respectively.

L	$\varepsilon_+^{(4)}(L)$	$\varepsilon_-^{(4)}(L)$
32	-0.996955(64)	-0.996962(67)
64	-0.993294(37)	-0.993383(36)
128	-0.992208(19)	-0.992275(18)

Table 4.15: Fitting values of the parameters $\varepsilon_\pm^{(4)}$ and $\varepsilon_{4,\pm}$.

Fitting parameters	constants	results	$\chi^2/d.o.f$
$\varepsilon_+^{(4)}$, $\varepsilon_{4,+}$	$D_4 = -0.326$	$\varepsilon_+^{(4)} = -0.99168(3)$ $\varepsilon_{4,+} = -1.67(3)$	1.5
$\varepsilon_-^{(4)}$, $\varepsilon_{4,-}$	$D_4 = -0.326$	$\varepsilon_-^{(4)} = -0.991755(8)$ $\varepsilon_{4,-} = -1.657(9))$	0.16

4.1.6 $n = \infty$, the spherical model

The spherical model has been introduced by Berlin and Kac [142] as an exactly solvable model of a ferromagnet and is described by the Hamiltonian

$$H^{sph} = -\sum_{\langle i,j \rangle}^{N} \eta_i \cdot \eta_j \ , \tag{4.26}$$

where the sum is intended over the pairs of nearest neighbors on a regular $d-$dimensional hypercubic lattice. At variance with the O(n) models the "spin variables" η_i are real numbers and their modulus is not fixed to unity. Instead, the spherical constraint

$$\sum_{i=1}^{N} \eta_i^2 = N \tag{4.27}$$

allows for a fluctuation of the modulus of the spin variables. The model is exactly solvable in any spatial dimension d in the thermodynamic limit, both in the canonical and in the microcanonical ensembles; for the canonical solution see e.g. Binney at al. [54] and references therein, for the microcanonical solution see e.g. [127]. Despite the long-range nature of the constrain in Eq.(4.27) the canonical and the microcanonical descriptions are equivalent and the model shows a continuous phase transition from a low-energy

(temperature) ferromagnetic phase to an high-energy (temperature) paramagnetic phase for all $d \geq 3$ [143].

In 1968, H. E. Stanley pointed out that the free energy of a class of models described by the Hamiltonian

$$\mathbb{H}^{(n)} = -\sum_{\langle i,j \rangle}^{N} \mu_i^{(n)} \cdot \mu_j^{(n)} = -\sum_{\langle i,j \rangle}^{N} \sum_{a=1}^{n} \mu_i^a \mu_j^a \tag{4.28}$$

with $|\mu_i|^2 = n \ \forall i = 1, \ldots, N$, approaches the free energy of the spherical model (4.26) in the $n \to \infty$ limit [144]. Moreover some "critical properties" of $\mathbb{H}^{(n)}$, like the value of the critical temperature $T_c^{(n)}$ or the value of some critical exponents [145], seems to be monotonic functions[6] of n. The class of models described by the Hamiltonian in Eq. (4.28) can be mapped in the class of classical O(n) models defined by Eq. (2.1), once the norm of the spins is properly scaled. In fact

$$\mathbb{H}^{(n)} = -\sum_{\langle i,j \rangle}^{N} \mu_i^{(n)} \cdot \mu_j^{(n)} = -n \sum_{\langle i,j \rangle}^{N} S_i \cdot S_j = n \ H^{(n)}, \tag{4.29}$$

and so

$$\lim_{n,\, N \to \infty} \frac{1}{n\ N} \mathbb{H}^{(n)} = \lim_{N \to \infty} \frac{1}{N} H^{(n)} = \lim_{N \to \infty} \frac{1}{N} H^{sph}. \tag{4.30}$$

This implies that the thermodynamic properties of the continuous O(n) models described by the Hamiltonian in Eq. (2.1) should converge to those of the spherical model, in the $n \to \infty$ limit. In particular, the discrete set of critical values of the energy density: $\{\varepsilon_c^{(1)}, \varepsilon_c^{(2)}, \varepsilon_c^{(3)}, \varepsilon_c^{(4)}, \ldots\}$ should converge pointwise to $\varepsilon_c^{(\infty)}$ —that is to the critical energy density value of H^{sph}— in the $n \to \infty$ limit. This means that, as a matter of fact, the spherical model can be considered as an O(∞) model in our analysis. The above property should be satisfied independently on the spatial dimensionality d of the lattice and so even in the case $d = 3$. In [127] an explicit expression for $\varepsilon_c^{(\infty)}$ is derived,

[6] In [145] the monotonicity is explicitly shown for the above quantities in $d = 1, 2, 3$ and for particular geometries of the lattices, i.e. spin chains, triangular lattices and fcc lattices. These results are supposed to hold also in more general cases but the generalization is not straightforward. In particular, it is not immediately clear whether the monotonicity is expected to hold also also for the energy density function $\varepsilon_c^{(n)}$ of models defined by Eq.(2.1) on regular cubic lattices in $d = 3$.

that reduces to

$$\varepsilon_c^{(\infty)} = -3 \ \frac{a_3}{1+a_3}, \ \text{ with } \ a_3 = \int_{[0,\pi)^3} \frac{d^3\phi}{\pi^3} \ \frac{\sum_{j=1}^3 \cos \ \phi_j}{3 - \sum_{j=1}^3 \cos \ \phi_j} \tag{4.31}$$

when adapted to our conventions in $d = 3$. From Eq.(4.31) we get

$$\varepsilon_c^{(\infty)} = -1.02161\ldots \tag{4.32}$$

as final best estimate of the critical energy density of the spherical model, or equivalently of the O(∞) model, in $d = 3$ and for $N \to \infty$.

4.2 Comparison of critical energy densities

The critical energy densities $\varepsilon_c^{(n)}$, discussed in the previous Sections for $n = 1, 2, 3, 4$ and ∞, are collected in Table 4.16 in function of $1/n = 1/\infty, 1/4, 1/3, 1/2$ and 1, together with their derivation method.

Table 4.16: Critical energy densities $\varepsilon_c^{(n)}$ and related values of $1/n$ with their derivation method for $n = 1, 2, 3, 4$ and $n = \infty$.

$\frac{1}{n}$	$\varepsilon_c^{(n)}$	Derivation method
$\frac{1}{\infty} \equiv 0$	-1.021611	Exact solution [127]
$\frac{1}{4}$	$-0.99174 \ \pm \ 0.00002 \ \pm \ 0.0006$	FSS this work, Eq. (4.25)
$\frac{1}{3}$	$-0.989556 \ \pm \ 0.000010 \ \pm \ 0.00010$	FSS this work, Eq. (4.20)
$\frac{1}{2}$	$-0.98904 \ \pm \ 0.00003 \ \pm \ 0.0003$	FSS this work, Eq. (4.14)
1	-0.99063 ± 0.00004	FSS [130]

Data in Table 4.16 allow to discuss the validity of Consequence 3.2.1 for 3−dimensional ferromagnetic nearest-neighbors O(n) models for every integer value of $n \in [1, \infty]$, and so for every rational value of $\frac{1}{n} \in [0, 1]$. Indeed, the function $\varepsilon_c(1/n)$ can be obtained with an interpolation procedure of data in the first two columns of Table 4.16; for every value of n, this function allows to estimate the critical energy density value $\varepsilon_c^{(n)} = \varepsilon_c(1/n)$ of the related three-dimensional O(n) and makes possible a direct comparison between $\varepsilon_c^{(n)}$ and $\varepsilon_c^{(1)}$.

In 1996, Campostrini et al. performed an analysis of the four-point renormalized coupling constant in classical O(n) models [146]. Interestingly, an

important requirement of this study was to posses an estimate of the critical value of the internal energy $\varepsilon_c^{(n)}$ for classical O(n) models, and authors found

$$\varepsilon_c^{(n)} = \varepsilon_c^{(\infty)} + b_1 \frac{1}{n} + O\left(\frac{1}{n^2}\right), \tag{4.33}$$

with $b_1 \simeq 0.21$, once adapted to our conventions. This result, particularly interesting for our discussion, suggests the way in which the interpolation procedure of data in Table 4.16 has to be performed: $\varepsilon_c(1/n)$ should be a polynomial function in $\frac{1}{n}$ in which the zero-order term is given by the critical energy density value $\varepsilon_c^{(\infty)}$ of the spherical model, and the coefficient b_1 of the linear term is fixed to 0.21.

We computed the interpolating function $\varepsilon_c(1/n)$ with the MATHEMATICA built-in routine `InterpolatingPolynomial` with the constraints on the zero-order term and on the coefficient b_1, set by Eq. (4.33). We found

$$\begin{aligned} \varepsilon_c(1/n) =& \varepsilon_c^{(\infty)} + 0.21\,\frac{1}{n} + b_2\,\frac{1}{n^2} + b_3\,\frac{1}{n^3} + b_4\,\frac{1}{n^4} = \\ =& -1.02161 + 0.21\,\frac{1}{n} - 0.402399\,\frac{1}{n^2} + \\ &+ 0.097314\,\frac{1}{n^3} + 0.256104\,\frac{1}{n^4}\,. \end{aligned} \tag{4.34}$$

In the interpolation procedure we did not consider the point $\{1, \varepsilon_c^{(1)}\}$ since our interest is in the comparison of $\varepsilon_c^{(n\geq 2)}$ and $\varepsilon_c^{(1)}$ in $\frac{1}{n} \in \left[0, \frac{1}{2}\right]$. Moreover, the function $\varepsilon_c(1/n)$ has to be computed with the lowest order polynomial function as possible. If we force $\varepsilon_c(1/n)$ to pass trough $\{1, \varepsilon_c^{(1)}\}$, the next-order term $b_5\,\frac{1}{n^5}$ becomes necessary although no useful informations on $\varepsilon_c^{(n)}$ are present in the range $1/n \in [1/2, 1]$.

As a further test on the form of the curve in Eq. (4.34), we performed a fit of data presented in Table 4.16 (without the point $\{1, \varepsilon_c^{(1)}\}$), with the following polynomial relation

$$\varepsilon_c(n) = \varepsilon_c^{(\infty)} + 0.21\frac{1}{n} + a_2\frac{1}{n^2} + a_3\frac{1}{n^3} + a_4\frac{1}{n^4} \tag{4.35}$$

where a_2, a_3 and a_4 are unknown fitting parameters. The results of the fit are given by $a_2 = 0.4025(2)$, $a_3 = 0.0975(8)$ and $a_4 = 0.256(1)$ and are in excellent agreement with the interpolation coefficients in Eq. (4.34). This notwithstanding, the $\chi^2/d.o.f$ of the fit is quite small, about 0. This fact can

be due to the problem of performing a three-parameters fit from a relative small set of data as in Table 4.16. We then choose to consider $\varepsilon_c(1/n)$ as given by the polynomial function in Eq. (4.34) where the parameters b_1, b_2 and b_3 are determined with the optimized routine `InterpolatingPolynomial` provided by MATHEMATICA.

In Fig. 4.7 we plot the following quantities: the interpolating curve given by Eq. (4.34) (dashed blue line), the curve in Eq. (4.33) (solid green line), the horizontal curve $\varepsilon_c^{(n)} = \varepsilon_c^{(1)}$ in correspondence of the critical energy density of the Ising model (dot-dashed black line), the critical energy densities $\varepsilon_c^{(1)}$ (blue circle), $\varepsilon_c^{(2)}$ (purple square), $\varepsilon_c^{(3)}$ (yellow diamond), $\varepsilon_c^{(4)}$ (green up-pointing triangle) and $\varepsilon_c^{(\infty)}$ (blue down-pointing triangle). For $n = 1/2, 1/3, 1/4$ the uncertainties on the points are given by the systematic uncertainties shown in Table 4.16. Eq. (4.34) allows to estimate the critical energy density values of the O(n) models for every value of n. As an example we computed $\varepsilon_c^{(n)}$ for $n = \{5, 6, 7, \ldots, 500\}$; the results are plotted in Fig. (4.7) as red crosses.

Fig. 4.7 shows that $\varepsilon_c^{(2)}$, $\varepsilon_c^{(3)}$ and $\varepsilon_c^{(4)}$ computed in the previous Sections are in agreement with results coming from the $\frac{1}{n}-$expansion around $\varepsilon_c^{(\infty)}$ given by Eq. (4.33). In fact the interpolating curve in Eq. (4.34) departing from $\varepsilon_c^{(\infty)}$ with slope 0.21, properly fits all the data for $n = 2, 3$ and 4 given in Table 4.16 and considered with the related systematic error bars.

Moreover, the interpolating curve provides a practical test for the approximation $\varepsilon_c^{(n)} \sim \varepsilon_c^{(1)}$ suggested by Consequence 3.2.1. In fact, if we admit that Eq. (4.34) correctly reproduces the real values of $\varepsilon_c^{(n)}$, for every $n \in [2, \infty]$ the discrepancy between $\varepsilon_c^{(n)}$ and $\varepsilon_c^{(1)}$ can be easily quantified as $|\varepsilon_c(1/n) - \varepsilon_c^{(1)}|$.

In particular: for $1/n \in [1, 1/8)$, that is up to $n = 8$, the error made by replacing $\varepsilon_c^{(n)}$ with $\varepsilon_c^{(1)}$ is $|\varepsilon_c(1/n) - \varepsilon_c^{(1)}| \leq 0.0108$, that is about the 1%; for $1/n \in [1/8, 1/18)$, that is up to $n = 18$, the error is about the 2%; for $1/n \in [1/18, 0]$, that is up to $n = \infty$, the error is about the 3%, and in any case smaller than $|\varepsilon_c^{(\infty)} - \varepsilon_c^{(1)}| \sim 0.031$.

The above analysis quantifies the level of approximation made assuming the Consequence 3.2.1 as satisfied, and concludes the discussion started in Chapter 3, at least for what concerns classical O(n) models with ferromagnetic interactions defined on regular cubic lattices in $d = 3$.

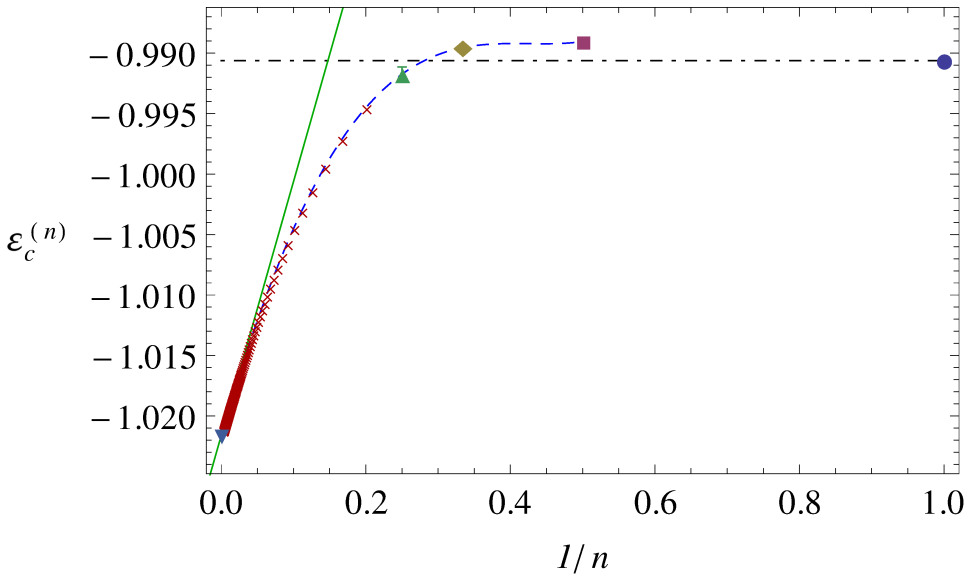

Figure 4.7: Plot of the critical energy densities $\varepsilon_c^{(n)}$ of $3d$-O(n) models as a function of $1/n$. $\varepsilon_c^{(1)}$ (blue circle), $\varepsilon_c^{(2)}$ (purple square), $\varepsilon_c^{(3)}$ (yellow diamond), $\varepsilon_c^{(4)}$ (green up-pointing triangle) and $\varepsilon_c^{(\infty)}$ (blue down-pointing triangle) are given in Table 4.16 and plotted with the statistical uncertainties when present. The dashed blue line represents the interpolating curve $\varepsilon_c(1/n)$ in Eq. (4.34), the solid green line represents the $\frac{1}{n}$ expansion in Eq. (4.33), the horizontal dot-dashed black line is the line of equation $\varepsilon_c(n) = \varepsilon_c^{(1)}$. The red crosses mark the critical energy density values $\varepsilon_c^{(n)}$ for $n \in [5, 500]$ as derived from Eq. (4.34).

4.3 Conclusions and remarks

In the present Chapter we have performed a numerical analysis of the Consequence 3.2.1 in the case of classical O(n) models defined on regular hypercubic lattices and with ferromagnetic interactions.

The critical values ε_c^n for $n = 2, 3$ and 4 have been evaluated with a FSS analysis together with the related statistical and systematic uncertainties due to the FSS procedure and to $\Delta T_c^{(n)}$, respectively; interestingly, the systematic uncertainties dominate on the statistical ones for every value of n. For $n = 2$ and 3, our results for the critical energy densities in Eqs. (4.10) and (4.16) improved the accuracy of the numerical estimates present in the literature.

Interpolating the data of $\varepsilon_c^{(n)}$ for $n = 2, 3, 4$ and $n = \infty$, the polynomial function $\varepsilon_c(1/n)$ has been computed to estimate the critical value of the energy density of a generic O(n) model with $n = \{2, 3, 4, 5, \ldots, \infty\}$. This function takes into account the results on the critical energy density values

of classical O(n) models derived with a $\frac{1}{n}-$expansion around $\varepsilon_c^{(\infty)}$ in [146], and produces a practical way to test the accuracy of Consequence 3.2.1 for every value of $n \in [2, \infty]$. Indeed, the error made by replacing $\varepsilon_c^{(n)} = \varepsilon_c(1/\bar{n})$ with $\varepsilon_c^{(1)}$ for a generic O(n) model happens to be less then 1% if $n \in [2, 8)$, from 1% and 2% if $n \in [8, 18]$ and less then 3% in all the other cases.

To conclude the Chapter, some considerations can be done as to possible continuation of this work.

The strong computational effort on one side and the necessity of the knowledge of the value of the critical temperature on the other side determined the limited number of representatives of O(n) models simulated in our analysis. In principle, O(n) models with $n > 4$ could have been studied with the algorithm we used, but in this case the critical temperatures $T_c^{(n>4)}$ should also have been determined with high accuracy, since their values are not known in literature up to our knowledge. Anyhow, knowing the critical energy density of at least another O(n) model with $n > 4$ would supply a further test of Eq. (4.34), so that it would be useful to compute it.

As briefly discussed in Sec. 4.1.6, a monotonic behavior in n is supposed to hold for some thermodynamic functions of classical O(n) models defined on particular lattice geometries, see [145]. From results reported in [145], it is not clear if such considerations could be applied also to $\varepsilon_c^{(n)}$ in the case of classical O(n) models defined on regular cubic lattices. This notwithstanding, starting from $n = \infty$, the interpolating function in Eq. (4.34) is a monotonic increasing function of $\frac{1}{n}$ up to $n = 2$. From Fig. 4.7 it is possible to see that the monotonicity fails for $n = 1$, but could be restored if an higher value $\varepsilon_c^{(1)\prime}$ is admitted for $\varepsilon_c^{(1)}$, such that $|\varepsilon_c^{(1)\prime} - \varepsilon_c^{(1)}| \simeq 10^{-3}$. Since the numerical value of $\varepsilon_c^{(1)}$ in Eq. (4.9) has been derived with high accuracy in [130], the only thing that can be possibly done in the future is to check the value of the critical temperature at which the Ising model is simulated.

However, a possible increase of less then 10^{-3} in $\varepsilon_c^{(1)}$ would affect neither the considerations made at the end of Sec. 4.2 nor the form of Eq. (4.34) that has been derived considering data for $n > 1$.

Chapter 5

Density of states of O(n) models and stationary points

A numerical study of critical energy densities has been presented in Chapter 4 in the case of three-dimensional O(n) models. This study revealed that the discrepancy between $\varepsilon_c^{(n)}$ and $\varepsilon_c^{(1)}$ is just below 3% for any value of n, and becomes even smaller when small values of n are considered. The aim of the present Chapter is to discuss how energy landscapes techniques presented in Chapter 3 can be applied to short-range O(n) models defined on $d-$dimensional hypercubic lattices, in order to extract informations on their thermodynamics.

Table 3.1 shows that, for any value of n, Consequence 3.2.1 correctly predicts the equality of the critical energy densities of the Ising model and of the O(n) models in case of long-range interactions. The same holds for O(n) models defined on one-dimensional lattices with nearest-neighbor interactions. In both cases the systems are exactly solvable and the critical energy density of the transition equals one of the boundaries of the energy density domain: the lower bound $\varepsilon_{\min}$ in the 1-d case, see i.e. [44, 94], and the upper bound $\varepsilon_{\max}$ in the long-range case, see i.e. [93]. The fact that a particular prediction made using Eq. (3.4) turns out to be exact does not imply that the equation itself is exact. This notwithstanding, it is reasonable to try to understand if, in some of the above cases where it gives the correct prediction for the critical energy, Eq. (3.4) can be derived with a lesser degree of approximation, or even exactly.

Indeed, we are going to show that in the case of the mean-field XY model and in the case of the one-dimensional XY model with nearest-neighbor

interactions, an expression very similar to Eq. (3.4), and which reduces to Eq. (3.4) when $\varepsilon \to \varepsilon_c$, can be derived exactly in the thermodynamic limit [40]. Besides confirming the reliability of the argument presented in Sec. 3.1, this analysis sets the energy range of validity of the approximation in Eq. (3.4) even if only for two particular models.

The technical aspects of the derivation strongly rely on the peculiarities of the two models so that the results cannot be generalized to other short-range O(n) models in $d > 1$ in a straightforward manner. However, something has been done in this sense. An approximation protocol has been developed in [41] to derive an approximate form of $\omega^{(n)}$ for—in principle any—short-range O(n) models defined on regular $d-$dimensional hypercubic lattices with periodic boundary conditions. The protocol, inspired by the energy landscape considerations made in Sec. 3.1, has been explicitly tested on the nearest-neighbor ferromagnetic XY model in $d = 2$ ad will be presented at the end of the Chapter. A generalization to other O(n) models is thought to be possible on the same lines but has not been carried out in detail.

The Chapter is organized as follows. In Sec. 5.1 the stationary points approach and the approximations introduced in [38] leading to Eq. (3.4) are recalled and discussed. Secs. 5.1.1 and 5.1.2 are devoted to the explicit derivation of the relation between the Ising model density of states and the density of states of the mean-field XY and 1-d XY models, respectively. In Sec. 5.1.3 the results are discussed in a more general perspective, with emphasis on the generalization to general $d-$dimensional lattices. In Sec. 5.2 the approximation protocol for the density of states $\omega^{(n)}$ will be discussed; its application to the XY model in $d = 2$ will be presented in Secs 5.2.1 et seq. Some conclusive comments will be listed in Sec. 5.2.4.

5.1 Stationary points and density of states

To perform our analysis we have to recall the derivation of Eq. (3.4) made in Chapter 3, that we rewrite for our convenience

$$\omega^{(n)}(\varepsilon) \simeq \omega^{(1)}(\varepsilon)\, g^{(n)}(\varepsilon)\,. \tag{5.1}$$

The approach followed in Sec. 3.1 is an "energy landscape" one and originates from the observation that, among all the stationary configurations of the Hamiltonian H in Eq. (2.1), the class of the Ising stationary configurations

introduced in Chapter 2 is the most relevant one for what concerns the thermodynamic properties of the continuous systems. This observation lead us to re-write the density of states of the O(n) models as a sum of integrals over a partition of the phase space. More precisely we had

$$\omega^{(n)}(\varepsilon) = \sum_p \int_{U_p} \delta(H^{(n)} - N\varepsilon)\, d\Gamma = \sum_p \int_{U_p \cap \Sigma_\varepsilon} \frac{d\Sigma}{|\nabla H^{(n)}|}\,, \tag{5.2}$$

where p run over the 2^N Ising stationary configurations, U_p is a neighborhood of the p-th Ising configuration such that $\{U_p\}_{p=1}^{2^N}$ is a proper partition of the configuration space Γ_N, that coincides with phase space for spin models defined by the Hamiltonian H in Eq. (2.1).

Then, two approximations were introduced in Sec. 3.1 to derive Eq. (5.1) from Eq. (5.2): (*i*) we assumed that the integrals in Eq. (5.2) depend only on ε, i.e., the neighborhoods U can be chosen, or deformed, such as

$$\int_{U_p} \delta(H^{(n)} - N\varepsilon)\, d\Gamma = \int_{U_q} \delta(H^{(n)} - N\varepsilon)\, d\Gamma = g^{(n)}(\varepsilon) \tag{5.3}$$

for any p, q such that $H^{(n)}(p) = H^{(n)}(q) = N\varepsilon$; (*ii*) Since it was assumed that non-Ising stationary configurations could be neglected, only neighborhoods centered around stationary configurations at energy density ε have been retained in the sum (5.2).

Both assumptions are needed to derive Eqs. (3.4) and (5.1), and are strictly related to each other. However, these two assumptions might well play a very different rôle. As we shall see in the following sections, in the two analytically tractable special cases, assumption (*ii*) does not hold in general: it holds only when $\varepsilon \to \varepsilon_c^{(n)}$. As a consequence, one has to include also stationary configurations with energy $\varepsilon' \neq \varepsilon$ in the sum. Clearly, if assumption (*ii*) does not hold, also assumption (*i*) is of little use as such, since also neighborhoods centered around stationary points with energy density different from ε have to be included in the sum.

One might then replace assumption (*i*) with

(*i'*) The integrals in Eq. (5.2) depend only on ε and on the energy density ε' of the stationary point, i.e.,

$$\int_{U_p} \delta(H^{(n)} - N\varepsilon)\, d\Gamma = G^{(n)}(\varepsilon, \varepsilon')\,, \tag{5.4}$$

for any p such that $H^{(n)}(p) = N\varepsilon'$.

The function $g^{(n)}(\varepsilon)$ would then be related to $G^{(n)}(\varepsilon, \varepsilon')$ by

$$g^{(n)}(\varepsilon) = G^{(n)}(\varepsilon, \varepsilon)\,. \tag{5.5}$$

Using assumption (*i'*) alone, without invoking[1] assumption (*ii*), one obtains from Eq. (5.2) the following expression for the density of states of a O(n) model:

$$\omega^{(n)}(\varepsilon) = \sum_{\varepsilon'} \omega^{(1)}(\varepsilon')\, G^{(n)}(\varepsilon, \varepsilon')\,, \tag{5.6}$$

i.e., a convolution between the Ising density of states $\omega^{(1)}$ and the function $G^{(n)}$. Then, in the thermodynamic limit $N \to \infty$ a saddle-point-like mechanism might single out a value $\tilde{\varepsilon}$ for ε', so that the convolution (5.6) becomes a product:

$$\omega^{(n)}(\varepsilon) = \omega^{(1)}(\tilde{\varepsilon})\, G^{(n)}(\varepsilon, \tilde{\varepsilon})\,, \tag{5.7}$$

where $\tilde{\varepsilon}$ is a suitable function of ε. If $\tilde{\varepsilon} = \varepsilon$, then using Eq. (5.5) one recovers Eq. (5.1). This is precisely what happens when $\varepsilon \to \varepsilon_c^{(n)}$ in the two special cases we are going to discuss in the following sections. In Sec. 5.1.3, we shall argue about the possible generality of this scenario.

5.1.1 The mean-field XY model

We shall now show that the density of states of the mean-field XY model can be written in the form (5.7), with $\tilde{\varepsilon} \to \varepsilon$ when $\varepsilon \to \varepsilon_{c,\mathrm{MF}}^{(2)}$, with $\varepsilon_{c,\mathrm{MF}}^{(2)} = \varepsilon_{\max} = 0$ its critical energy density.

The mean-field XY model is described by the Hamiltonian (2.5) that we recall here for $n = 2$:

$$H_{\mathrm{MF}}^{(2)} = -\frac{1}{2N} \sum_{i,j=1}^{N} \cos\left(\vartheta_i - \vartheta_j\right)\,, \tag{5.8}$$

where $\vartheta_i \in [0, 2\pi)$, so that the configuration (or phase) space of the system is the torus $\mathbb{T}^N$.

[1] One may wonder whether the removal of assumption (*ii*) has any consequence on the robustness of the hypothesis of dominance of the Ising configurations. In our opinion it does not have any consequence, because the latter hypothesis is preliminary to the others, and relies on that Ising configurations are exponentially large in N, as the total number of stationary points is expected to be, so that they are at least a non-negligible fraction of the whole.

By introducing the magnetization density vector $\mathbf{m} = (m_x, m_y)$, where

$$m_x = \frac{1}{N}\sum_{i=1}^{N} \cos\vartheta_i \,, \tag{5.9}$$

$$m_y = \frac{1}{N}\sum_{i=1}^{N} \sin\vartheta_i \,, \tag{5.10}$$

$$\tag{5.11}$$

we can write the total energy of the system as a function of the modulus $m = |\mathbf{m}|$ of the magnetization density:

$$H^{(2)}_{\mathrm{MF}} = -\frac{Nm^2}{2} \,. \tag{5.12}$$

For XY models, Ising stationary points are configurations where the angles ϑ_i differ from each other by either 0 or π, as discussed in Sec. 2.2.1. To break the $O(2)$ invariance of the Hamiltonian we set $\vartheta_N = 0$, so that the Ising stationary configurations are all the configurations $\overline{\vartheta} = \left\{\overline{\vartheta}_i\right\}_{i=1}^{N}$ where the angles are either 0 or π, and can be parametrized by the number N_π of angles equal to π. The configurations with given N_π are

$$\overline{\vartheta}_i = \pi \quad \forall\, i = 1, \ldots, N_\pi \tag{5.13}$$

$$\overline{\vartheta}_i = 0 \quad \forall\, i = N_\pi + 1, \ldots, N \tag{5.14}$$

and all the others obtained by permutations of the indices i. The number $\nu(N_\pi)$ of such configurations is given by the binomial coefficient

$$\nu(N_\pi) = \frac{N!}{N_\pi!(N - N_\pi)!} \,, \tag{5.15}$$

while their magnetization and energy density depend only on N_π and are given by

$$m(N_\pi) = m_x(N_\pi) = \frac{N - 2N_\pi}{N} = 1 - 2n_\pi \,, \tag{5.16}$$

$$\varepsilon(N_\pi) = -\frac{m^2(N_\pi)}{2} = -\frac{(N - 2N_\pi)^2}{2N^2} = -\frac{(1 - 2n_\pi)^2}{2} \,, \tag{5.17}$$

where, coherently with Sec. 2.2.1, we have introduced the fraction of angles equal to π, $n_\pi = N_\pi/N$.

Given a stationary configuration $p = \left\{\overline{\vartheta}_1, \ldots, \overline{\vartheta}_N\right\}$, let us define the neighborhood

$$U_{p(\vartheta_i)} = \begin{cases} \left[\dfrac{\pi}{2}, \dfrac{3\pi}{2}\right] & \text{if} \quad \overline{\vartheta}_i = \pi \\ \\ \left[\dfrac{3\pi}{2}, \dfrac{\pi}{2}\right] & \text{if} \quad \overline{\vartheta}_i = 0 \end{cases} \tag{5.18}$$

so that $\{U_p\}_{p=1}^{2^N}$ is a partition of the phase space $\mathbb{T}^N$. The density of states $\omega_{\mathrm{MF}}^{(2)}$ of the mean-field XY model can thus be written as

$$\omega_{\mathrm{MF}}^{(2)}(\varepsilon) = \sum_{N_\pi=0}^{N} \nu(N_\pi)\, G_{\mathrm{MF}}^{(2)}(\varepsilon, N_\pi) \tag{5.19}$$

where

$$\begin{aligned} G_{\mathrm{MF}}^{(2)}(\varepsilon, N_\pi) = \int_{\pi/2}^{3\pi/2} d\vartheta_1 \cdots d\vartheta_{N_\pi} \int_{3\pi/2}^{\pi/2} d\vartheta_{N_\pi+1} \cdots d\vartheta_N \times \\ \times\, \delta\left[H_{\mathrm{MF}}(\vartheta_1, \ldots, \vartheta_N) - N\varepsilon\right] \ . \end{aligned} \tag{5.20}$$

We note that $\nu(N_\pi)$ given by Eq. (5.15) is nothing but the density of states $\omega_{\mathrm{MF}}^{(1)}$ of the mean-field Ising model

$$H_{\mathrm{MF}}^{(1)} = -\frac{1}{2N} \sum_{i,j=1}^{N} \sigma_i \sigma_j \,, \tag{5.21}$$

as a function of the number of "up" spins $\sigma = 1$; using the relation (5.17) to obtain the energy density ε' of the Ising stationary configuration as a function of N_π, Eq. (5.19) can be written as

$$\omega_{\mathrm{MF}}^{(2)}(\varepsilon) = \sum_{\varepsilon'} \omega_{\mathrm{MF}}^{(1)}(\varepsilon')\, G_{\mathrm{MF}}^{(2)}(\varepsilon, \varepsilon') \,, \tag{5.22}$$

where the sum runs over the energy density levels of the Ising mean-field Hamiltonian (5.21), so that it is exactly Eq. (5.6) written in the special case of the mean-field XY model. It is important to stress that this result is a consequence of the fact that the energy of a Ising stationary configuration depends only on N_π and that all the neighborhoods $U_{p(\vartheta_i)}$ with the same N_π contribute equally to the sum (5.19).

Let us now compute the function $G_{\mathrm{MF}}^{(2)}$ defined in Eq. (5.20). To make the calculation simpler it is useful to express $G_{\mathrm{MF}}^{(2)}$ as a function of m instead of

ε; one then gets back to ε using Eq. (5.12). Since we fixed the magnetization to be along the x axis, the function $G^{(2)}_{\mathrm{MF}}(m, N_\pi)$ is given by

$$G^{(2)}_{\mathrm{MF}}(m, N_\pi) = \int_{\pi/2}^{3\pi/2} d\vartheta_1 ... d\vartheta_{N_\pi} \int_{3\pi/2}^{\pi/2} d\vartheta_{N_\pi+1} ... d\vartheta_N \times \\ \times \delta\left(\sum_{i=1}^{N} \cos\vartheta_i - Nm\right) \delta\left(\sum_{i=1}^{N} \sin\vartheta_i\right) . \tag{5.23}$$

Using the integral representation of the Dirac delta distribution, Eq. (5.23) becomes

$$G^{(2)}_{\mathrm{MF}}(m, N_\pi) = \left(\frac{1}{2\pi}\right)^2 \int_{\pi/2}^{3\pi/2} d\vartheta_1 ... d\vartheta_{N_\pi} \int_{3\pi/2}^{\pi/2} d\vartheta_{N_\pi+1} ... d\vartheta_N \times \\ \times \int_{-\infty}^{\infty} dq_1 \int_{-\infty}^{\infty} dq_2 \, e^{iq_1\left(\sum_{i=1}^{N} \cos\vartheta_i - Nm\right)} \, e^{iq_2\left(\sum_{i=1}^{N} \sin\vartheta_i\right)} ; \tag{5.24}$$

by writing

$$A(q_1, q_2) = \int_{\pi/2}^{3\pi/2} d\vartheta \, \exp\left[iq_1 \cos\vartheta + iq_2 \sin\vartheta\right] , \tag{5.25}$$

and

$$B(q_1, q_2) = \int_{3\pi/2}^{\pi/2} d\vartheta \, \exp\left[iq_1 \cos\vartheta + iq_2 \sin\vartheta\right] = \\ = \int_{\pi/2}^{3\pi/2} d\vartheta \, \exp\left[iq_1 \cos(\vartheta - \pi) + iq_2 \sin(\vartheta - \pi)\right] , \tag{5.26}$$

we get

$$G^{(2)}_{\mathrm{MF}}(m, N_\pi) = \left(\frac{1}{2\pi}\right)^2 \int_{-\infty}^{\infty} dq_1 \int_{-\infty}^{\infty} dq_2 \times \\ \times e^{N(-imq_1 + n_\pi \log A(q_1,q_2) + (1-n_\pi)\log B(q_1,q_2))} . \tag{5.27}$$

The integrals in Eq. (5.27) can be computed with the saddle-point method [147] in the limit $N \to \infty$. The saddle point is given by $q_2 = 0$ e $q_1 = -i\gamma$, where $\gamma \in \mathbb{R}$ satisfies the self-consistency equation

$$m = n_\pi \frac{I_1(\gamma) - L_{-1}(\gamma)}{I_0(\gamma) - L_0(\gamma)} + (1 - n_\pi) \frac{I_1(\gamma) + L_{-1}(\gamma)}{I_0(\gamma) + L_0(\gamma)} ; \tag{5.28}$$

in Eq. (5.28), $I_k(\gamma)$ are modified Bessel functions of order k and $L_k(\gamma)$ are modified Struve functions of order k [148]. We can thus write, in the limit $N \gg 1$,

$$G^{(2)}_{\rm MF}(m, n_\pi) = \left(\frac{1}{2\pi}\right)^2 e^{N\left[-m\gamma + n_\pi \log \tilde{A}(\gamma,0) + (1-n_\pi)\log \tilde{B}(\gamma,0)\right]}, \tag{5.29}$$

where we have written n_π instead of N_π since we are approaching the $N \to \infty$ limit; γ must be numerically determined solving Eq. (5.28), and the functions $\tilde{A}$ and $\tilde{B}$ are given by

$$\tilde{A}(\gamma, 0) = \pi[I_0(\gamma) - L_0(\gamma)], \tag{5.30}$$

$$\tilde{B}(\gamma, 0) = \pi[I_0(\gamma) + L_0(\gamma)]. \tag{5.31}$$

In the large N limit, we can thus write the density of states as a function of m as

$$\omega^{(2)}_{\rm MF}(m) = \int_0^1 dn_\pi \, e^{N(-m\gamma + n_\pi \log \tilde{A}(\gamma,0) + (1-n_\pi)\log \tilde{B}(\gamma,0) - n_\pi \log n_\pi - (1-n_\pi)\log(1-n_\pi))}, \tag{5.32}$$

where we have neglected the sub-leading contributions in N. Again, the integral (5.32) can be computed with the saddle-point method as $N \to \infty$, so that, given m and thus ε, only a particular value of n_π (and thus of m' and, in turn, of ε') is singled out and the density of states $\omega^{(2)}_{\rm MF}$ assumes the product form (5.7). The particular value of n_π which is singled out is the one such that the exponent in Eq. (5.32) is maximum; it has to be computed numerically.

The saddle point on Eq. (5.32) singles out a value $\tilde{m}$ of the magnetization such that

$$\omega^{(2)}_{\rm MF}(m) = \omega^{(1)}(\tilde{m})\, G^{(2)}_{\rm MF}(m, \tilde{m}). \tag{5.33}$$

In order to show that the value of $\tilde{m}$ as a function of m converges to m as $m \to m_c$, where $m_c = 0$ is the critical value of the magnetization, in Fig. 5.1 we plot the function

$$h(m) = m - \tilde{m}. \tag{5.34}$$

Figure 5.1 shows that $h \to 0$ as $m \to 0$, so that the density of states $\omega^{(2)}_{\rm MF}(m)$ is such that

$$\omega^{(2)}_{\rm MF}(m) \to \omega^{(1)}(m)\, g^{(2)}_{\rm MF}(m), \tag{5.35}$$

where $g^{(2)}_{\rm MF}(m) = G^{(2)}_{\rm MF}(m, m)$, for $m \to m_c$. More precisely, h appears to be a linear function of m as $m \to 0$, $h(m) \propto -m$. When $m \to 1$ the numerical

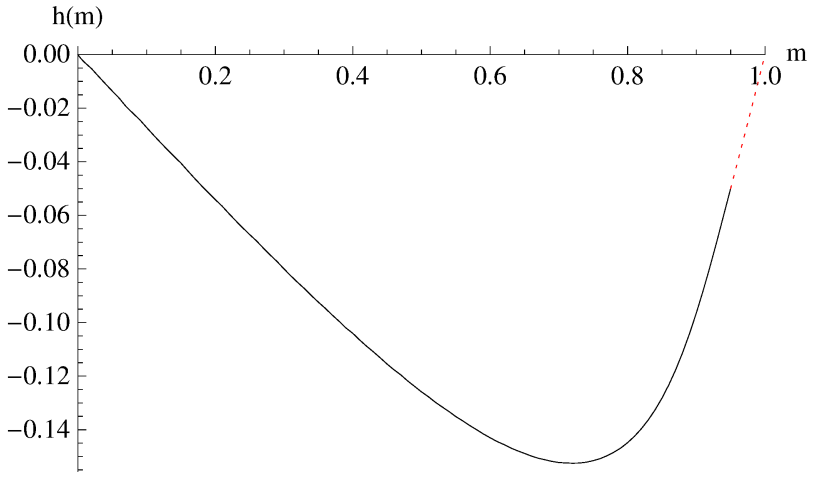

Figure 5.1: Numerical results for the function $h(m)$ defined in Eq. (5.34) for the mean-field XY model. The red (dotted) part of the curve is obtained by interpolation (see text).

procedure we used to compute $h(m)$ had some convergence problems. Since $m = 1$ implies $h(m) = 0$ and $n_\pi = 1$, to avoid these numerical problems the curve plotted in Fig. 5.1 in the range $m \in [0.97, 1]$ has been evaluated interpolating the numerical results obtained for $m < 0.97$ with the constraint $h(1) = 0$. The interpolating curve is drawn in red and in dotted style in Figure 5.1. We stress that the part of the curve relevant to the phase transition is that in the opposite limit, $m \to 0$, where the numerical procedure easily converges.

We can now go back to the energy, using $\varepsilon = -m^2/2$, and write

$$\omega^{(2)}_{\rm MF}(\varepsilon) = \omega^{(1)}(\tilde{\varepsilon})\, G^{(2)}_{\rm MF}(\varepsilon, \tilde{\varepsilon})\,, \tag{5.36}$$

where $\tilde{\varepsilon} \to \varepsilon$ as $\varepsilon \to \varepsilon^{(2)}_{c,\rm MF} = 0$. One can thus write, as $\varepsilon \to \varepsilon^{(2)}_{c,\rm MF}$,

$$\omega^{(2)}_{\rm MF}(\varepsilon) \to \omega^{(1)}(\varepsilon)\, g^{(2)}_{\rm MF}(\varepsilon)\,, \tag{5.37}$$

where $g^{(2)}_{\rm MF}(\varepsilon) = G^{(2)}_{\rm MF}(\varepsilon, \varepsilon)$, for $\varepsilon \to \varepsilon^{(2)}_{c,\rm MF}$. Figure 5.2 shows the function

$$\eta(\varepsilon) = h(\sqrt{-2\varepsilon}) = \varepsilon - \tilde{\varepsilon}\,; \tag{5.38}$$

as $\varepsilon \to \varepsilon^{(2)}_{c,\rm MF} = 0$, $\eta(\varepsilon) \propto -\sqrt{-\varepsilon}$. Since $|\eta(\varepsilon)|$ is the difference between the energy $\tilde{\varepsilon}$ singled out by the saddle point and the energy ε at which the density of states is calculated, it somehow measures also the "distance" between the

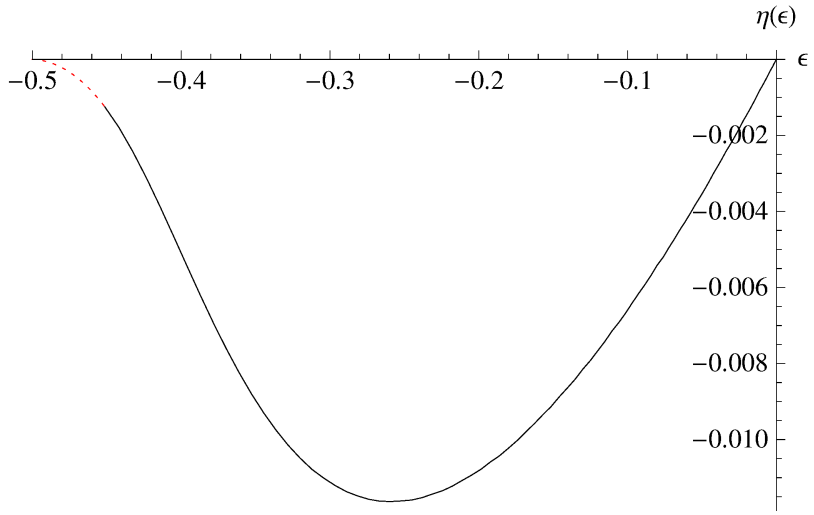

Figure 5.2: Numerical results for the function $\eta(\varepsilon) = h(-\sqrt{2\varepsilon})$ defined in Eq. (5.38) for the mean-field XY model. The red (dotted) part is obtained by interpolation (see Fig. 5.1 and text).

function $G^{(2)}_{\mathrm{MF}}(\varepsilon, \tilde{\varepsilon})$ and the function $g^{(2)}_{\mathrm{MF}}(\varepsilon) = G^{(2)}_{\mathrm{MF}}(\varepsilon, \varepsilon)$. From Fig. 5.2 we see that this difference reaches its maximum (roughly equal to 1.2×10^{-2}) around the center of the energy density range. Comparing this value to the width of the energy range itself we see that this difference is at most of the order of 2%.

5.1.2 The one-dimensional XY model

Let us now consider the one-dimensional XY model, which is a system of N planar spins with nearest-neighbor coupling, described by the Hamiltonian in Eq. (2.19), that we rewrite as

$$H^{(2)}_{1d} = -\sum_{i=1}^{N-1} \cos\left(\vartheta_{i+1} - \vartheta_i\right) , \tag{5.39}$$

where, as in the mean-field XY model, $\vartheta_i \in [0, 2\pi)$, so that the configuration (or phase) space of the system is the torus $\mathbb{T}^N$. This model is ordered only in its state of minimum energy, hence for $\varepsilon^{(2)}_{c,1d} = \varepsilon_{\min} = -1$.

As we shall see in the following, also for this model the density of states can be written as

$$\omega^{(2)}_{1d}(\varepsilon) = \omega^{(1)}(\tilde{\varepsilon})\, G^{(2)}_{1d}(\varepsilon, \tilde{\varepsilon}) , \tag{5.40}$$

where, in this case, $\omega^{(1)}$ is the density of states of the one-dimensional Ising model

$$H_{1d}^{(1)} = -\sum_{i=1}^{N-1} \sigma_i \sigma_{i+1} \,, \tag{5.41}$$

and $\tilde{\varepsilon} \to \varepsilon$ as $\varepsilon \to \varepsilon_{c,1d}^{(2)} = \varepsilon_{\min}$. One can thus write, as $\varepsilon \to \varepsilon_{c,1d}^{(2)}$,

$$\omega_{1d}^{(2)}(\varepsilon) \to \omega^{(1)}(\varepsilon)\, g_{1d}^{(2)}(\varepsilon) \,, \tag{5.42}$$

where $g_{1d}^{(2)}(\varepsilon) = G_{1d}^{(2)}(\varepsilon, \varepsilon)$, for $\varepsilon \to \varepsilon_{c,1d}^{(2)}$. The derivation follows very closely that of the mean-field model, with a few differences that will be underlined.

Let us fix $\vartheta_N = 0$, and leave open the boundary condition at the other side of the chain. As in the mean-field case, the Ising stationary configurations are those where the angles $\overline{\vartheta}$ are either 0 or π. However, their energy is no longer parametrized by N_π. On an Ising stationary configuration, the energy can be written as

$$H_{1d}^{(2)}(\overline{\vartheta}_1, \ldots, \overline{\vartheta}_{N-1}) = H_{1d}^{(1)} = 2N_d - N + 1 \;, \tag{5.43}$$

where N_d is the number of the domain walls in the configuration, i.e., the number of flips between $\overline{\vartheta} = 0$ and $\overline{\vartheta} = \pi$ (and viceversa) along the chain. This implies that one can no longer use the definition (5.18) of the neighborhoods U_p to build the partition of the configuration space, because this would imply that stationary points with the same energy would give different contributions.

Let us then change variables from $(\vartheta_1, \ldots, \vartheta_N)$ to $(x_1, \ldots, x_N)$ as follows:

$$\begin{cases} x_k &= \vartheta_{k+1} - \vartheta_k \quad \text{if } k = 1, \ldots, N-1, \\ \\ x_N &= \vartheta_N = 0 \,. \end{cases} \tag{5.44}$$

In the new variables the Ising stationary points are still such that $\overline{x}_k = 0$ or $\overline{x}_k = \pi$, but now the energy is given in terms of the number of x's equal to π, because the number of domain walls N_d is precisely that number. One can thus define the partition of the configuration space using the neighborhoods $U_{p(x_i)}$ defined as

$$U_{p(x_i)} = \begin{cases} \left[\dfrac{\pi}{2}, \dfrac{3\pi}{2}\right] & \text{if} \quad \overline{x}_i = \pi \\ \\ \left[\dfrac{3\pi}{2}, \dfrac{\pi}{2}\right] & \text{if} \quad \overline{x}_i = 0 \end{cases} \tag{5.45}$$

and write the density of states of the 1-d XY model as

$$\omega_{1d}^{(2)}(\varepsilon) = \sum_{N_d=0}^{N-1} \nu(N_d)\, G_{1d}^{(2)}(\varepsilon, N_d) \tag{5.46}$$

where

$$\nu(N_d) = \frac{(N-1)!}{N_d!(N-N_d-1)!} \tag{5.47}$$

is the number of Ising configurations with N_d domain walls, i.e., the density of states $\omega^{(1)}(\varepsilon')$ of the one-dimensional Ising model with energy density

$$\varepsilon' = \frac{2N_d - N + 1}{N}\,, \tag{5.48}$$

and

$$\begin{aligned} G_{1d}^{(2)}(\varepsilon, N_d) = \int_{\pi/2}^{3\pi/2} dx_1 \cdots dx_{N_d} \int_{3\pi/2}^{\pi/2} dx_{N_d+1} \cdots dx_{N-1} \times \\ \times\ \delta\left(-\sum_{k=1}^{N-1} \cos x_k - N\varepsilon \right)\,. \end{aligned} \tag{5.49}$$

The computation then proceeds following very closely what already done for the mean-field case. The 1-d case is even simpler, because one can directly compute $G_{1d}^{(2)}$ as a function of the energy density, without the need to consider it as a function of the magnetization. Using the integral representation of the δ and integrating on the x variables we can write in the large N limit

$$G_{1d}^{(2)}(\varepsilon, n_d) = \frac{1}{2\pi} \int_{-\infty}^{\infty} dq\, e^{N[-iq\varepsilon + n_d \log b(q) + (1-n_d)\log a(q)]}\,, \tag{5.50}$$

where $n_d = N_d/N$ and the functions a and b are given by

$$a(q) \;=\; \int_{3\pi/2}^{\pi/2} dx\; e^{-iq\cos x}\,, \tag{5.51}$$

$$b(q) \;=\; \int_{\pi/2}^{3\pi/2} dx\; e^{-iq\cos x}\,. \tag{5.52}$$

Performing again a saddle point with $q = -i\gamma$ we get, in the $N \to \infty$ limit,

$$G_{1d}^{(2)}(\varepsilon, n_d) = \frac{1}{\pi}\, e^{N\left[-\gamma\varepsilon + n_d \log \tilde{b}(\gamma) + (1-n_d)\log \tilde{a}(\gamma)\right]}\,, \tag{5.53}$$

where

$$\tilde{a}(\gamma) = \tilde{A}(\gamma, 0)\,, \tag{5.54}$$
$$\tilde{b}(\gamma) = \tilde{B}(\gamma, 0)\,, \tag{5.55}$$

with $\tilde{A}$ and $\tilde{B}$ given by Eqs. (5.30) and (5.31), respectively, and where γ satisfies the self-consistency equation

$$\varepsilon = (1 - n_d)\,\frac{I_1(\gamma) - L_{-1}(\gamma)}{I_0(\gamma) - L_0(\gamma)} + n_d\,\frac{I_1(\gamma) + L_{-1}(\gamma)}{I_0(\gamma) + L_0(\gamma)}\,. \tag{5.56}$$

We can thus realize that Eqs. (5.53) and (5.56) coincide with the same equations derived for the mean-field case, i.e., Eqs. (5.29) and (5.28), provided

$$\begin{cases} m & \to & \varepsilon \\ n_\pi & \to & 1 - n_d \end{cases} \tag{5.57}$$

The latter reflect the fact that in the 1-d case the transition occurs at the minimum value of ε instead of at the maximum.

From now on, the calculation of $\omega^{(2)}_{1d}(\varepsilon)$ is exactly the same as that of $\omega^{(2)}_{\rm MF}(m)$, with the substitutions (5.57). A certain value $\tilde{n}_d$ of n_d will be singled out, which corresponds to an energy density $\tilde{\varepsilon}$ via Eq. (5.48). We thus obtain

$$\omega^{(2)}_{1d}(\varepsilon) = \omega^{(1)}(\tilde{\varepsilon})\, G^{(2)}_{1d}(\varepsilon, \tilde{\varepsilon})\,, \tag{5.58}$$

where $\tilde{\varepsilon} \to \varepsilon$ as $\varepsilon \to \varepsilon^{(2)}_{c,1d} = \varepsilon_{\rm min}$; more precisely, defining the function

$$\zeta(\varepsilon) = \varepsilon - \tilde{\varepsilon} = h(m = \varepsilon + 1)\,, \tag{5.59}$$

where $h(m)$ is the function (5.34) defined for the mean-field XY model, we have that $\zeta \to 0$ when $\varepsilon \to \varepsilon^{(2)}_{c,1d} = \varepsilon_{\rm min} = -1$, and in particular $\zeta \propto -(1+\varepsilon)$ for ε close to $\varepsilon^{(2)}_{c,1d} = -1$. If one plots ζ as a function of ε one thus obtains exactly the same curve reported in Fig. 5.1, with the horizontal axis shifted so that $\varepsilon \in [-1, 0]$. Since $|h(m)|$ is maximum for $m \simeq 0.75$, the function $|\zeta(\varepsilon)|$ reaches its maximum value (roughly equal to 0.15) around $\varepsilon \simeq -0.25$; the maximum difference between ε and $\tilde{\varepsilon}$ in this case is around 15% of the full energy density range, larger than in the mean-field case.

5.1.3 Concluding remarks, part I

The previous Sections have been mainly devoted to discuss the validity of the relation (3.4), recalled in Eq. (5.1), in the special cases of the mean-field

and 1-d XY models. We have shown that the slightly more general formula (5.7) holds, which reduces to the previous one in the limit $\varepsilon \to \varepsilon_c^{(n)}$.

The present work confirms that Eq. (5.1) can not be exact for a generic O(n) model since the specific heat critical exponent α of a O(n) model would then have the correct sign, but the wrong absolute value. More precisely, Eq. (5.1) implies that if α_I is the microcanonical specific heat exponent of the Ising model on a given lattice, then the microcanonical specific heat exponent of the O(n) model on the same lattice and with the same interactions is $\alpha = -\alpha_I$, regardless of n. In $d = 3$, for instance, this yields the correct sign of the O(n) exponents, because $\alpha_I > 0$ so that $\alpha < 0$; the O(n) specific heat is not divergent, but cuspy at the transition. However, the absolute value of the exponent is wrong, because it should depend on n, as shown by well-established results for the O(n) universality classes [121]. It is worth noting that, here and in the following, we are dealing with the specific heat critical exponents defined in the microcanonical ensemble: these are related to the usual critical exponents $\bar{\alpha}$ defined in the canonical ensemble by $\alpha = \bar{\alpha}/(1 - \bar{\alpha})$ [48], so that microcanonical results can be easily carried over to the canonical ensemble[2]. The result $\alpha = -\alpha_I$ follows from Eq. (5.1) by assuming that the function $g^{(n)}(\varepsilon)$ is a generic function which does not contain any explicit information on the phase transition, i.e., is analytic with a generic Taylor expansion. If we proceed in an analogous way assuming that Eq. (5.7) holds for a generic O(n) model, we still find the correct sign of the specific heat critical exponents as with Eq. (5.1), but we do no longer have any contradiction with the known results on the values of the exponents. Indeed, assuming that $G^{(n)}(x, y)$ is a generic (i.e., analytic) function because it should not contain any information about the phase transition, it can be shown that the critical exponent α of the continuous model can be any real number in $[-1, 0)$. This range of values is in agreement with known results [121]; moreover, although it does not predict a precise value of α, it still correctly implies that the specific heat of O(n) lattice spin models does not diverge for $n > 1$. The details about the predictions of Eqs. (5.1) and (5.7) as to the critical exponent α are reported in Appendix C.1.

[2]In particular, if $\bar{\alpha} \in [-1, 0]$ then $\alpha \in \left[-\frac{1}{2}, 0\right]$; we note that the relation $\alpha = \bar{\alpha}/(1 - \bar{\alpha})$ given in [48] holds for any $\bar{\alpha} < 1$.

The two models we have dealt with are very special and both of them are exactly solvable in the microcanonical ensemble. In particular, in these two cases the degeneracy factors $\nu(N_\pi)$ and $\nu(N_d)$ in Eqs. (5.15) and (5.47) can be computed exactly together with the continuous factors $G^{(2)}_{MF}(\varepsilon, N_\pi)$ and $G^{(2)}_{1d}(\varepsilon, N_d)$ in Eqs. (5.20) and (5.49) respectively. This feature is crucial for the derivation we have presented and does not hold for generic short-range O(n) models, the difficulties being similar to exactly solve their thermodynamics in the microcanonical ensemble. To generalize these procedures to short-range O(n) models in $d > 1$ suitable approximations become necessary to compute the above quantities.

Two possible approximation procedures will be presented in the next Sections and their application to the nearest-neighbor XY model in $d = 2$ will be explicitly discussed.

5.2 O(n) models with short-range interactions in $d > 1$

In this Section we are going to give some hints on the generalization of techniques presented in this Chapter to short-range O(n) models in $d > 1$. The results we are discussing are collected in [41] and can be grouped into two different categories according to the approach involved in their derivation.

Supported by the results presented in this Chapter and in [40], the first attempt in the generalization is to set an approximation procedure that allows to evaluate the density of states $\omega^{(n)}(\varepsilon)$ from the sum given by Eq. (5.2). The equation can be rewritten as

$$\omega^{(n)}(\varepsilon) = \sum_{p \in \Gamma} \int_{U_p} d\Gamma \; \delta(H^{(n)} - N\varepsilon) \tag{5.60}$$

where p denotes any Ising stationary configuration of $H^{(n)}$. This approach is the direct generalization of the techniques already applied to the mean-field and to the one-dimensional XY models to generic short-range O(n) models. The approximation protocol we are going to develop will be denoted as "first-principles" approximation, its starting point being simply the density of states $\omega^{(n)}$ expressed in terms of a suitable partition of the phase space Γ of the system. The procedure will be presented in Sec. 5.2.2 and the two-dimensional XY model will be considered as a test model of our analysis.

The second approach starts from the ansatz on the form of the density of states proposed in [38] and discussed in Chapter 3, Eq. (3.4), and given by

$$\omega^{(n)}(\varepsilon) = \omega^{(1)}(\varepsilon)\; g^{(n)}(\varepsilon) \tag{5.61}$$

with $\omega^{(1)}(\varepsilon)$ density of states of the Ising model and $g^{(n)}(\varepsilon)$ is the continuous factor given by Eq. (5.3). From Eq. (5.5) we have that $g^{(n)}(\varepsilon) = G^{(n)}(\varepsilon, \varepsilon)$ with $G^{(n)}(\varepsilon, \varepsilon)$ given by Eq. (5.4) for Ising stationary points p with energy density $\varepsilon' = H^{(n)}/N$ such that $\varepsilon' = \varepsilon$. In this approach it is assumed that the integral in Eq. (5.4) does not depend on the specific point considered but only on its energy density ε' and that only Ising point with energy density $\varepsilon' = \varepsilon$ contribute to the density of states $\omega^{(n)}(\varepsilon)$ in Eq. (5.61). We will denote this kind of analysis as "ansatz-based" approximation. The general aspects of the method will be presented in Sec. 5.2.3 and its application to the XY model in two-dimensions will be discussed in detail.

Both in the "ansatz-based" and "first-principles" approximations, the main point is to evaluate the quantity

$$\int_{U_p} d\Gamma\; \delta\left(H^{(n)} - N\varepsilon\right) = \int_{U_p} d\Gamma\; \delta\left(-\frac{1}{2}\sum_{i=1}^{N}\sum_{j\in\mathcal{N}(i)}\sum_{a=1}^{n} S_i^a S_j^a - N\varepsilon\right); \tag{5.62}$$

where $\mathcal{N}(i)$ denotes the set of nearest-neighbors of lattice site i and we have introduced the explicit expression of $H^{(n)}$ given by Eq. (2.1) in the case of short-range O(n) models. According to the analysis presented in Secs. 5.1.1 and 5.1.2, we suppose that the neighborhoods U_p in Eq. (5.62) can be chosen in such a way that

$$\int_{U_p} d\Gamma\; \delta\left(H^{(n)} - N\varepsilon\right) = \int_{U_q} d\Gamma\; \delta\left(H^{(n)} - N\varepsilon\right) \tag{5.63}$$

for any Ising stationary points p and q such that $H^{(n)}(p) = H^{(n)}(q)$. Among the O(n) class of models, Eq. (5.62) can be analytically evaluated only in the cases of the mean-field and one-dimensional XY models; its computation in the general case being as difficult as to find an exact solution of the models. However some computational procedures can be set up to carry on the calculations, albeit approximate. In [41, 55] a particular scheme of approximation has been introduced, named the Local-Mean-Field (LMF) approximation [41]. This is a model-dependent procedure that allows to reduce

the $N-$dimensional integral in Eq. (5.62) over the configuration space Γ to N one-dimensional integrals over single uncoupled variables. The uncoupling procedure becomes possible once suitable model-dependent collective variables are defined, whose rôle reminds the one played by N_π and N_d in Eqs. (5.20) and (5.49), respectively. The LMF procedure can be applied to any O(n) model with short-range (or long-range, see i.e. [55]) interactions and in any spatial dimensions d; the difference from case to case is simply given by the number and by the type of global variables needed in the calculations. The proof of the technique is constructive and will be presented in Sec. 5.2.1. For simplicity we restrict the presentation to the case $n = 2$ and to two-dimensional square lattices with periodic boundary conditions. Generalizations to higher-dimensional lattices and different values of n are possible along similar lines, but we did not work this out in detail although something similar has been done in [55] for the case $n = 2$ and $d = 3$.

5.2.1 The Local Mean-Field (LMF) approximation

In the case $n = 2$ and $d = 2$, i.e. for the XY models in two spatial dimensions, the parametrization (2.3) can be chosen such that the integral in Eq. (5.62) becomes

$$\begin{aligned}
&\int_{U_p} d\vartheta_1 \dots d\vartheta_N \, \delta\left(-\frac{1}{2} \sum_{\langle i,j \rangle}^{N} \cos\left(\vartheta_i - \vartheta_j\right) - N\varepsilon \right) = \\
&= \int_{U_p} d\vartheta_1 \dots d\vartheta_N \times \\
&\quad \times \delta\left(- \sum_{i=1}^{N} \left[\cos\vartheta_i \sum_{j=1}^{2} \cos\vartheta_i^{(j)} + \sin\vartheta_i \sum_{j=1}^{2} \sin\vartheta_i^{(j)} \right] - N\varepsilon \right) = \\
&= \int_{-\infty}^{\infty} \frac{dk}{2\pi} e^{-ikN\varepsilon} \times \\
&\quad \times \int_{U_p} d\vartheta_1 \dots d\vartheta_N \; e^{-ik \sum_{i=1}^{N} \left[\cos\vartheta_i \sum_{j=1}^{2} \cos\vartheta_i^{(j)} + \sin\vartheta_i \sum_{j=1}^{2} \sin\vartheta_i^{(j)} \right]}
\end{aligned} \tag{5.64}$$

where we have introduced the integral representation of the $\delta-$function, $\delta(x) = \frac{1}{2\pi} \int_{-\infty}^{\infty} e^{-ikx} dk$; $\vartheta_i^{(j)}$ denotes the nearest-neighbor spin j of the lattice site i considered according to the convention reported in Fig. 5.3. The two spins identified by $\vartheta_i^{(1)}$ and $\vartheta_i^{(2)}$ are said to be second-neighbors spins. A generalization of Eq. (5.64) to $n > 2$ and $d > 2$ should be straightforward

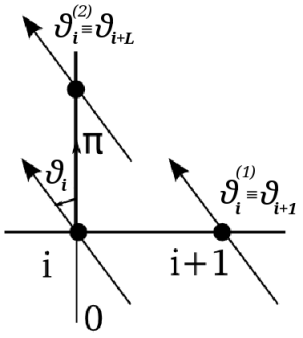

Figure 5.3: Index convention for the nearest-neigbors spins $\vartheta_i^{(1)}$ and $\vartheta_j^{(2)}$ of ϑ_i for the XY model on a square lattice of edge $L = \sqrt[3]{N}$ and periodic boundary conditions. The spins in the lattice sites $i+1$ and $i+L$ are said to be second-neighbors.

once a proper parametrization for the angular variables as in Eq. (2.3) is chosen and the spins are properly labeled.

In Eq. (5.64), p denotes any Ising stationary point; the LMF approximation can then be introduced as follows.

Let us consider a particular Ising point, i.e. $\bar{p} = \left(\bar{\vartheta}_1, \ldots, \bar{\vartheta}_N\right)$ with $\bar{\vartheta}_i \in \{0, \pi\}$ $\forall i = 1, \ldots, N$. For each angular variable ϑ_i, in Eq. (5.64) we replace the $N-1$ variables ϑ_j with $j \neq i$ with their numerical values $\bar{\vartheta}_j$ assumed on the specific point $\bar{p}$. The variable ϑ_i is left free to vary in all the range specified by $U_{\bar{p}(\vartheta_i)}$. In this way the angular variables in Eq. (5.64) become uncoupled and we have that

$$\begin{aligned} &\int_{-\infty}^{\infty} \frac{dk}{2\pi} e^{-ikN\varepsilon} \times \\ &\times \int_{U_p} d\vartheta_1 \ldots d\vartheta_N \; e^{-ik\sum_{i=1}^{N}\left[\cos\vartheta_i \sum_{j=1}^{2}\cos\vartheta_i^{(j)} + \sin\vartheta_i \sum_{j=1}^{2}\sin\vartheta_i^{(j)}\right]} = \\ &= \int_{-\infty}^{\infty} \frac{dk}{2\pi} e^{-ikN\varepsilon} \prod_{i=1}^{N} \int_{U_{\bar{p}(\vartheta_i)}} d\vartheta_i \, e^{-ik\cos\vartheta_i\left(\cos\bar{\vartheta}_i^{(1)} + \cos\bar{\vartheta}_i^{(2)}\right)} \end{aligned} \tag{5.65}$$

with $H(\bar{p}) = N\varepsilon'$. Eq. (5.65) clarifies the choice of Local Mean-Field as the name for the approximation. In fact, after LMF approximation is applied, the angular variables ϑ_i's in Eq. (5.65) become independent variables in $U_{\bar{p}(\vartheta_i)}$; each degree of freedom interacts only with a sort of local mean-field given by $\sum_{j=1}^{2}\cos\bar{\vartheta}_i^{(j)}$, generated by the spins in the nearest-neighbor lattice sites. It is worth to stress that the approximation is not a proper mean-field approximation; indeed the *local* field applied to every spin depends on

the values of its nearest-neighbors and can possibly vary from site to site. Remarkably, with this approximation the contribution of the sines in the exponent of Eq. (5.65) vanishes, since $\sin\vartheta_i = 0$ when $\vartheta_i \in \{0, \pi\}$, and the expression in Eq. (5.65) simplifies.

Since the analysis is restricted to Ising stationary configurations, in Eq. (5.65) only two facts are possible:

(a) The second neighbor spins are equal. In this case $\cos\bar{\vartheta}_i^{(1)} = \cos\bar{\vartheta}_i^{(2)} = \pm 1$, and so

$$\int_{U_{\bar{p}(\vartheta_i)}} d\vartheta_i \; e^{-ik\cos\vartheta_i\left(\cos\bar{\vartheta}_i^{(1)}+\cos\bar{\vartheta}_i^{(2)}\right)} = \int_{U_{\bar{p}(\vartheta_i)}} d\vartheta_i \; e^{\mp 2ik\cos\vartheta_i}; \qquad (5.66)$$

(b) The second neighbor spins are opposite. In this case $\cos\bar{\vartheta}_i^{(1)} = -\cos\bar{\vartheta}_i^{(2)}$, and so

$$\int_{U_{\bar{p}(\vartheta_i)}} d\vartheta_i \; e^{-ik\cos\vartheta_i\left(\cos\bar{\vartheta}_i^{(1)}+\cos\bar{\vartheta}_i^{(2)}\right)} = \int_{U_{\bar{p}(\vartheta_i)}} d\vartheta_i \; . \qquad (5.67)$$

To evaluate Eqs. (5.66) and (5.67) the only missing thing is the definition of the neighborhoods $U_{\bar{p}(\vartheta_i)}$. A priori there are no particular clues on the best choice of $U_{\bar{p}(\vartheta_i)}$; the only request being that $\{U_{p(\vartheta_1)}, \ldots, U_{p(\vartheta_N)}\}_{p=1}^{2^N}$ has to be a partition of the phase space of the system. In the following, two different choices of $U_{p(\vartheta_i)}$ will be considered:

- *Choice 1*

$$U_{p(\vartheta_i)} = \begin{cases} [-\pi, \pi], & \text{if } \bar{\vartheta}_i = 0, \\ [0, 2\pi], & \text{if } \bar{\vartheta}_i = \pi. \end{cases} \qquad (5.68)$$

- *Choice 2*

$$U_{p(\vartheta_i)} = \begin{cases} \left[-\frac{\pi}{2}, \frac{\pi}{2}\right], & \text{if } \bar{\vartheta}_i = 0, \\ \left[\frac{\pi}{2}, \frac{3\pi}{2}\right], & \text{if } \bar{\vartheta}_i = \pi. \end{cases} \qquad (5.69)$$

In principle choice 1 should be avoided, the neighborhoods $U_{p(\vartheta_i)}$'s being partially superposed. We will consider it in any case, since it is the easiest choice that can be done a priori for these systems. For the "first-principles" approximation only the first choice for the $U_{p(\vartheta_i)}$ will be considered, the convergence problems in the numerical evaluation of $\omega^{(n)}(\varepsilon)$ with $U_{p(\vartheta_i)}$ as in choice 2 being difficult to control. For the "ansatz-based" approximations,

instead, both choice 1 and choice 2 will be considered and the effect of neighborhood superposition will be explicitly discussed.

Once the LMF approximation is defined the "first-principles" and the "ansatz-based" approach can be discussed in detail and their application to the two-dimensional XY model in $d = 2$ will be the subject of the next Sections.

5.2.2 "First-principles" approximation

Let us consider the form of the density of state $\omega^{(n)}(\varepsilon)$ given by Eq. (5.60). In the following we are going to apply our procedure to derive an approximate form of the density of states $\omega^{(2)}(\varepsilon)$ for the XY model in $d = 2$. A generalization of these techniques to O(n) models with $n > 2$ in $d > 2$ is thought to be possible on the same lines and the key points will be highlighted in the following discussion.

Once the XY model in $d = 2$ is considered, Eq. (5.60) can be written as

$$\begin{aligned}\omega_N^{(2)}(\varepsilon) \simeq \sum_{p\in\Gamma} \frac{1}{2\pi} \int_{-\infty}^{\infty} dk\, e^{-iNk\varepsilon} \int_{U_p} d\vartheta_1 \dots d\vartheta_N \times \\ \times \quad e^{-ik\sum_{i=1}^{N}\left[\cos\vartheta_i \sum_{j=1}^{2}\cos\vartheta_i^{(j)} + \sin\vartheta_i \sum_{j=1}^{2}\sin\vartheta_i^{(j)}\right]},\end{aligned} \tag{5.70}$$

where p is any Ising stationary configuration. The integral over the angular variables ϑ_i can be evaluated by applying the LMF approximation procedure presented in Sec. 5.2.1. In this case we choose a definition of the integration neighbors as in Eq. (5.68). Similar results are supposed to hold also for a choice of $U_{p(\vartheta_i)}$ as in Eq. (5.69) but the calculations have not been carried out in this case. As discussed in Sec. 5.2.1, the generalization of Eq. (5.70) to other O(n) models is straightforward and depends on the parametrization chosen to describe the spin variables and on the number of nearest neighbors (that is, on the dimensionality of the lattice).

From Eqs. (5.66) and (5.67) we have

$$\int_{-\pi}^{\pi} d\vartheta\; e^{\mp 2ik\cos\vartheta} = 2\pi J_0(2|k|) \tag{5.71}$$

whenever a couple of equal second-neighbors spins is present in the system, and

$$\int_{0}^{2\pi} d\vartheta\; 1 = 2\pi \tag{5.72}$$

every time a couple of opposite second-neighbors spins is present in the system; $J_0(x)$ is the zero order Bessel function of the first kind [148]. We will denote by N_c the number of pairs of equal second-neighbor spins present in the system[3] and by $n_c = N_c/N$ its number density.

The collective parameter N_c plays the same rôle as N_π and N_d for the mean-field and the one-dimensional XY models, respectively. Indeed, for any given value of N_c, a particular family of Ising stationary configurations is selected and the integral in Eq. (5.70) becomes the product of two different contributions: the first one is $(2\pi J_0(2|k|))^{N_c}$ and it is due to number of pairs of equal second neighbors spins, and the second one is $(2\pi)^{N-N_c}$ that is due to the number of opposite pairs. In this way Eq. (5.70) becomes

$$\omega_N^{(2)}(\varepsilon) \simeq \sum_{N_c=0}^{N} \nu(N_c) \frac{(2\pi)^{N(1-n_c)}}{2\pi} \int_{-\infty}^{\infty} dk\; e^{N\left[-i\,k\;\varepsilon + n_c \log\left(2\pi J_0(2\sqrt{k^2})\right)\right]}, \quad (5.73)$$

where $\nu(N_c)$ is the degeneracy factor analogous to $\nu(N_\pi)$ and $\nu(N_d)$ in Eqs. (5.15) and (5.47), respectively, that counts how many Ising configurations are present for a certain value N_c of the collective variable. Thanks to the choice of periodic boundary conditions in the system, N_c can vary from 0 to N; moreover the problem of determining $\nu(N_c)$ in Eq. (5.73) is reduced to a combinatorial problem analogous to the one of disposing N_c distinct elements over N possible empty spaces. The solution to the latter is given by the binomial factor $\nu(N_c) = \binom{N}{N_c} = \frac{N!}{N_c!(N-N_c)!}$. The evaluation of the degeneracy factor $\nu(N_c)$ is crucial for our analysis and we will come back on this point at the end of this Section.

Since we are interested in the large N behavior of the system, the integration over k in Eq. (5.73) can be computed with the saddle-point method. The saddle-point equation is given by $k = i\tau$ with τ satisfying the self-consistency equation

$$\frac{I_1(2\tau)}{I_0(2\tau)} = \frac{\varepsilon}{2n_c}. \quad (5.74)$$

[3]The number of pairs of opposite spins will be simply given by $N_D = N - N_c$.

Eq. (5.73) can then be written as

$$\begin{aligned}\omega_N^{(2)}(\varepsilon) \simeq \sum_{Nn_c=0}^{N} \frac{N!}{N_c!(N-N_c)!}\, e^{N[-\tau\,\varepsilon+\log 2\pi+\, n_c \log(I_0(2\tau))]} \simeq \\ \simeq N \int_0^1 dn_c\; e^{N[-\tau\,\varepsilon-\, n_c \log n_c-(1-n_c)\log(1-n_c)+\log 2\pi+\, n_c \log(I_0(2\tau))]},\end{aligned} \tag{5.75}$$

where we have replaced the sum over N_c with an integration over n_c, we have neglected the term $-\frac{1}{N}\log 2\pi$ in the exponent since its contribution will vanish in the limit $N \gg 1$, and we have introduced the Stirling approximation of the factorial terms in the binomial coefficient to get

$$\frac{N!}{N_c!(N-N_c)!} \simeq e^{N[-n_c \log n_c-(1-n_c)\log(1-n_c)]}. \tag{5.76}$$

For each value of the energy density ε, we can approximate Eq. (5.75) as

$$\omega_N^{(2)} \simeq\; N\; e^{N\;\max_{n_c\in[0,1]}\,[-\tau\,\varepsilon-\, n_c \log n_c-(1-n_c)\log(1-n_c)+\log 2\pi+\, n_c \log(I_0(2\tau))]}; \tag{5.77}$$

In this way the entropy density $s^{(2)}(\varepsilon)$ of the system in the thermodynamic limit is finally given by:

$$s^{(2)}(\varepsilon) \simeq \max_{n_c\in[0,1]} f(n_c,\tau), \tag{5.78}$$

with

$$\begin{aligned}f(n_c,\tau) = -\,\tau\,\varepsilon -\; n_c \log n_c - (1-n_c)\log(1-n_c)+ \\ +\log 2\pi +\; n_c \log\left(I_0(2\tau)\right)\end{aligned} \tag{5.79}$$

and τ numerically determined from Eq. (5.74). The maximization procedure in Eq. (5.78) can be performed numerically with the help of MATHEMATICA. The temperature T and the specific heat c as a function of the energy density have been computed from Eq. (5.78) by numerical differentiation and are displayed as red circles in Figs. 5.4 and 5.5, respectively. As a comparison, data for T and c as functions of the energy density ε have been computed with a Monte Carlo simulation of the XY model with edge $L = 32$ in $d = 2$, performed with the optimized cluster algorithm `spinmc` provided by the ALPS project [132]. The numerical data are plotted in Figs. 5.4 and 5.5 as blue triangles together with the results from our approximation. The error bars in the numerical data lie inside the symbols.

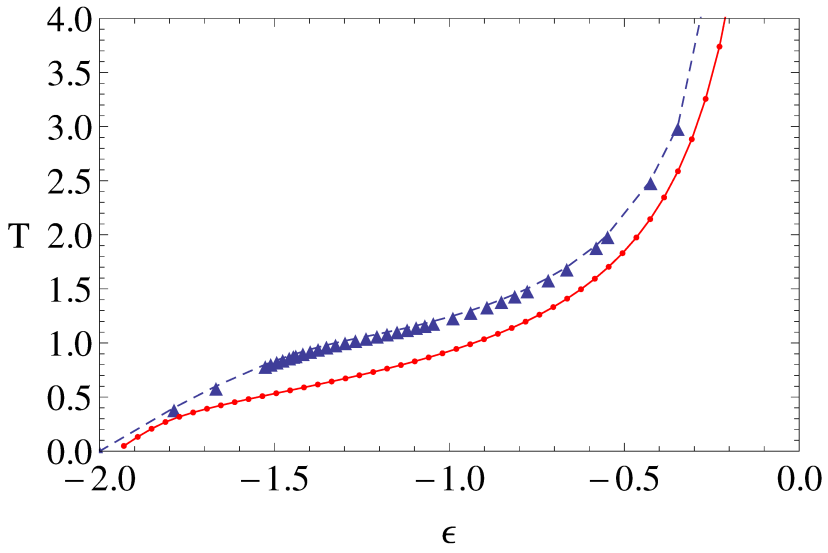

Figure 5.4: Temperature T as a function of the energy density ε as derived from Eq. (5.78) for the XY model in $d = 2$. Our results (red circles) are plotted together with the data obtained by a Monte Carlo simulation (blue triangles). The dashed blue line and the solid red line connecting the two sets of data are meant as guide to the eyes. The error bars in the Monte Carlo data lie inside the symbols.

Fig. 5.4 shows that our approximation correctly reproduces the asymptotic behavior of the function $T(\varepsilon)$ both in the low and in the high energy regime, at a semiquantitative level. In particular, for $\varepsilon \simeq -2$ our results and the simulation data are almost coincident. For $\varepsilon \geq -1.8$ the discrepancy between the numerical and the approximate results increases; the approximate value of the temperature remains lower than the results obtained from the simulations although essentially at a constant distance. The difference between the calculated and the simulated temperatures never exceeds the 15%.

Our results for the specific heat are reported in Fig. 5.5 (red circles). They reveal a peak for $\varepsilon_{p,1} \simeq -1.495$ marked by the vertical red dot-dashed line, at a slightly lower energy density value then $\varepsilon_p \simeq -1.24$ where the peak occurs in the simulation data (vertical dashed blue line). The overall shape of the specific heat sketched by our results is in qualitative agreement with the numerical results for $\varepsilon \in [\varepsilon_{p,1}, -0.6]$ although it is shifted to lower energies with respect to the blue triangles. For $\varepsilon \geq -0.6$ the agreement increases also quantitatively and two sets of points become essentially indistinguishable.

On the other side, for $\varepsilon < \varepsilon_{p,1}$ the agreement becomes worse. Both from

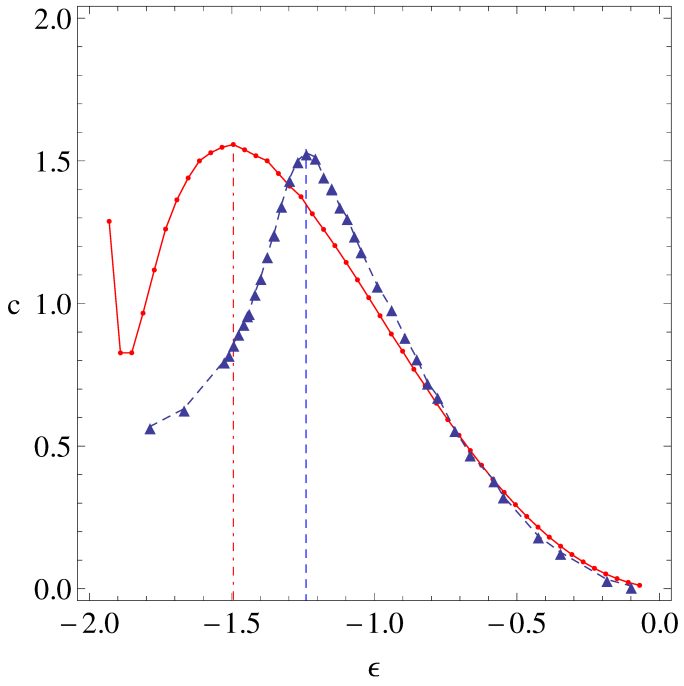

Figure 5.5: Specific heat c as a function of the energy density ε as derived from Eq. (5.78) for the XY model in $d = 2$. Our results (red circles) are plotted together with the data obtained by a Monte Carlo simulation (blue triangles). The dashed blue line and the solid red line connecting the two sets of data are meant as guide to the eyes. The error bars in the Monte Carlo data lie inside the symbols.

theoretical and numerical results, we know that $c(\varepsilon) \to 0.5$ when $\varepsilon \to 0$, see i.e. [96, 97]. Our results show an abrupt increase for $\varepsilon \simeq -1.85$ which is not physical but is due to a shortcoming of our approximation that is still under investigation.

The degeneracy factor ν and a different approximation for $\omega^{(n)}$

The analysis presented in this Section shows that the "first-principles" procedure provides a practical method to derive an approximate form of the density of states $\omega^{(2)}$ in two dimensions. In fact, the thermodynamic functions derived from Eq. (5.78) are in reasonably good agreement with the simulations, as shown in Figs. 5.4 and 5.5.

This fact suggests that our idea of considering only Ising stationary points in the derivation of $\omega^{(2)}(\varepsilon)$ is trustworthy and it provides a good strategy to approximate the thermodynamic properties of continuous O(n) models, in

principle for any value of n and d.

An important feature of the "first-principles" approximation is the natural emergence of collective variables, like N_c, in terms of which the stationary configurations can be parametrized and the density of states re-written as in Eq. (5.73). The number and the type of the collective variables depend on several aspects: the model considered, the dimensionality of the lattice, the definition of the integration neighbors $U_{p(\vartheta_i)}$, the specific Ising point p considered, and the approximation strategy applied to evaluate the integral in Eq. (5.62). Indeed, instead of applying the LMF approximation, other strategies could have been adopted to compute the integral in Eq. (5.62), like a harmonic expansion of the Hamiltonian $H^{(n)}$ around the Ising stationary points. In this case other quantities, as the reduced determinant of the Hessian matrix $\mathcal{D}(p)$ or the density of index ι, would have emerged in the analysis.

Let us denote by $\mathbf{z}(n, d, p)$ the vector of collective variables needed in the evaluation. In the "first-principle" approach the density of states $\omega_N^{(n)}(\varepsilon)$ can always be reduced to a form of the type

$$\omega_N^{(n)}(\varepsilon) = \sum_{\mathbf{z}(n,d,p)}^{N} \nu(\mathbf{z}(n, d, p), N)\ f(\mathbf{z}(n, d, p), N), \tag{5.80}$$

as shown in Eq. (5.73). In the above expression $\nu(\mathbf{z}(n, d, p), N)$ represents the degeneracy factor[4] associated to the collective vector of parameters $\mathbf{z}$ which counts how many Ising configurations are present in the system for given values $\mathbf{z}(n, d, p)$ and N of the collective variables and of the number of degrees of freedom of the system, respectively.

The degeneracy factor ν can not be evaluated analytically but in some specific cases like those discussed so far, and its computation may require additional approximations that can vary from case to case. As an example, if the continuous factor in Eq. (5.62) is approximated by expanding $H^{(n)}$ around each Ising point p up to harmonic order, the vector of collective variables $\mathbf{z}(n, d, p)$ becomes $\{\mathcal{D}(p), \iota(p), H^{(n)}(p)/N\}$ and the analytical expression of $\nu(\mathcal{D}(p), \iota(p), H^{(n)}(p)/N)$ is hard to find, see [41]. To carry on the calculation one may then estimate $\nu(\mathbf{z}(n, d, p))$ numerically. This can be done for instance by performing a Monte Carlo simulation in which the Ising

[4]Like i.e. $\nu(N_\pi)$, $\nu(N_d)$ and $\nu(N_c)$ in Eqs. (5.15), (5.47), (5.73), respectively.

configurations are grouped and counted according to their value of $\mathbf{z}$. This method, although possibly correct, would require a strong computational effort. We leave its investigation to future work.

On the other hand the ansatz on the form of the density of states $\omega^{(n)}$ proposed in [38] and discussed in Chapter 3 was able to reproduce with unexpected accuracy both the emergence of the phase transitions in the O(n) models and even the critical energy density values at which the transitions are located.

Then, one may consider Eq. (5.61) as the new starting point to approximate the thermodynamic functions of the O(n) system in the whole energy density range $[-d, d]$. In this kind of approach, called "ansatz-based" approach, the main point remains the estimation of $g^{(n)}(\varepsilon)$; this implies the emergence of collective variables $\mathbf{z}(n, p, d)$, as before. This notwithstanding, it is now reasonable to assume that, given a particular Ising point p with energy density $\varepsilon' = H^{(n)}(p)/N$, the possible values of the collective variables $\mathbf{z}(n, d, p)$ would narrow around a typical value $\tilde{\mathbf{z}}(n, d, p)$ when $N \to \infty$. Results reported in Secs. 2.3.1 and 2.3.2 for the reduced determinant $\mathcal{D}$ and for the density of index ι for the two- and three-dimensional nearest-neighbors XY models confirm this idea and suggest that the typical value $\tilde{\mathbf{z}}(n, d, p)$ would not depend on p anymore but only on its energy density ε', when $N \gg 1$. We then have $\tilde{\mathbf{z}}(n, d, p) \sim \tilde{\mathbf{z}}(n, d, \varepsilon')$. Since the ansatz in Eq. (5.61) imposes that only stationary points with energy density $\varepsilon' = \varepsilon$ have to be considered in the evaluation of $\omega^{(n)}(\varepsilon)$, we have that $g^{(n)}(\mathbf{z}(d, p)) \to g^{(n)}(\mathbf{z}(d, \varepsilon)) = g^{(n)}(\varepsilon)$ in $d-$dimensions, with $\mathbf{z}(d, \varepsilon)$ suitable functions that can be easily computed with numerical fits of simulation data.

All these concepts will be clarified in the next Sections where the "ansatz-based" approximation will be applied to the XY model in $d = 2$.

5.2.3 "Ansatz-based" approximation

Let us consider the density of states $\omega^{(n)}$ as given by Eq. (5.61); then, our purpose is to estimate the continuous factor $g^{(n)}(\varepsilon)$. This can be done for instance by applying the LMF approximation introduced in Sec. 5.2.1. Let us consider the XY model in $d = 2$ as test model of our procedure so that all the technical tools presented in Sec. 5.2.1 can be immediately applied to this case; the generalization to other O(n) models should be straightforward.

LMF approximation for $g^{(2)}(\varepsilon)$ and $U_{p(\vartheta_i)}$ given by Eq. (5.68).

We start considering the LMF approximation with the first choice of the neighbors $U_{p(\vartheta_i)}$ given by Eq. (5.68). In this case the calculations proceed on the same lines as in the case of the "first-principles" approximation, the only difference being that only Ising points with energy density ε are considered and the collective variable $\mathbf{z}(2, 2, \varepsilon) = N_c(\varepsilon)$ does not depend on the specific Ising point p anymore but only on its energy density ε.

The density of states can then be written as

$$\omega_N^{(2)}(\varepsilon) = \omega_N^{(1)}(\varepsilon) \frac{(2\pi)^{N(1-n_c(\varepsilon))}}{2\pi} \int_{-\infty}^{\infty} e^{N\left[-ik\varepsilon + n_c(\varepsilon)\log\left(2\pi J_0\left(2\sqrt{k^2}\right)\right)\right]} \tag{5.81}$$

where $\omega_N^{(1)}(\varepsilon)$ plays the rôle of $\nu(N_c, N)$ in Eq. (5.73) and is analytically known thanks to the Onsager solution [95]. On the other hand, $n_c = n_c(\varepsilon)$ is an unknown function that has to be determined. This has be done interpolating the numerical data obtained by a Monte Carlo simulation of the two-dimensional XY model with edge $L = 32$. The interpolation has been performed with the MATHEMATICA built-in routine `Interpolation` and the result is shown as a solid blue line in Fig. 5.6, together with the simulation data.

The integral in Eq. (5.81) can be computed with the saddle-point method and the saddle-point equation is given by $k = i\lambda$; λ satisfies a self-consistency equation analogous to Eq. (5.74) given by

$$\frac{I_1(2\lambda)}{I_0(2\lambda)} = \frac{\varepsilon}{2n_c(\varepsilon)}. \tag{5.82}$$

Eq. (5.81) can then be written as

$$\begin{aligned} \omega_N^{(2)}(\varepsilon) &\simeq \omega_N^{(1)}(\varepsilon) e^{N[-\lambda\varepsilon + \log 2\pi + n_c(\varepsilon)\log(I_0(2\lambda))]} = \\ &= e^{N\left[s_N^{(1)}(\varepsilon) - \lambda\varepsilon + \log 2\pi + n_c(\varepsilon)\ \log(I_0(2\lambda))\right]} \end{aligned} \tag{5.83}$$

valid for $N \gg 1$; $s_N^{(1)}(\varepsilon)$ represents is the entropy density of the two-dimensional Ising model. Dividing by N the logarithm of the above expression, letting $N \to \infty$ and neglecting the sub-leading terms in N, we finally get the following expression for the entropy density of the XY model in $d = 2$

$$s^{(2)}(\varepsilon) \sim s^{(1)}(\varepsilon) + \log 2\pi - \lambda\varepsilon + n_c(\varepsilon)\log\left[I_0(2\lambda)\right]; \tag{5.84}$$

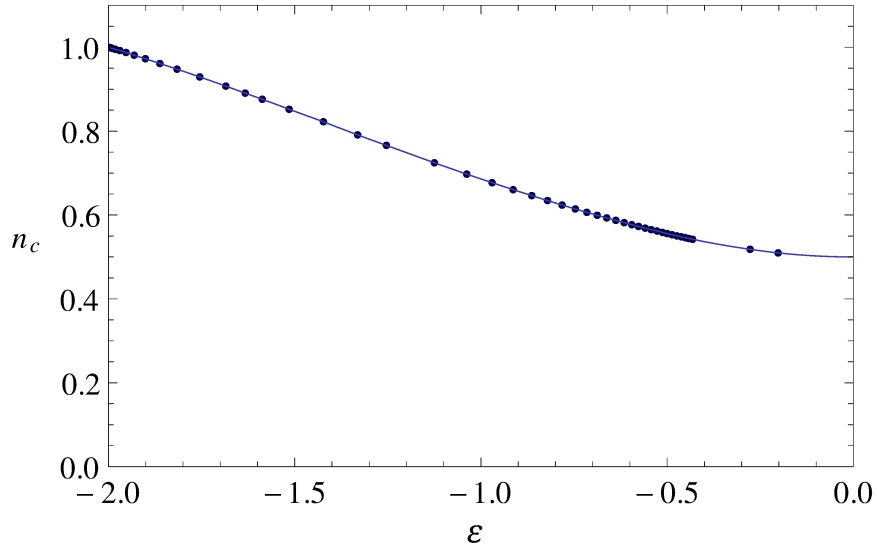

Figure 5.6: Numerical data for n_c obtained from a Monte Carlo simulation of the two-dimensional Ising model with edge $L = 32$, blue points. The solid blue line represents the interpolating function $n_c(\varepsilon)$. Error bars lie inside the points.

with λ satisfying the self-consistency equation (5.82). In Fig. 5.7 we plot the temperature T as a function of the energy density ε as obtained from numerical differentiation of Eq. (5.84) (red points) according to Eq. (1.6). As in Fig. 5.4, the values obtained with a Monte Carlo simulation are shown for comparison (blue triangles). The error bars in the Monte Carlo data lie inside the symbols

Fig. 5.7 shows that the asymptotic behavior of the function $T(\varepsilon)$, in the harmonic regime (very low-energy), in the low-energy regime and in the high-energy limit is well reproduced at a semiquantitative level by our approximation; the agreement is extremely good for low energies. For $\varepsilon \gtrsim -1.9$ the approximate results move away from the numerical ones and, $\varepsilon \gtrsim \tilde{\varepsilon} = -1.9$ the approximate value of the temperature remains lower than the results obtained from the simulation[5]. The largest difference between theoretical and numerical values of T is about 50%.

In Fig. 5.8 the values of the specific heat c obtained with a numerical differentiation of Eq. (5.84) as in Eq. (1.7) are plotted as a function of

[5]This behavior is analogous to the one obtained in [55] with a similar procedure applied to the partition function of the system.

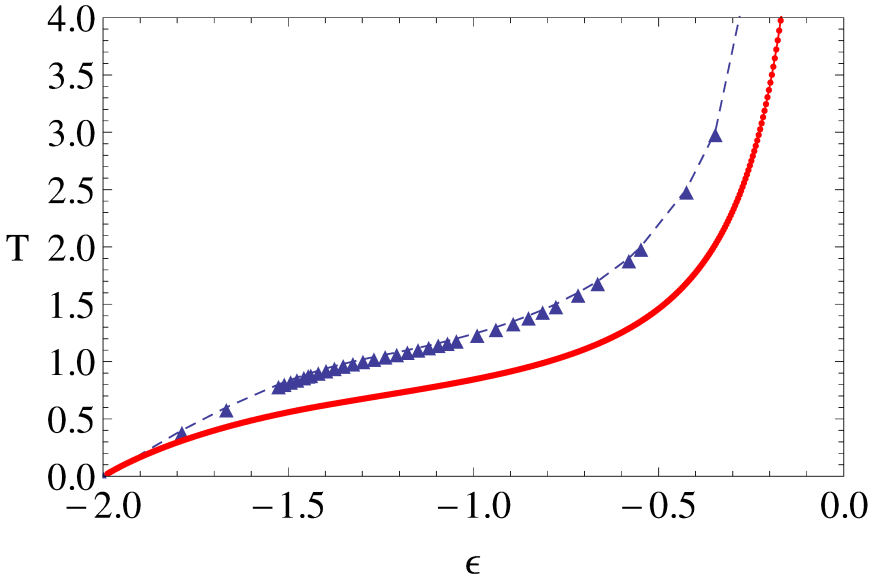

Figure 5.7: Temperature T as a function of the energy density ε as derived from Eq. (5.84) for the XY model in $d = 2$. Our results (red circles) are plotted together with the data obtained by a Monte Carlo simulation (blue triangles). The dashed blue line and the solid red line connecting the two sets of data are meant as guide to the eyes. The error bars in the Monte Carlo data lie inside the symbols

the energy density ε. As in Fig. 5.7 the theoretical results are displayed as red circles and are plotted together with the values of c computed by Monte Carlo simulation (blue triangles). The specific heat shows a peak for $\varepsilon_{p,2} \simeq -1.258$ marked by the vertical red dot-dashed line. This value of the energy density is very close to $\varepsilon_p \simeq -1.24$ that is the energy density value at which the peak occurs in the simulation data. Our approximation is able to reproduce the correct behavior of the specific heat in the high-energy regime, while the agreement becomes slightly worse in the low-energy case, although qualitatively correct. The difference between calculated and simulated values of c is about 20% for $\varepsilon < \varepsilon_p$ and smaller for $\varepsilon > \varepsilon_p$. Trend of the theoretical results up to $\varepsilon \simeq -1.9$ seems to suggests a value for $c(-2) \in [0.5, 0.6]$, a bit higher than expected. For $\varepsilon \simeq -2$ a shortcoming of the approximation procedure produces the abrupt increase of our results as in Fig. 5.5.

The calculations presented in this Section have been repeated using the expression of $U_{p(\vartheta_i)}$ given in Eq. (5.69). The results are presented in the following.

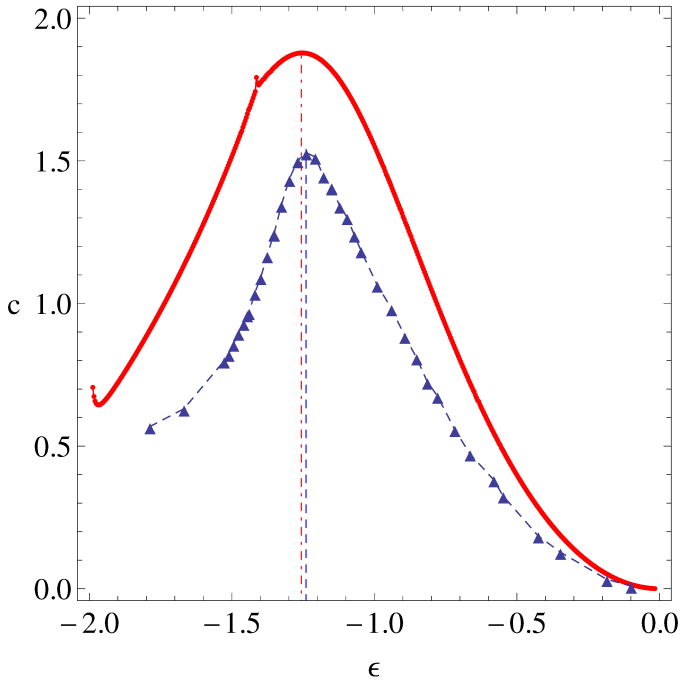

Figure 5.8: Specific heat c as a function of the energy density ε as derived from Eq. (5.84) for the XY model in $d = 2$. Our results (red circles) are plotted together with the data obtained by a Monte Carlo simulation (blue triangles). The dashed blue line and the solid red line connecting the two sets of data are meant as guide to the eyes. The error bars in the Monte Carlo data lie inside the symbols

LMF approximation for $g^{(2)}(\varepsilon)$ and $U_{p(\vartheta_i)}$ given by Eq. (5.69).

We now consider the LMF approximation with the neighborhoods $U_{p(\vartheta_i)}$ given by Eq. (5.69). Given a particular Ising configuration p, from Eq. (5.66) we have:

- if $\bar{\vartheta}_i^{(1)} = \bar{\vartheta}_i^{(2)} = 1$ (resp. -1) and $\bar{\vartheta}_i = 1$ (resp. -1), i.e., the configuration looks locally like

$$\begin{array}{ccc} \cdot & \uparrow & \cdot \\ \cdot & \uparrow & \uparrow \\ \cdot & \cdot & \cdot \end{array} \quad \text{or respectively} \quad \begin{array}{ccc} \cdot & \downarrow & \cdot \\ \cdot & \downarrow & \downarrow \\ \cdot & \cdot & \cdot \end{array}, \tag{5.85}$$

then

$$\begin{aligned}&\int_{-\frac{\pi}{2}}^{\frac{\pi}{2}} e^{-ik\cos\vartheta_i(\cos\bar{\vartheta}_i^{(1)}+\cos\bar{\vartheta}_i^{(2)})}d\vartheta_i = \\ &\int_{\frac{\pi}{2}}^{\frac{3\pi}{2}} e^{-ik\cos\vartheta_i(\cos\bar{\vartheta}_i^{(1)}+\cos\bar{\vartheta}_i^{(2)})}d\vartheta_i = \pi\left(J_0(2k) - iH_0(2k)\right)\end{aligned} \tag{5.86}$$

independently on whether $\bar{\vartheta}_i = 0$ or π; $H_0(x)$ denotes the zero-order Struve function.

- If $\bar{\vartheta}_i^{(1)} = \bar{\vartheta}_i^{(2)} = 1$ (resp. -1) and $\bar{\vartheta}_i = -1$ (resp. 1), i.e., the configuration looks locally like

$$\begin{array}{ccc}\cdot & \uparrow & \cdot \\ \cdot & \downarrow & \uparrow \\ \cdot & \cdot & \cdot\end{array} \quad \text{or respectively} \quad \begin{array}{ccc}\cdot & \downarrow & \cdot \\ \cdot & \uparrow & \downarrow \\ \cdot & \cdot & \cdot\end{array}, \tag{5.87}$$

then

$$\begin{aligned}&\int_{-\frac{\pi}{2}}^{\frac{\pi}{2}} e^{-ik\cos\vartheta_i(\cos\bar{\vartheta}_i^{(1)}+\cos\bar{\vartheta}_i^{(2)})}d\vartheta_i = \\ &\int_{\frac{\pi}{2}}^{\frac{3\pi}{2}} e^{-ik\cos\vartheta_i(\cos\bar{\vartheta}_i^{(1)}+\cos\bar{\vartheta}_i^{(2)})}d\vartheta_i = \pi\left(J_0(2k) + iH_0(2k)\right)\end{aligned} \tag{5.88}$$

independently on whether $\bar{\vartheta}_i = 0$ or π.

On the other hand, Eq. (5.67) is simply given by

$$\int_{-\frac{\pi}{2}}^{\frac{\pi}{2}} d\vartheta_i\, 1 = \int_{\frac{\pi}{2}}^{\frac{3\pi}{2}} d\vartheta_i\, 1 = \pi. \tag{5.89}$$

We will denote by $n_3 = N_3/N$ the density of triplets of equal spins forming a local configuration as in Eq.(5.85). In this way, combining Eqs. (5.86), (5.88) with Eq. (5.65) we get

$$\begin{aligned}g^{(2)}(\varepsilon) = &\frac{\pi^N}{2\pi}\int_{-\infty}^{\infty} dk\; e^{ikN\varepsilon}\; e^{N[n_3(\varepsilon)\log(J_0(2k)-iH_0(2k))]}\times \\ &\times e^{N[(n_c(\varepsilon)-n_3(\varepsilon))\log(J_0(2k)+iH_0(2k))]}.\end{aligned} \tag{5.90}$$

In this case, the vector of parameters $\mathbf{z}(2,2,\varepsilon)$ is given by $\mathbf{z}(2,2,\varepsilon) = n_c(\varepsilon) \cup n_3(\varepsilon)$.

The integral in Eq. (5.90) can be computed with the saddle point method in the limit $N \gg 1$. The saddle point equation is given by $k = -i\zeta$; making use of the properties of the Bessel and of the Struve functions and performing some algebra, Eq. (5.90) can be written as

$$\begin{aligned} g^{(2)}(\varepsilon) \simeq & e^{N[-\zeta\varepsilon + \log\pi + n_3(\varepsilon)\log(I_0(2\zeta) - L_0(2\zeta))]} \\ & e^{N[(n_c(\varepsilon) - n_3(\varepsilon))\log(I_0(2k) + L_0(2\zeta))]} \end{aligned} \tag{5.91}$$

with ζ satisfying the self-consistency equation

$$\begin{aligned} & -\varepsilon + \frac{n_3(\varepsilon)}{I_0(2\zeta) - L_0(2\zeta)} \left(2I_1(2\zeta) - \left(\frac{2}{\pi} + L_{-1}(2\zeta) + L_1(2\zeta) \right) \right) + \\ & + \frac{n_c(\varepsilon) - n_3(\varepsilon)}{I_0(2\zeta) + L_0(2\zeta)} \left(2I_1(2\zeta) + \left(\frac{2}{\pi} + L_{-1}(2\zeta) + L_1(2\zeta) \right) \right) = 0. \end{aligned} \tag{5.92}$$

As in the case of $n_c(\varepsilon)$, the function $n_3(\varepsilon)$ can be obtained as interpolation of the numerical data arising from a Monte Carlo simulation of the system; the simulation data for n_3 are not shown here.

We can now insert Eq. (5.91) in Eq. (5.61). By taking the logarithm of the resulting expression and neglecting the sub-leading term in N, we finally arrive to the following expression for the entropy density

$$\begin{aligned} s^{(2)}(\varepsilon) \simeq s^{(1)}(\varepsilon) \, - \, \zeta\,\varepsilon + \, \log\pi \, + \, n_3(\varepsilon) \, \log\left[I_0(2\zeta) - L_0(2\zeta)\right] + \\ + \left(n_c(\varepsilon) - n_3(\varepsilon)\right) \, \log\left[I_0(2\zeta) + L_0(2\zeta)\right] \end{aligned} \tag{5.93}$$

valid in the $N \to \infty$ limit; ζ has to be determined numerically from Eq. (5.92).

Fig. 5.9 shows the behavior of T as function of the energy density ε obtained by numerical differentiation from Eq. (5.93) (red points). As in Fig. 5.7 the theoretical values are plotted together with the data obtained with a Monte Carlo simulation of the system (blue triangles). The error bars in the Monte Carlo data lie inside the symbols

For Fig. 5.9 the same comments can be done as for Fig. 5.7. The theoretical results are in good agreement with the numerics in the entire energy density range. In comparison with the theoretical caloric curve in Fig. 5.7, the caloric curve resulting from this approximation and shown Fig. 5.9 is closer to the numerical results: the largest difference between theory and simulation is here around 20%. This fact is the effect of the different choice of the integration neighborhoods. In particular, if the integration neighborhoods are superposed, as in Eq. (5.68), the continuous factor $g^{(2)}(\varepsilon)$ is

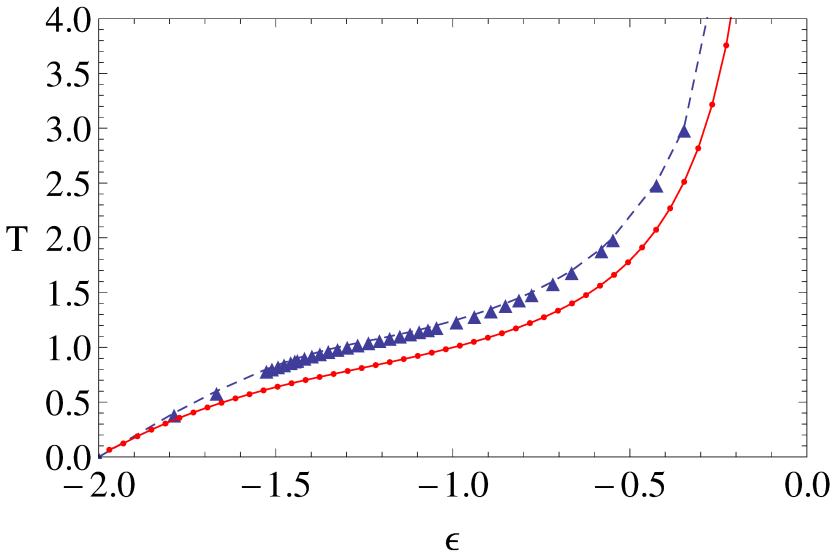

Figure 5.9: Temperature T as a function of the energy density ε as derived from Eq. (5.93) for the XY model in $d = 2$. Our results (red circles) are plotted together with the data obtained by a Monte Carlo simulation (blue triangles). The dashed blue line and the solid red line connecting the two sets of data are meant as guide to the eyes. The error bars in the Monte Carlo data lie inside the symbols

over-estimated and the discrepancy between the theoretical and the numerical results is larger than in case of a choice of the integration neighborhoods as in Eq. (5.69).

This fact is even more evident for the specific heat. The theoretical results are plotted in red in Fig. 5.10. With a choice of the integration neighborhoods of Eq. (5.90) as in Eq. (5.69), the energy value of the peak of the specific heat derived with our approximation is $\varepsilon_{p,3} \simeq -1.3 \simeq \varepsilon_p \simeq -1.24$; moreover, all the high energy regime for $\varepsilon > \varepsilon_p$ is in good quantitative agreement with the numerics. On the other hand, for $\varepsilon < \varepsilon_p$ the two sets of data separate themselves and in the low energy regime the same considerations as for Figs. 5.5 and 5.8 can be done on the shortcoming of our approximation.

5.2.4 Concluding remarks, part II

In Sec. 5.2 we have shown how the concepts presented in Sec. 5.1 can be generalized to non solvable short-range O(n) models in $d > 1$; the two-dimensional XY model has been explicitly discussed. This part of the analysis revealed that, even if some extra approximations are required to perform

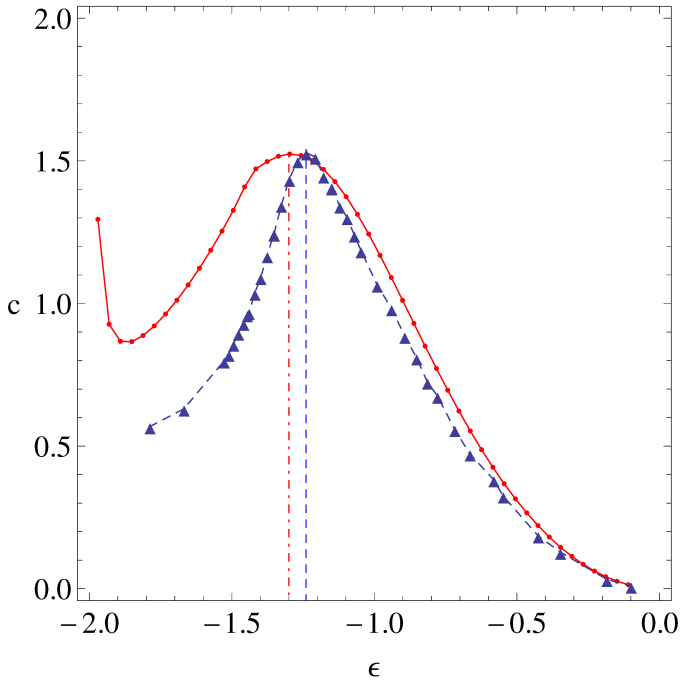

Figure 5.10: Specific heat c as a function of the energy density ε as derived from Eq. (5.84) for the XY model in $d = 2$. Our results (red circles) are plotted together with the data obtained by a Monte Carlo simulation (blue triangles). The dashed blue line and the solid red line connecting the two sets of data are meant as guide to the eyes. The error bars in the Monte Carlo data lie inside the symbols

the calculations (like the LMF approximation), the original idea of considering only Ising stationary configurations in the derivation of the thermodynamic properties of the continuous models is sound.

The XY model in $d = 2$ is not exactly solvable and any approximation scheme has to be compared with the results coming from numerical simulations. Calculated thermodynamic functions always show a qualitative agreement with the numerical data and in some cases also a quantitative agreement. Particularly interesting is the presence of the peak in the specific heat reported in Figs. 5.5, 5.8 and 5.10. Despite the approximations involved in its derivation, the specific heat correctly shows a peak and not a divergence as happens, instead, for the Ising model in $d = 2$ at $\varepsilon_c^{(1)} \simeq 1.41$ [95]. For this particular value of the energy density our numerical procedure correctly produces a finite value of c although the numerical convergence is more delicate as highlighted by the scattered data present in Figs. 5.8 and 5.10 for

$\varepsilon \simeq \varepsilon_c^{(1)}$. In case of Fig. 5.10 the agreement is also quantitative as far as the location of the peak of the specific heat is concerned.

Apart from technical limitations, the concepts presented in Sec. 5.2 can be generalized in principle to any other O(n) model in any spatial dimensions and possibly can give an hint towards the development of approximation techniques to study these models for which an exact solution is still missing.

Chapter 6

Energy landscapes and Smale's 7th problem

Besides carrying out the energy landscape analysis of classical O(n) spin models presented in the previous chapters, during my graduate studies I had the opportunity to work on a related topic. This is Smale's 7th problem concerning the $N-$points configurations on the sphere $\mathbb{S}^2$ which minimize the logarithmic pair-energy $V_0(r) = \ln \frac{1}{r}$ averaged over the $\binom{N}{2}$ pairs in a configuration; here, r is the chordal distance between the points forming a pair. More generally, the same question can be asked when the logarithmic pair energy is replaced with an s-Riesz pair energy (see below). Empirically, the number of local minimum energy configurations which are not global seems to grow exponentially with N [163]. The growth rate should have a significance similar to the complexity of the energy landscape. Empirical studies about this s-Riesz energy landscape for N-point configurations on $\mathbb{S}^2$ have begun recently, see [165] and references therein. Thus the problem fits into the general topic of energy landscape analysis presented in this Thesis.

However, the analysis of the energy landscape of these s-parametrized systems is much more difficult than the analysis of the O(n) models discussed so far. Even the analysis of the optimal energy N-point configurations is largely unsettled and necessitates computer-assisted empirical studies. We have carried out such a study, collected in [42], in collaboration with M. K.-H. Kiessling and J. Brauchart, which started in 2011 and is still in force. In this last Chapter we present a brief summary of the theoretical motivation and of the principal findings extensively discussed in [42]. We refer the interested reader to the cited paper for an in-depth analysis of the problem.

6.1 Smale's 7th problem

In various fields of science, ranging from biology over chemistry and physics to computer science, one encounters N-point optimization problems of which the following one is archetypical. Consider $N \geq 2$ distinct points on the standard two-sphere $\mathbb{S}^2$. Any such N-point configuration will be denoted by $\omega_N \subset \mathbb{S}^2$. The positions of the N points are conveniently given by N vectors $\boldsymbol{q}_k \in \mathbb{R}^3$ of Euclidean length $|\boldsymbol{q}_k| = 1$, $k = 1, \ldots, N$, and the distance between the two points in the pair (i, j) is taken to be the chordal distance $|\boldsymbol{q}_i - \boldsymbol{q}_j|$. Any pair (i, j) is now assigned a *standardized Riesz pair-energy*[1] $V_s(|\boldsymbol{q}_i - \boldsymbol{q}_j|)$, with

$$V_s(r) \equiv s^{-1}\left(r^{-s} - 1\right), \qquad s \in \mathbb{R}, \quad s \neq 0; \tag{6.1}$$

$$V_0(r) \equiv -\ln r \qquad \left(= \lim_{s\to 0} V_s(r)\right). \tag{6.2}$$

The *average standardized Riesz pair-energy of a configuration* is given by

$$\langle V_s \rangle(\omega_N) \equiv \frac{2}{N(N-1)} \sum_{1\leq i<j\leq N} \sum V_s(|\boldsymbol{q}_i - \boldsymbol{q}_j|), \tag{6.3}$$

and the *minimal average standardized Riesz pair-energy* by

$$v_s(N) \equiv \inf_{\omega_N \subset \mathbb{S}^2} \langle V_s \rangle(\omega_N). \tag{6.4}$$

The problem is to determine $v_s(N)$ together with the minimizing configuration(s) ω_N^s (also known as N-tuple of s-Fekete points) whenever such exist.[2] In general this is a hard mathematical problem. Only for one distinguished value of s has it been solved for all N, and only for a few N-values has it been conquered for all s.

The distinguished special value for which this problem has been completely solved for all N by explicit calculation is $s = -2$, which yields the

[1] Traditionally the Riesz pair-energy is defined as $\widetilde{V}_s(r) = r^{-s}$ for $s \neq 0$, and $\widetilde{V}_0(r) = -\ln r$ for $s = 0$. This has the disadvantages that $\widetilde{V}_0(r) \neq \lim_{s\to 0} \widetilde{V}_s(r)$, and that one has to seek energy-minimizing configurations for $s \geq 0$ yet energy-maximizing ones for $s < 0$.

[2] By the lower semi-continuity of the standardized Riesz pair-energy and the compactness of the sphere, there always exist N labeled points (not necessarily pairwise different if $s \leq -2$) whose average pair-energy equals $v_s(N)$. A minimizing set of N labeled points is not a proper minimizing *N-point configuration* unless all points are pairwise different.

energy law for the completely integrable Newtonian N-body problem with repulsive harmonic forces. Any N-point configuration satisfying $\sum_{i=1}^{N} \boldsymbol{q}_i = \mathbf{0}$ is a minimizing configuration of $\langle V_s \rangle(\omega_N)$, and only such are. The minimal energy reads

$$v_{-2}(N) = -\frac{1}{2}\frac{N+1}{N-1}. \tag{6.5}$$

For $s < -2$ one is confronted with the observation that for large N the N-tuple Fekete points accumulate around two opposite points, and the localization sharpens as N is getting larger; this is a consequence of Theorem 7 in [150]. In particular, for even N the infimum $v_s(N)$, $s < -2$, is achieved[3] if and only if half of the particles each are placed at two antipodal points, yielding

$$v_s(N) = -\frac{1}{|s|}\,\frac{\left(2^{|s|-1}-1\right)N+1}{N-1}, \qquad s < -2, \qquad N = 2n, \tag{6.6}$$

which converges to $v_{-2}(N)$ when taking the limit $s \uparrow -2$ of Eq. (6.6).

When N is odd the situation is already more tricky. For instance, for the smallest allowed odd $N = 3$ it is suggestive to conjecture that the minimizing configuration consists of the corners of an equilateral triangle in an arbitrary equatorial plane; yet comparison with an antipodal "configuration" (arrangement) with two labeled points in the North and one in the South Pole reveals that the equilateral configuration yields a lower average standardized Riesz pair-energy only for $s_3 < s < -2$, where $s_3 \equiv \ln(4/9)/\ln(4/3)$, while for $s < s_3$ the antipodal arrangement yields the lower average standardized Riesz pair-energy; in this case one can easily show rigorously that the antipodal arrangement is in fact optimal: namely, the equilateral triangle and the antipodal arrangement are the only equilibrium arrangements of 3 labeled points. When comparing the average standardized Riesz pair-energy for antipodal and equilateral arrangements for other odd N, this changeover happens only if N is a multiple of 3. The critical $s_{3(2n-1)}$ tends monotonically to -2 as $N = 3(2n-1) \to \infty$. Of course, this does not prove that either arrangement is optimal in the respective range of s. To the best of our knowledge, the optimal arrangement of odd-N points as a function of $s < -2$ is far from being settled.

[3] By Theorem 7 of [150], the infimum is *not* achieved by a proper N-point configuration since the points are not all distinct.

When $s > -2$ the problem becomes drastically more complicated. One needs to distinguish the cases $-2 < s < 2$, $s = 2$, $s > 2$, and the limit $s \to \infty$.

The interval $-2 < s < 2$ is known as the *potential-theoretical regime*, since concepts and methods of potential theory can be applied to study both the discrete and the continuous (i.e. $N \to \infty$) optimization problems.

Within this regime the integer values $s = -1$, $s = 0$, and $s = 1$ are of particular interest. When $s = -1$ the minimal average standardized Riesz pair-energy problem is equivalent to the maximal average pairwise chordal distance problem; see [151–153]. The case "$s = 0$," i.e. the limit $s \to 0$, which yields the logarithmic pair-energy in Eq. (6.2) (also known as the Coulomb energy for a pair of "two-dimensional unit point charges" on $\mathbb{S}^2$, respectively the Kirchhoff energy of a pair of unit point vortices on $\mathbb{S}^2$), occurs in a stunning variety of problems (on $\mathbb{S}^2$ and other manifolds) in the sciences and mathematics, see [42] for references. Originally Smale's 7th problem for the 21st century [154] was formulated for the logarithmic energy, see below. Lastly, the value $s = 1$ yields the Coulomb pair-energy of "three-dimensional unit point charges" associated with the so-called *Thomson problem* (see [42] for references).

Amongst the values $s \geq 2$, the borderline value $s = 2$ is special in the sense that the finite-N behavior is qualitatively different from both, the regime $-2 < s < 2$, and the regime $s > 2$. Yet it can be understood by considering a certain limit process $s \to 2$. The Riesz pair interaction for $s = 2$, in physics considered as correction term to Newton's gravity [155], is also special in the sense that it yields a Newtonian N-body problem in $\mathbb{R}^3$ with additional isolating integrals of motion, see i.e. [156], besides those associated with Galilei invariance. Restricted to $\mathbb{R}$ the motion is even completely integrable for all N [157, 158].

Also the limit $s \to \infty$ is of interest; though, applied to $V_s(r)$ it only gives impenetrable calottes with pair energy

$$V_\infty(r) \equiv \lim_{s\to\infty} V_s(r) = \begin{cases} \infty & \text{if } r < 1 \\ 0 & \text{if } r \geq 1 \end{cases} . \tag{6.7}$$

In that case $v_\infty(N) = 0$ for $N < N_*$, while $v_\infty(N) = \infty$ for $N \geq N_*$, where $N_* = 12$, see [42] and references therein. More interesting is it to take the limit $s \to \infty$ of the minimizing configuration(s) for $v_s(N)$, after factoring out of the rotation group. This leads to the so-called Tamm problem, or *hard*

sphere (best-packing) problem; that is, to find a configuration of N points on the sphere with the minimal pairwise (chordal) distance between the points being as large as possible, see [42] for a discussion on this point and useful references.

To our best knowledge, the following point sets are the only ones for which one can rigorously prove that they have minimal average standardized Riesz pair-energy for *all* $s > -2$. One can *easily* characterize the minimizing configuration explicitly only when $N = 2$ or 3 (as the antipodal and equilateral configuration, respectively). The minimizing configuration has been characterized explicitly also for $N = 4$, 6, and 12 as the vertices of Platonic solids[4] (tetrahedron, octahedron, and icosahedron), which are known to be *universally optimal* (see [159]); such configurations minimize the potential energy of *completely monotonic* pair-energy functions. The standardized Riesz pair-energies for $s > -2$ (including the logarithmic pair-energy at $s = 0$) fall into this category. The listed configurations for $N = 2$, 3, 4, 6, and 12 exhaust the possibilities for universally optimal configurations on $\mathbb{S}^2$; cf. [159, 160].

The difficult task of finding a proof of minimality can, perhaps, be best illustrated with the only partly resolved —partially with our results— *five point problem on* $\mathbb{S}^2$, see [42].

The truly hard regime is the vast intermediate range of N which are generically too large to allow for an explicit determination of the minimizing configuration, but not large enough for the asymptotic formulas to yield sufficiently accurate results. Empirical insight can be gained from computer experiments (e.g. [161], [162], see also [42] for additional references), which help finding candidates for the minimizing configuration, and in any event yield empirical upper bounds $v_s^x(N)$ on the minimal average standardized Riesz pair-energy $v_s(N)$. Up to $N \approx 100$ one can pretty much trust the computational results: several different computational routines all have yielded the same putatively minimizing configurations. For larger N, fewer independent computer experiments have been carried out, and since the number of local minimum energy configurations which are not global seems to grow

[4]Surprisingly, perhaps, the vertices of the Platonic cube ($N = 8$) have a higher average pair-energy than the square-antiprism derived from the cube by twisting (angle of 45 degrees) and squeezing together two opposite faces of the cube. Similarly, the dodecahedron (N=20) is not a minimizing configuration either, for any $s > -2$.

exponentially[5] with N [163], it becomes quite likely that a computer-assisted (random) search finds only one of these non-global minima when N is too large. Since it is so difficult to find the optimizing configurations, one may need to settle for less. Smale's 7th problem is formulated in this spirit:

> *Find an algorithm which, upon input N, in polynomial time returns a configuration ω_N on $\mathbb{S}^2$ whose average standardized Riesz pair-energy does not deviate from the optimal value obtained with ω_N^s by more than a certain conjectured s-specific function of N.*

Remark 6.1.1. *Smale's problem was originally posed for $s = 0$, viz. $V_0(r) = -\ln r$, and then not for the average logarithmic pair-energy but for the total logarithmic energy of the N-point configurations, i.e. for $\binom{N}{2} v_0(N)$. The "s-specific function of N" in this original formulation is the fourth term of the partially proved, partially conjectured large-N asymptotic expansion of the optimal logarithmic energy of N-point configurations on $\mathbb{S}^2$ [161, 162],*

$$\binom{N}{2} v_0(N) = aN^2 + bN \ln N + cN + d \ln N + \mathcal{O}(1), \tag{6.8}$$

with $a = \frac{1}{4} \ln \frac{e}{4}$ and $b = -\frac{1}{4}$ rigorously known, and with rigorous upper and lower bounds on c,[6] and numerical estimates for d, given in [161] (for an update, see [164]). The coefficient "d" in Smale's problem is unspecified and allowed to be bigger than any asymptotically determined[7] "d."

Subsequently Smale extended his problem to other values of $s \in (0, 2)$; and he remarked that analogous problems can be formulated for higher-dimensional spheres $\mathbb{S}^{\mathrm{d}}, \mathrm{d} = 3, 4, \ldots$ [154].

---

[5] The growth rate should have a significance similar to "the *complexity* of the energy landscape." Studies about the s-Riesz energy landscape for N-point configurations on $\mathbb{S}^2$ have only begun recently, see [165] and references therein. For background information on energy landscapes and their complexity, see [1].

[6] In [164] it is conjectured that $c = \ln\big(2(2/3)^{1/4}\pi^{3/4}/\Gamma(1/3)^{3/2}\big)$. Recently, a rigorous determination of c for weighted logarithmic Fekete problems in $\mathbb{R}^2$, to which the logarithmic Fekete problem on $\mathbb{S}^2$ is related by stereographic projection, was proposed in [166]; unfortunately, the conditions on the weights imposed in [166] just barely miss the particular weight obtained by stereographic projection.

[7] Currently only numerical evidence is available for the fourth term in the putative asymptotic expansion, and it is also conceivable that this term is actually not truly asymptotic.

This concludes our brief introduction into this fascinating field. Further information can be found in the survey articles cited in [42]. We next explain what we are up to in our work.

6.2 “Magic” numbers in Smale’s 7th problem

Our starting point is the observation that the strict monotonic increase of the sequence $N \mapsto v_s(N)$ (see [167] for a proof) and its boundedness above for $s < 2$ (a simple variational estimate see [42]) together imply that the *overall shape* of the graph $\{(N, v_s(N)) : N = 2, 3, ...\}$ must be “concave in the large” for each $s < 2$. This raises the question whether this graph is perhaps even *locally*, at each $N > 2$, strictly concave when $s < 2$. Explicitly, the question is whether the discrete second derivative of $v_s(N)$, given by

$$\ddot{v}_s(N) = v_s(N-1) - 2v_s(N) + v_s(N+1), \qquad N > 2, \tag{6.9}$$

is perhaps strictly negative for all $N > 2$ when $s < 2$.

Moreover, although $v_s(N)$ is not bounded above for $s \geq 2$, since the leading-order terms of the asymptotic large-N expansion of $v_s(N)$, namely $v_2(N) \propto \ln N$ [168] and $v_s(N) \propto N^{(s-2)/2}$ for $s > 2$ [169], are strictly locally concave for $2 \leq s < 4$, it is even conceivable that so is $N \mapsto v_s(N)$.

An affirmative answer is readily obtained for the special value $s = -2$ simply by differentiating the expression (6.5) for $v_{-2}(N)$ twice. Furthermore, twofold discrete differentiation of $v_s(2n)$ when $s < -2$, see (6.6), shows that also $2n \mapsto v_s(2n)$ is strictly locally concave for $s < -2$; of course, this does not prove that $N \mapsto v_s(N)$ is strictly concave for all $N > 2$ when $s < -2$.

In the absence of any closed form representation of $v_s(N)$ for $s > -2$ we turned to the empirical data published in [162, 163, 170, 171], and to those publicly available at the website [172] (some of which we generated ourselves), to gather some experimental input. All the experimental data $\mathcal{E}_s^x(N)$ reported in [162, 163, 170–172] have been computed with the conventional expression for the Riesz s-energy; if optimal, these Riesz s-energies are related to our minimal average standardized Riesz pair-energies by $\mathcal{E}_s(N) = \frac{N(N-1)}{2}\big(sv_s(N) + 1\big)$ for $s \in \{-1, 1, 2, 3\}$. We converted the computer-experimental data $\mathcal{E}_s^x(N)$ into putatively minimal (empirical) average standardized Riesz pair-energies $v_s^x(N)$ for $s \in \{-1, 0, 1, 2, 3\}$ and inspected these as functions of N. A first impression was gained by plotting $\ddot{v}_s^x(N)$ computed

from the first 200 or so empirical data $v_s^x(N)$ versus N, for the five chosen s-values. The plots can be found in [42] together with a detailed discussion of the results. Here we can summarize our findings as:

First, the map $N \mapsto v_{-2}(N)$ is strictly locally concave. Second, based on our empirical data analysis, we conjecture that the map $N \mapsto v_s(N)$ is strictly locally concave also for $s = -1$, while its strict local concavity is occasionally violated, $\ddot{v}_s^x(N) \geq 0$ for some N-values, when $s \in \{0, 1, 2, 3\}$.

"Magic" numbers: "Optimally optimal" configurations?

From our results the N-values at which $\ddot{v}_s^x(N) \geq 0$ seem to become more frequent, and apparently more random, the larger s is. Interestingly, for the smallest s-value for which we found empirical violations of strict local N-concavity, namely $s = 0$, i.e. for the logarithmic pair interaction invoked in the original formulation of Smale's 7th problem, the violations of strict local concavity were few and far between. They occurred at the following experimental sequence of integers:

$$\mathcal{C}_+^x(0) = \big\{\underline{6}, \underline{12}, \underline{24}, 32, \underline{48}, \underline{60}, 67, \underline{72}, 80, 104, \underline{108}, 122, \underline{132}, 137, ...\big\}. \quad (6.10)$$

Curiously, the majority of the numbers in the sequence (6.10) are multiples of 6 (underlined), or almost multiples (like 67 and 137) — coincidence?

We note that the logarithmic-energy minimizers for the first two "integers of convexity," i.e. $N = 6$ and $N = 12$, are two "optimally symmetric" configurations, namely Platonic polyhedra: the octahedron ($N = 6$) and icosahedron ($N = 12$); also the (putative) minimizers for $N \in \{24, 48, 60\}$ are highly symmetric configurations; in particular, the one for $N = 24$ is an Archimedean polyhedron (also for $N \in \{48, 60\}$ there are Archimedean polyhedra, but these are NOT log-energy optimizers). To be sure, there is an integer inbetween which is not divisible by 6, namely $N = 32$ (the highly symmetric optimizer is a Catalan polyhedron), and also the "odd-balls" $N = 67$ and (of all integers!) $N = 137$ show up.

Yet it is an intriguing thought that the N-values in $\mathcal{C}_+^x(0)$ may correspond to log-energy-optimizing configurations which are "optimally symmetric" in the following sense. Most of the log-energy-optimizing configurations associated with $\mathcal{C}_+^x(0)$ are separated by longer N-intervals in which $N \mapsto v_0^x(N)$ is strictly concave. This suggests that, perhaps, the configurations in an interval of concavity form a family of more-and-more symmetric optimizers which

better-and-better approximate a highly symmetric endpoint configuration. Once an endpoint configuration is reached, the addition of the next point inevitably will destroy a high amount of symmetry, for which an extra large amount of energy may be required.

These “concave families” would thus be vaguely analogous to the “periods” in the so-called periodic table of the chemical atoms. The endpoints of the periods are the chemically very inert noble gases which are associated with highly symmetric “electronic configurations”[8] about the nuclei with charge number $Z \in \{2, 10, 18, ...\}$. Incidentally, also the atomic nuclei seem to form something akin to “periods,” in the sense that the set of nucleon numbers $\{2, 8, 20, 28, 50, 82, 126, ...?...\}$ is associated with nuclei that have a particular high binding energy per nucleon. This set of nucleon numbers is known as the *Magic Numbers* of nuclear physics.[9] By analogy, we call the set $\mathcal{C}^x_+(0)$ the “Magic Numbers of Smale’s 7th problem.”

[8] Actually, what is symmetric is the structure of the wave function of the electrons.

[9] Since there are protons and neutrons in the nucleus, some nuclei are “doubly magic.”

Conclusions and future perspectives

Based on the knowledge about the stationary points of the energy function, energy landscape methods can be applied to determine both dynamical and equilibrium properties of a system. Several methods have been proposed in the past years to connect equilibrium phase transitions and energy landscapes properties of classical Hamiltonian systems, either focused on specific models or trying to shed light on the general mechanism. However, a general picture is still missing. Indeed most of the techniques introduced required the knowledge of all the stationary configurations to be implemented, so that their applicability was effectively limited to one-dimensional or mean-field models.

The main purpose of this work has been to go beyond mean-field or one-dimensional models, considering systems such as classical O(n) spin models with short range interactions in $d > 1$, and to develop approximation procedures capable of giving hints on their thermodynamic behavior even in case of partial knowledge of the stationary points of the systems. This is in fact the general scenario once energy landscape techniques are applied to "realistic" models.

In particular, in Chapter 2, we observed that a special class of stationary configurations of the Hamiltonian $H^{(n)}$ in Eq. (2.1) can be constructed, given by all the configurations of the corresponding Ising model. More precisely, we showed that a one-to-one correspondence between a class of stationary points of the O(n) classical spin models (Ising stationary points) and the configurations of an Ising model defined on the same hypercubic lattice and with the same interactions exists. Ising stationary points do not exhaust all the stationary configurations possibly present in the system. However, the Ising points exhibit important features: they are exponentially many in N,

their energy densities cover densely all the energy range allowed for O(n) models, they are robust to generic external perturbations. This suggests they might be the most important stationary points for what concerns the thermodynamics of the continuous models.

We took seriously this idea and in Sec. 2.3 we applied the KSS criterion (1.5.2) for the search of phase transitions on this class of configurations to detect the transitions in the XY models with short-range interactions in $d = 2$ and 3. The KSS criterion is the only result in this research area that can be applied to generic models also in case of partial knowledge of the stationary configurations (the only requirement being that the potentials are Morse functions). However, the KSS criterion was not able to single out the phase transitions in the XY models in $d = 2$ and 3 (neither on the Ising class nor on other classes of stationary points we eventually defined). This study led to important considerations. The Ising stationary points had to be sampled numerically with a Monte Carlo scheme as well as numerical had been the computation of the reduced determinant $\mathcal{D}$ on these configurations ($\mathcal{D}$ is the key quantity in the application of the criterion). The fact that in our analysis $\mathcal{D}$ remained well above zero in all the energy density range suggested that from a practical point of view the KSS criterion is of little use when short-range interacting systems are considered. Indeed, a purely numerical approach to the criterion is not useful unless a numerical sampling scheme able to efficiently detect stationary configurations with zero—or at least small—determinant is devised, which is currently lacking. Despite the very different nature of the phase transitions in the two cases, the results on the reduced determinant for the XY models in $d = 2$ and 3 were essentially the same; this fact led us to conjecture that analogous results would hold also for other O(n) models and could be possibly connected with the short-range nature of the interactions.

Apart from the considerations on the criterion, the study conducted in Sec. 2.3 led to other interesting results. The potential energy functions of the XY models turned out not to be Morse functions even after the explicitly breaking of the continuous O(2) symmetry (by fixing the value of one angular variable of the system). Indeed singular solutions were present in the systems that could be removed only with the application of an external perturbation to the systems. One interesting fact is that the external perturbation killed all the classes of stationary points we have been able to construct, but the Ising one. Moreover, the results on the reduced determi-

nant $\mathcal{D}$ (and on the density of index ι) suggested that the energy landscape of the XY models around the Ising points depends only on its energy density and not on the specific point considered. These two extra properties of the Ising class reinforced our belief on the importance of these configurations to the thermodynamics of the continuous models.

Since the KSS criterion failed to detect the critical behavior of these systems we looked for another mechanism at the basis of the origin of phase transitions in short-range O(n) models. In Chapter 3 we discussed some assumptions, that led to an approximate form of the density of states of continuous O(n) models. This form, given by Eq. (3.4), expresses the density of states of a generic O(n) model in terms of the same quantity of the corresponding Ising model. This equation leads to Consequence 3.2.1 according to which phase transitions in ferromagnetic O(n) models defined on regular $d-$dimensional hypercubic lattices occur at the same value of the energy density as in the Ising model defined on the same lattice and with same interactions. Even if we do not expect relation (3.4) to be exact neither for finite N nor in the thermodynamic limit, according to the results available in literature Consequence 3.2.1 holds exactly for long-range and one-dimensional nearest-neighbor O(n) models. In $d = 2$ the discrepancy between the critical energy values is about 2% but it is hard to understand if it is due to the assumptions made in the derivation of (3.4) or to the different nature of the phase transitions present in the Ising and XY models. The $d = 3$ case, instead, is more interesting. In fact from available data in the literature it turned out that the critical energy densities of the O(n) models with $n = 2$ and 3 were almost consistent with that of the Ising model. Moreover, all models in $d = 3$ have a ferromagnetic phase transition with spontaneous symmetry breaking. This case can then be seen as a good test case for the accuracy of the prediction made by Eq. (3.4).

Since the assumptions involved in the derivation of Eq. (3.4) were difficult to control, we performed two different analyses to discuss their reliability: in Chapter 4 we tested the accuracy of the prediction made by Consequence 3.2.1 with a numerical study of the three-dimensional O(n) models, while in Chapter 5 we performed an analytical derivation of an exact expression for the density of states of the mean-field and of the one-dimensional XY models that reduces to Eq. (3.4) at the phase transition; moreover, a possible generalization of these concepts to short-range O(n) models has been proposed at the end of Chapter 5.

For what concerns the numerical analysis, the problem has been settled in $d = 3$. Indeed, thanks to a finite-size scaling analysis of the numerically obtained critical energies of O(n) models with $n = 2, 3$ and 4 and a comparison with the analytical results for the critical energy density of the spherical model ($n = \infty$), we derived an interpolation formula for the critical energy density of any three-dimensional O(n) model. This expression, given by Eq. (4.34), allowed to test the accuracy of Consequence 3.2.1 for any n. Our results showed that the discrepancy between the critical energy values of the O(1) model and of the O($n > 1$) is always less than 3% and becomes less than 1% when O($2 < n < 8$) are considered, that is for the O(n) models one typically deals with.

For what concerns the analytical analysis a slightly more general formula, given in Eq. (5.7), was shown to hold exactly in the case of the mean-field and of the one-dimensional XY models. Eq. (5.6) reduces to Eq. (3.4) when the limit $\varepsilon \to \varepsilon_c^{(n)}$ is considered, with $\varepsilon_c^{(n)}$ critical value of the energy density. For these models the derivation made in Chapter 3 to reach Eq. (3.4) can be followed rigorously and relies on the exact solutions of the systems. This fact limits the generalization of these concepts to other O(n) models in $d > 1$ and with short range interactions. This notwithstanding, some results have been obtained also in the general case (see Sec. 5.2). Two approximation schemes have been developed to estimate the density of states of a generic O(n) model in any spatial dimension. The first one considers Eq. (5.2) as the basic form of the density of states, while the second one originates from the ansatz on $\omega^{(n)}$ given by Eq. (5.61). The procedures presented in these last Sections have been tested on the XY model in $d = 2$. In both cases we found that the results on the behavior of some thermodynamic functions, such as the caloric curve or the specific heat, are in good agreement with data from numerical simulations.

Both the analyses presented in Chapter 4 and 5 support the original idea that Ising stationary points may play a special rôle for the thermodynamics of classical O(n) spin models. Our analysis showed that usually trustworthy results, such as the KSS criterion, have to be taken with special care when short-range systems are considered and when only some classes of stationary points are known. On the other hand, the last Sections of Chapter 5 suggested a possible procedure to give an estimation of some important thermodynamic functions, such as the caloric curve or the specific heat, even in case of partial knowledge of the stationary configurations. The application of

these techniques to other O(n) models represents an interesting perspective of our work.

In the very last Chapter we drew the attention to the problem of the energy landscape of the local minimizers of the s-Riesz pair energy averaged over all pairs in an N-point configuration. We mentioned that computer-experimental evidence suggests that the number of non-globally minimizing configurations (modulo rotations on $\mathbb{S}^2$), is growing exponentially with N [163]. Such a growth rate is reminiscent of "the *complexity* of the energy landscape," see [1]. As far as we know, not much is known about the s-Riesz energy landscape for N-point configurations on $\mathbb{S}^2$. With the help of catalogs of non-globally minimizing configurations and their energies it should be feasible to determine the experimental number counts of the local minimizers *below a certain energy* E; see [165] and references therein. To make a modest contribution, we discussed the results of an empirical study of the N and s dependence of the s-Riesz energies of putatively optimal N-point configurations, fruit of a collaboration with M. K.-H. Kiessling and J. Brauchart. Based on our empirical findings, we conjectured that there exists an $s_* \in (-1, 0)$ such that $N \mapsto v_s^x(N)$ is locally strictly concave for all $s < s_*$, while local strict concavity is violated at some N-values whenever $s \geq s_*$. In [42] we presented some rigorous, and some quasi-rigorous upper bounds on s_*; together with some rigorous bounds on the second discrete derivative, $\ddot{v}_s(N)$, of $N \mapsto v_s(N)$. For each studied s-value, the N-values at which the map $N \mapsto v_s^x(N)$ is strictly convex were collected into a set $\mathcal{C}_+^x(s)$. We found that the empirical map $s \mapsto \mathcal{C}_+^x(s)$ is set-theoretically monotonic increasing, based on which we have conjectured that the actual map $s \mapsto \mathcal{C}_+(s)$ is set-theoretically monotonic increasing, indeed. Surprisingly, the set $\mathcal{C}_+^x(0)$ exhibits some intriguing quasi-regular patterns which reminded us of the periodic table of the chemists, or the "magic" numbers in nuclear physics. Thus we decided to call the N-values in $\mathcal{C}_+^x(0)$ the "Magic Numbers of Smale's 7th problem." We have speculated that those "magic" numbers could be associated with "optimally symmetric" endpoints of families of more-and-more symmetric configurations; the first few configurations associated with $\mathcal{C}_+^x(0)$ being in fact highly symmetric. We hope that our work should trigger future research into the regime of concavity of the minimal average standardized Riesz pair-energies on $\mathbb{S}^2$, and the structure of its convexity sets as functions of s.

Appendix A

Appendix to Chapter 2

A.1 Singular stationary points of the three-dimensional XY model

Similar considerations as for the two-dimensional case in Sec. 2.3.4 motivate the following construction of singular stationary configurations in three dimensions, which for illustrational purposes is shown here for a lattice of side length $L = 8$. The scheme consists of four different planar configurations

$$A = \begin{array}{cccccccc} \leftarrow & \uparrow & \updownarrow & \updownarrow & \updownarrow & \updownarrow & \updownarrow & \uparrow \\ \downarrow & \updownarrow & \updownarrow & \updownarrow & \updownarrow & \updownarrow & \downarrow & \rightarrow \\ \updownarrow & \updownarrow & \updownarrow & \updownarrow & \updownarrow & \uparrow & \leftarrow & \uparrow \\ \updownarrow & \updownarrow & \updownarrow & \updownarrow & \downarrow & \rightarrow & \downarrow & \updownarrow \\ \updownarrow & \updownarrow & \updownarrow & \uparrow & \leftarrow & \uparrow & \updownarrow & \updownarrow \\ \updownarrow & \updownarrow & \downarrow & \rightarrow & \downarrow & \updownarrow & \updownarrow & \updownarrow \\ \updownarrow & \uparrow & \leftarrow & \uparrow & \updownarrow & \updownarrow & \updownarrow & \updownarrow \\ \downarrow & \rightarrow & \downarrow & \updownarrow & \updownarrow & \updownarrow & \updownarrow & \updownarrow \end{array}, \tag{A.1}$$

$$B = \begin{array}{cccccccc}
\downarrow & \updownarrow & \updownarrow & \updownarrow & \updownarrow & \updownarrow & \downarrow & \rightarrow \\
\updownarrow & \updownarrow & \updownarrow & \updownarrow & \updownarrow & \uparrow & \leftarrow & \uparrow \\
\updownarrow & \updownarrow & \updownarrow & \updownarrow & \downarrow & \rightarrow & \downarrow & \updownarrow \\
\updownarrow & \updownarrow & \updownarrow & \uparrow & \leftarrow & \uparrow & \updownarrow & \updownarrow \\
\updownarrow & \updownarrow & \downarrow & \rightarrow & \downarrow & \updownarrow & \updownarrow & \updownarrow \\
\updownarrow & \uparrow & \leftarrow & \uparrow & \updownarrow & \updownarrow & \updownarrow & \updownarrow \\
\downarrow & \rightarrow & \downarrow & \updownarrow & \updownarrow & \updownarrow & \updownarrow & \updownarrow \\
\leftarrow & \uparrow & \updownarrow & \updownarrow & \updownarrow & \updownarrow & \updownarrow & \uparrow
\end{array}, \tag{A.2}$$

$$C = \begin{array}{cccccccc}
\rightarrow & \downarrow & \updownarrow & \updownarrow & \updownarrow & \updownarrow & \updownarrow & \downarrow \\
\uparrow & \updownarrow & \updownarrow & \updownarrow & \updownarrow & \updownarrow & \uparrow & \leftarrow \\
\updownarrow & \updownarrow & \updownarrow & \updownarrow & \updownarrow & \downarrow & \rightarrow & \downarrow \\
\updownarrow & \updownarrow & \updownarrow & \updownarrow & \uparrow & \leftarrow & \uparrow & \updownarrow \\
\updownarrow & \updownarrow & \updownarrow & \downarrow & \rightarrow & \downarrow & \updownarrow & \updownarrow \\
\updownarrow & \updownarrow & \uparrow & \leftarrow & \uparrow & \updownarrow & \updownarrow & \updownarrow \\
\updownarrow & \downarrow & \rightarrow & \downarrow & \updownarrow & \updownarrow & \updownarrow & \updownarrow \\
\uparrow & \leftarrow & \uparrow & \updownarrow & \updownarrow & \updownarrow & \updownarrow & \updownarrow
\end{array}, \tag{A.3}$$

$$D = \begin{array}{cccccccc}
\uparrow & \updownarrow & \updownarrow & \updownarrow & \updownarrow & \updownarrow & \uparrow & \leftarrow \\
\updownarrow & \updownarrow & \updownarrow & \updownarrow & \updownarrow & \downarrow & \rightarrow & \downarrow \\
\updownarrow & \updownarrow & \updownarrow & \updownarrow & \uparrow & \leftarrow & \uparrow & \updownarrow \\
\updownarrow & \updownarrow & \updownarrow & \downarrow & \rightarrow & \downarrow & \updownarrow & \updownarrow \\
\updownarrow & \updownarrow & \uparrow & \leftarrow & \uparrow & \updownarrow & \updownarrow & \updownarrow \\
\updownarrow & \downarrow & \rightarrow & \downarrow & \updownarrow & \updownarrow & \updownarrow & \updownarrow \\
\uparrow & \leftarrow & \uparrow & \updownarrow & \updownarrow & \updownarrow & \updownarrow & \updownarrow \\
\rightarrow & \downarrow & \updownarrow & \updownarrow & \updownarrow & \updownarrow & \updownarrow & \downarrow
\end{array}. \tag{A.4}$$

All these planar configurations consist of a pattern similar to the two-dimensional configuration (2.51), but in A and C the pattern is shifted one site away from

the diagonal. Moreover, C is obtained from A by rotating all spins by π, and the same is true for D and B. As before, the lattice sites marked with gray $\updownarrow$-arrows can be filled with an arbitrary 'Ising-type'-pattern of $\uparrow$ and $\downarrow$ arrows. Arranging these planar configurations in the sequence $ABCDABCD$ results in a stationary configuration on a cubic lattice with vanishing Hessian determinant. The scheme works in just the same way for larger lattice sizes with side lengths that are multiples of 4.

Appendix B

Appendix to Chapter 4

B.1 Monte Carlo simulations

In Chapter 4 we considered classical O(n) models with $n = 2, 3$ and 4, defined on regular cubic lattices in $d = 3$ and with ferromagnetic nearest-neighbor interactions.

The simulations have been performed on the PLX machine in the CINECA cluster in Casalecchio di Reno (Bologna). For the system architecture of the PLX machine, please see [173]. The total local Cluster CPU time spent on PLX for the simulations has been of about 40690 h.

The simulation algorithm applied in our work is the optimized canonical Monte Carlo cluster algorithm for classical O(n) spin models, `spinmc`, provided by the ALPS project [132].

In some cases, marked with the symbol ($*$) in the following, the simulations have been performed with the same `spinmc` algorithm on the cluster farm of the department of Physics and Astronomy of the Università degli Studi di Firenze in Sesto Fiorentino (Firenze).

In the following Sections we will denote by: THERMALIZATION the number of pure Monte Carlo steps set for the thermalization of the system, SWEEPS the number Monte Carlo steps in which the thermodynamic observables are accumulated, t the duration time of the simulation (in seconds).

The technical details of the simulations of the O(n) models with $n = 2, 3$ and 4 are summarized in Secs. 4.1.3, 4.1.4 and 4.1.5, respectively.

B.1.1 O(2) model

Simulations details for the O(2) models with nearest-neighbor ferromagnetic interactions in $d = 3$ and periodic boundary conditions.

Table B.1: Canonical Monte Carlo simulations of the O(2) model at $T_c^{(2)} = 2.201673$ as in [104], for different values of the lattice edge L. For $(*)$, see Sec. B.1.

L	THERMALIZATION	SWEEPS	t (sec.)
32	$2 \cdot 10^5$	10^6	$0.642 \cdot 10^4$
40	$5 \cdot 10^5$	$5 \cdot 10^6$	$0.4794 \cdot 10^5$
50	$5 \cdot 10^5$	$5 \cdot 10^6$	$0.9462 \cdot 10^5$
64	$2 \cdot 10^5$	10^6	$0.197783 \cdot 10^6$ $(*)$
80	$5 \cdot 10^5$	$5 \cdot 10^6$	$0.18 \cdot 10^5$
100	$5 \cdot 10^5$	$5 \cdot 10^6$	$0.12599 \cdot 10^5$
128	$5 \cdot 10^5$	$5 \cdot 10^6$	$0.1517701 \cdot 10^7$ $(*)$

Table B.2: Canonical Monte Carlo simulations of the O(2) model at $T_+^{(2)} = T_c^{(2)} + \Delta T_c^{(2)} = 2.20177$, for different values of the lattice edge L.

L	THERMALIZATION	SWEEPS	t (sec)
32	$2 \cdot 10^5$	10^6	$0.564 \cdot 10^4$
64	$4 \cdot 10^5$	$4 \cdot 10^6$	$0.178539 \cdot 10^6$
128	$5 \cdot 10^5$	$5 \cdot 10^6$	$0.14256 \cdot 10^7$

Table B.3: Canonical Monte Carlo simulations of the O(2) model at $T_-^{(2)} = T_c^{(2)} - \Delta T_c^{(2)} = 2.201576$, for different values of the lattice edge L.

L	THERMALIZATION	SWEEPS	t (sec)
32	$2 \cdot 10^5$	10^6	$0.588 \cdot 10^4$
64	$5 \cdot 10^5$	$5 \cdot 10^6$	$0.15918 \cdot 10^6$
128	$5 \cdot 10^5$	$5 \cdot 10^6$	$0.14256 \cdot 10^7$

B.1.2 O(3) model

Simulations details for the O(3) models with nearest-neighbor ferromagnetic interactions in $d = 3$ and periodic boundary conditions.

Table B.4: Canonical Monte Carlo simulations of the O(3) model at $T_c^{(3)} = 1.44298$ given in [106], for different values of the lattice edge L. For $(*)$, see Sec. B.1.

L	THERMALIZATION	SWEEPS	t (sec.)
32	$0.25 \cdot 10^7$	10^7	$0.219596 \cdot 10^6$ $^{(*)}$
40	$0.25 \cdot 10^7$	10^7	$0.1776 \cdot 10^6$
50	$0.25 \cdot 10^7$	10^7	$0.4743 \cdot 10^4$
64	$0.25 \cdot 10^7$	10^7	$0.6048 \cdot 10^6$ $^{(*)}$
80	$0.25 \cdot 10^7$	10^7	$0.24191 \cdot 10^5$
100	$0.25 \cdot 10^7$	10^7	$0.50754 \cdot 10^5$
128	$0.25 \cdot 10^7$	10^7	$0.66528 \cdot 10^7$

Table B.5: Canonical Monte Carlo simulations of the O(3) model at $T_+^{(3)} = T_c^{(3)} + \Delta T_c^{(3)} = 1.443$, for different values of the lattice edge L. For $(*)$, see Sec. B.1.

L	THERMALIZATION	SWEEPS	t (sec)
32	$0.25 \cdot 10^7$	10^7	$0.328273 \cdot 10^6$ $(*)$
64	$0.25 \cdot 10^7$	10^7	$0.8416 \cdot 10^6$
128	$0.25 \cdot 10^7$	10^7	$0.66528 \cdot 10^7$

Table B.6: Canonical Monte Carlo simulations of the O(3) model at $T_-^{(3)} = T_c^{(3)} - \Delta T_c^{(3)} = 1.44296$, for different values of the lattice edge L. For $(*)$, see Sec. B.1.

L	THERMALIZATION	SWEEPS	t (sec)
32	$0.25 \cdot 10^7$	10^7	$0.214172 \cdot 10^6$ $(*)$
64	$0.25 \cdot 10^7$	10^7	$0.171337 \cdot 10^6$
128	$0.25 \cdot 10^7$	10^7	$0.66528 \cdot 10^7$

B.1.3 O(4) model

Simulations details for the O(4) models with nearest-neighbor ferromagnetic interactions in $d = 3$ and periodic boundary conditions.

Table B.7: Canonical Monte Carlo simulations of the O(4) model at $T_c^{(4)} = 1.06835$ given in [141], for different values of the lattice edge L. For $(*)$, see Sec. B.1.

L	THERMALIZATION	SWEEPS	t (sec.)
32	$0.25 \cdot 10^7$	10^7	$0.7117910^{5\ (*)}$
40	$0.25 \cdot 10^7$	10^7	$0.13902110^{6\ (*)}$
64	$0.25 \cdot 10^7$	10^7	$0.81842710^{6\ (*)}$
80	$0.25 \cdot 10^7$	10^7	$0.87203810^{6\ (*)}$
100	$0.25 \cdot 10^7$	10^7	$0.345610^{7\ (*)}$
128	$0.25 \cdot 10^7$	10^7	$0.7084810^{7\ (*)}$

Table B.8: Canonical Monte Carlo simulations of the O(4) model at $T_+^{(4)} = T_c^{(4)} + \Delta T_c^{(4)} = 1.06848$, for different values of the lattice edge L. For $(*)$, see Sec. B.1.

L	THERMALIZATION	SWEEPS	t (sec)
32	$0.25 \cdot 10^7$	10^7	$0.11460710^{6\ (*)}$
64	$0.25 \cdot 10^7$	10^7	$0.78555310^{6\ (*)}$
128	$0.25 \cdot 10^7$	10^7	$0.7084810^{7\ (*)}$

Table B.9: Canonical Monte Carlo simulations of the O(4) model at $T_-^{(4)} = T_c^{(4)} - \Delta T_c^{(4)} = 1.06822$, for different values of the lattice edge L. For $(*)$, see Sec. B.1.

L	THERMALIZATION	SWEEPS	t (sec)
32	$0.25 \cdot 10^7$	10^7	$0.10321710^{6\ (*)}$
64	$0.25 \cdot 10^7$	10^7	$0.83640310^{6\ (*)}$
128	$0.25 \cdot 10^7$	10^7	$0.7084810^{7\ (*)}$

Appendix C

Appendix to Chapter 5

C.1 Critical exponent of the specific heat from Eqs. (3.4) and (5.7)

In Sec. 5.1.3, we have discussed the implications of Eqs. (3.4) and (5.7) in case they would exactly hold. Here we give the details about the predictions on the specific heat critical exponent α obtained by assuming that the density of states has the form given by Eqs. (3.4) or (5.7), respectively[1]. Let us recall that, in the microcanonical ensemble, the specific heat is defined as

$$C(\varepsilon) = -\frac{[s'(\varepsilon)]^2}{s''(\varepsilon)}\,, \tag{C.1}$$

where $s(\varepsilon)$ is the entropy density and the temperature is defined as $T(\varepsilon) = 1/s'(\varepsilon)$. With $s'(\varepsilon)$ and $s''(\varepsilon)$ we denote the first and second derivative of the function $s(\varepsilon)$.

Let us consider a short-range $O(n)$ model and assume the relation (3.4) holds as an equality. We assume in the following that the phase transition occurs for a value of the energy density in the interior of the domain of the entropy density[2]. Without loss of generality, let us shift the energy density

[1] We recall that the specific heat critical exponent α in the microcanonical ensemble, is related to the specific heat critical exponent $\bar{\alpha}$ in the canonical ensemble by the relation $\alpha = \bar{\alpha}/(1-\bar{\alpha})$.

[2] As a consequence, what follows does not apply to the mean-field and one-dimensional XY models.

ε such that $\varepsilon_c = 0$. The entropy density of the continuous model can then be written as:

$$s(\varepsilon) = s_I(\varepsilon) + \log f(\varepsilon)\,, \tag{C.2}$$

where here and in the following we use the notation $s_I(\varepsilon)$ instead of $s^{(1)}(\varepsilon)$ for the entropy density of the Ising model, to avoid possible misunderstanding with derivatives. We also omit the symbol (n) indicating which $O(n)$ model we are considering because our arguments do not depend on it. Finally, we denoted $g^{(n)}(\varepsilon)^{1/N}$ by $f(\varepsilon)$.

Let us now consider, for the moment, only energy densities larger than the critical one, i.e., $\varepsilon > 0$. Three facts are relevant for the following:

1. we consider $0 < \alpha_I < 1$, i.e., the case $d > 2$. Moreover, because the critical temperature of the Ising models is finite, $s_I''(\varepsilon) \propto \varepsilon^{\alpha_I}$ for $\varepsilon \to 0^+$.

2. $s'(\varepsilon)$ is finite around $\varepsilon = 0$ because the critical temperature of the continuous model does not vanish at the transition.

3. we assume $f(\varepsilon)$ is analytical, consistently with the discussion in Sec. 5.1. We can then expand $f(\varepsilon)$ in a Taylor series around $\varepsilon = 0$.

Inserting Eq. (C.2) into Eq. (C.1), we get

$$C(\varepsilon) = -\frac{\left[s_I'(\varepsilon) + \frac{g'(\varepsilon)}{f(\varepsilon)}\right]^2}{s_I''(\varepsilon) + \frac{g''(\varepsilon)}{f(\varepsilon)} - \left[\frac{g'(\varepsilon)}{f(\varepsilon)}\right]^2}\,. \tag{C.3}$$

Using the expansions described above around $\varepsilon = 0$, neglecting the higher order terms and expanding the fraction, we obtain

$$C(\varepsilon) \simeq a_+ + b_+\,\varepsilon^{\alpha_I} \qquad (\varepsilon \to 0^+), \tag{C.4}$$

where a_+ and b_+ are constants whose exact value is irrelevant to our purposes. We can repeat the same calculations for $\varepsilon < 0$, obtaining the same result as in Eq. (C.4) but for that $\varepsilon \to -\varepsilon$ and that the constants may be different. Hence the specific heat close to $\varepsilon = 0$ is

$$C(\varepsilon) \simeq a_\pm + b_\pm\,|\varepsilon|^{\alpha_I}\,. \tag{C.5}$$

We then obtain the result stated in Sec. 5.1.3: the specific heat of the continuous model does not diverge at the transition and the critical exponent α of the continuous model is related to the one of the Ising model via $\alpha = -\alpha_I$.

With a similar reasoning we can also deal with the case in which we consider Eq. (5.7) to be exact. As before, we start by considering $\varepsilon > 0$. Assuming Eq. (5.7) holds as an equality, the entropy density of the continuous model is

$$s(\varepsilon) = s_I(\varepsilon) + f(\varepsilon, \tilde{\varepsilon}(\varepsilon)) \,, \tag{C.6}$$

where we denoted by $f(\varepsilon, \tilde{\varepsilon}(\varepsilon))$ the function $(1/N) \log g^{(n)}(\varepsilon, \tilde{\varepsilon}(\varepsilon))$. In this case, f is a function of two variables: again, we assume it is analytic and expand it around $\varepsilon = 0$, such that

$$f(x, y) \simeq f_0 + f_1 x + f_2 y + f_3 xy + f_4 x^2 + f_5 y^2 + f_6 x^2 y + f_7 xy^2 + f_8 x^3 + f_9 y^3 \,, \tag{C.7}$$

where x and y are shorthands for ε and $\tilde{\varepsilon}$ and the f_i's are constants whose exact value is irrelevant to our purposes. At variance with the previous case, $\tilde{\varepsilon}(\varepsilon)$ contains some information about the transition because it vanishes for $\varepsilon \to 0$; we should then admit the possibility of a singular dependence on ε, writing $\tilde{\varepsilon}(\varepsilon) \propto \varepsilon^\theta$ with $\theta > 0$ for $\varepsilon \to 0^+$.

Using the information on the behavior of $s_I''(\varepsilon)$ around $\varepsilon = 0$ and integrating two times, we get

$$s_I(x) \simeq a_0 + a_1 x + a_2 x^{\alpha_I + 2} \,, \tag{C.8}$$

where the a_i's are suitable constants. Inserting Eqs. (C.7) and (C.8) into the equation for the entropy of the continuous model, Eq. (C.6), we get:

$$\begin{aligned} s(\varepsilon) \simeq a_0 + a_1 \varepsilon^\theta + a_2 \varepsilon^{\theta(\alpha_I+2)} + f_0 + f_1 \varepsilon + f_2 \varepsilon^\theta + f_3 \varepsilon^{\theta+1} + f_4 \varepsilon^2 + \\ + f_5 \varepsilon^{2\theta} + f_6 \varepsilon^{2+\theta} + f_7 \varepsilon^{1+2\theta} + f_8 \varepsilon^3 + f_9 \varepsilon^{3\theta} \,. \end{aligned} \tag{C.9}$$

Taking the first and the second derivative of the previous expression and renaming the constants, we obtain

$$\begin{aligned} s'(\varepsilon) \simeq b_1 \varepsilon^{\theta-1} + b_2 \varepsilon^{\theta(\alpha_I+2)-1} + h_1 + h_2 \varepsilon^{\theta-1} + h_3 \varepsilon^\theta + h_4 \varepsilon + \\ + h_5 \varepsilon^{2\theta-1} + h_6 \varepsilon^{\theta+1} + h_7 \varepsilon^{2\theta} + h_8 \varepsilon^2 + h_9 \varepsilon^{3\theta-1} \,, \end{aligned} \tag{C.10}$$

and

$$\begin{aligned} s''(\varepsilon) \simeq c_1 \varepsilon^{\theta-2} + m_3 \varepsilon^{\theta-1} + m_4 + m_5 \varepsilon^{2\theta-2} + m_6 \varepsilon^\theta + m_7 \varepsilon^{2\theta-1} + \\ + m_8 \varepsilon + m_9 \varepsilon^{3\theta-2} \,. \end{aligned} \tag{C.11}$$

The quantity θ is unknown. However, since the specific heat of the continuous model does not vanish at the transition, the above expressions imply the

constraint $\theta \geq 2$. Moreover, if $\theta > 3$, the linear term in Eq. (C.11) would dominate. Hence the range of values for θ to be considered is $\theta \in (2, 3]$; if $\theta > 3$ or $\theta = 2$, the leading behavior of $s''(\varepsilon)$ would be the same as that given by Eq. (C.11) with $\theta = 3$.

The leading behavior of Eqs. (C.10) and (C.11) is then $s'(\varepsilon) \simeq h_1 + h_4\varepsilon$ and $s''(\varepsilon) \simeq m_4 + c_1\varepsilon^{\theta-2}$. Inserting these results into the expression (C.1) for the specific heat, we obtain

$$C(\varepsilon) \simeq -\frac{(h_1 + h_4\varepsilon)^2}{m_4 + c_1\varepsilon^{\theta-2}} \simeq c_+ + d_+\,\varepsilon^{\theta-2} \qquad (\varepsilon \to 0^+)\,. \tag{C.12}$$

Repeating the same calculations for $\varepsilon < 0$ and combining the result with Eq. (C.12) we obtain the behavior of the specific heat close to the transition,

$$C(\varepsilon) \simeq c_\pm + d_\pm\,|\varepsilon|^{\theta-2}\,. \tag{C.13}$$

The above expression, together with the above bounds on θ, shows that the specific heat of the continuous model does not diverge and its critical exponent α is determined by θ, which is model dependent. Varying θ in its allowed range we obtain $\alpha \in [-1, 0)$.

Bibliography

[1] D. J. Wales, *Energy Landscapes*. Cambridge: Cambridge University Press, 2004.

[2] P. G. Debenedetti and F. H. Stillinger, "Supercooled liquids and the glass transition," *Nature*, vol. 410, pp. 259–267, 2001.

[3] F. Sciortino, "Potential energy landscape description of supercooled liquids and glasses," *J. Stat. Mech: Theory Exp.*, vol. 2005, no. 05, p. P05015, 2005.

[4] J. N. Onuchic, Z. Luthey-Schulten, and P. G. Wolynes, "Theory of protein folding: The energy landscape perspective," *Annu. Rev. Phys. Chem.*, vol. 48, no. 1, pp. 545–600, 1997.

[5] F. H. Stillinger, "A topographic view of supercooled liquids and glass formation," *Science*, vol. 267, pp. 1935–1939, 1995.

[6] F. H. Stillinger and T. A. Weber, "Packing structures and transitions in liquids and solids," *Science*, vol. 225, pp. 983–989, 1984.

[7] B. Strodel and D. J. Wales, "Free energy surface from an external harmonic superposition approach and kinetics for alanine dipeptide," *Chem. Phys. Lett.*, vol. 466, p. 105, 2008.

[8] D. Mehta, C. Hughes, M. Schröck and D. J. Wales, "Potential Energy Landscapes for the 2D XY Model: Minima, Transition States and Pathways," *J. Chem. Phys.*, vol. 139, p. 194503, 2013.

[9] L. Angelani, R. Di Leonardo, G. Ruocco, A. Scala, and F. Sciortino, "Saddles in the energy landscape probed by supercooled liquids," *Phys. Rev. Lett.*, vol. 85, pp. 5356–5359, Dec 2000.

[10] T. S. Grigera, A. Cavagna, I. Giardina, and G. Parisi, "Geometric approach to the dynamic glass transition," *Phys. Rev. Lett.*, vol. 88, p. 055502, 2002.

[11] L. Casetti, E. G. D. Cohen, and M. Pettini, "Exact result on topology and phase transitions at any finite n," *Phys. Rev. E*, vol. 65, no. 3, p. 036112, 2002.

[12] L. Caiani, L. Casetti, C. Clementi, and M. Pettini, "Geometry of dynamics, lyapunov exponents, and phase transitions," *Phys. Rev. Lett.*, vol. 79, no. 22, pp. 4361–4364, Dec 1997.

[13] L. Casetti, E. G. D. Cohen, and M. Pettini, "Topological origin of the phase transition in a mean-field model," *Phys. Rev. Lett.*, vol. 82, no. 21, pp. 4160–4163, 1999.

[14] L. Casetti, M. Pettini, and E. G. D. Cohen, "Phase transitions and topology changes in configuration space," *J. Stat. Phys.*, vol. 111, pp. 1091–1123, 2003.

[15] L. Casetti, M. Pettini, and E. G. D. Cohen, "Geometric approach to hamiltonian dynamics and statistical mechanics," *Phys. Rep.*, vol. 337, pp. 237–341, 2000.

[16] M. Kastner, "Phase transitions and configuration space topology," *Rev. Mod. Phys.*, vol. 80, no. 1, pp. 167–187, 2008.

[17] M. Pettini, *Geometry and Topology in Hamiltonian Dynamics and Statistical Mechanics*. New York: Springer, 2007.

[18] M. Kastner, "Topological approach to phase transitions and inequivalence of statistical ensembles," *Physica A*, vol. 359, pp. 447–454, 2006.

[19] H. Federer, *Geometric Measure Theory*. New York: Springer, 1969.

[20] M. Kastner, O. Schnetz, and S. Schreiber, "Nonanalyticities of the entropy induced by saddle points of the potential energy landscape," *J. Stat. Mech: Theory Exp.*, vol. 2008, no. 04, p. P04025, 2008.

[21] R.B.Griffiths, "Rigorous results and theorems," in *Phase Transitions and Critical Phenomena*, C. Domb and M. S. Green, Eds. London: Academic Press, 1972, vol. 1.

[22] L. Casetti, M. Kastner, and R. Nerattini, "Kinetic energy and microcanonical nonanalyticities in finite and infinite systems," *J. Stat. Mech: Theory Exp.*, vol. 2009, no. 07, p. P07036, 2009.

[23] A. Andronico, L. Angelani, G. Ruocco, and F. Zamponi, "Topological properties of the mean-field ϕ^4 model," *Phys. Rev. E*, vol. 70, p. 041101, Oct 2004.

[24] L. Angelani and G. Ruocco, "Phase transitions and topology in $2 + k$ XY mean-field models," *Phys. Rev. E*, vol. 76, p. 051119, 2007.

[25] L. Angelani, G. Ruocco, and F. Zamponi, "Relationship between phase transitions and topological changes in one-dimensional models," *Phys. Rev. E*, vol. 72, p. 016122, 2005.

[26] F. Baroni, "Transizioni di fase e topologia dello spazio delle configurazioni di modelli di campo medio," Master's thesis, Università di Firenze, 2002.

[27] D. A. Garanin, R. Schilling, and A. Scala, "Saddle index properties, singular topology, and its relation to thermodynamic singularities for a ϕ^4 mean-field model," *Phys. Rev. E*, vol. 70, p. 036125, Sep 2004.

[28] I. Hahn and M. Kastner, "The mean-field φ^4 model: Entropy, analyticity, and configuration space topology," *Phys. Rev. E*, vol. 72, p. 056134, 2005.

[29] M. Kastner and D. Mehta, "Phase transitions detached from stationary points of the energy landscape," *Phys. Rev. Lett.*, vol. 107, p. 160602, Oct 2011.

[30] M.Kastner, "Unattainability of a purely topological criterion for the existence of a phase transition for nonconfining potentials," *Phys. Rev. Lett.*, vol. 93, p. 150601, 2004.

[31] L. Angelani, L. Casetti, M. Pettini, G. Ruocco, and F. Zamponi, "Topology and phase transitions: From an exactly solvable model to a relation between topology and thermodynamics," *Phys. Rev. E*, vol. 71, no. 3, p. 036152, Mar 2005.

[32] L. Casetti and M. Kastner, "Nonanalyticities of entropy functions of finite and infinite systems," *Phys. Rev. Lett.*, vol. 97, no. 10, p. 100602, Sep 2006.

[33] L. Angelani, L. Casetti, M. Pettini, G. Ruocco, and F. Zamponi, "Topological signature of first-order phase transitions in a mean-field model," *Europhys. Lett.*, vol. 62, no. 6, p. 775, 2003.

[34] M. Kastner and O. Schnetz, "Phase transitions induced by saddle points of vanishing curvature," *Phys. Rev. Lett.*, vol. 100, no. 16, p. 160601, Apr 2008.

[35] M. Kastner, S. Schreiber, and O. Schnetz, "Phase transitions from saddles of the potential energy landscape," *Phys. Rev. Lett.*, vol. 99, no. 5, p. 050601, Jul 2007.

[36] C. Nardini and L. Casetti, "Energy landscape and phase transitions in the self-gravitating ring model," *Phys. Rev. E*, vol. 80, no. 6, p. 060103, Dec 2009.

[37] R. Nerattini, M. Kastner, D. Mehta, and L. Casetti, "Exploring the energy landscape of XY models," *Phys. Rev. E*, vol. 87, p. 032140, 2013.

[38] L. Casetti, C. Nardini, and R. Nerattini, "Microcanonical relation between continuous and discrete spin models," *Phys. Rev. Lett.*, vol. 106, no. 5, p. 057208, Feb 2011.

[39] R. Nerattini, L. Casetti, and A. Trombettoni, "Critical energy densities of classical three-dimensional O(n) models," *In preparation*, 2013.

[40] C. Nardini, R. Nerattini, and L. Casetti, "Density of states of continuous and discrete spin models: a case study," *J. Stat. Mech: Theory Exp.*, vol. 2012, no. 02, p. P02007, 2012.

[41] C. Nardini, R. Nerattini, and L. Casetti, "Density of states of the two-dimensional XY model: an energy landscape approach," *In preparation*, 2013.

[42] R. Nerattini, J. S. Brauchart, and M. K. H. Kiessling, " "Magic" numbers in Smale's 7th problem," *arXiv:1307.2834*, submitted to J. Stat. Phys; 106 pages, of which 30 are numerical data table not included in the J. Stat. Phys. version.

[43] N. Goldenfeld, *Lectures on Phase Transitions and the Renormalisation Group.* Cambridge: Perseus Publishing, 1992.

[44] K. Wang, *Introduction to Statistical Physics –2nd ed.* New York: CRC Press, Taylor & Francis Group, 2010.

[45] P. Labastie and R. L. Whetten, "Statistical Thermodynamics of the Cluster Solid-Liquid Transition," *Phys. Rev. Lett.*, vol. 65, no. 13, pp. 1567–1570, 1990.

[46] M. Kastner, "Critical phenomena in the entropy formalism and microcanonical finite-size scaling", Ph.D. thesis, Erlangen, 2000.

[47] M. Kastner, M. Promberger and A. Hüller, "Magnetic Properties of Finite 3D Ising Systems: A Microcanonical Approach", in *Computer Simulation Studies in Condensed Matter Physics XI*, D. P. Landau and H. -B. Schüttler Eds., Heildelberg, 1998.

[48] M. Kastner, M. Promberger, and A. Hüller, "Microcanonical finite-size scaling," *J. Stat. Phys.*, vol. 99, pp. 1251–1264, 2000.

[49] H. Touchette, "Equivalence and nonequivalence of the microcanonical and canonical ensembles: a large deviations study," PhD thesis, McGill University, 2003.

[50] R. S. Ellis, H. Touchette and B. Turkington, "Thermodynamic versus statistical nonequivalence of ensembles for the mean-field BlumeâEmeryâGriffiths model," *Physica A*, vol. 335, pp. 518–538, 2004.

[51] A. Campa, T. Dauxois, and S. Ruffo, "Statistical mechanics and dynamics of solvable models with long-range interactions," *Phys. Rep.*, vol. 480, no. 3-6, pp. 57–159, 2009.

[52] J. L. Lebowitz, "Statistical mechanics: A selective review of two central issues," *Rev. Mod. Phys.*, vol. 71, pp. 346–357, 1999.

[53] H. A. Kramers and G. H. Wannier, "Statistics of the two-dimensional ferromagnet. part i," *Phys. Rev.*, vol. 60, p. 252, 1941.

[54] J. J. Binney, N. J. Dowrick, A. J. Fisher, and M. Newman, *The Theory of Critical Phenomena: An Introduction to the Renormalization Group.* New York: Oxford University Press, 1992.

[55] R. Nerattini, "Paesaggio energetico dei modelli XY," Master's thesis, Università di Firenze, 2010.

[56] L. van Hove, "Sur l'integrale de configuration pour les systèmes de particules á une dimension," *Physica (Amsterdam)*, vol. 16, pp. 137–143, 1950.

[57] R. B. Griffiths, "Peierls proof of spontaneous magnetization in a two-dimensional ising ferromagnet," *Phys. Rev.*, vol. 136, p. A437, 1964.

[58] N. D. Mermin and H. Wagner, "Absence of ferromagnetism in one- or two-dimensional isotropic heisenberg models," *Phys. Rev. Lett.*, vol. 17, pp. 1133–1307, 1966.

[59] C. N. Yang and T. D. Lee, "Statistical theory of equations of states and phase transitions. i. theory of condensation," *Phys. Rev.*, vol. 87, pp. 404–409, 1952.

[60] M. E. Fisher, "The nature of critical points," in *Lectures in Theoretical Physics.* Boulder, Colorado: University of Colorado Press, vol. VII, pp. 73–109, 1965.

[61] D. J. Wales, "Coexistence in small inert gas clusters," *Mol. Phys.*, vol. 78, pp. 151–171, 1993.

[62] F. Baroni, "A simple topological model with continuous phase transition," *J. Stat. Mech: Theory Exp.*, vol. 2011, no. 08, p. P08010, 2011.

[63] F. Baroni and L. Casetti, "Topological conditions for discrete symmetry breaking and phase transitions," *J. Phys. A: Math. Gen.*, vol. 39, no. 3, p. 529, 2006.

[64] G. Carlsson, J. Gorham, M. Kahle, and J. Mason, "Computational topology for configuration spaces of hard disks," *Phys. Rev. E*, vol. 85, p. 011303, 2012.

[65] M. Farber and V. Fromm, "Telescopic linkages and a topological approach to phase transitions," *J. Aust. Math. Soc.*, vol. 90, no. 02, pp. 183–195, 2011.

[66] P. Grinza and A. Mossa, "Topological Origin of the Phase Transition in a Model of DNA Denaturation," *Phys. Rev. Lett.*, vol. 92, p. 158102, Apr 2004.

[67] M. Kastner, "Stationary-point approach to the phase transition of the classical XY chain with power-law interactions," *Phys. Rev. E*, vol. 83, p. 031114, Mar 2011.

[68] L.Angelani and G.Ruocco, "Role of saddles in topologically driven phase transitions: The case of the d-dimensional spherical model," *Phys. Rev. E*, vol. 77, p. 052101, 2008.

[69] D. Mehta and M. Kastner, "Stationary point analysis of the one-dimensional lattice landau gauge fixing functional, aka random phase XY hamiltonian," *Ann. Phys. (NY)*, vol. 326, no. 6, pp. 1425–1440, 2011.

[70] M. Antoni and S. Ruffo, "Clustering and relaxation in hamiltonian long-range dynamics," *Phys. Rev. E*, vol. 52, no. 3, pp. 2361–2374, Sep 1995.

[71] D. Mehta, "Finding All the Stationary Points of a Potential Energy Landscape via Numerical Polynomial Homotopy Continuation Method," *Phys. Rev. E*, vol. 84, p. 025702, 2011.

[72] C. Nardini, "Paesaggio energetico e transizioni di fase in un modello con interazioni gravitazionali," Master's thesis, Università di Firenze, 2009.

[73] A. C. Ribeiro Teixeira and D. A. Stariolo, "Topological hypothesis on phase transitions: The simplest case," *Phys. Rev. E*, vol. 70, p. 016113, Jul 2004.

[74] S. Risau-Gusman, A. C. Ribeiro-Teixeira, and D. Stariolo, "Topology and phase transitions: The case of the short range spherical model," *J. Stat. Phys.*, vol. 124, pp. 1231–1253, 2006.

[75] S. Risau-Gusman, Ana C. Ribeiro-Teixeira, and Daniel A. Stariolo, "Topology, phase transitions, and the spherical model," *Phys. Rev. Lett.*, vol. 95, p. 145702, Sep 2005.

[76] F. A. N. Santos and M. D. Coutinho-Filho, "Topology, symmetry, phase transitions, and noncollinear spin structures," *Phys. Rev. E*, vol. 80, p. 031123, Sep 2009.

[77] J. W. Milnor, *Morse theory.* Princeton Univeristy Press, vol. 51 of Annals of Mathematical Studies, 1963.

[78] M. Demazure, *Bifurcations and Catastrophes: Geometry of Solutions to Nonlinear Problems.* Springer, Berlin, 2000.

[79] R. Franzosi and M. Pettini, "Topology and phase transitions II. theorem on a necessary relation," *Nucl. Phys. B*, vol. 782, no. 3, pp. 219–240, 2007.

[80] R. Franzosi, M. Pettini, and L. Spinelli, "Topology and phase transitions I. preliminary results," *Nucl. Phys. B*, vol. 782, no. 3, pp. 189–218, 2007.

[81] R. Franzosi and M. Pettini, "Theorem on the origin of phase transitions," *Phys. Rev. Lett.*, vol. 92, no. 6, p. 060601, Feb 2004.

[82] J. Dunkel and S. Hilbert, "Phase transitions in small systems: Microcanonical vs. canonical ensembles," *Physica A*, vol. 370, pp. 390–406, 2006.

[83] S. Hilbert and J. Dunkel, "Nonanalytic microscopic phase transitions and temperature oscillations in the microcanonical ensemble: An exactly solvable one-dimensional model for evaporation," *Phys. Rev. E*, vol. 74, p. 011120, 2006.

[84] M. Kastner and O. Schnetz, "On the mean-field spherical model," *J. Stat. Phys.*, vol. 122, pp. 1195–1214, 2006.

[85] D. Ruelle, *Statistical mechanics: rigorous results.* Benjamin, Reading, 1969.

[86] R. Schilling, "Energy landscape properties studied using symbolic sequences," *Physica D*, vol. 216, no. 1, pp. 157–166, 2006.

[87] C. Nardini, "Energy landscapes, equilibrium and out of equilibrium physics of long and short range interacting systems," Ph.D. thesis, Università degli Studi di Firenze and Ecole Normale Supérieure de Lyon, 2012.

[88] Y. Sota, O. Iguchi, M. Morikawa, T. Tatekawa, and K. ichi Maeda, "Origin of scaling structure and non-gaussian velocity distribution in a self-gravitating ring model," *Phys. Rev. E*, vol. 64, no. 5, p. 056133, Oct 2001.

[89] T. Tatekawa, F. Bouchet, T. Dauxois, and S. Ruffo, "Thermodynamics of the self-gravitating ring model," *Phys. Rev. E*, vol. 71, no. 5, p. 056111, May 2005.

[90] S. T. Bramwellt and P. C. W. Holdswortht, "Magnetization and universal sub-critical behaviour in two-dimensional XY magnets", *J. Phys: Condens. Matter*, vol. 5, pp. L53–L59, 1993.

[91] S. T. Bramwellt and P. C. W. Holdswortht, "Magnetization: A characteristic of the Kosterlitz-Thouless-Berezinskii transition", *Phys. Rev. B*, vol. 49, no. 13, pp. 8811–8814, 1994.

[92] D. Mehta, J. D. Hauenstein, and M. Kastner, "Energy landscape analysis of the two-dimensional nearest-neighbor ϕ^4 model," *Phys. Rev. E*, vol. 85, p. 061103, 2012.

[93] A. Campa, A. Giansanti, and D. Moroni, "Canonical solution of classical magnetic models with long-range couplings," *J. Phys. A: Math. Gen.*, vol. 36, no. 25, p. 6897, 2003.

[94] H. E. Stanley, *Introduction to Phase Transitions and Critical Phenomena*. Clarendon Prees, Oxford, 1971.

[95] L. Onsager, "Crystal statistics. I. a two-dimensional model with an order-disorder transition," *Phys. Rev.*, vol. 65, pp. 117–149, 1944.

[96] V. L. Berežinskij, "Violation of long range order in one-dimensional and two-dimensional systems with a continuous symmetry group. I. classical systems," *Sov. Phys. JETP*, vol. 32, p. 493, 1971.

[97] J. M. Kosterlitz and D. J. Thouless, "Ordering, metastability and phase transitions in two-dimensional systems," *J. Phys. C: Solid State Phys.*, vol. 6, no. 7, p. 1181, 1973.

[98] J. B. Kogut, "An introduction to lattice gauge theory and spin systems", *Rev. Mod. Phys.*, vol. 51, p. 659, 1979.

[99] C. Itzykson e J. M. Drouffe, "Statistical Field Theory I: From Brownian motion to renormalization and lattice gauge theory", Cambridge University Press, 1989.

[100] S. Coleman, "There are no Goldstone Bosons in Two Dimensions", *Commun. Math. Phys.*, vol. 31, pp. 259-264, 1973.

[101] R. Kenna, "The XY Model and the Berezinskii-Kosterlitz-Thouless Phase Transition", *arXiv:cond-math/0512356v1*, 2005.

[102] R. Gupta and C. F. Baillie, "Critical behavior of the two-dimensional XY model," *Phys. Rev. B*, vol. 45, pp. 2883–2898, Feb 1992.

[103] M. Hasenbusch, "The two-dimensional XY model at the transition temperature: a high-precision Monte Carlo study," *J. Phys. A: Math. Gen.*, vol. 38, no. 26, p. 5869, 2005.

[104] A. P. Gottlob and M. Hasenbusch, "Critical behaviour of the 3D XY-model: a Monte Carlo study," *Physica A*, vol. 201, pp. 593–613, 1993.

[105] A. J. F. de Souza and F. G. B. Moreira, "Microcanonical renormalization-group simulation of Ising systems," *Phys. Rev. B*, vol. 48, pp. 9586–9594, 1993.

[106] R. G. Brown and M. Ciftan, "Critical behavior of the helicity modulus for the classical heisenberg model," *Phys. Rev. B*, vol. 74, p. 224413, 2006.

[107] D. Mehta, A. Sternbeck, L. von Smekal, and A. G. Williams, "Lattice landau gauge and algebraic geometry," *PoS*, vol. QCD-TNT09, p. 25, 2009.

[108] L. von Smekal, D. Mehta, A. Sternbeck, and A. G. Williams, "Modified Lattice Landau Gauge," *PoS*, vol. LAT2007, p. 382, 2007.

[109] D. J. Bates, J. D. Hauenstein, A. J. Sommese, and C. W. Wampler, "Bertini: Software for numerical algebraic geometry," `http://www.nd.edu/~sommese/bertini`.

[110] E. L. Allgower and K. Georg, *Introduction to Numerical Continuation Methods*. John Wiley & Sons, New York, 1979.

[111] C. Hughes, D. Mehta, and J.-I. Skullerud, "Enumerating Gribov copies on the lattice," *Ann. Phys.*, vol. 331, pp. 188–215, 2013.

[112] D. Mehta, "Numerical polynomial homotopy continuation method and string vacua," *Adv. High Energy Phys.*, vol. 2011, p. 263937, 2011.

[113] D.Mehta, "Lattice vs. continuum: Landau gauge fixing and 't hooft-polyakov monopoles," Ph.D. thesis, The University of Adelaide, australasian Digital Theses Program, 2009.

[114] M. Maniatis and D. Mehta, "Minimizing Higgs Potentials via Numerical Polynomial Homotopy Continuation," *Eur. Phys. J. Plus*, vol. 127, p. 91, 2012.

[115] D. Mehta, D. Stariolo and M. Kastner, "Energy Landscape of the Finite-Size Mean-field 3−Spin Spherical Model," *Phys.Rev. E*, vol. 87, p. 052143, 2013.

[116] B. Greene, D. Kagan, A. Masoumi, D. Mehta, E. J. Weinberg and X. Xiao, "Tumbling through a landscape: Evidence of instabilities in high-dimensional moduli spaces," *Phys.Rev. D*, vol. 88, p. 026005, 2013.

[117] D. Mehta, Y.-H. He, and J. D. Hauenstein, "Numerical Algebraic Geometry: A New Perspective on String and Gauge Theories," *JHEP*, vol. 1207, p. 018, 2012.

[118] A. J. Sommese, J. Verschelde, and C. W. Wampler, "Introduction to numerical algebraic geometry," in *Solving Polynomial Equations: Foundations, Algorithms, and Applications*, ser. Algorithms and Computation in Mathematics, A. Dickenstein and I. Z. Emiris, Eds. Berlin: Springer, vol. 14, pp. 339–392, 2005.

[119] Y. Lu, D. J. Bates, A. J. Sommese, and C. W. Wampler, "Finding all real points of a complex curve," in *Algebra, Geometry and Their Interactions*, ser. Contemporary Mathematics, A. Corso, J. Migliore, and C. Polini, Eds. American Mathematical Society, vol. 448, pp. 183–205, 2006.

[120] S. Strogatz and R. Mirollo, "Stability of incoherence in a population of coupled oscillators," *Journal of Statistical Physics*, vol. 63, no. 3, pp. 613–635, 1991.

[121] A. Pelissetto and E. Vicari, "Critical phenomena and renormalization-group theory," *Phys. Rep.*, vol. 368, no. 6, pp. 549–727, 2002.

[122] T. Niemeijer, "On the high-density limit of heisenberg and ising ferromagnets," *Physica (Amsterdam)*, vol. 48, p. 467, 1970.

[123] M. Kastner, "Nonequivalence of ensembles for long-range quantum spin systems in optical lattices," *Phys. Rev. Lett.*, vol. 104, p. 240403, 2010.

[124] R. Kenna and A. C. Irving, "The Kosterlitz-Thouless universality class," *Nucl. Phys. B*, vol. 485, p. 583, 1997.

[125] X. Leoncini, A. D. Verga, and S. Ruffo, "Hamiltonian dynamics and the phase transition of the XY model," *Phys. Rev. E*, vol. 57, no. 6, pp. 6377–6389, 1998.

[126] J. Tobochnik and G. V. Chester, "Monte carlo study of the planar spin model," *Phys. Rev. B*, vol. 20, pp. 3761–3769, 1979.

[127] M. Kastner, "Microcanonical entropy of the spherical model with nearest-neighbour interactions," *J. Stat. Mech.*, p. P12007, 2009.

[128] M. Suzuki, "New Universality of Critical Exponents", *Prog. Theor. Phys.*, vol. 51, 1974.

[129] P. Archambault, S. T. Bramwell and P. C. W. Holdsworth, "Magnetic fluctuations in a finite two-dimensional XY model," *J. Phys. A:Math*, vol. 30, pp. 8363–8378, 1997.

[130] M. Hasenbusch and K. Pinn, "a_+/a_-, α, ν, and $f_s\xi^3$ from 3d ising energy and specific heat," *J. Phys. A:Math*, vol. 31, p. 6157, 1998.

[131] J. Engels and F. Karsch, "Scaling functions of the free energy density and its dertivatives for the $3d$ O(4) model," *Phys. Rev. D*, vol. 85, p. 094506, 2012.

[132] "Alps project," Web page: *http://alps.comp-phys.org/*.

[133] E.Brèzin, "An investigation of finite size scaling," *J. Physique*, vol. 43, no. 1, pp. 15–22, 1982.

[134] M. E. Fisher, "The renormalization group in the theory of critical behavior," *Rev. Mod. Phys.*, vol. 46, no. 4, pp. 597–615, 1974.

[135] H. E. Stanley, "Scaling, universality, and renormalization: Three pillars of modern critical phenomena," *Rev. Mod. Phys.*, vol. 71, no. 2, pp. S358–S366, 1999.

[136] N. Schultka and E. Manousakis, "Specific heat of superfluids near the transition temperature," *Phys. Rev. B*, vol. 52, no. 10, pp. 7528–7536, 1995.

[137] L. Goldner and G. Ahlers, *Phys. Rev. B*, vol. 40, p. 13129, 1992.

[138] M. Hasenbusch and T. Török "High precision Monte Carlo study of the 3d XY-universality class," *J. Phys. A*, vol. 32, p. 6361, 1999.

[139] C. L. Guillou and J. Zinn-Justin, "Critical exponents from field theory," *Phys. Rev. B*, vol. 21, p. 3976, 1980.

[140] C. Holm and W. Janke, "Monte carlo study of topological defects in the 3d Heisenberg model," *J. Phys. A*, vol. 27, p. 2553, 1994.

[141] K. Kanaya and S. Kaya, "Critical exponents of a three dimensional O(4) spin model," *Phys. Rev. D*, vol. 51, pp. 2404–2410, 1995.

[142] T. H. Berlin and M. Kac, "The spherical model of a ferromagnet," *Phys. Rev.*, vol. 86, pp. 821–835, 1952.

[143] G. S. Joyce, "Critical properties of the spherical model," in *Phase Transitions and Critical Phenomena*, C. Domb and M. S. Green, Eds. Academic Press, 1972, vol. 2.

[144] H. E. Stanley, "Spherical model as the limit of infinite spin dimensionality," *Phys. Rev.*, vol. 176, pp. 718–722, 1968.

[145] H. E. Stanley, "Dependence of critical properties on dimensionality of spins," *Phys. Rev. Lett.*, vol. 20, pp. 589–592, 1968.

[146] P. R. M. Campostrini, A. Pellissetto and E. Vicari, "Four-point renormalized coupling constant in O(n) models," *Nuc. Phys. B*, vol. 459, pp. 207–242, 1996.

[147] C. M. Bender and S. A. Orszag, *Advanced Mathematical Methods for Scientists and Engineers*. New York: Springer, 1999.

[148] M. Abramowitz and I. A. Stegun, Eds., *Handbook of Mathematical Functions*. New York: Dover, 1965.

[149] M. G. Bulmer, *Principles of Statistics*. New York: Dover, 1979.

[150] G. Björck, "Distributions of positive mass, which maximize a certain generalized energy integral," *Ark. Mat.*, vol. 3, pp. 255–269, 1956.

[151] J. Beck, "Sums of distances between points on a sphere — an application of the theory of irregularities of distribution to discrete geometry," *Mathematica*, vol. 31, pp. 33–41, 1984.

[152] K. Stolarsky, "Spherical distributions of N points with maximal distance sums are well spaced," *Proc. Amer. Math. Soc.*, vol. 48, pp. 203–206, 1975.

[153] L. F. Tóth, "On the sum of distances determined by a point set," *Acta. Math. Acad. Sci. Hungar.*, vol. 7, pp. 397–401.

[154] S. Smale, "Mathematical problems for the next century," *Math. Intelligencer*, vol. 20, pp. 7–15, 1998, see also version 2 on Steve Smale's home page: http://math.berkeley.edu/∼smale/.

[155] G. Manev, "Die gravitation und das prinzip von wirkung und gegenwirkung," *Z. Phys.*, vol. 31, pp. 786–802, 1925.

[156] D. Lynden-Bell and R. Lynden-Bell, "Exact general solutions to extraordinary n-body problems," *Proc. R. Soc. Lond. A*, vol. 445, pp. 475–489, 1999.

[157] F. Calogero, "Solution of the one-dimensional N-body problem with quadratic and/or inversely quadratic pair potentials," *J. Math. Phys.*, vol. 12, pp. 419–436, 1971. Erratum ibid. vol. 37, p. 3646, 1996.

[158] J. Moser, "Three integrable hamiltonian systems connected with isospectral deformations," *Adv. Math.*, vol. 16, pp. 197–220, 1975.

[159] H. Cohn and A. Kumar, "Universally optimal distribution of points on spheres," *J. Amer. Math. Soc.*, vol. 20:1, pp. 99–148, 2007.

[160] J. Leech, "Equilibrium of sets of particles on a sphere," *Math. Gaz.*, vol. 41, pp. 81–90, 1957.

[161] E. A. Rakhmanov, E. B. Saff, and Y. M. Zhou, "Minimal discrete energy on the sphere," *Math. Res. Lett.*, vol. 1, pp. 647–662, 1994.

[162] E. Rakhmanov, E. Saff, and Y. Zhou, "Electrons on the sphere," in *Computational Methods and Function Theory*, R. M. Ali, S. Ruscheweyh, and E. B. Saff, Eds. World Scientific, pp. 111–127, 1995.

[163] T. Erber and G. M. Hockney, "Complex systems: equilibrium configurations of n equal charges on a sphere ($2 \leq n \leq 112$)," in *Adv. Chem. Phys.*, I. Prigogine and S. A. Rice, Eds. Wiley, New York, vol. XCVIII, pp. 495–594, 1997.

[164] J. S. Brauchart, D. P. Hardin, and E. B. Saff, "The next-order term for optimal Riesz and logarithmic energy asymptotics on the sphere," in *Recent advances in orthogonal polynomials, special functions, and their applications*, J. Arvesú and G. L. Lagomasino, Eds. Contemporary Mathematics, AMS, Providence, RI, 2012, vol. 578, pp. 31–61.

[165] M. Calef, C. Fichtl, W. Goulart, D. Hardin, and A. Schulz, "Asymptotic differences in energies of stable and minimal point configurations on $\mathbb{S}^2$ and the role of defects," *eprint arXiv:1307.0409*, 2013.

[166] E. Sandier and S. Serfaty, "2d coulomb gases and the renormalized energy," *(eprint) arXiv:1201.3503v2 [math-ph]*, 2013.

[167] N. S. Landkof, *Foundations of modern potential theory.* Berlin: Springer Verlag, 1972.

[168] A. Kuijlaars and E. Saff, "Asymptotics for minimal discrete energy on the sphere," *Trans. Amer. Math. Soc.*, vol. 350, pp. 523–538, 1998.

[169] D. P. Hardin and E. Saff, "Minimal riesz energy point configurations for rectifiable d-dimensional manifolds," *Adv. Math.*, vol. 193, pp. 174–204, 2005.

[170] M. Calef, "Theoretical and computational investigations of minimal energy problems," Ph.D. thesis, Vanderbilt University, 2009.

[171] R. H. Hardin, N. J. A. Sloane, and W. D. Smith, "Minimal energy arrangements of points on a sphere",©(1994) hss;
"http://www.research.att.com/~njas/electrons."

[172] C. Cecka, *http://thomson.phy.syr.edu/shells/shelltable.php*.

[173] "PLX system achitecture," Web page: *http://www.hpc.cineca.it/content/ibm-plx-gpu-user-guide-0#systemarchitecture*.